Preliminary Report
of
The Hakuho Maru Cruise KH 86-5

November 22 - December 14, 1986

Geophysical and Geological Investigation of the Nankai Trough,
Boso Triple Junction, Zenisu Ridge and Muroto Trough

(ODP Site Survey)

Ocean Research Institute
University of Tokyo
1988

Preliminary Report
of
The Hakuho Maru Cruise KH 86-5

November 22 - December 14, 1986

Geophysical and Geological Investigation of the Nankai Trough,
Boso Triple Junction, Zenisu Ridge and Muroto Trough

(ODP Site Survey)

by
The Scientific Members of the Expedition
Edited by
Asahiko Taira

PREFACE

The subduction of the Philippine Sea Plate at the margin of southwestern Honshu results remarkable tectono-sedimentology processes important to the understanding of evolution of active margin.

Such processes include:

1. Origin of sediment accretionary prism
2. Hydrogeology and fluid circulation within accretionary prism
3. Tectono-sedimentary evolution of trench-trench-trench triple junction
4. Intra-oceanic plate shortening related to arc-arc collision

These are the main objectives of this cruise and have been examined by means of geophysical and geological techniques; seismic reflection analysis, seismic refraction velocity determination using ocean bottom seismometers, 3.5 kHz subbottom profiling and PDR depth sounding, heat flow, underwater photography, piston coring and hauling.

The main results of this cruise can be summarized as follows:

1. Accretion of sediment is ensured at the triple junction zone suggesting that the rapid sediment yield is a primary factor of sediment accretion.
2. Intra-plate shortening related to the Izu-Bonin Arc collision zone is recognized within a much wider and more diffused zone than as previously thought.
3. Heat flow measurements, seismic studies and undersea photography showed an active fluid circulation and over pore-pressuring within the accretionary prism of the Nankai Trough.

In spite of the damage to the streamer cable at the summit of Takuyo-Daini Seamount due to the encounter with fish trap, the cruise was quite successful and achieved most of initial objectives.

We thank very much for the cooperation of ship's officers and crews. This cruise was also planned for the ODP (Ocean Drilling Program) site survey for the Nankai Trough and Zenisu Ridge.

Much of the editorial work was assisted by W. Soh and I thank especially for his contribution.

June, 1988

Ashahiko TAIRA

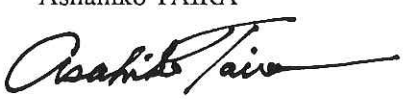

Chief Scientist of the Cruise

Contents

SCIENTIST LIST OF THE R/V HAKUHO MARU, KH-86-5 CRUISE

Asahiko TAIRA (Chief Scientist)	Ocean Research Institute, University of Tokyo
Toshio ASANUMA	Department of Earth Sciences, Chiba University
Peter BLUM	Department of Geology & Mineralogy, Kyoto University
Nicolas CHAMOT-ROOKE	Ecole Normale Superiere
Hiromi FUJIMOTO	Ocean Research Institure, University of Tokyo
Toshio FURUTA	Ocean Research Institute, University of Tokyo
Xiaoli GYO	Department of Earth Sciences, Shizuoka University
Chiaki IGARASHI	Ocean Research Institute, University of Tokyo
Shin'ichi ISEKI	Department of Earth Sciences, Shizuoka University
Yoshinobu KASUMI	Department of Earth Sciences, Chiba University
Hajimu KINOSHITA	Department of Earth Sciences, Chiba University
Masataka KINOSHITA	Earthquake Research Institute, University of Tokyo
Kazuaki KOJIMA	Department of Earth Sciences, Kanazawa University
Naoko MATSUDA	Department of Earth Sciences, Chiba University
Masao NAKANISHI	Ocean Research Institute, University of Tokyo
Ei'ichiro NISHIYAMA	Ocean Research Institute, University of Tokyo
Azusa NISHIZAWA	Observation Center for Earthquake Prediction,Tohoku University
Yujiro OGAWA	Department of Geology, Kyushu University
Tadashi OHTA	Department of Earth Sciences, Kanazawa University
Keni'ichi OTUKA	Department of Earth Sciences, Shizuoka University
Masaharu WATANABE	Ocean Research Institute, University of Tokyo
Koji YAGISHITA	Ocean Research Institute, University of Tokyo
Tetsuzo SENO	International Institute of Seismology & Earthquake Engineering, Building Research Institute, Tsukuba
Lallemant SIEGFRIED	Ecole Normale Superiere, Paris
Wonn SOH	Ocean Research Institute, University of Tokyo
Makoto SUEMASU	Department of Earth Sciences, Chiba University
Bong Chool SUK	Ocean Research Institute, University of Tokyo
Yoshihiko TAMURA	Department of Geology, University of Tokyo
Hidekazu TOKUYAMA	Ocean Research Institute, University of Tokyo
Ikuko UNO	Department of Earth Sciences, Kobe University
Chul Soo YANG	Ocean Research Institute, University of Tokyo
Jian-hua YIN	Department of Earth Sciences, Shizuoka University

Work Log and Index Maps

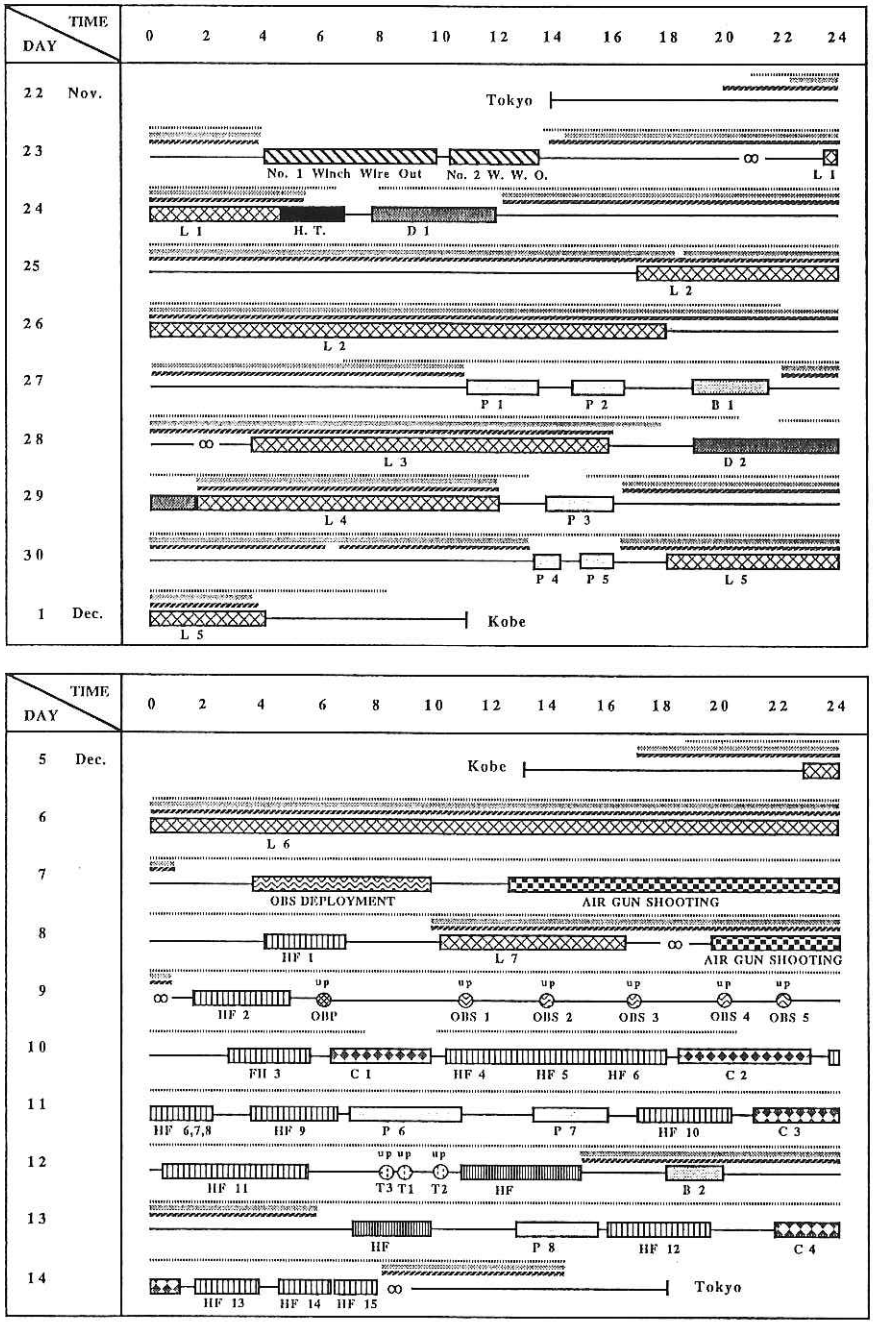

KEYS

3.5 kHz acousitic profiling

Geomagnetometers

12 kHz precision depth meter

L : multichannel sesimic reflection profiler HT : heat flow measurement
D : dredge sampling P : pistone coring OBP : ocean bottom pressure measurement
OBS : ocean bottom seismic refraction measurement C : deep-sea camera

Fig. 1 Work log of KH 86-5

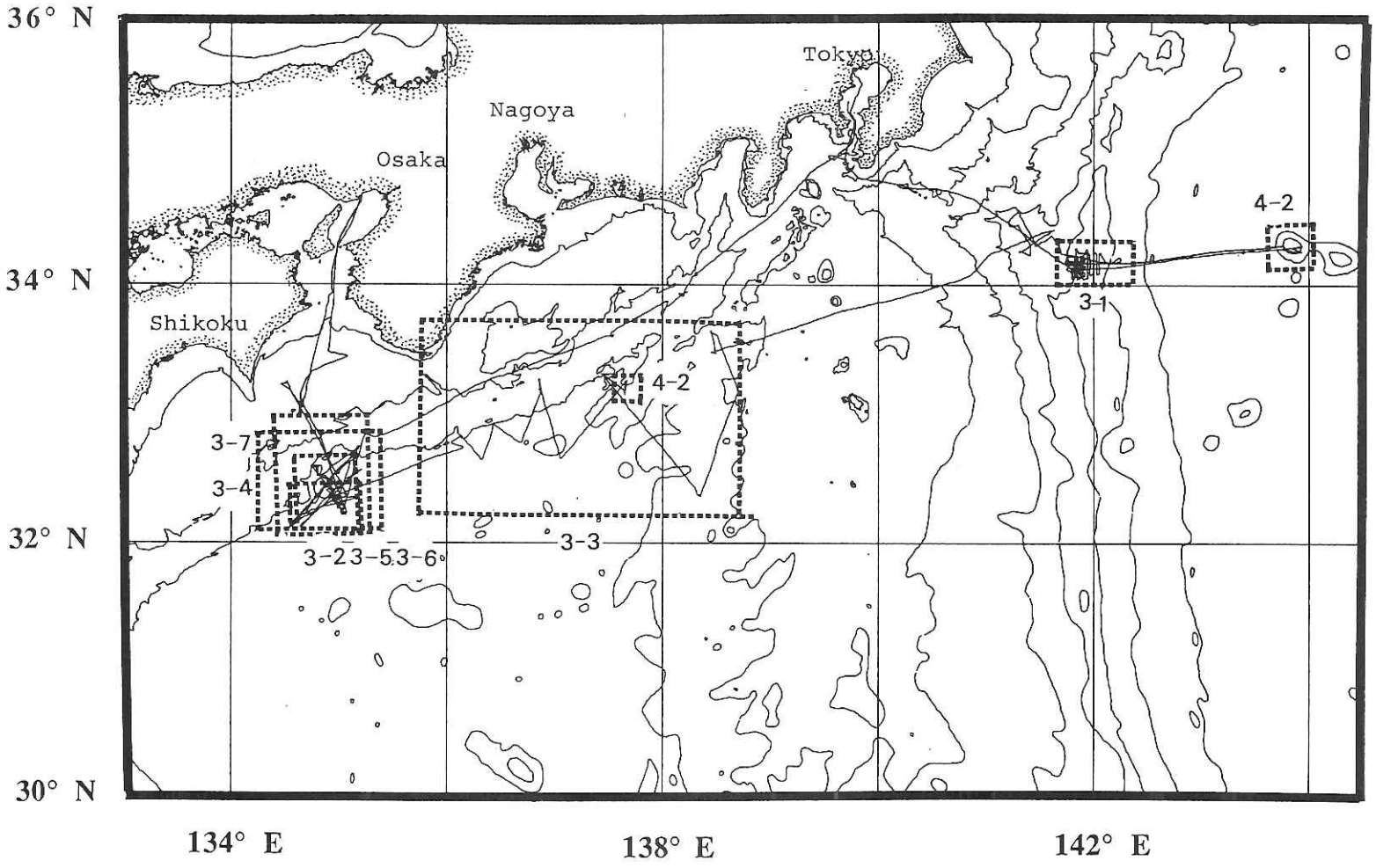

Fig. 2 Ship's tracks of KH86-5. (index map)

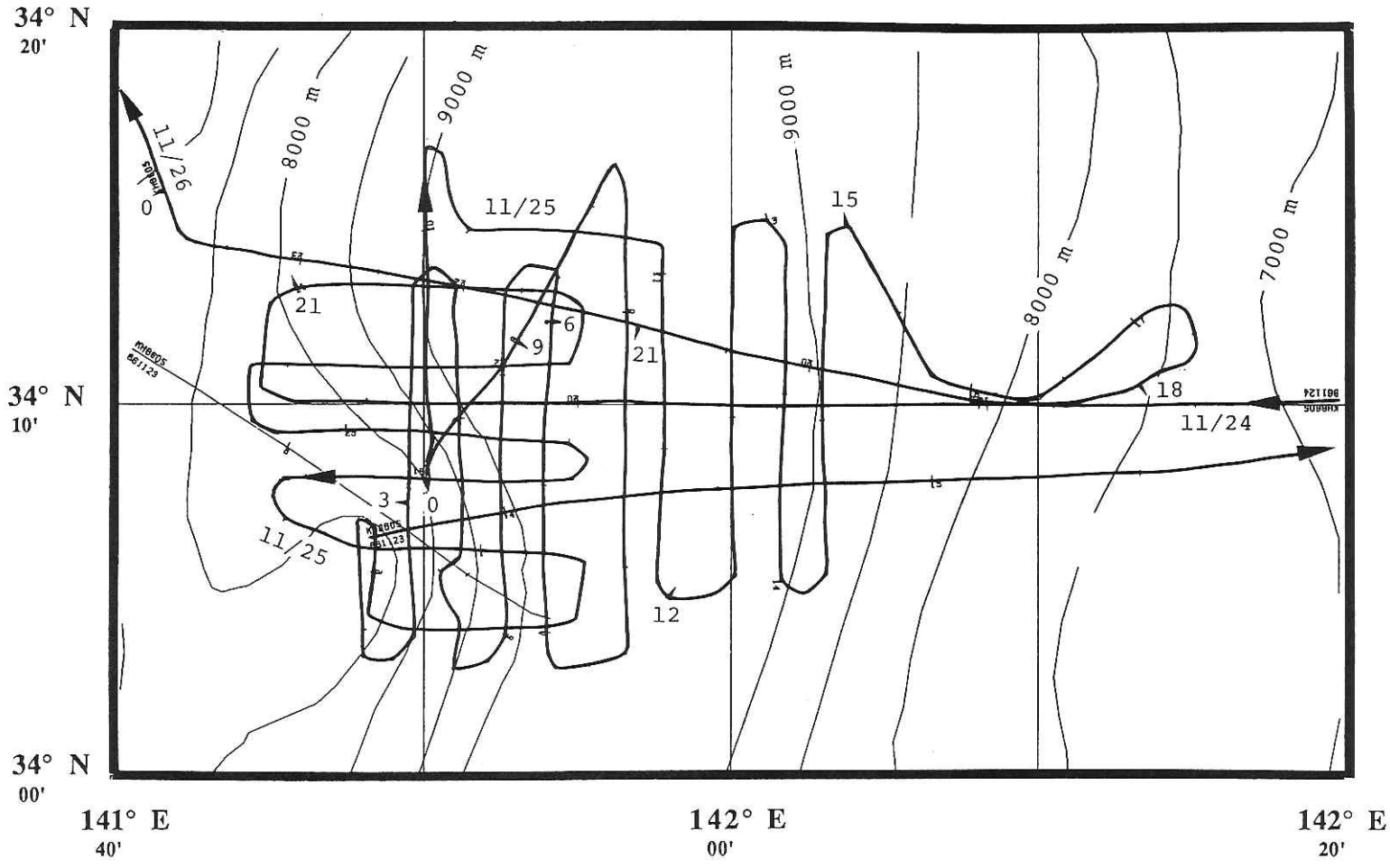

Fig. 3–1 Ship's track chart around the Boso Trench–trench–trench Triple Junction off Boso Peninsula. The numbers are date and time.

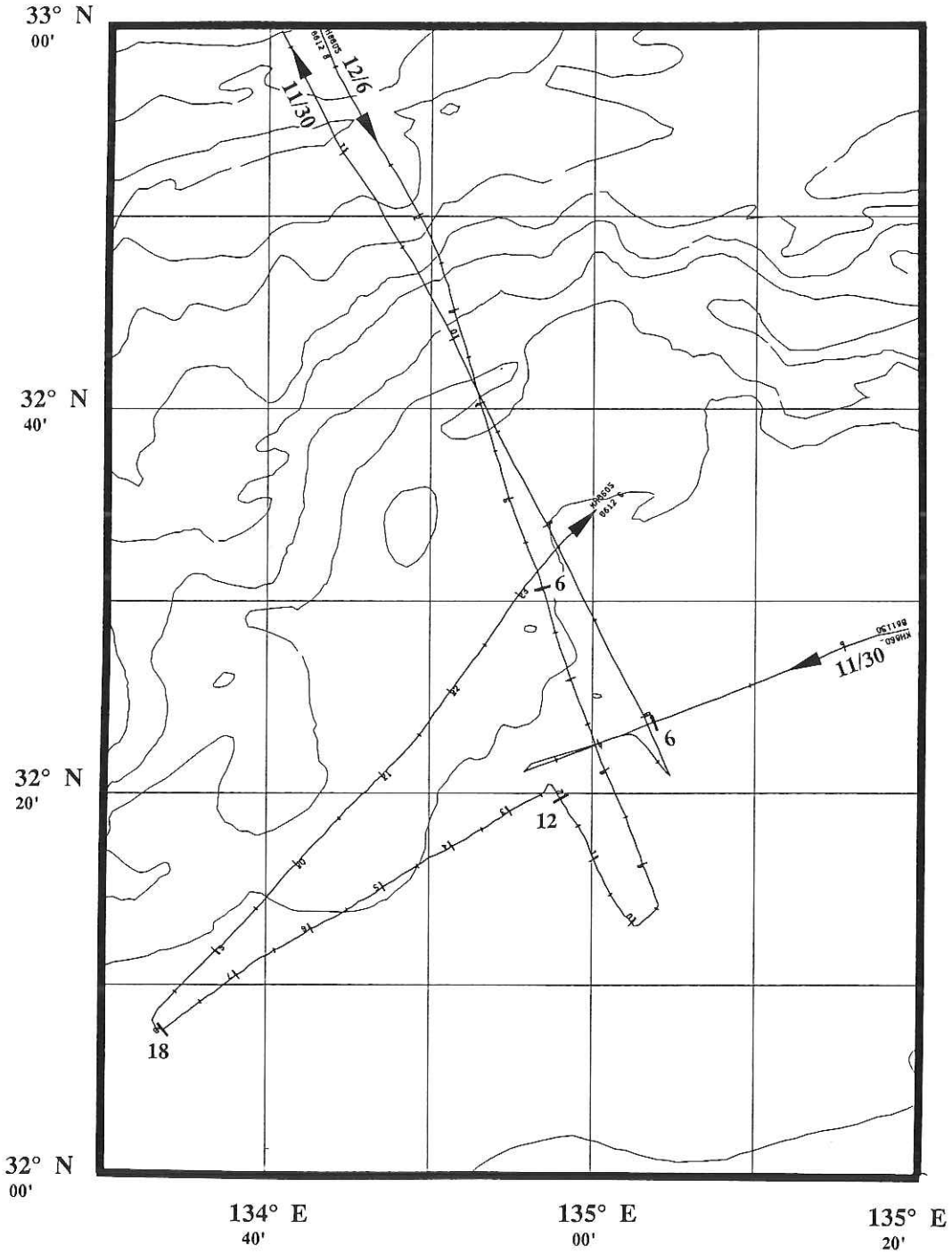

Fig. 3–2 Ship's track chart around off Muroto Basin.

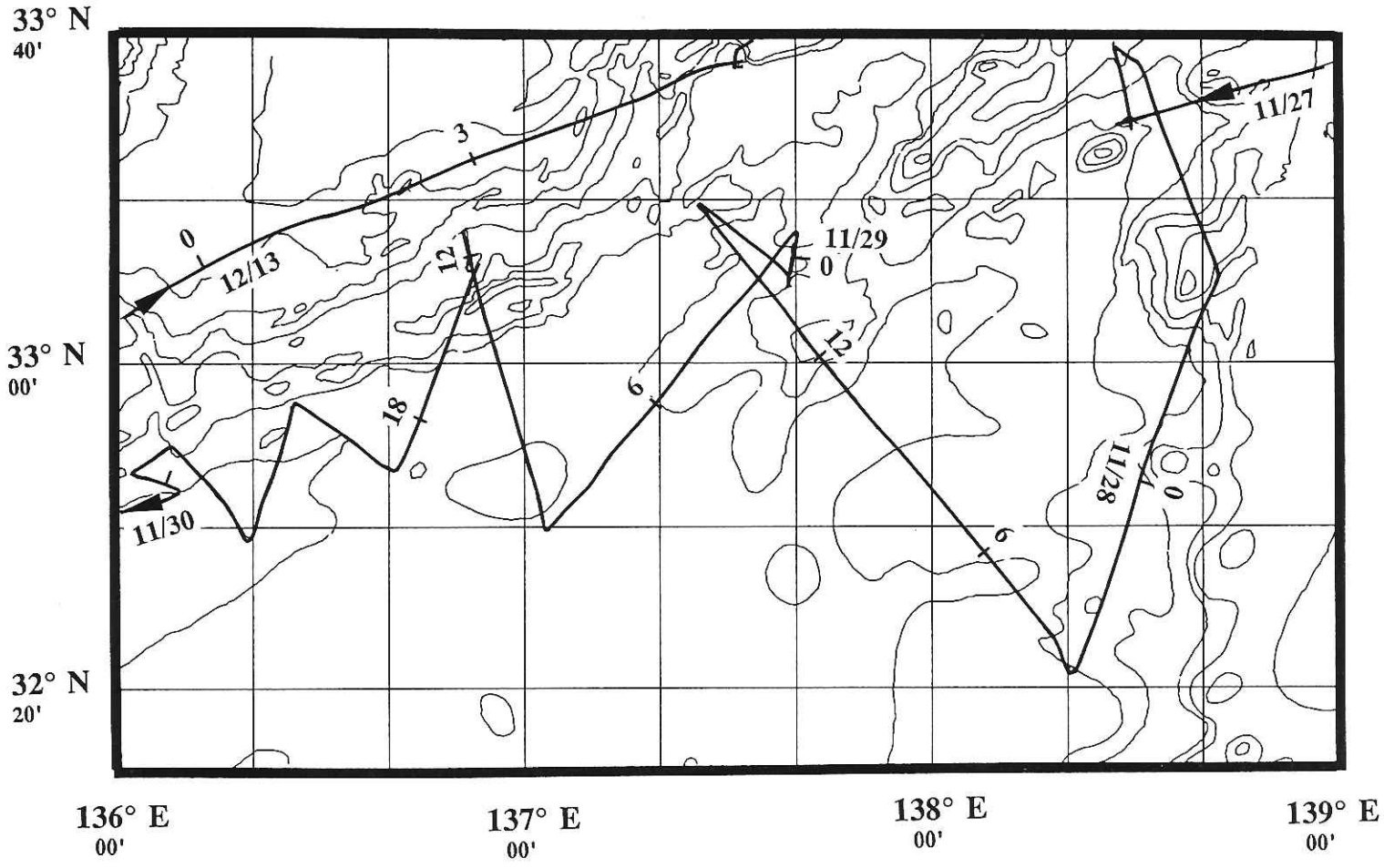

Fig. 3–3 Ship's track chart around the Nankai Trough off Kumano Basin.

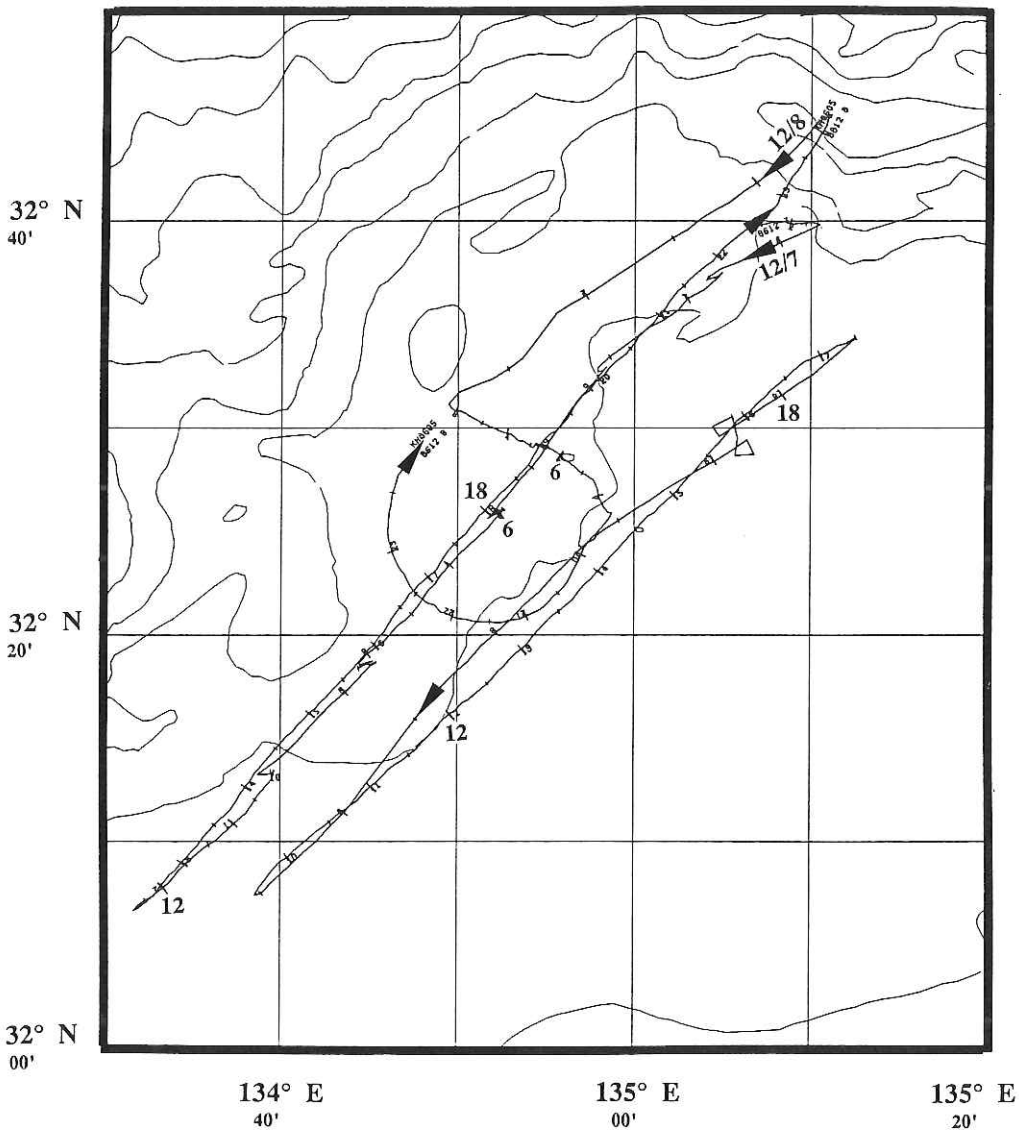

Fig. 3–4 Ship's track chart around the Nankai Trough off Muroto Basin.

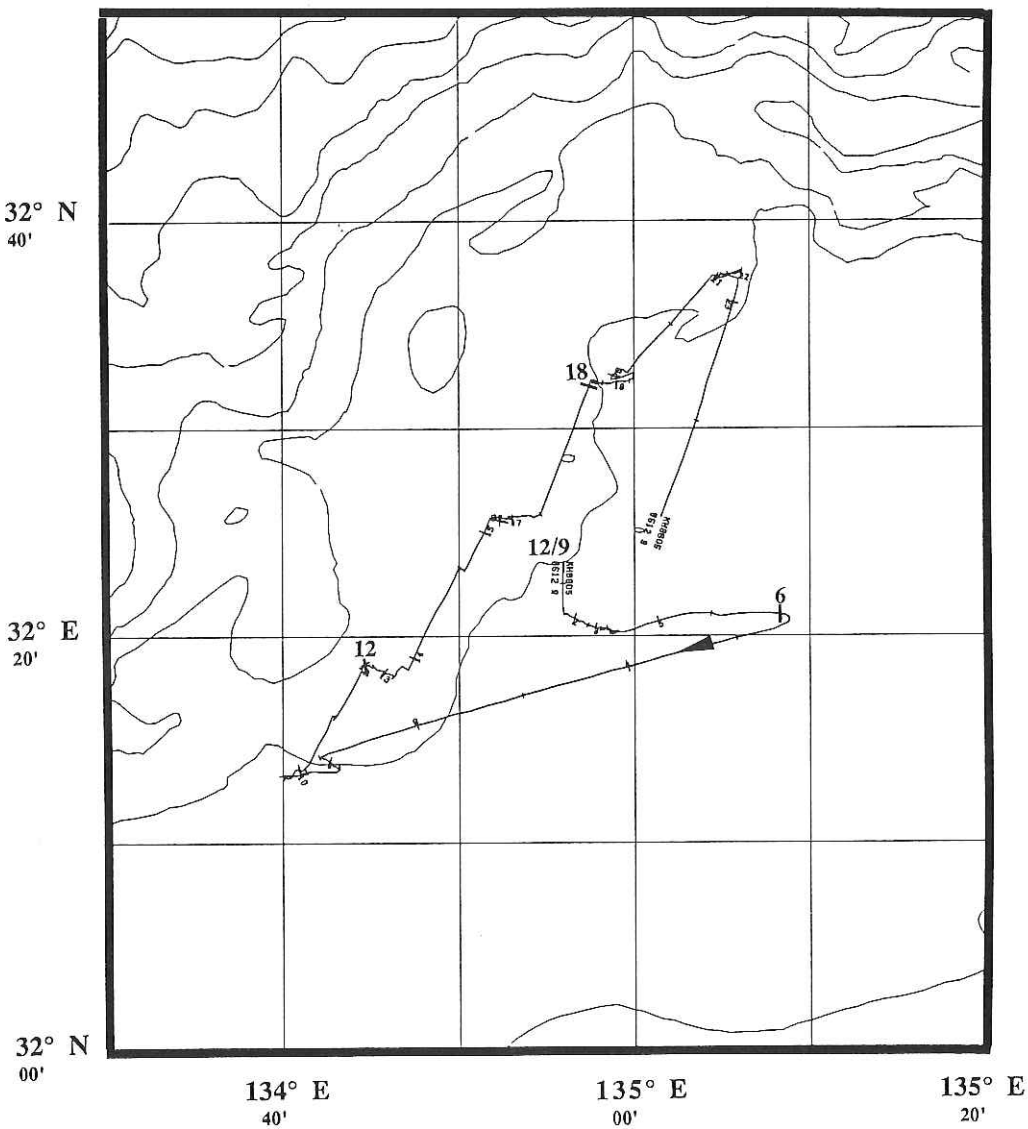

Fig. 3–5 Ship's track chart around off Muroto Basin during 6h–18h, 9th December.

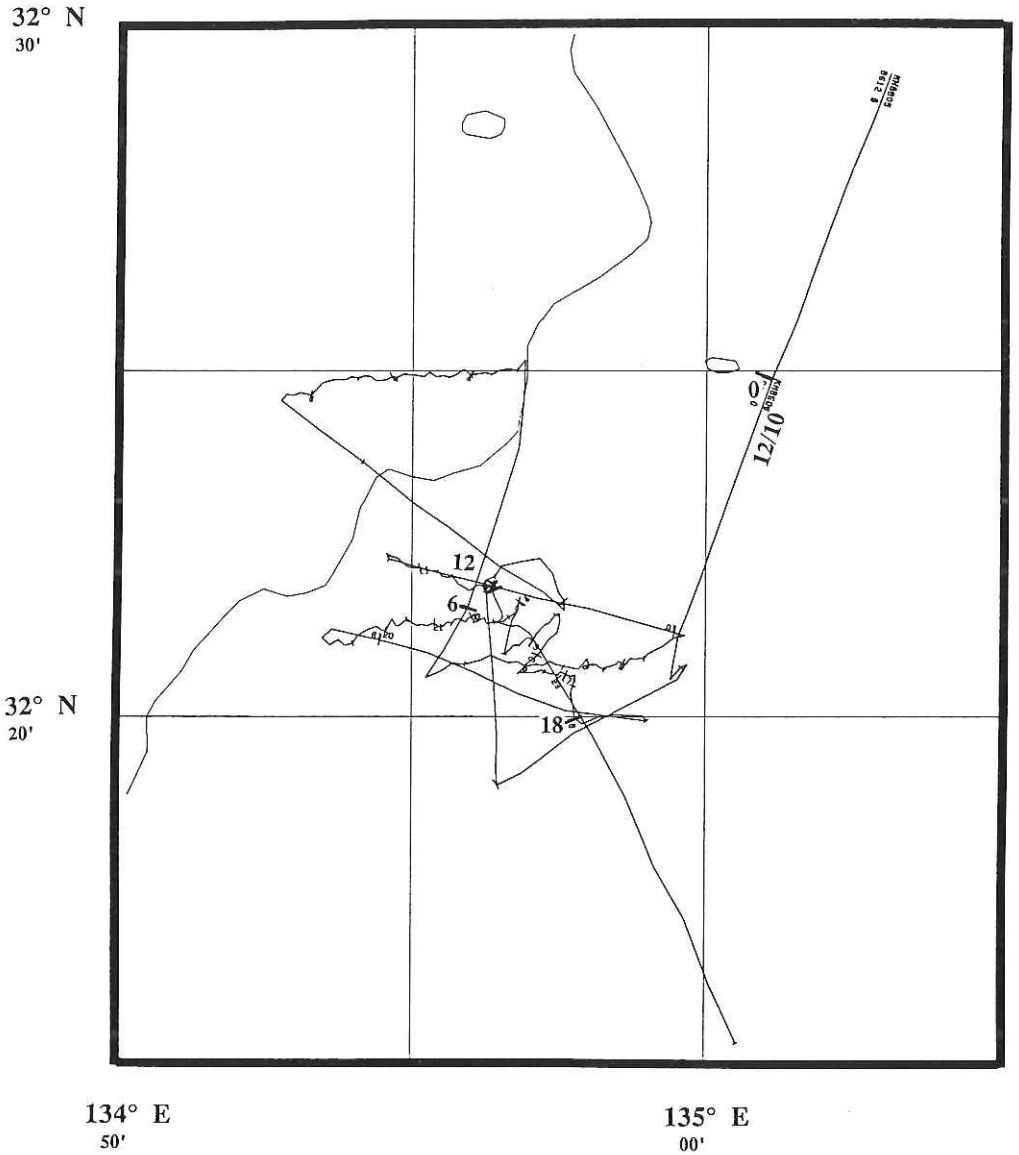

Fig. 3–6 Ship's track chart during 6h–18h, 10th December.

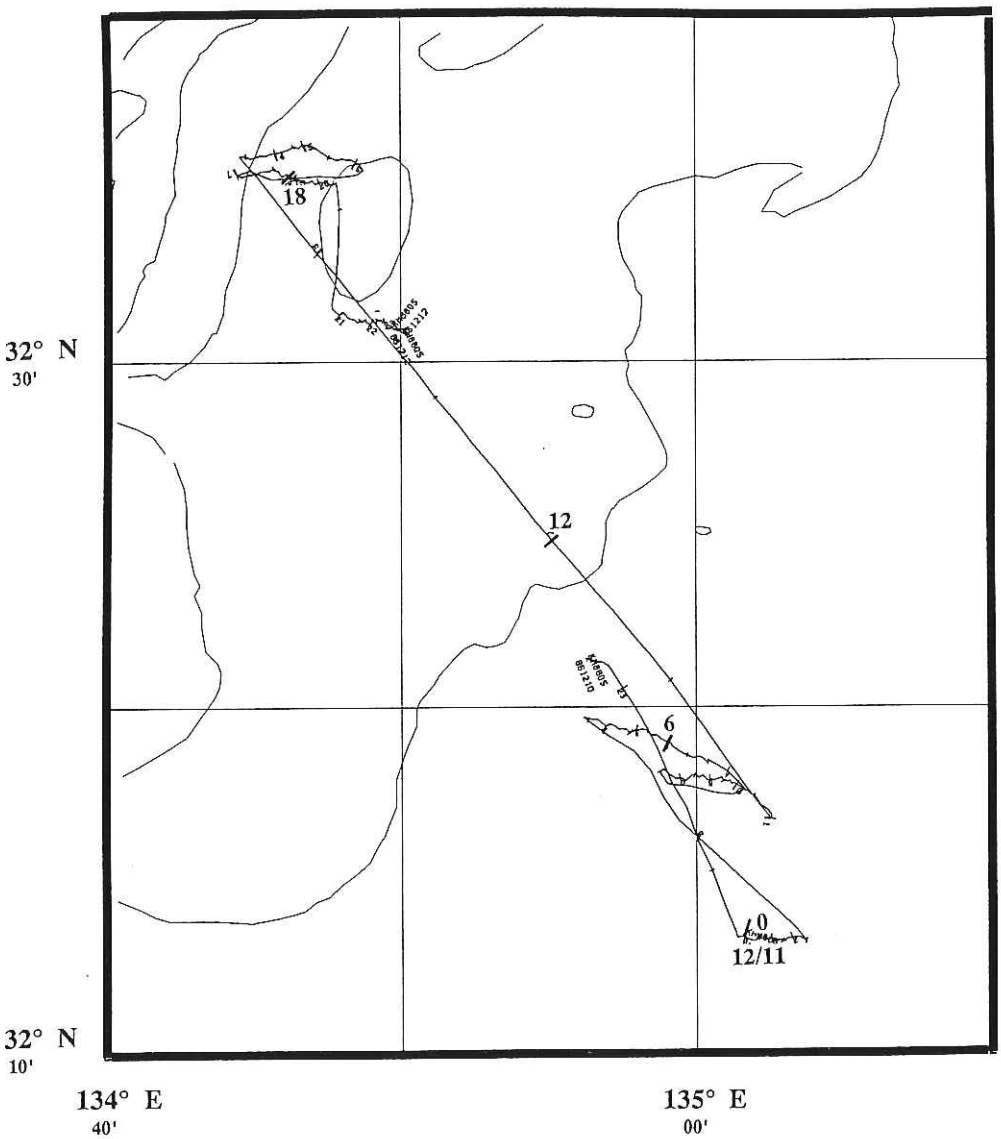

Fig. 3–7 Ship's track chart during 6h–18h, 11th December.

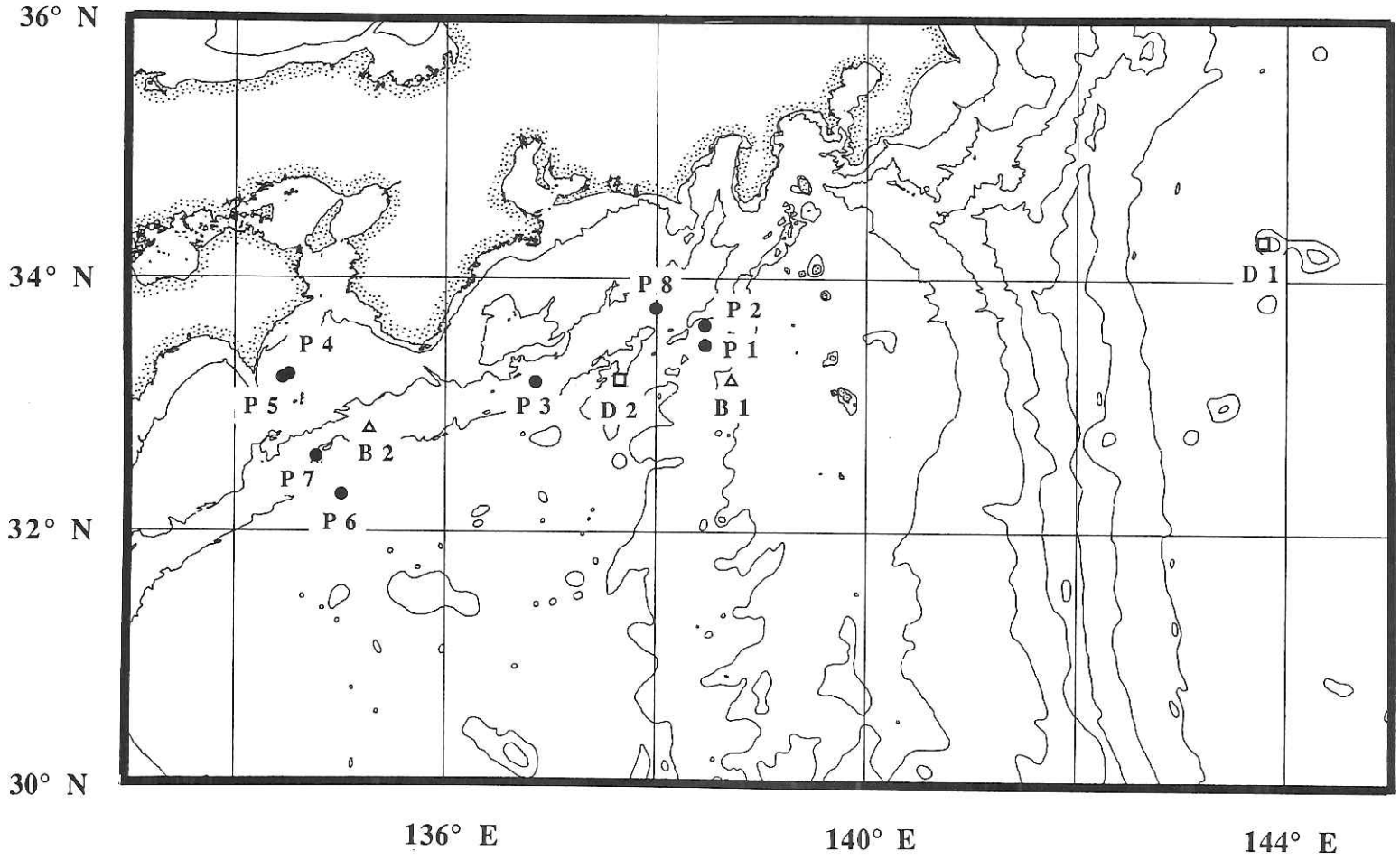

Fig. 4–1 Sampling sites of piston coring (P), box sampling (B) and dredging (D).

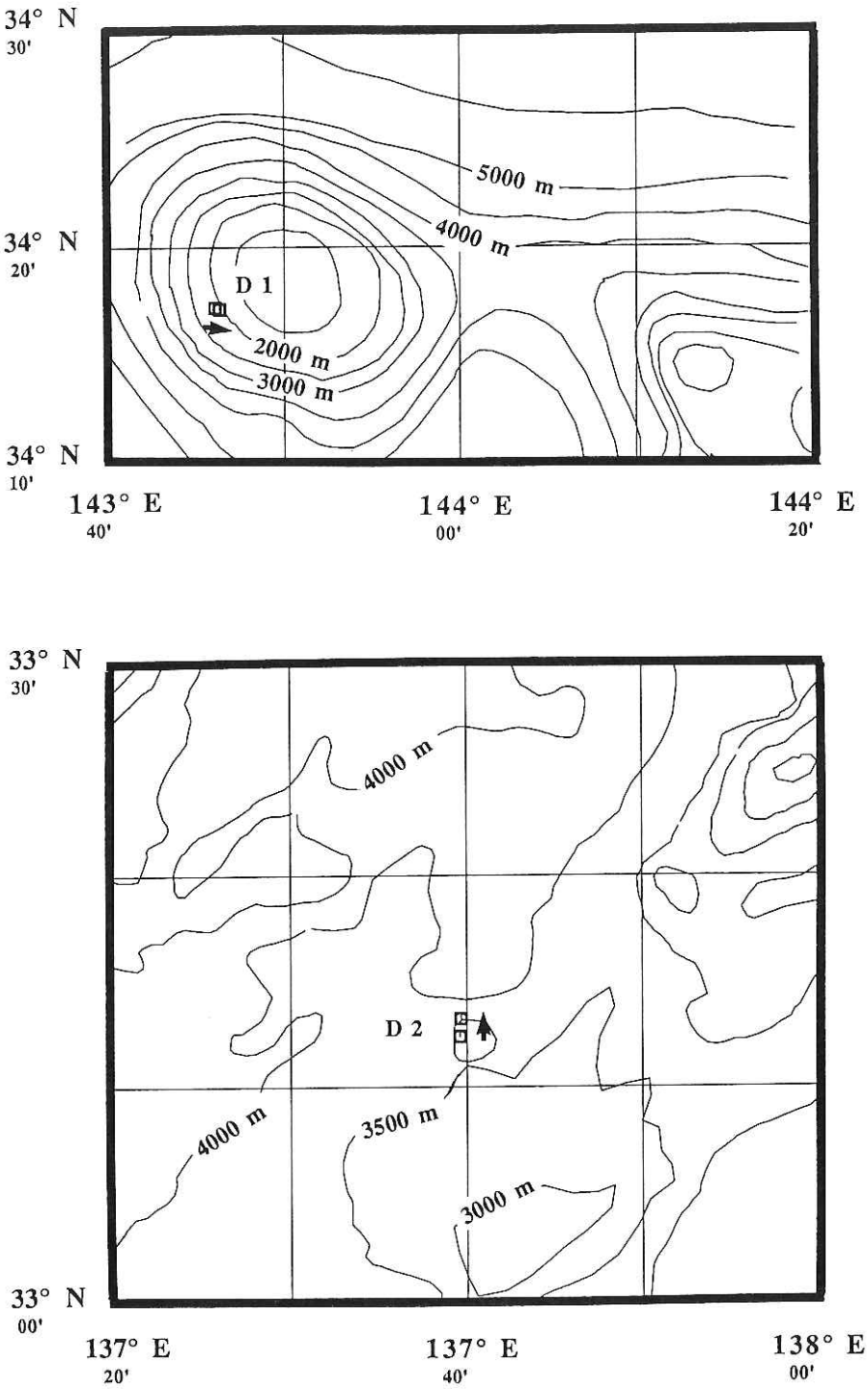

Fig. 4–2 Detail bathymetric map showing the tracks of dredgings, D1 and D2.

Geophysical Data

SEISMIC REFLECTION SURVEY

E. NISHIYAMA
Ocean Research Institute, University of Tokyo, Nakano, Tokyo 164
M. SUYEMASU and T. ASANUMA
Department of Earth Sciences, Chiba University, Yayoi, Chiba 260
H. TOKUYAMA
Ocean Research Institute, University of Tokyo, Nakano, Tokyo 164

DATA ACQISITION

Field data were recorded with NEC NE-128 digital recording system. The hydrophone streamer cable which was deployed in this cruise consists of a 200 meter lead-in cable, a 50 meter stretch section, twelve units of detector with unit length of 50 meter and a tail section as a stabilizer. In this construction of streamer cable, the shortest offset distance (shot to receiver distance) is 275 meter and the largest one is 825 meter. As a sound source, Bolt type air gun with 550 cubic inch chamber size was used and fired every 50 meter at the pressure range of 80 to 100 kg/cm^2. The combination of shot interval and unit length of detector permitted twelve fold CDP coverage. The analogue signals detected by the hydrophones were amplified and filtered in a filtering circuit. The pre-amplifier gain was 48 dB and a 0 to 128 Hz band-pass filter was applied to input signals. The output signals from a filtering circuit were transmitted to a A/D (analogue to digital) converter with resolution of 15 bits. The analogue signals from 12 detectors were sampled every 4 ms at the same time and were amplified up to a proper amplitude range. They were then digitized and digital signals were recorded on 2400 ft magnetic tapes. Recording length was 8 second per shot.

LOCATIONS OF REFLECTION LINES

Locations of all exploring lines obtained in the cruise are shown in figures 1 to 3. Fig. 1 gives an outline of entire lines. Fig. 2 is a detailed track chart of line 2 and numbers indicate shot points. Fig. 3 is an enlarged chart for lines 6 and 7.

Line 1 was planned to investigate the internal structure of Takuyo-daini seamount for the coming ODP drilling and running from the west to the east across the outer slope of the Japan trench. Unfortunately, operation was abandoned on the top of the seamount because of unexpected accident. Streamer cable was caught by fishermen's net and several units were lost into the sea. After few hours, the detached hydrophones were recovered. Instantaneous validity check of hydrophones was made

on board. Consequently it was made sure that ten units hydrophones have not been damaged.

Line 2 was recorded around the triple junction area off Boso peninsula. The objective of this line was to delineate subsurface structure made by reciprocal reaction of three major plates. An attempt to detect reflectors showing subducting Pacific Plate and Philippine Sea Plate was not achieved.

Line 3 was to investigate the intra-plate deformation of south Zenisu region.

Lines 4 and 5 were explored by singlechannel technique.

Investigation of lines 6 and 7 were performed around the inner slope of the Nankai trough off Shikoku Island. Line 6 consists of four minor lines. Line 6-1 gives a preliminary information to heat flow measurement operated in this cruise. Line 6-2 is the southeastern extension of JAPEX line 55-2 and the purpose of this line was to take an information of undeformed zone. Line 6-3 is a transit from line 6-2 to line 6-4. Line 6-4 was planned as a reference line for OBS experiment performed in the cruise.

DATA PROCESSING OF MULTICHANNEL PROFILES

Using digital computer in the institute, reflection data recorded with multichannel technique were processed to obtain high resolution sections. Processing procedure consists of the following steps.

(1) Conversion of data format from SEG-B to SEG-X.
(2) Editing of CDP traces.
(3) Band pass filtering with band range of 5 to 100 Hz.
(4) True Amplitude Recovery process.
(5) Deconvolution before stack to eliminate the effect of source reverberation (prediction distance is 20 ms).
(6) Velocity analysis with constant velocity stack method to construct stacking velocity profiles. Velocity (RMS velocity) structures are obtained every 100 or 200 shots.
(7) Normal move-out correction with derived RMS velocity.
(8) Common depth point stacking (600 % or 500%).
(9) Deconvolution after stack to remove multiple reflections (prediction distance is 200 ms).
(10) Band pass filtering with band width from 10 to 50 Hz to give the final sections.

Processed profiles are shown in Figs. 4 to 14.

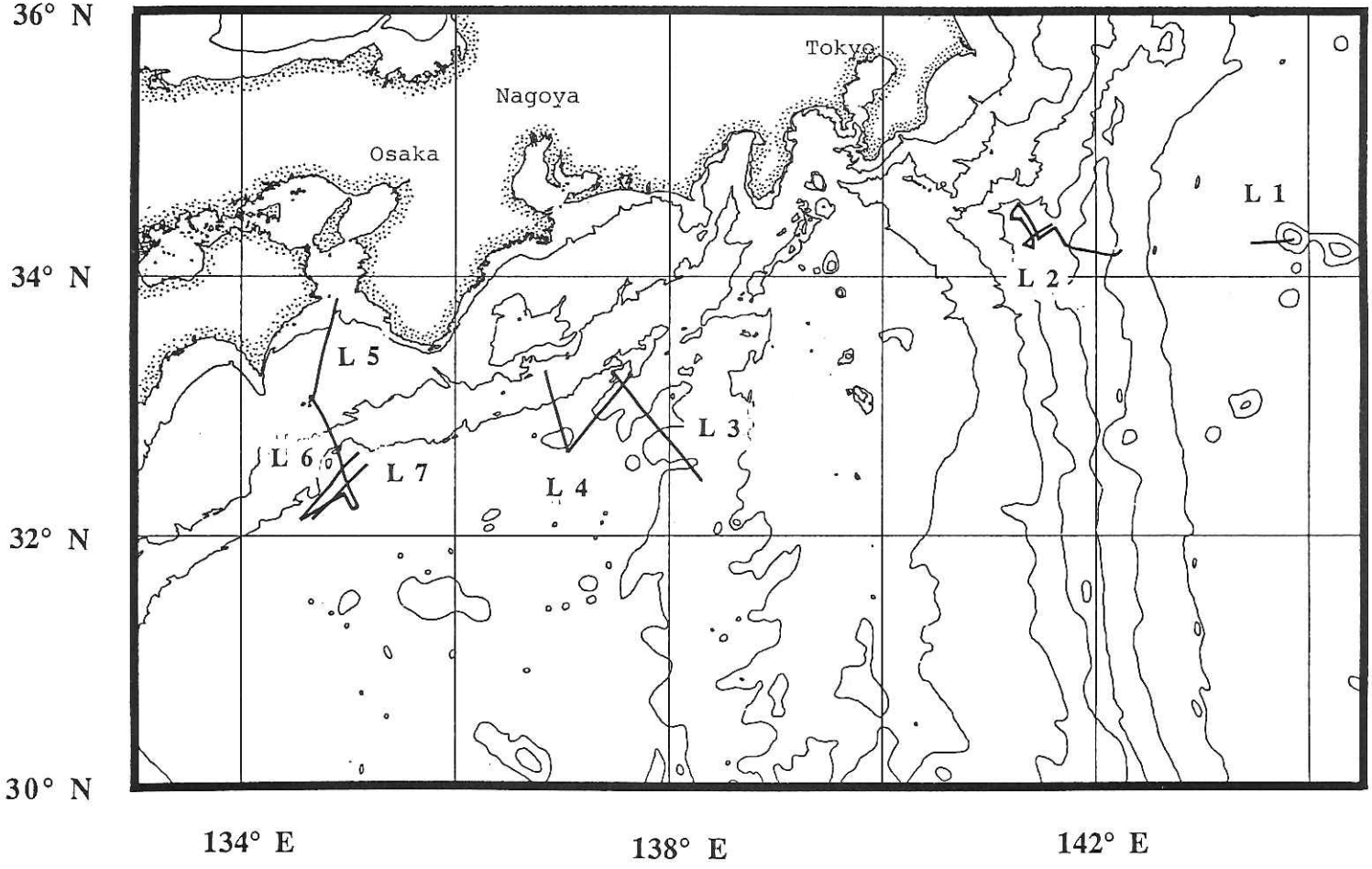

Fig. 1 Track lines of seismic reflection survey performed during KH86–5 cruise.

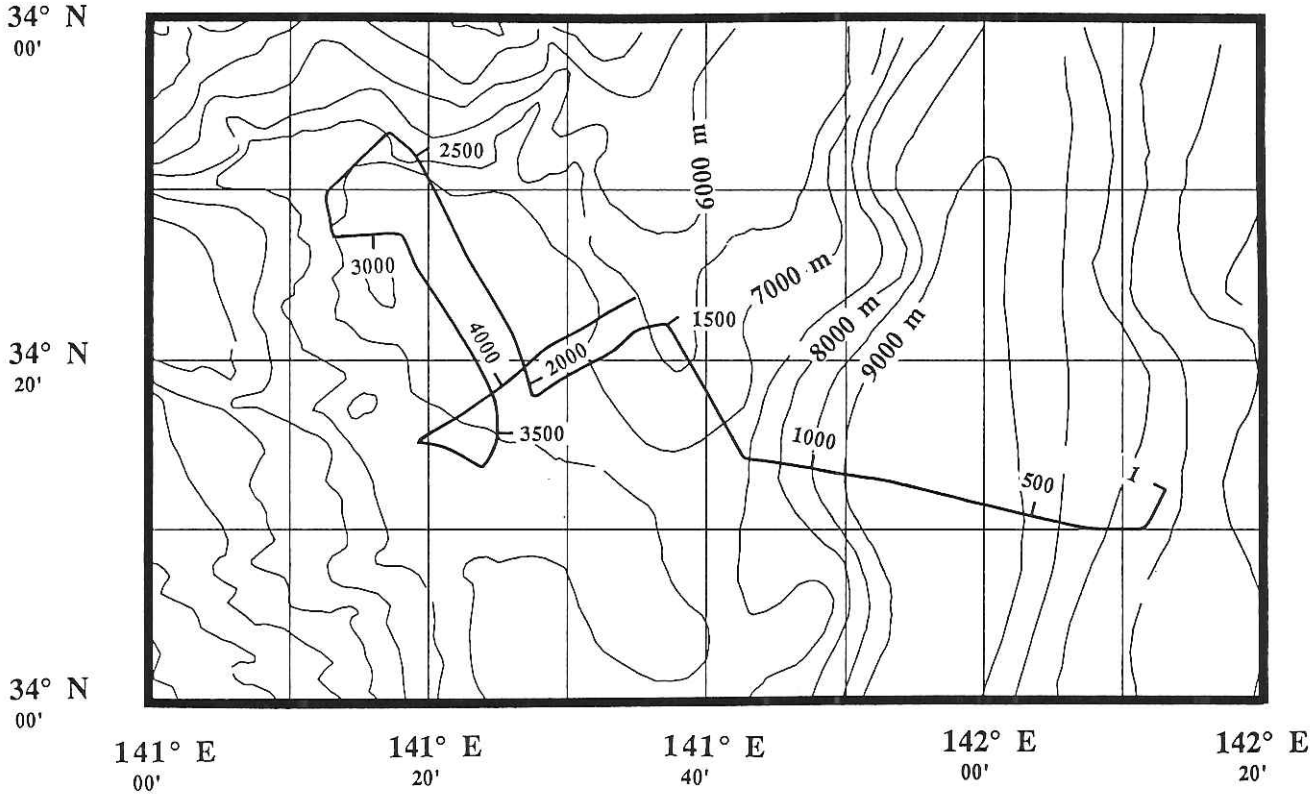

Fig. 2 A detailed track chart of line 2. Numbers indicate the shot points.

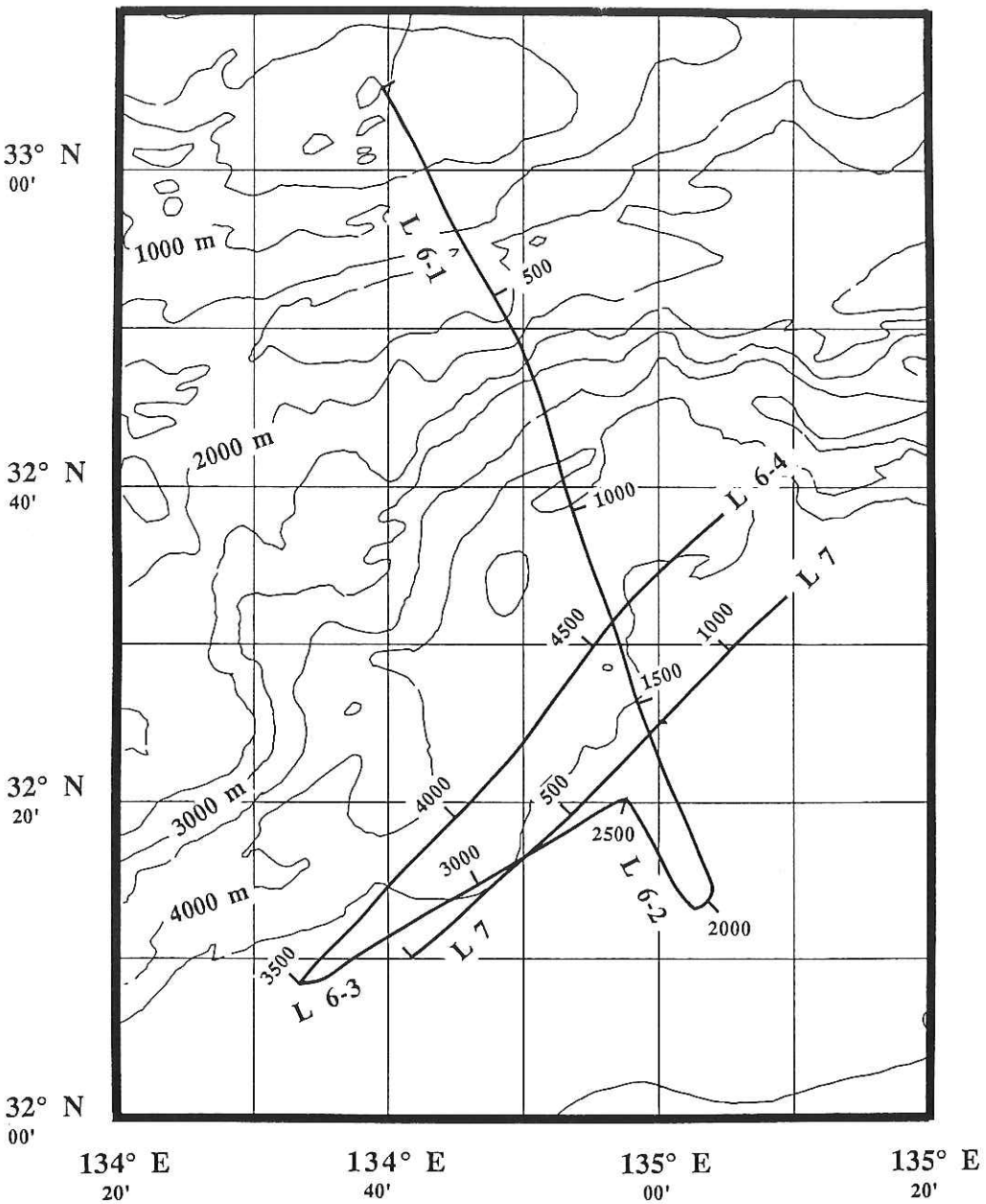

Fig. 3 An enlarged chart for lines 6 and 7. Numbers indicate the shot points.

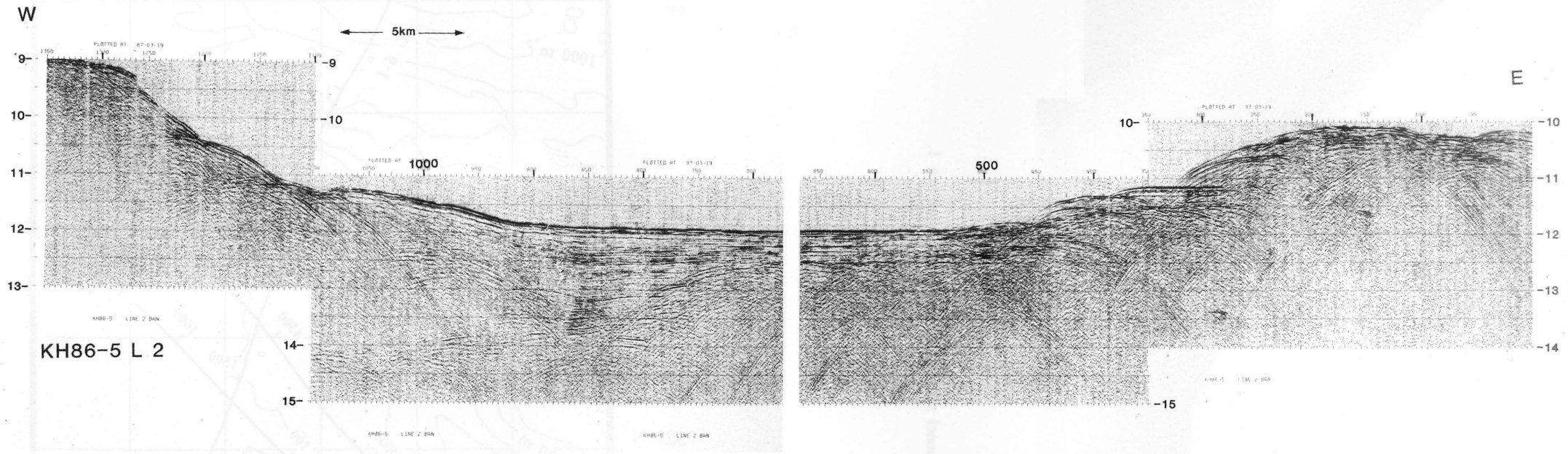

Fig. 5 A multichannel seismic reflection profile of line 2, shot points between1 and 1350.

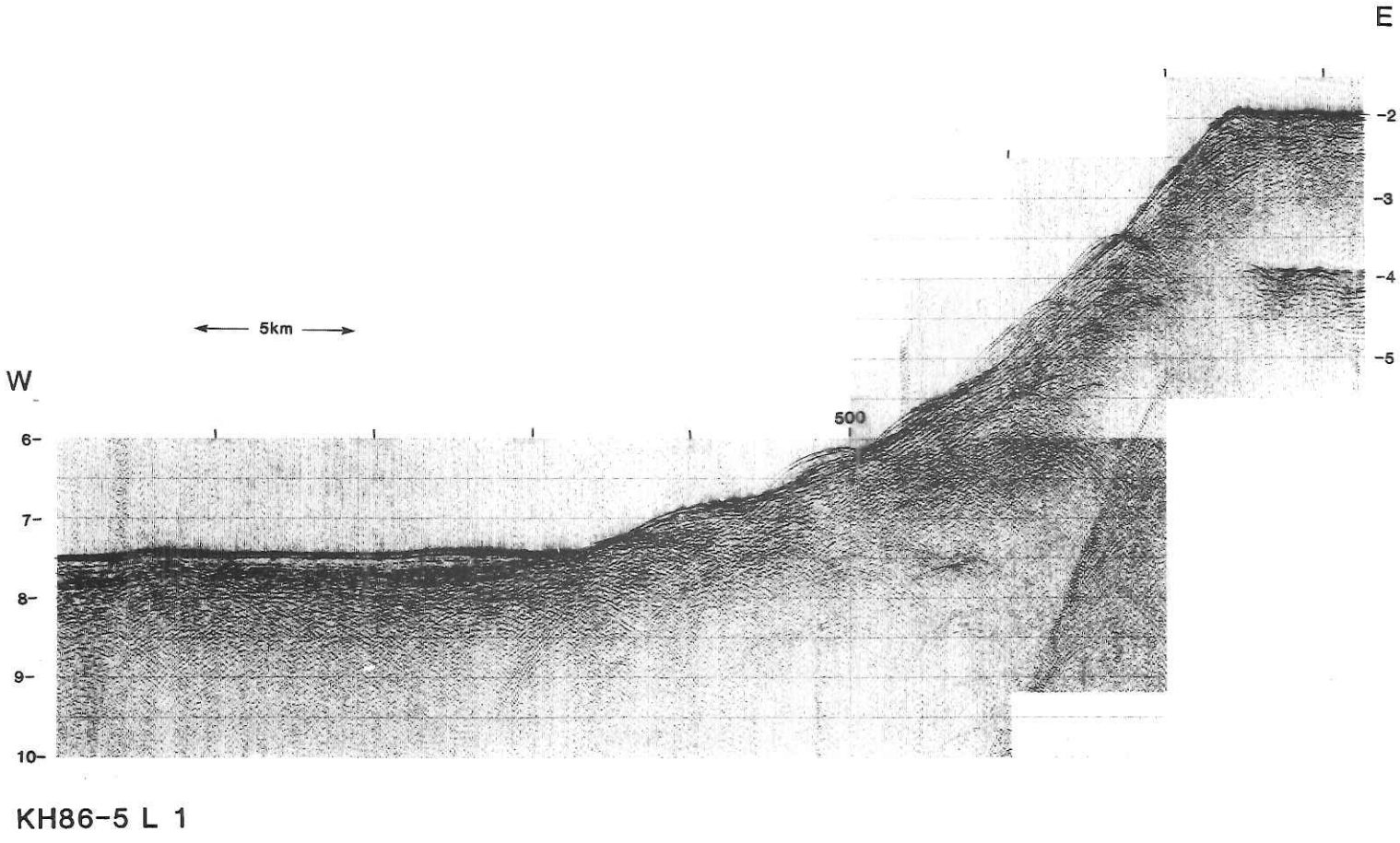

Fig. 4 A multichannel seismic reflection profile of line 1.

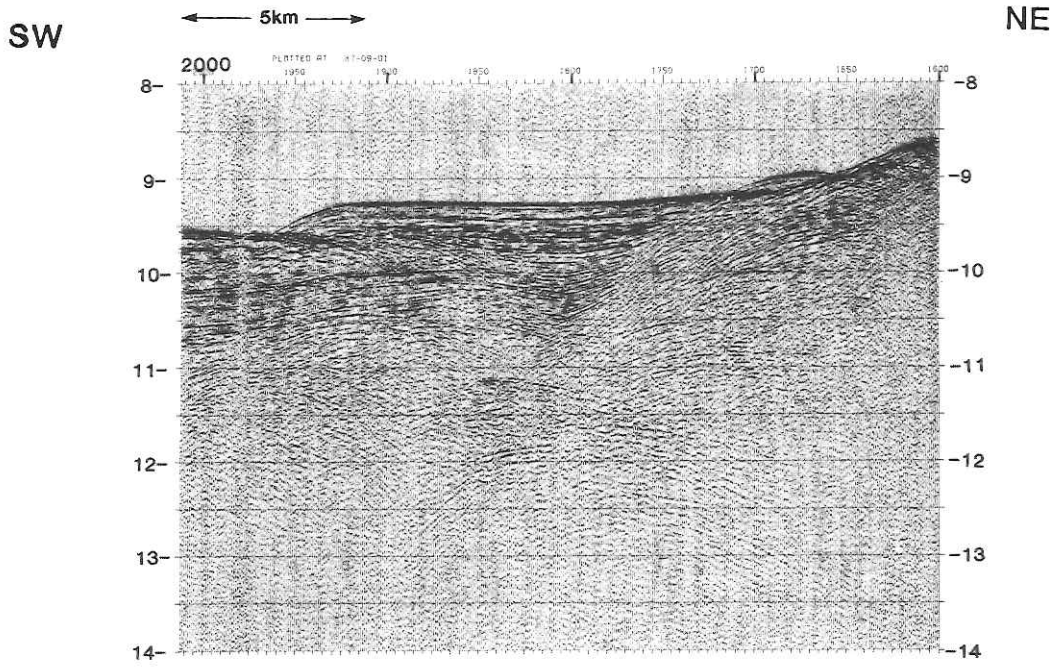

Fig. 6 A multichannel seismic reflection profile of line 2, shot points between1600 and 2012.

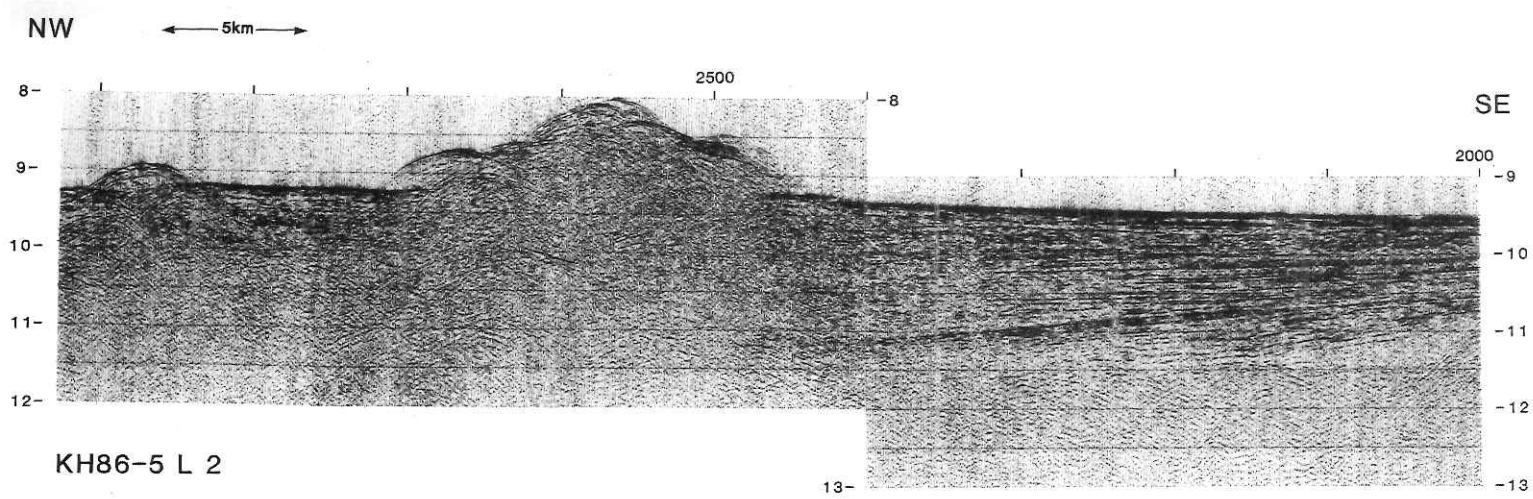

Fig. 7 A multichannel seismic reflection profile of line 2, shot points between 2000 and 2925.

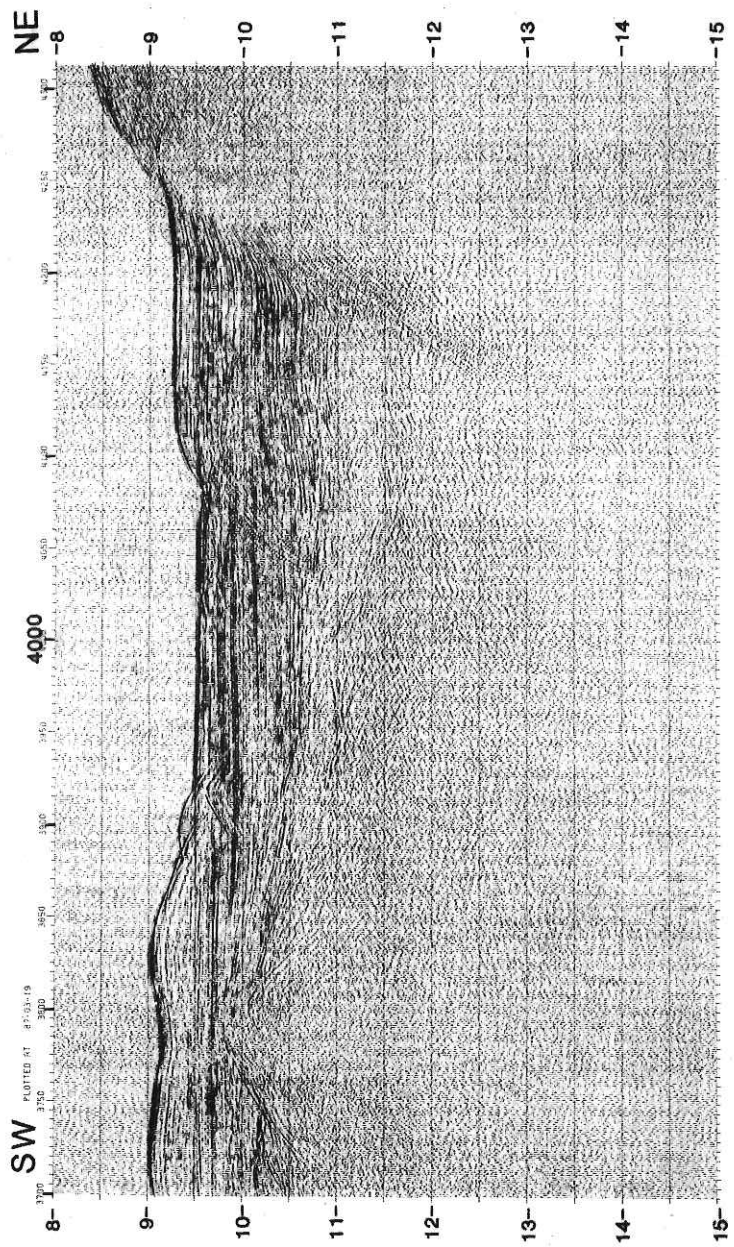

Fig. 8 A multichannel seismic reflection profile of line 2, shot points between 3700 and 4311.

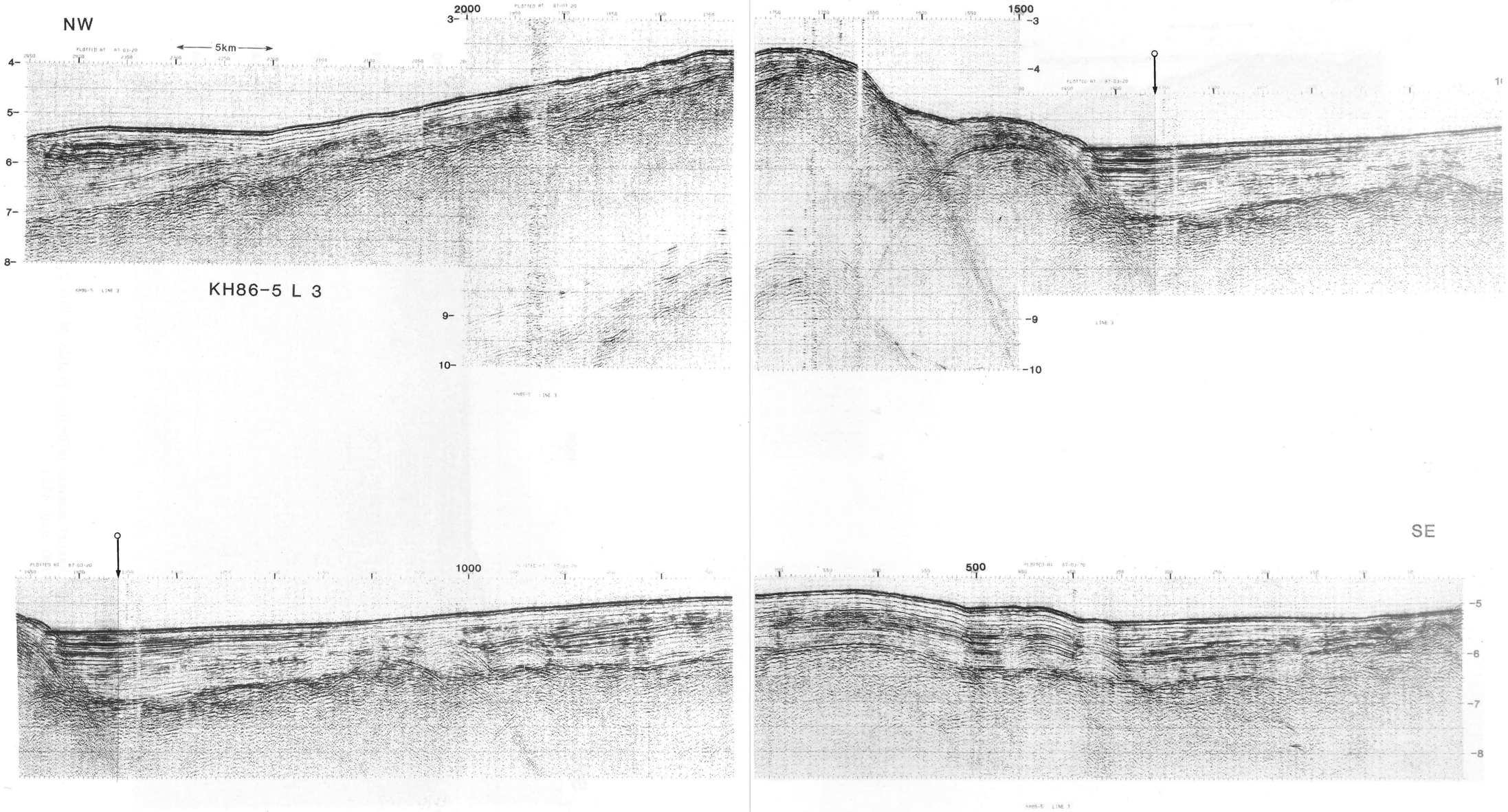

Fig.9 A multichannel seismic reflection profile of line 3.

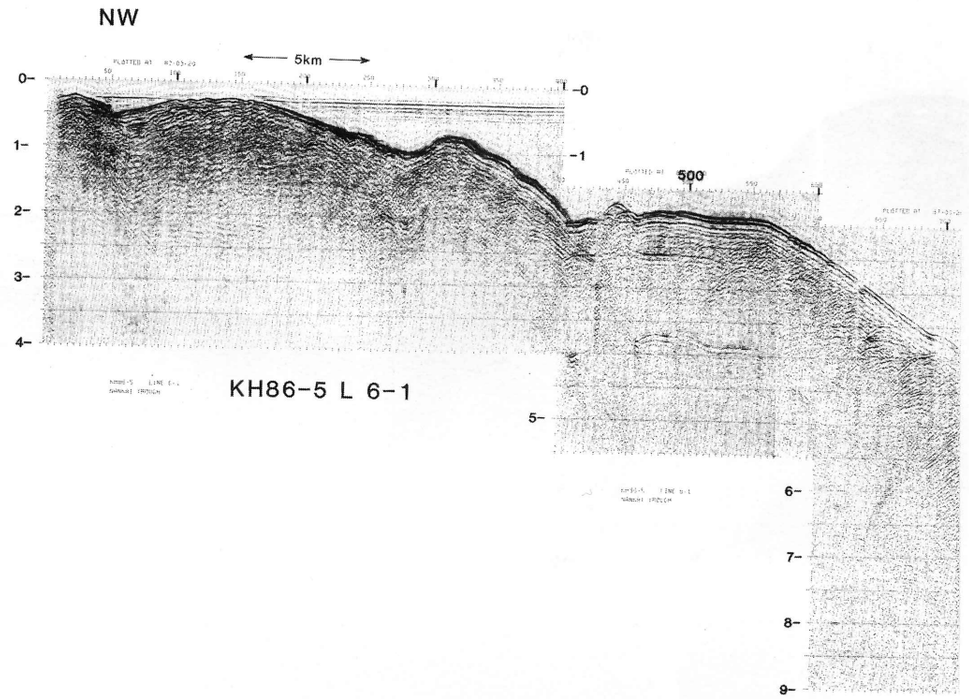

Fig. 10 A multichannel seismic reflection profile of line 6–1.

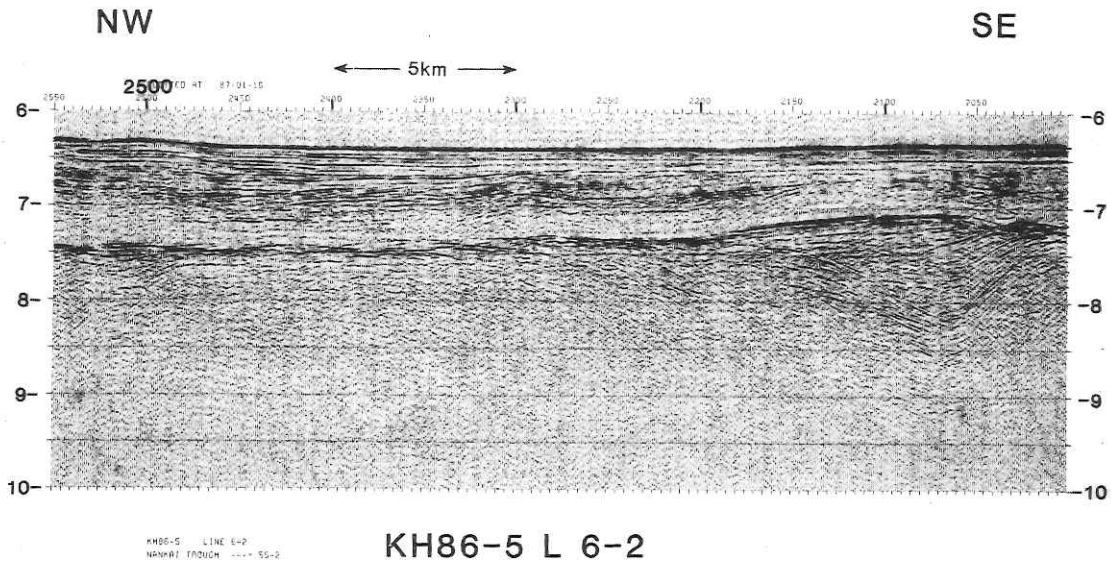

Fig. 11 A multichannel seismic reflection profile of line 6–2.

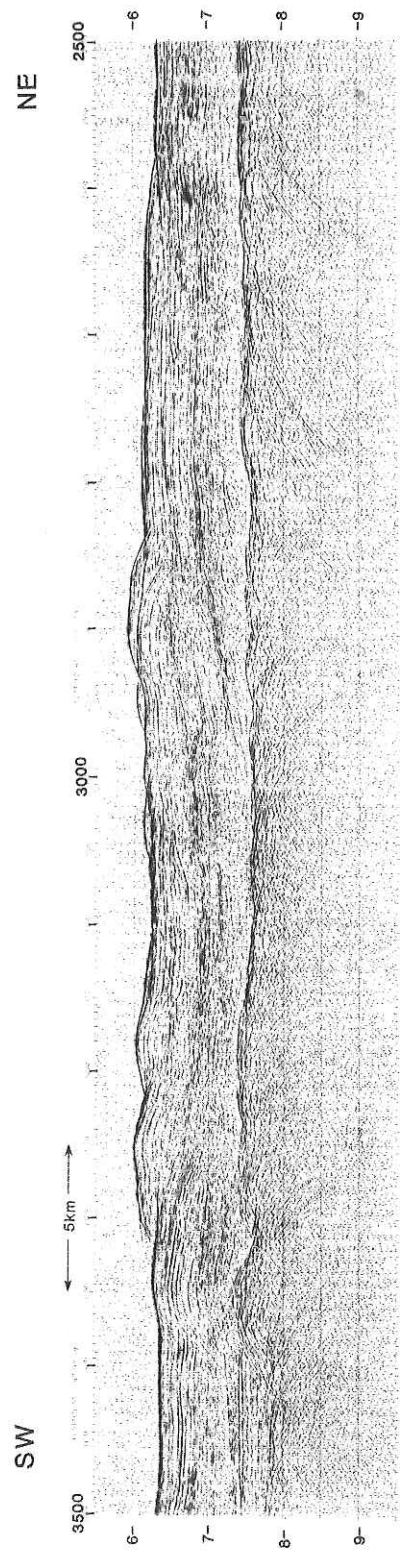

Fig. 12 A multichannel seismic reflection profile of line 6–3.

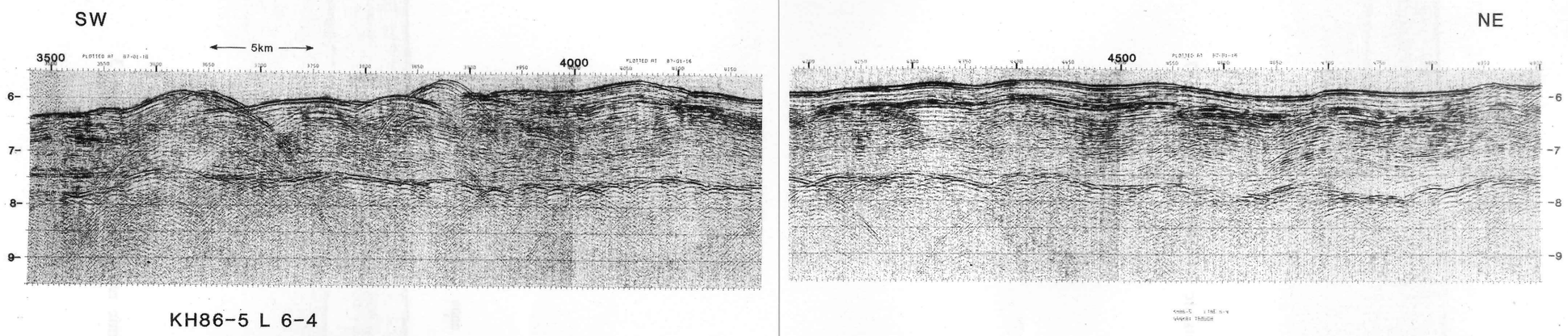

Fig. 13 A multichannel seismic reflection profile of line 6–4.

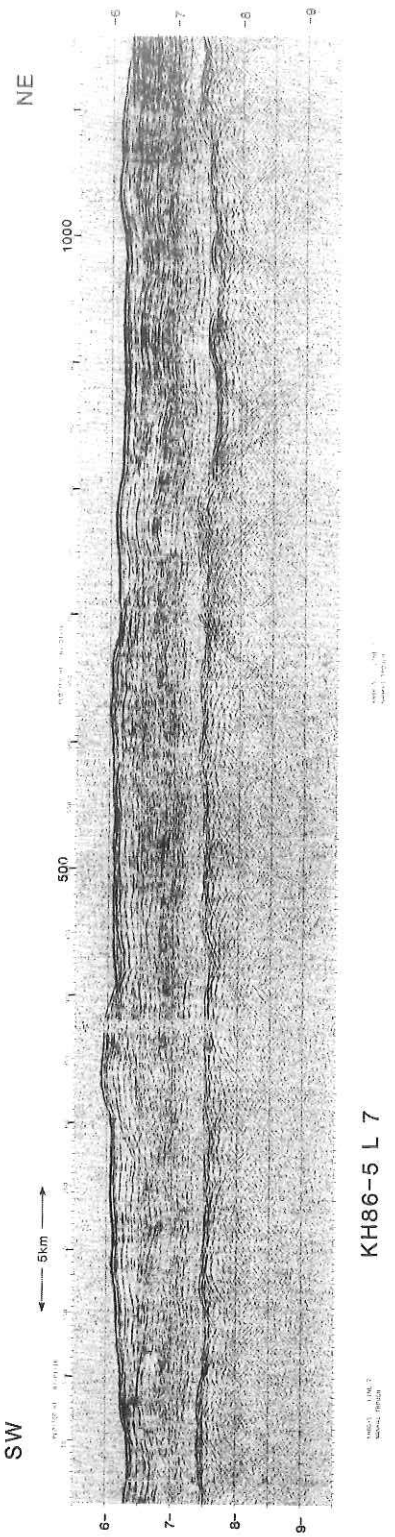

Fig. 14 A multichannel seismic reflection profile of line 7.

3.5 kHz SUBBOTTOM PROFILING SURVEY

C. IGARASHI, B.C. SUK and A. TAIRA
Ocean Research Institute, University of Tokyo, Nakano, Tokyo 164

A subbottom profiling survey for investigation the topography and the structure of surface sediments was carried out through the entire cruise (Appendix I and Fig. in this volume), using the equipment of the Raytheon 3.5 kHz subbottom profiling system. This system is composed of twelve transducers at 3.5 kHz (type TR75A) installed within the sonar dome beneath the bow bottom, a transceiver (PTR105A), a correlation echo sounder processor (CESP II) and an universal graphic recorder (UGR 196C). The reflected signals were recorded on the graphic recorder at a two second sweep rate. The survey covered, topographically, the Japan Triple Junction area, the Takuyo No. 2 Seamount, the Zenisu Ridge, the Muroto Trough and the Nankai Trough. In particular at the Japan Triple Junction region, a detailed grid survey was done for 26 hours to study the morphology and structure of so-called Mogi Fan within the Izu-Bonin Trench. The records have shown that the trench fan (Mogi Fan) at the triple junction deformed due to the subduction of the Pacific Plate (Fig. 1). Turbidites are well-developed at the Muroto basin (Fig. 2), and other flat plain area. Sliding and slumping deposits were found at trench slope and lower slope of the seamounts. Rock-fall deposits showing irregular hyperbolae imposed each other on high resolution (3.5 kHz) reflection echogram developed at the rugged seamount and submarine canyon wall.

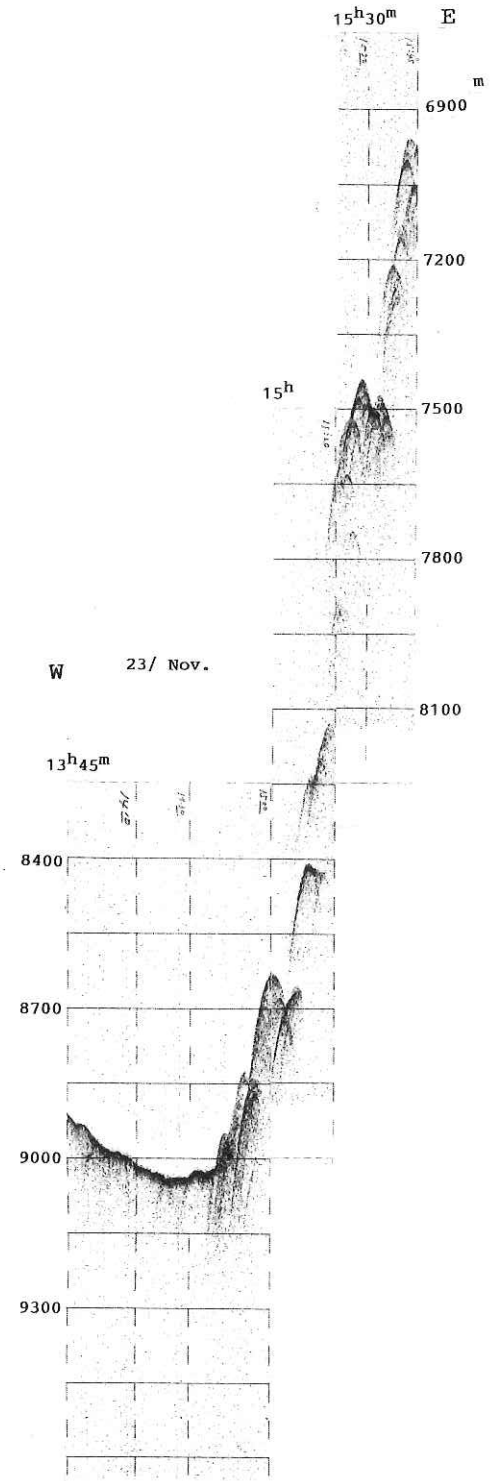

Fig. 1 Trench fan and depormation front in near the center of the trench floor of the Mogi Fan.

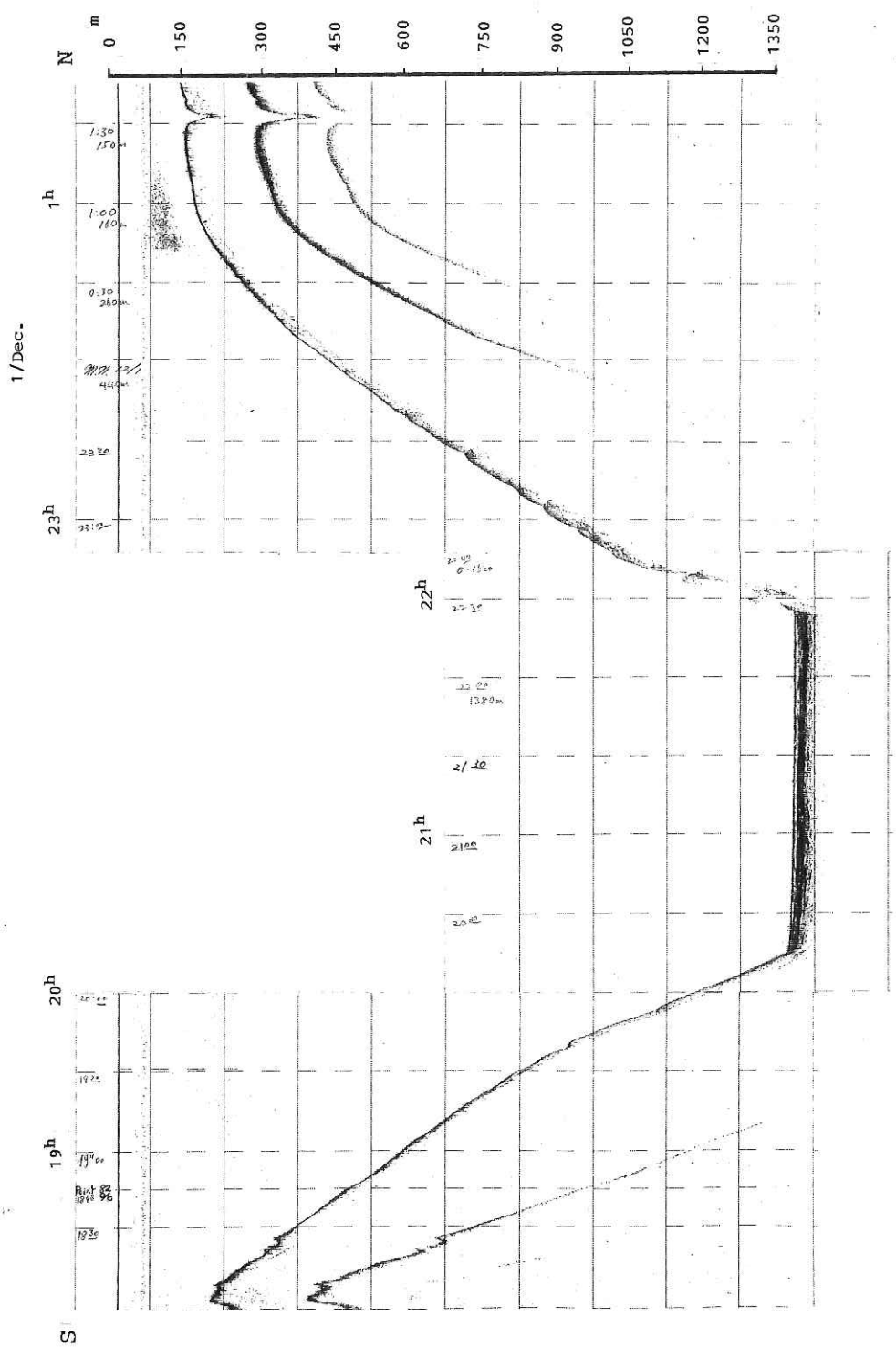

Fig. 2 Well developed turbidites from the Muroto basin.

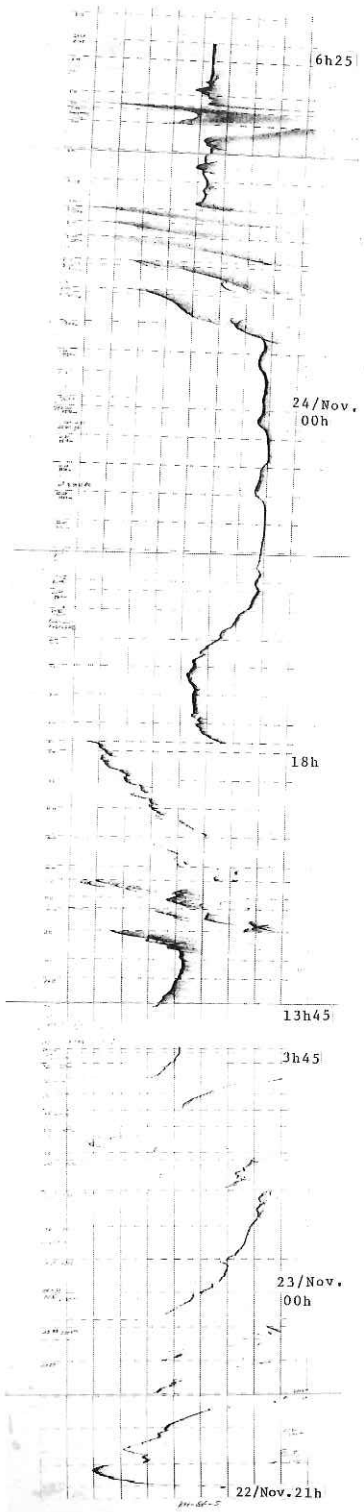

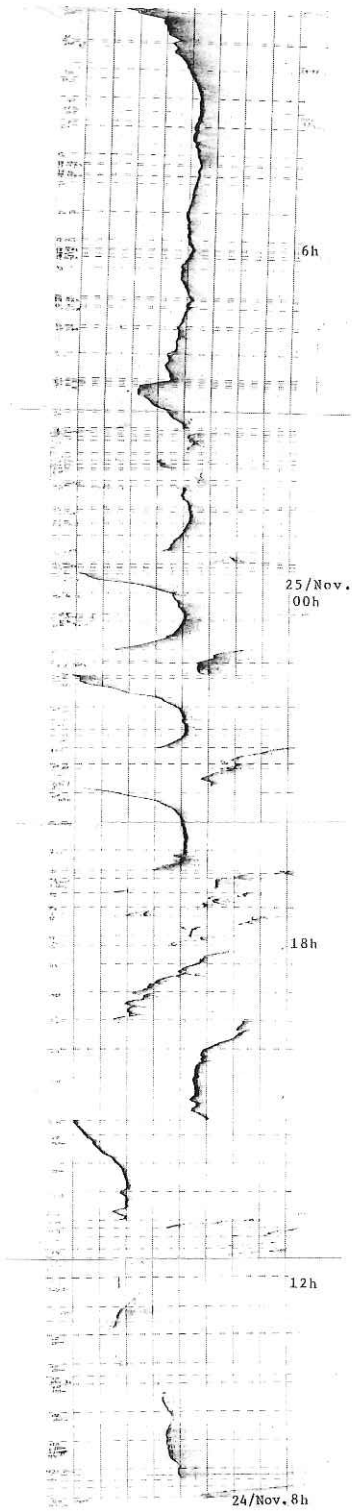

Appendex I 3.5kHz subbottom profiles through all the cruise.

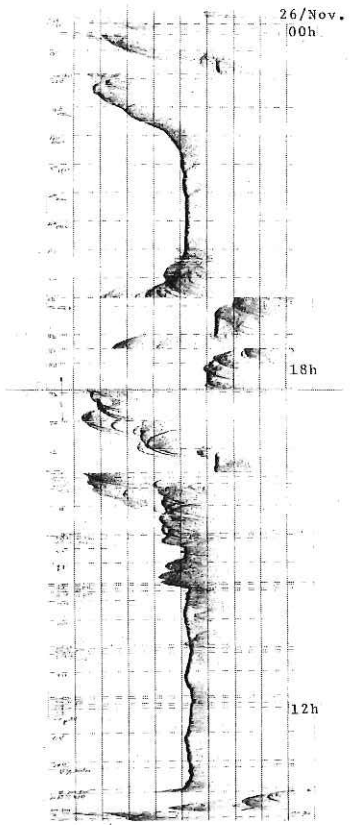
26/Nov.
00h
18h
12h

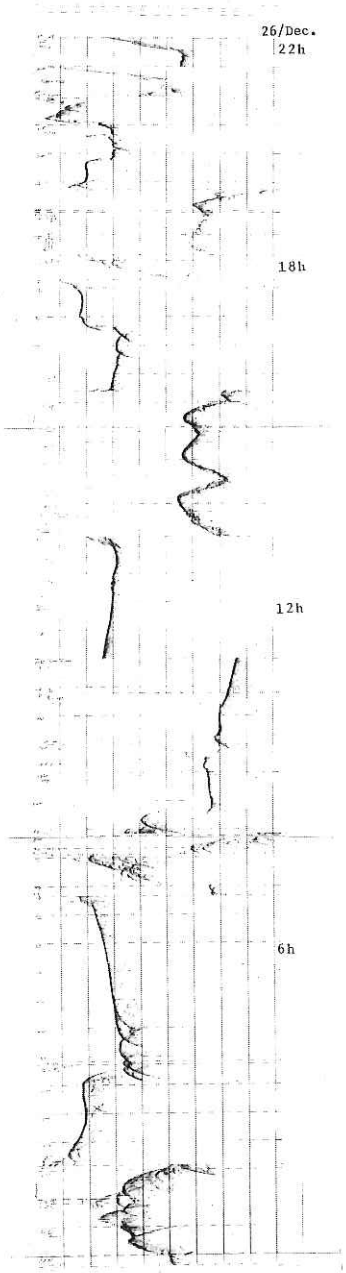
26/Dec.
22h
18h
12h
6h

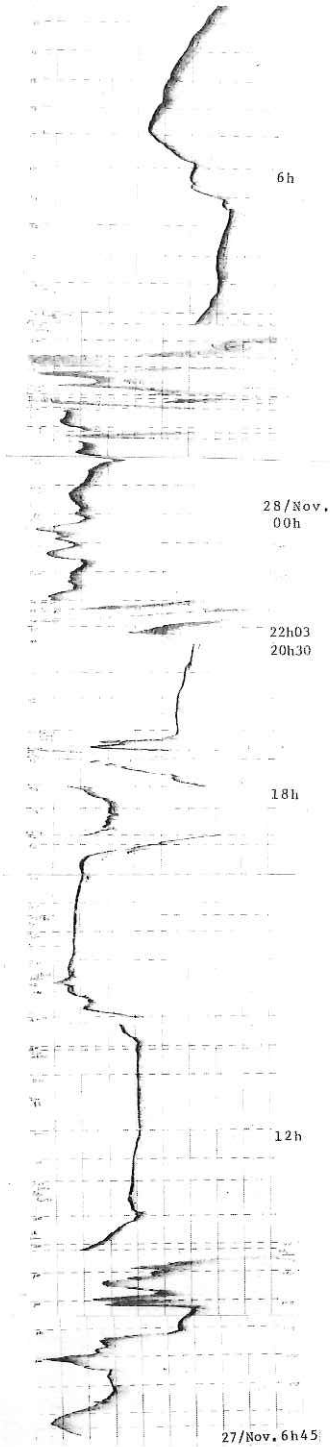
6h
28/Nov.
00h
22h03
20h30
18h
12h
27/Nov. 6h45

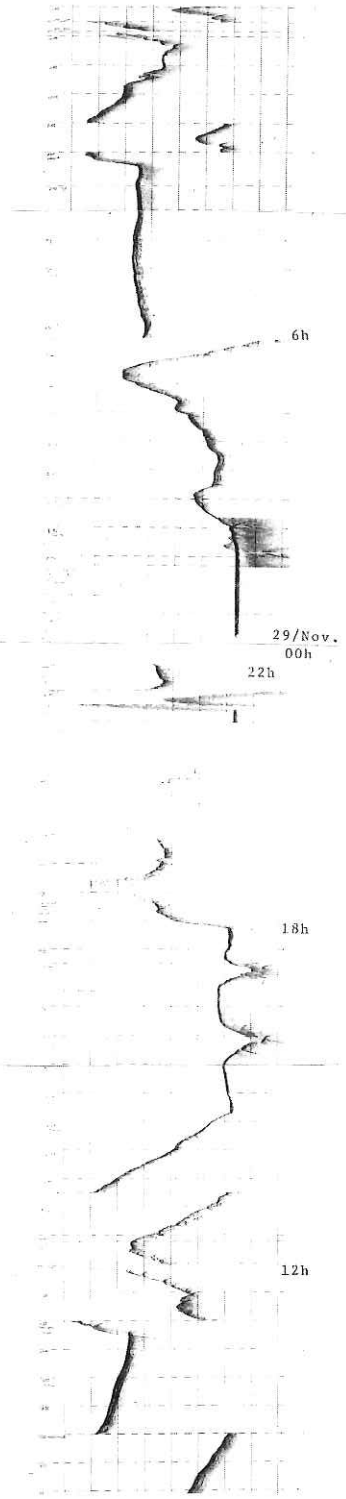
6h
29/Nov.
00h
22h
18h
12h

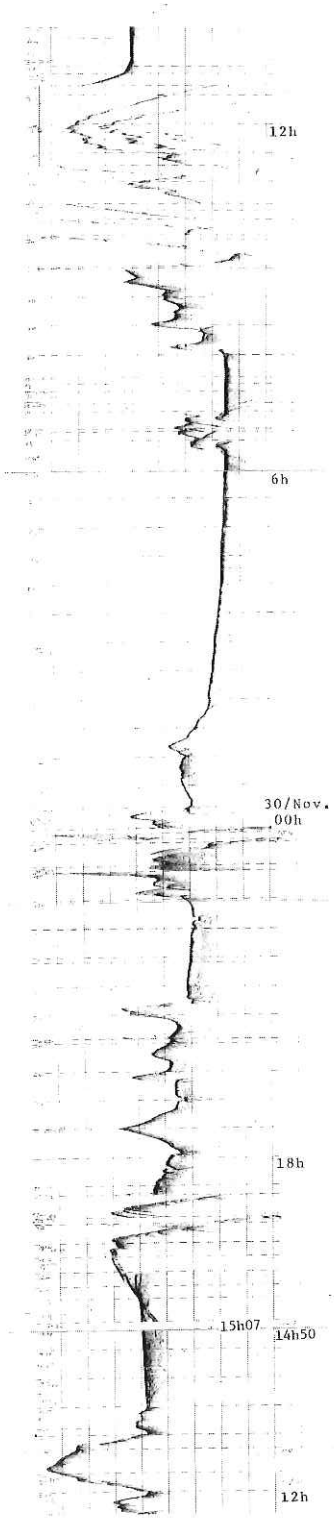
12h
6h
30/Nov.
00h
18h
15h07
14h50
12h

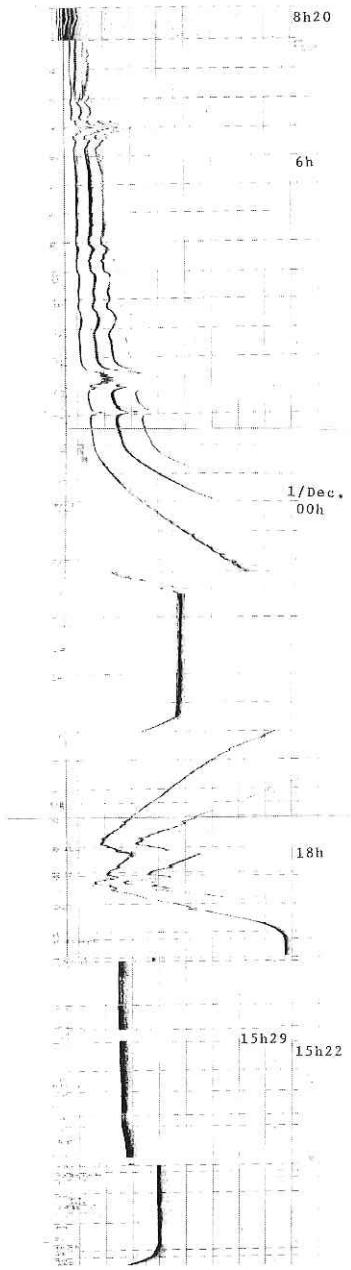
8h20
6h
1/Dec.
00h
18h
15h29
15h22

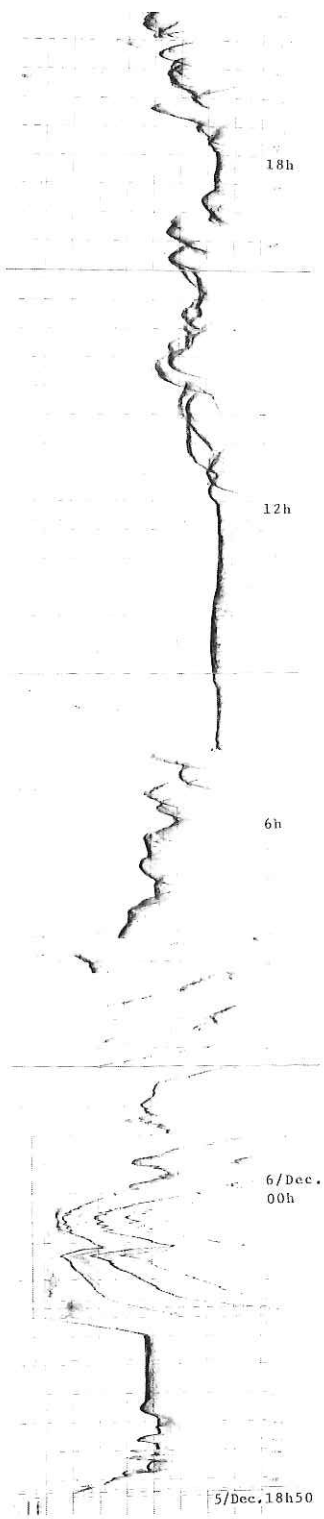
18h
12h
6h
6/Dec.
00h
5/Dec.18h50

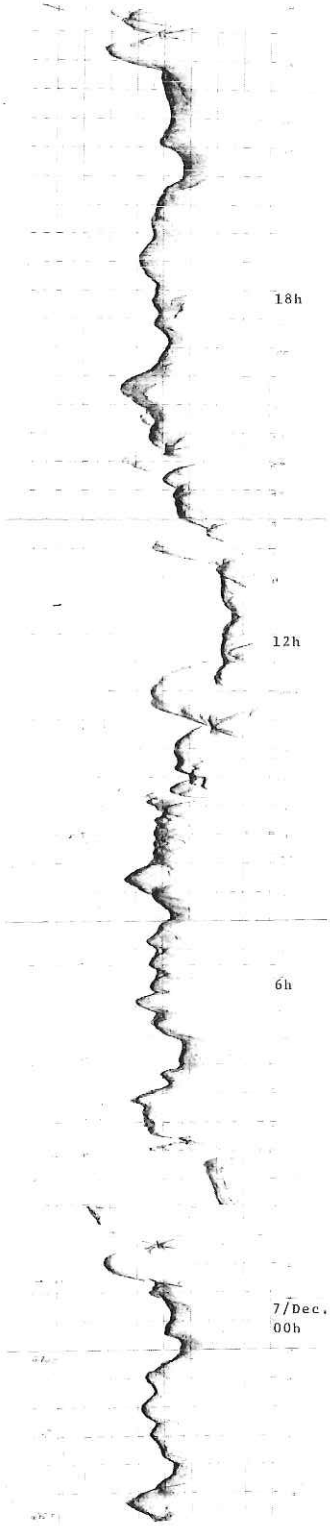
18h
12h
6h
7/Dec.
00h

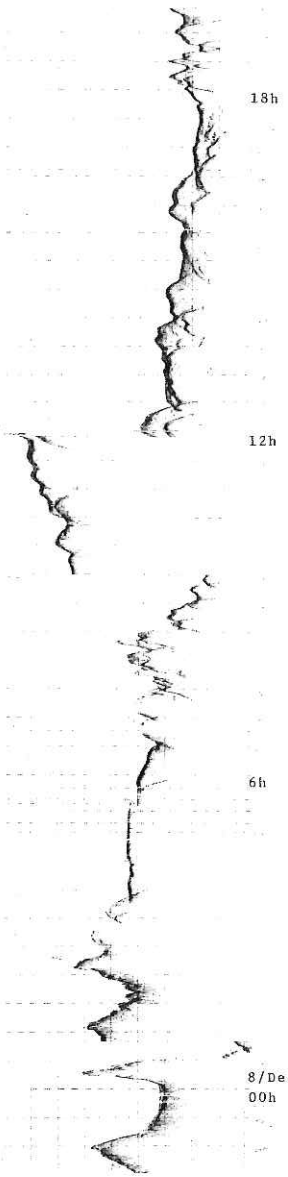
18h
12h
6h
8/Dec.
00h

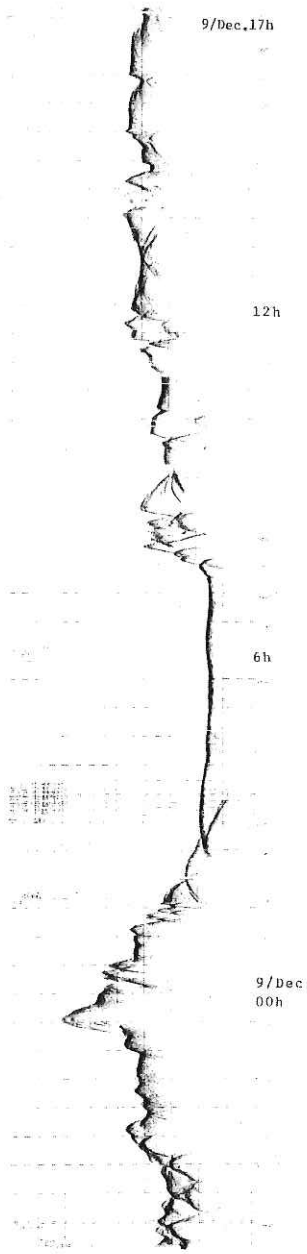
9/Dec.17h
12h
6h
9/Dec.
00h

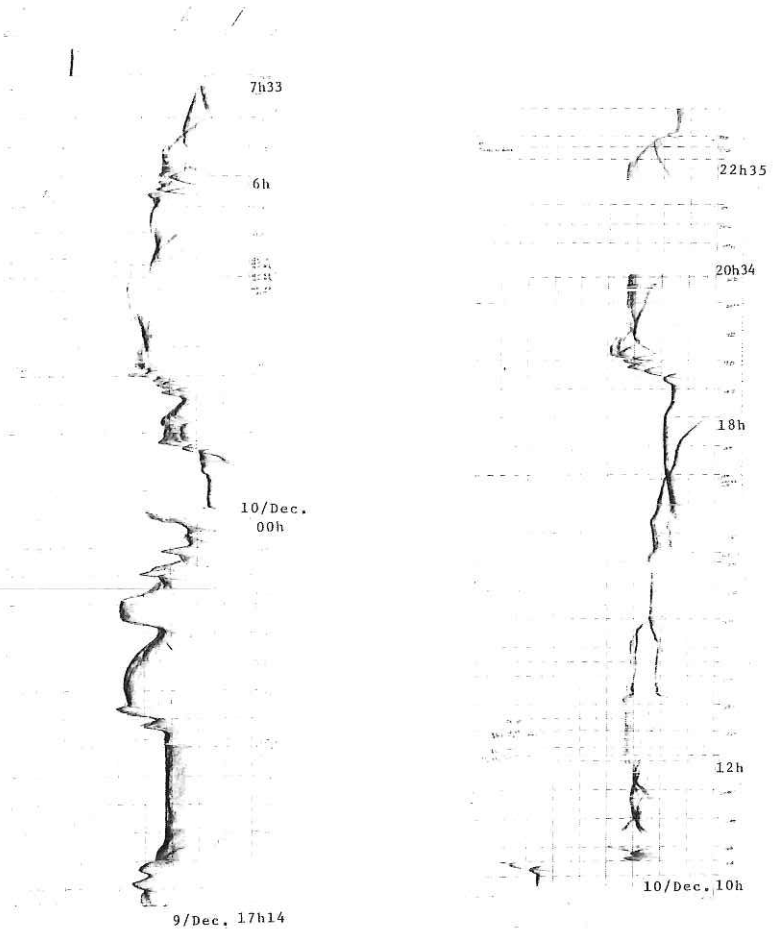
7h33
6h
10/Dec.
00h
9/Dec. 17h14
22h35
20h34
18h
12h
10/Dec. 10h

AIRGUN-OBSH REFRACTION STUDY IN THE NANKAI TROUGH

H. KINOSHITA
Department of EarthSciences, Chiba University, Yayoi, Chiba 260
A. NISHIZAWA
Observation Center for Earthquake Prediction, Tohoku University, Sendai,980
N. MATSUDA and T. ASANUMA
Department of Earth Sciences, Chiba University, Yayoi, Chiba,260

During 6th-9th December, 1986, a seismic refraction experiment was carried out in the Nankai Trough. Five OBSH's were developed almost every 15 km, along 4,300 m depth contour line nearly parallel to the trough axis. Detailed position of OBSH's are listed in Table 1.

The ORI (Ocean Research Institute, University of Tokyo) airgun (Bolt type 1,500c, 12 liter, 100 atm) was used as a seismic source along the main profile (Fig. 1) for determination of detailed crustal structure. The length of the track line was 90 km and along which 1,035 shots were fired every 40 sec for about 12 hours. Location of ship while towing the airgun are listed in Table 2.

Of five OBSH's, three were developed at Chiba University (P1, P2 and P3) and others belonged to Geophysical Institute, University of Tokyo (P4 and P5). All of the OBSH's are pop-up type equipped with an acoustic release system and Chiba type OBSH has also a timed release device for back up. Each OBSH carries three geophones (one vertical component and two horizontal components with 4.5 Hz natural frequency) and a hydrophone. The signals from these sensors were amplified and recorded on an 8-channel direct analog recorder. The gains of recorded signals are listed in Table 3. Chiba type OBSH's had devices for determining directions of horizontal geophones st the seafloor developed by A. Nishizawa.

All OBSH's were successfully recovered and the quality of recorded data were found almost good, although the data had a less signal-to-noise ratio. All the analog data were converted to digital data to produce record sections.

For example, the record section of vertical component from P2 is presented in Fig. 2. Arrivals from layers can be traced in this record section. The wavespeeds of layers are estimated by use of 2D ray tracing method which gives layers of 2.00-2.05 km/s, 2.55-2.70 km/s, 4.6-4.9 km/s and 6.3-6.6 km/s. However, it is noted that arrivals from the

layers with wavespeeds of 2.0-2.05 km/s and 4.6-4.9 km/s are less clear than those of 2.55-2.7 km/s and 6.3-6.6 km/s layers.

Multi-channel seismic (MCS) reflection data along the same track obtained in this cruise are shown in Fig. 13 of Nishiyama et al.(this cruise report). In comparison with the MCS structure feature, the layers from refraction data, 2.0-2.05 km/s. 2.55-2.7 km/s and 4.6-4.9 km/s correspond to the layers which appear between reflection interfaces, with the 2-way travel time of 5.8s-6.2s, 6.2s-7.7s and 7.7s- at the shot point 4,000 close to P2 of our refraction study. The travel time calculated from wavespeeds and thickness of layers beneath P2 almost coincides with one of the reflections.

A preliminary model of the crustal structure obtained from P2 and P3 is shown in Fig. 3.

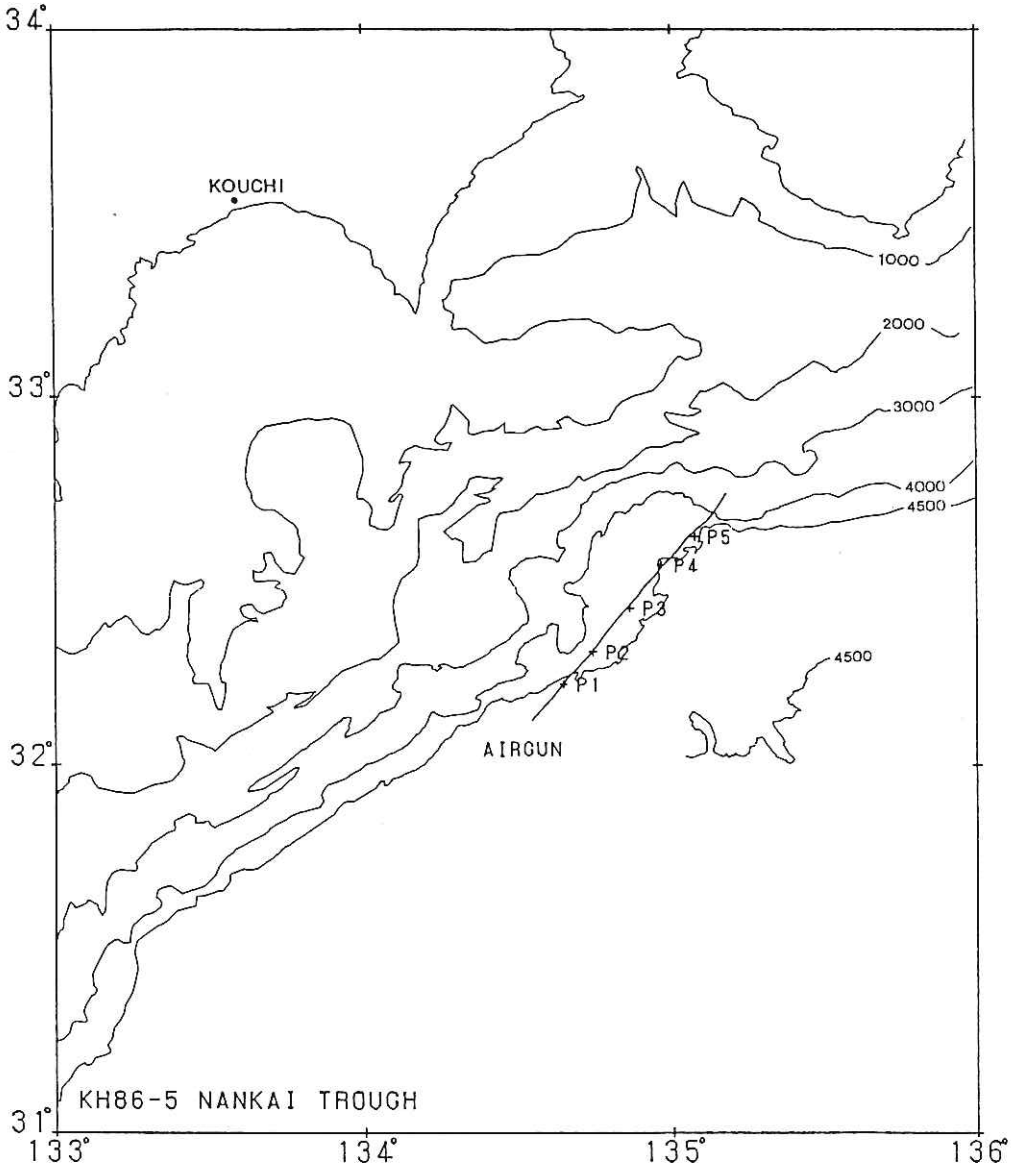

Fig. 1 Bathymetry map of the Nankai trough. The airgun profile is shown. The lenght of profile is about 90km. Cross marks indicate the OBSH location.

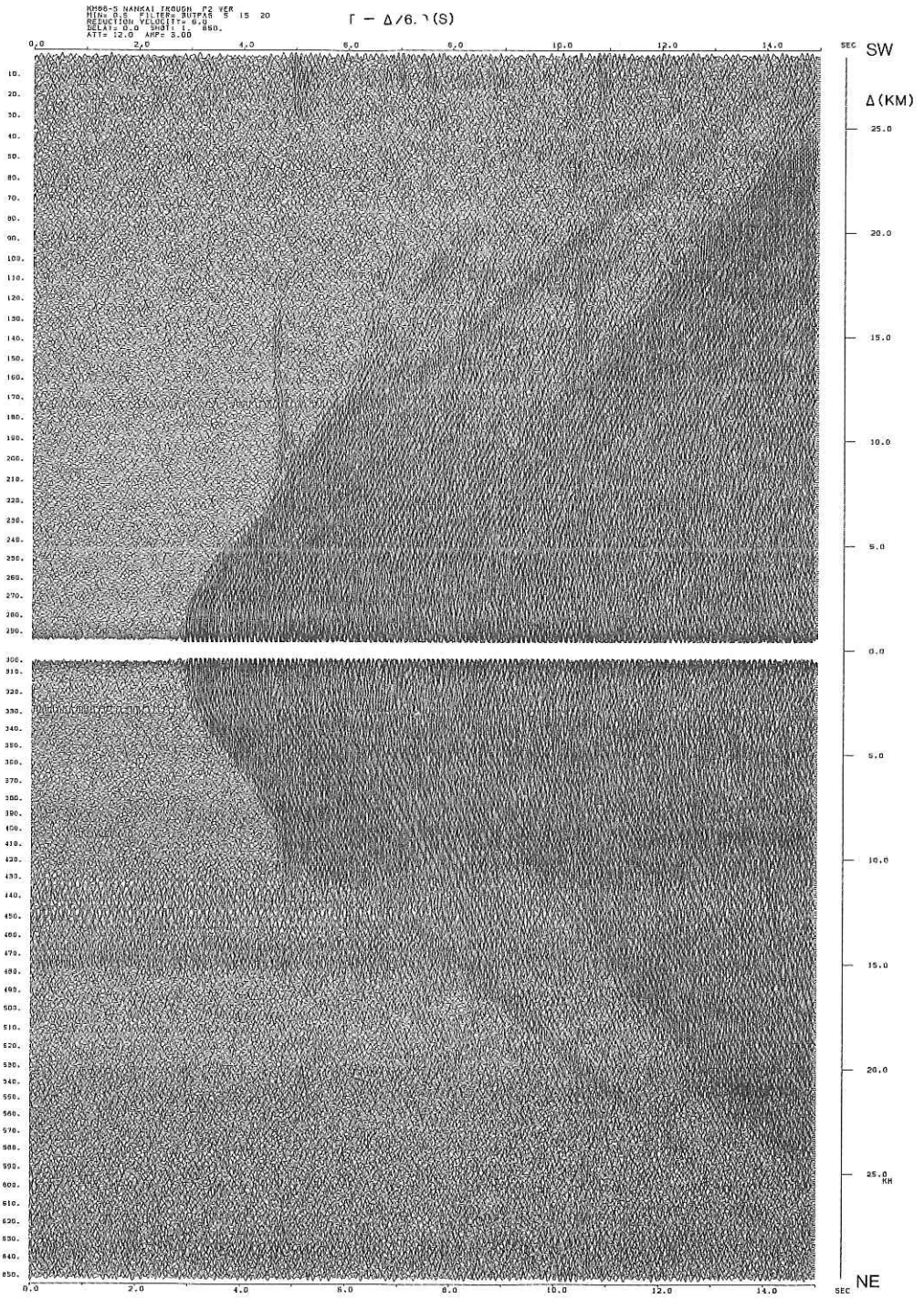

Fig. 2 A record section of vertical component from P2. The reduction velocity is 6.0km/s.

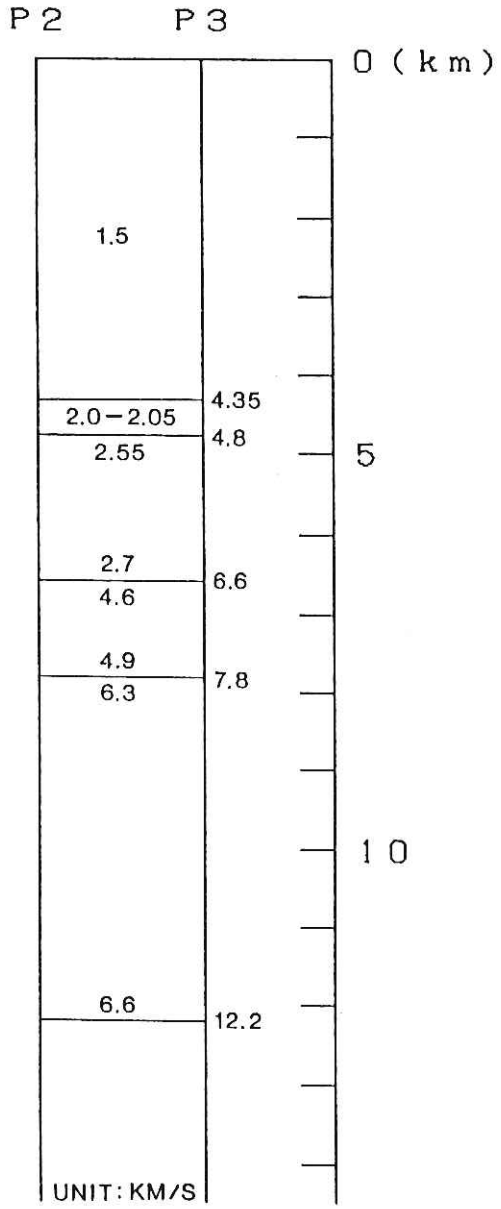

Fig. 3 Preliminary velocity model obtained from P2 and P3.

Table 1. KH86-5 NANKAI TROUGH OBSH POSITION

No.	LAT.	LONG.	DEPTH(m)	DEPLOYMENT	RETLIEVAL
P1	32° 13.30'	134° 38.70'	4500	12-07 09:49	12-09 11:00
P2	32° 18.53'	134° 44.50'	4370	12-07 08:31	12-09 13:46
P3	32° 25.64'	134° 51.74'	4350	12-07 06:16	12-09 17:22
P4	32° 32.65'	134° 57.82'	4510	12-07 04:38	12-09 20:07
P5	32° 37.25'	135° 04.39'	4310	12-07 03:33	12-09 22:46

Table 2. KH86-5 NANKAI TROUGH AIRGUN PROFILE
(START 12-07 12:31:05 END 12-08 00:00:25)

TIME	LAT.	LONG.
12-07 12:33	32° 07.4'	134° 32.7'
13:00	32° 09.0'	134° 34.4'
13:30	32° 10.8'	134° 36.3'
13:40	32° 11.4'	134° 36.9'
14:00	32° 12.6'	134° 38.0'
14:15	32° 13.6'	134° 38.9'
14:25	32° 14.2'	134° 39.4'
14:30	32° 14.5'	134° 39.7'
15:00	32° 16.3'	134° 41.7'
15:15	32° 16.5'	134° 42.0'
15:30	32° 17.9'	134° 43.6'
16:00	32° 19.6'	134° 45.3'
16:30	32° 21.4'	134° 46.8'
16:40	32° 21.9'	134° 47.3'
17:00	32° 22.8'	134° 48.3'
17:30	32° 24.4'	134° 49.8'
18:00	32° 26.0'	134° 51.5'
18:30	32° 27.6'	134° 53.3'
19:00	32° 29.2'	134° 54.6'
19:30	32° 30.7'	134° 56.4'
20:00	32° 32.4'	134° 58.0'
20:30	32° 33.8'	134° 59.8'
21:00	32° 35.4'	135° 01.4'
21:30	32° 36.9'	135° 02.8'
22:00	32° 38.4'	135° 04.7'
22:30	32° 39.8'	135° 06.8'
23:00	32° 41.2'	135° 08.3'
23:30	32° 43.0'	135° 09.6'
12-08 00:00	32° 44.3'	135° 10.6'

Table 3. THE GAINS OF RECORDED SIGNALS

	CHANNEL	COMPONENT	GAIN
Recorder1	1ch	Horizontal1	66dB
	2ch	Time code	----
	3ch	Vertical	62dB
	4ch	Vertical	90dB
Recorder2	1ch	Horizontal2	66dB
	2ch	Time code	----
	3ch	Hydorophone	60dB
	4ch	* Hydorophone	66dB

* Hydorophone signal(Rec.2. 4ch) are recorded after rectification and filtering for high frequency signal(50-250Hz).

HEAT FLOW --BASIC DATA--

M. KINOSHITA
Earthquake Research Institute, University of Tokyo, Bunkyo, Tokyo 113
Y. KASUMI
Department of Earth Sciences, Chiba University, Yayoi, Chiba 260

Heat flow measurements were made in the Nankai Trough area during the KH86-5 cruise. The measurement areas were concentrated on two points; near the trough axis off Cape Muroto and the easternmost part of the trough.

METHODS OF MEASUREMENT

A surface heat flow value is usually determined as the product of the temperature gradient and thermal conductivity.

We used three types of ordinary geothermal probe for the measurements of the temperature gradient. One is the Ewing type probe which has been in use in ERI since 1983 (Yamano, 1985; Fig. 1-a and 1-b). It has six sensors (thermisters) outriggered at regular intervals, and has two version as:

A) Heavy weight (450 kg) and lance of 4.5 m long,
B) Light weight (200 kg) and lance of 3.0 m long.

The lance is made of a strong steel rod, which allows multiple penetrations into the sediment. This drastically improved the efficiency of the data collection and enabled closely spaced measurements. The data is logged in a digital form and recorded in a cassette tape every 30 seconds for each sensor, and at the same time these logged data are telemetered to the ship with 12 kHz acousitic pulses. The logged data and telemetered signal also includes the information about the instrument tilt, by which, together with temperature information, we can know if the probe penetrates vertically or not, and it is possible to try again soon when the penetration is unsuccessful.

Another is also the Ewing type probe which was developed at the Chiba University (Nagihara et al., 1986; Fig. 1-c). The instrument weights about 200 kg and the lance is 4 m long. It has six sensors and enables to measure the thermal conductivity in situ, which unfortunately did not work well in this cruise.

The last one is the Bullard type probe. It is about 3 m long and seven sensors are installed (Fig. 1-d). As is recognized from the shape of the probe, it is easier to penetrate than the Ewing type, but it usually bends when pulled out from the mud and therefore does not allow multiple penetrations.

The measurement of the temperature in the sediment is performed as follows. First, at about 30 m above the seafloor, the probe stand still for five minutes in order to measure the seawater temperature, which is used as the reference. After that we lower the probe quickly into the mud and wait for about ten to fifteen minutes for the sensors to equilibrate to the temperature of the sediment around, because they are frictionally heated when penetrating. The temperature gradient is determined by the seawater temperature versus depth for each sensor to a straight line.

Furthermore, in case of oblique penetration that is known from the record, we can make a tilt correction following the tilt angle, which is divided into three categories; almost vertical (0°-7°), 7°-40° and more than 40°. For the data of more than 7° tilt we made the correction and results were given in parentheses.

The thermal conductivity was measured by the needle probe method (von Herzen and Maxwell, 1959) of the core samples taken by the piston corer. The measured values were corrected for the in-situ pressure and temperature conditions, following Ratcliffe (1960).

THE DATA

All the results are listed in Table 1.

Temperature gradients were measured at twelve stations (HF1-HF12) off Cape Muroto, while at five stations (HF13-17) in the easternmost part of the Nankai Trough, which is shown in Figs. 2 and 3. The obtained temperature versus depth profiles are presented in Fig. 4.

HF1 : The (B) type was used. Stations HF1 and HF3 were located in the imbricated thrust zone (Kagami, 1986) on the landward slope. For HF1A the probe penetrated though tilted, whereas for HF1B it fell completely. Because of a strong wind the wire angle was as large as 30° and we could not catch any acoustic signal that made the operation dufficult.

HF2 : The (B) type was lowered. It was located on the trough floor slightly seaward of the deformation front. None of five trials resulted in vertical penetrations, however, the corrected values are in good agreement with each other.

HF3 : The (B) type was used. One of two trials were successful. This was located in the close vicinity of the previous heat flow station (Yamano. 1986), and the obtained value (109 mW/m^2) is consistent with this former value (93 mW/m^2) within the error.

At HF4 to HF7, measurements were made usingh (A) type probe, and all these measurements were made without raising up the instrument fully; e.g. after finishing measurements at one station the probe was raised up by about 2,000 m from the bottom while running the ship to the next station, and it was again lowered at the next station. This method greatly increased the efficiency of the measurement. Station HF4 to HF7 were located from the northwest (landward side) to the southeast (seaward) on the deformation front.

HF4 : One trial was successful, and the other three results were in good agreement with the successful one.

HF5 : Probably due to the hard bottom, the probe tilted and only the minimum estimates were obtained. At HF5C the negative temperature gradient was obtained, though the temperature change for each sensor was small.

HF6 : Although none of four trials ended in a success, corrected values are in agreement with each other.

HF7 : One of two trials was successful. The obtained value was slightly higher than at HF4.

HF8 : It was located on the trough floor. The probe penetrated fully, and the obtained heat flow value (160 mW/m^2) was a little higher as compared with the previous values on the trough.

HF9 : The (B) type was lowered. It was also on the trough floor and much closer to the deformation front. None of five were successful and temperature profiles were not linear.

HF10, HF11 : The (B) type was used. Both were in the upper part of the imbricated thrust zone. Because of the coarse sediment no trials were successful.

HF12 : The instrument developed at the Chiba University was used. It was located between the deformation front and the station HF8 on the trough floor. The penetration was tried two times, and one was successful. The obtained temperature versus depth profile was convex upwards, though it was less reliable because only three of six sensors were working. The best fit line of the data gives the heat flow value 113 mW/m^2, which is lower than the Value at HF8.

HF13 : The (B) type was used. It was located at the southern end of the Tenryu Canyon, and the coarse sediment prevented the probe from penetrating at all.

HF14 : The (B) type probe was lowered. This station was located slightly seaward of the main thrust. Five trials were made and none of them was successful.

HF15 : The (B) type was used. We aimed at the ponding structure located just seaward of the main thrust. The probe penetrated fully, and the results indicate that the heat flow is lower than in the western part of the Nankai Trough floor.

HF16 : The (B) types was used. It was located on the landward slope where the east-west trneding channle existed. Probably due to the bad bottom condition, the probe did not penetrate well.

HF17 : The Bullard type probe was used. Its postion was almost the same as HF16. Four of seven sensors were in the mud.

Thermal conductivity measurements were made on three core samples taken by the piston corer (P-6 to P-8, see Figs. 2 and 3). The thermal conductivity versus depth profiles are given in Fig. 5. Other than these results, the thermal conductivity value for the previous heat flow station in the vicinity was also used (Yamano, 1986) on the landward slope of the trough off Cape Muroto.

REFERENCES

von Herzen, R. P. and Maxwell, A. E., 1959, The measurement of thermal conductivity of deep-sea sediments by a needle-probe method, Jour. Geophys. Res., 64, 1557-1566.

Kagami, H., 1986, The accretionary prism of the Nankai Trough off Shikoku, southeastern Japan, In: Initial Rep. DSDP (Whalen, E., ed.), 87, pp.941-953, U. S. Govement Printing Off., Washington, D. C.

Nagihara, S., Suzuki, S., Boh, R. and Kinoshita, H., 1986, Development of a 16-channel heat flow measuring system and its test application on the deep sea floor, Zisin, 39, 277-287. (Japanese with English abstract)

Ratcliffe, E. H., 1960, The thermal conductivities of ocean sediments, Jour. Geophys. Res., 65, 1535-1541.

Yamano, M., Heat flow studies of the Circum-Pacific subduction zones, (Doctor Thesis, University of Tokyo)15-16.

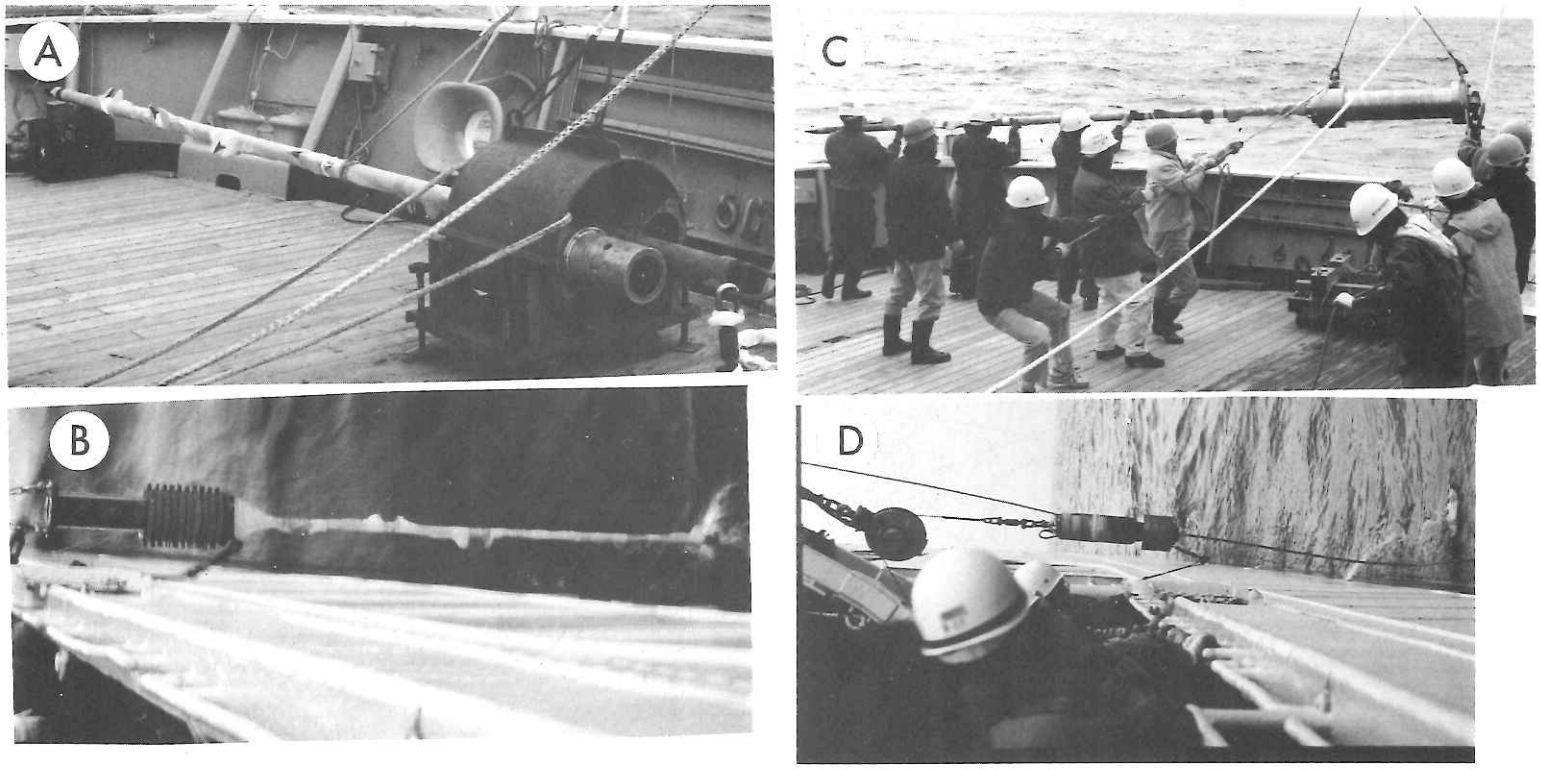

Fig. 1 (a) The Ewing type probe; (A) type (ERI).
(b) The Ewing type probe; (B) type (ERI).
(c) The Ewing type probe (Chiba University).
(d) The Bullard type probe.

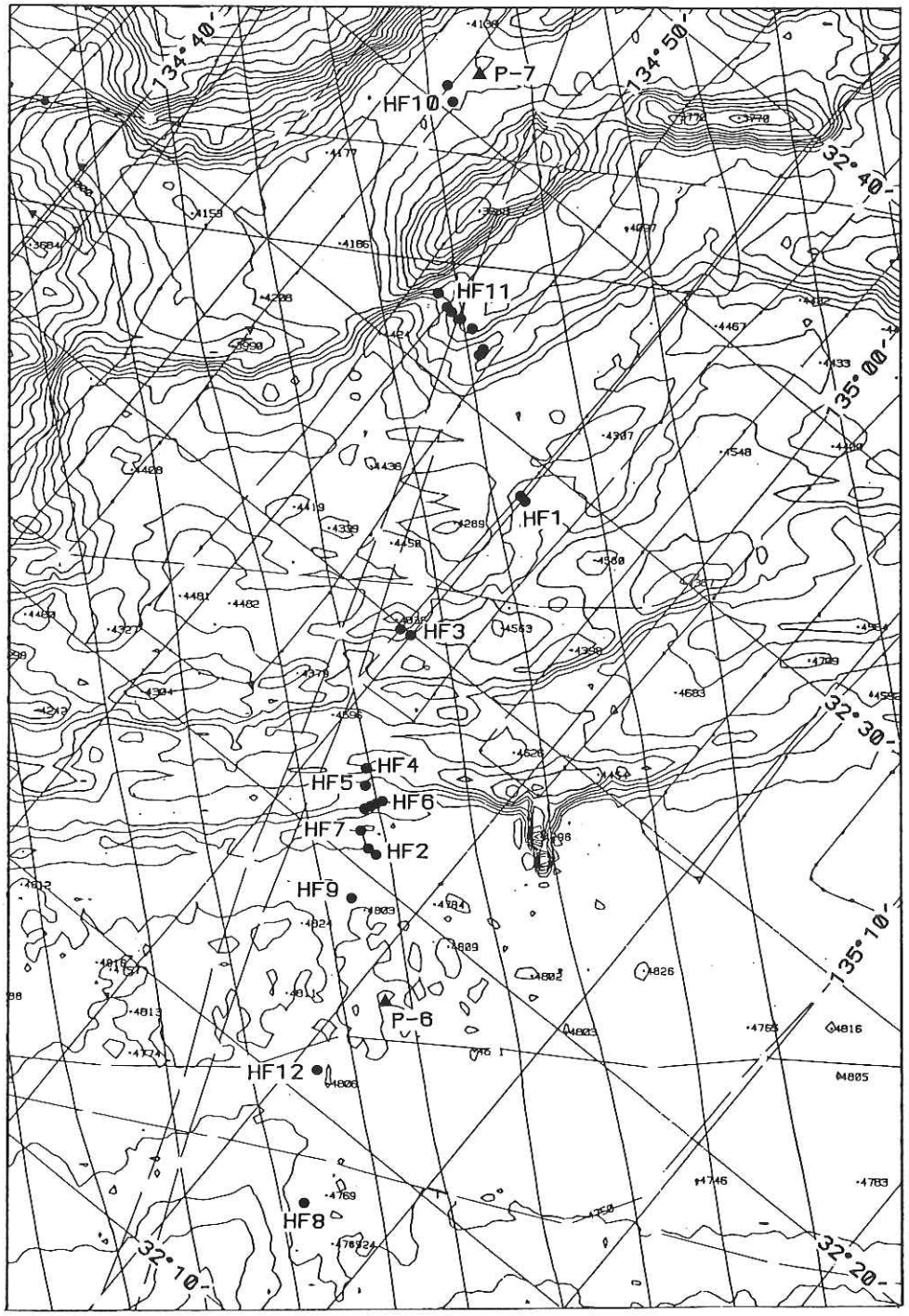

Fig. 2 The heat flow stations in the Nankai Trough area. Solid circles are stations by this study; solid square the previous value; and the solid triangle the sampling station by the piston corer. This is the detailed map for the hatched area in Fig. (1). Thick solid line marked "55-2" is the multichannel seismic line by JAPEX.

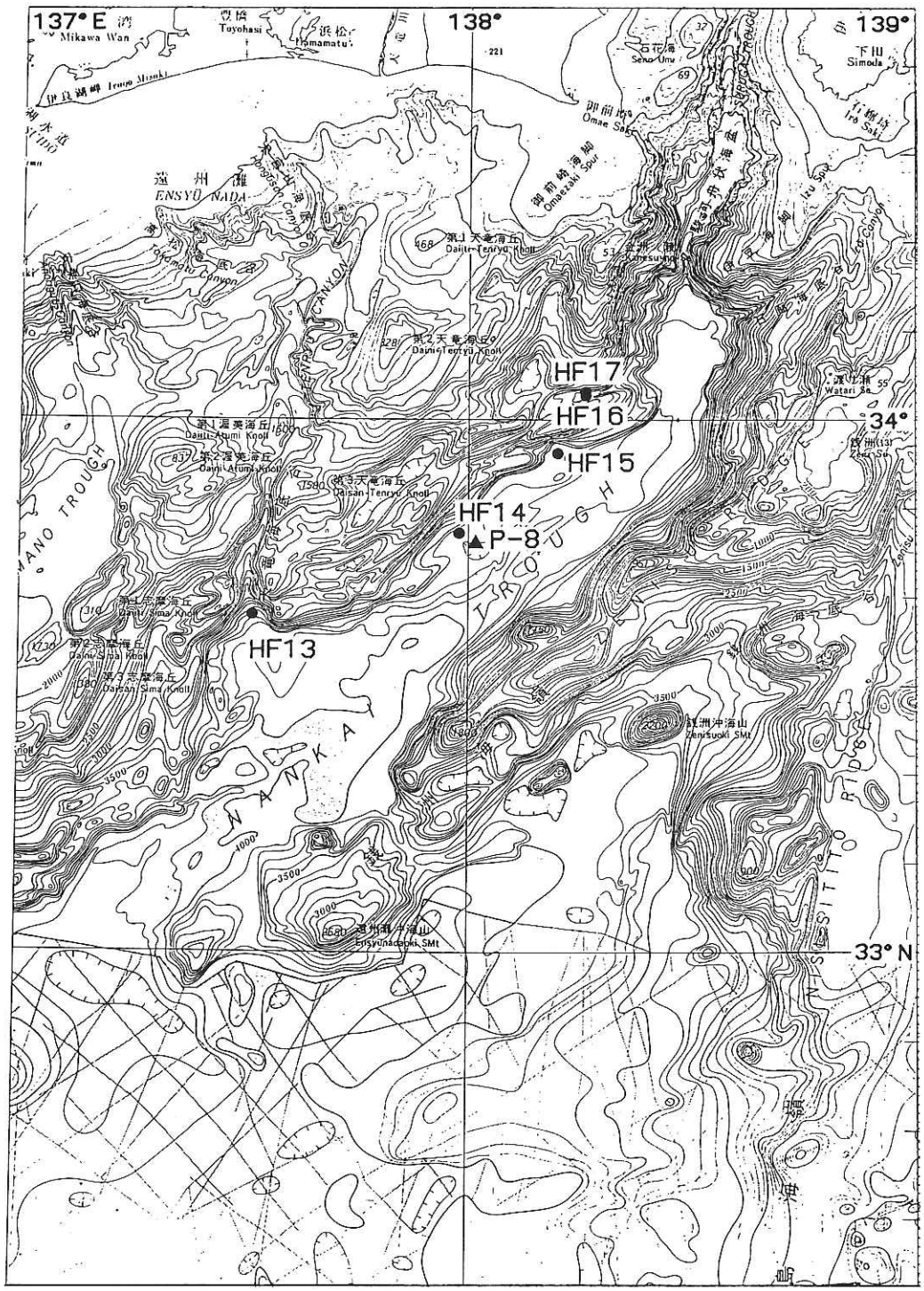

Fig. 3 The heat flow stations in the eastern part of the Nankai Trough. P-8 is the sampling site by the piston corer.

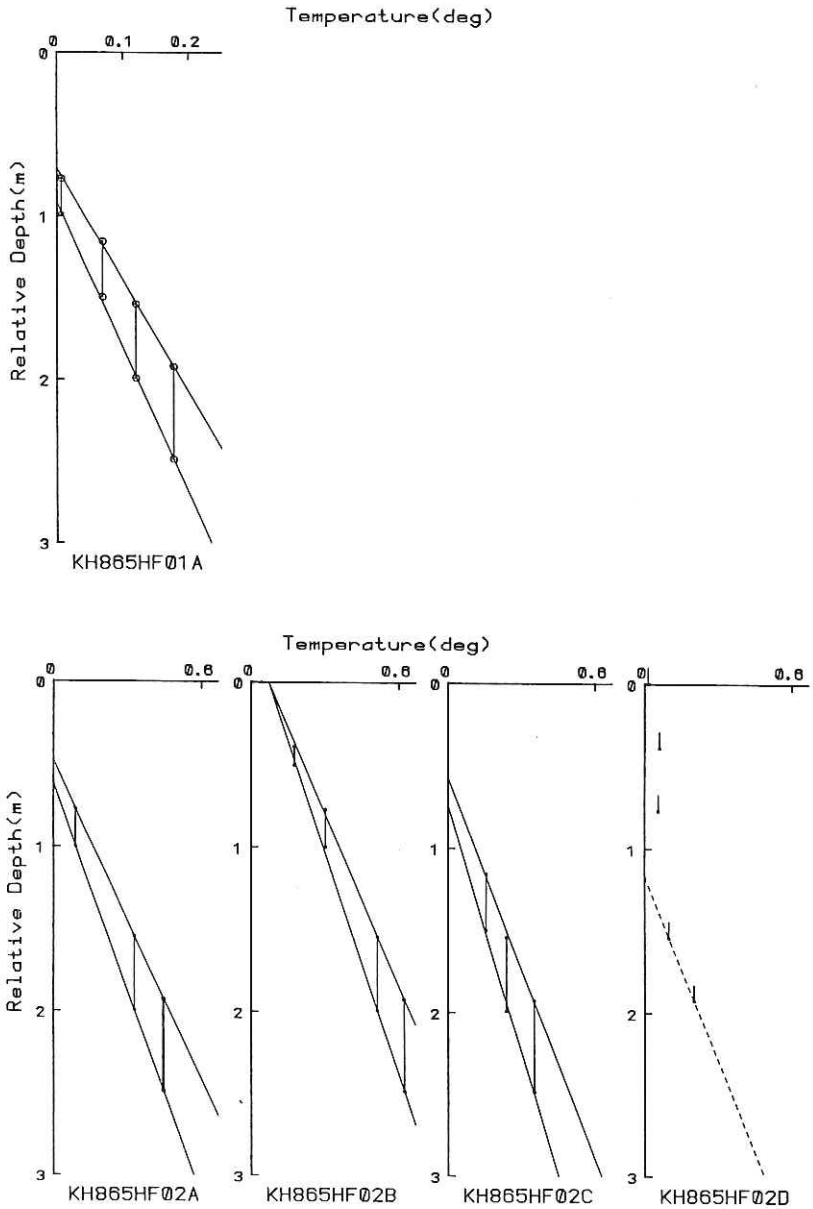

Fig. 4(a-g) Temperature versus depth profiles obtained in the Nankai Trough area. The depth is taken relative to the position of the topmost sensor. Temperature indicates the difference between the equilibrium temperature (Teq) and reference temperature (Tw). Straight lines are the best fit to the straight lines. Solid line means that the result is reliable, while dotted lines indicates that it is less reliable. The cross-marked data is excluded form the estimation of the temperature gradient due to the instability of the sensor. Note that the temperature scale differs for each station. Data that range in depth are the estimation with consideration of the instrument tilt, where the lower value corresponds to the tilt of 7° and upper tilt of 40°. Two lines are the best fit for each case. Data with tips upward correspond to the tilt angle of more than 40°, and therefore the temperature gradient is the minimum estimation.

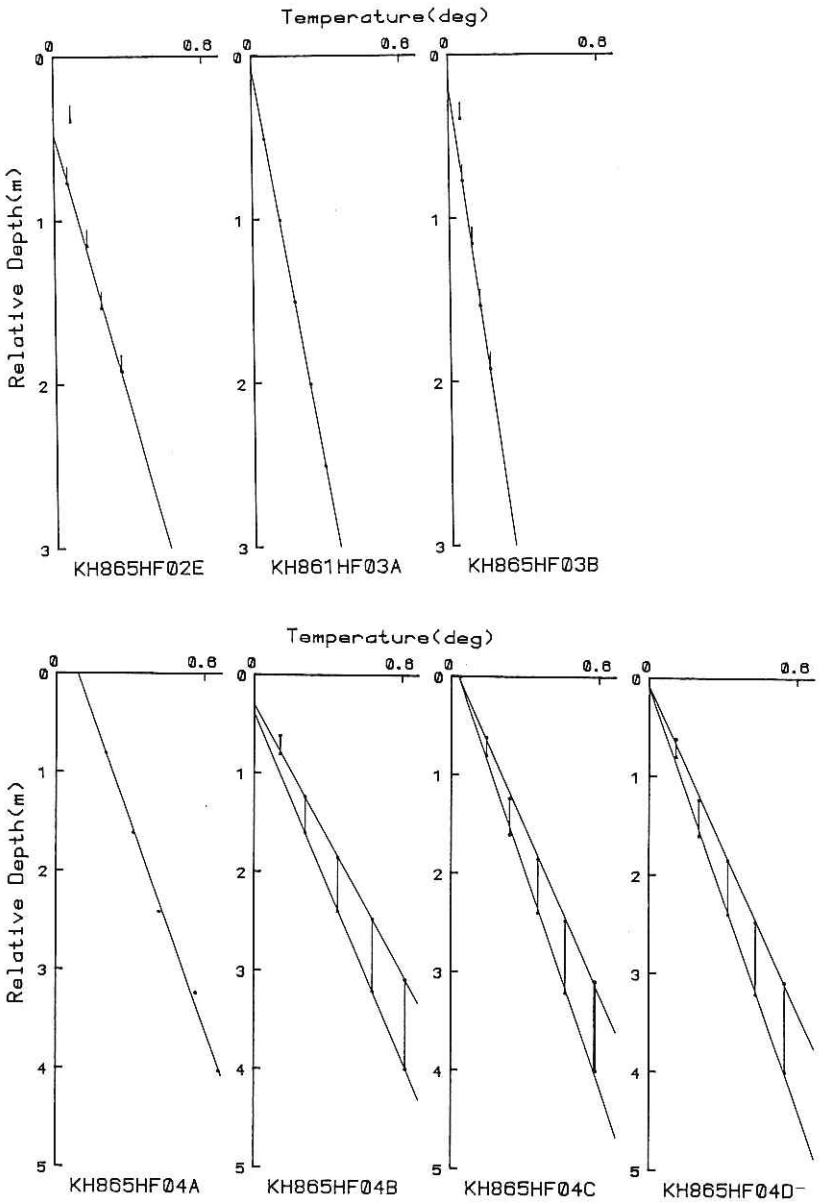
Temperature(deg)
0
0.8
Relative Depth(m)
1
2
3
KH865HF02E
KH861HF03A
KH865HF03B
Temperature(deg)
0
0.8
Relative Depth(m)
1
2
3
4
5
KH865HF04A
KH865HF04B
KH865HF04C
KH865HF04D

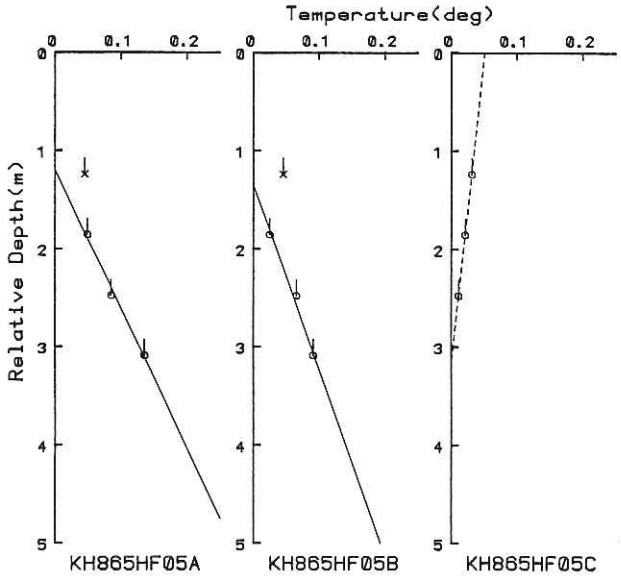
Temperature(deg)
0
0.1
0.2
Relative Depth(m)
0
1
2
3
4
5
KH865HF05A
KH865HF05B
KH865HF05C

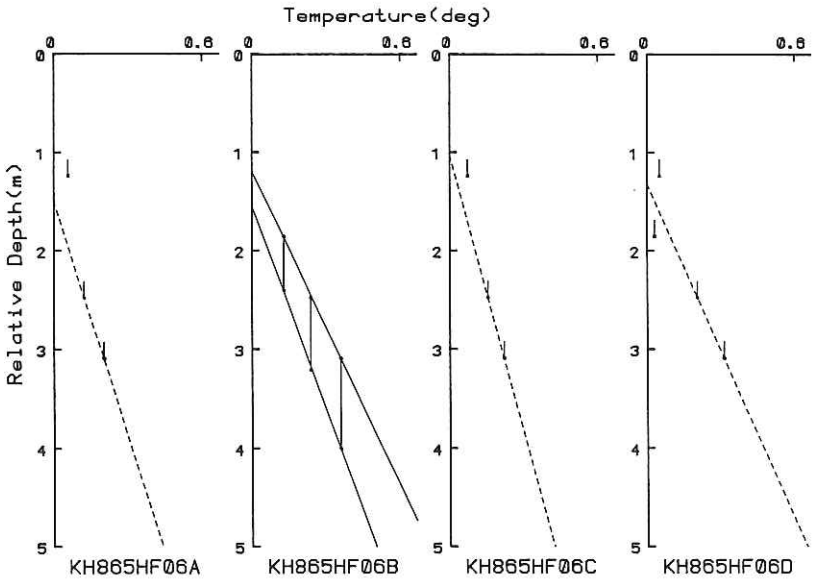
Temperature(deg)
0
0.6
Relative Depth(m)
0
1
2
3
4
5
KH865HF06A
KH865HF06B
KH865HF06C
KH865HF06D

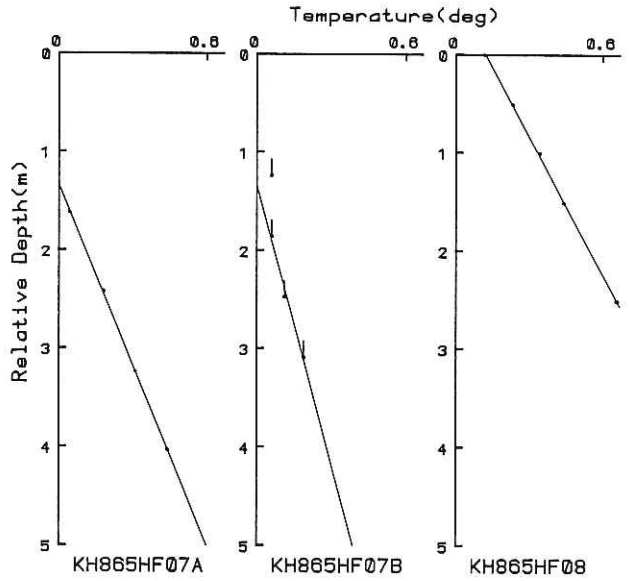
Temperature(deg)
0
0.6
Relative Depth(m)
1
2
3
4
5
KH865HF07A
KH865HF07B
KH865HF08

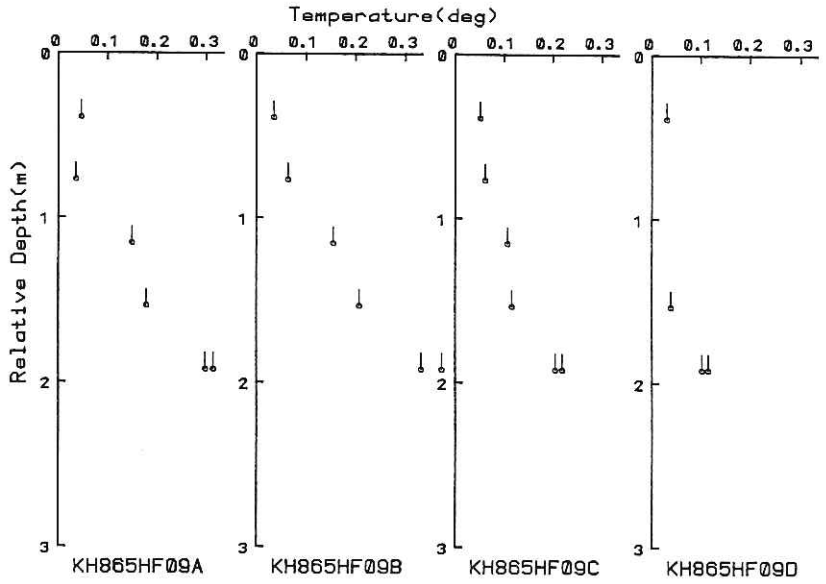
Temperature(deg)
0
0.1
0.2
0.3
Relative Depth(m)
1
2
3
KH865HF09A
KH865HF09B
KH865HF09C
KH865HF09D

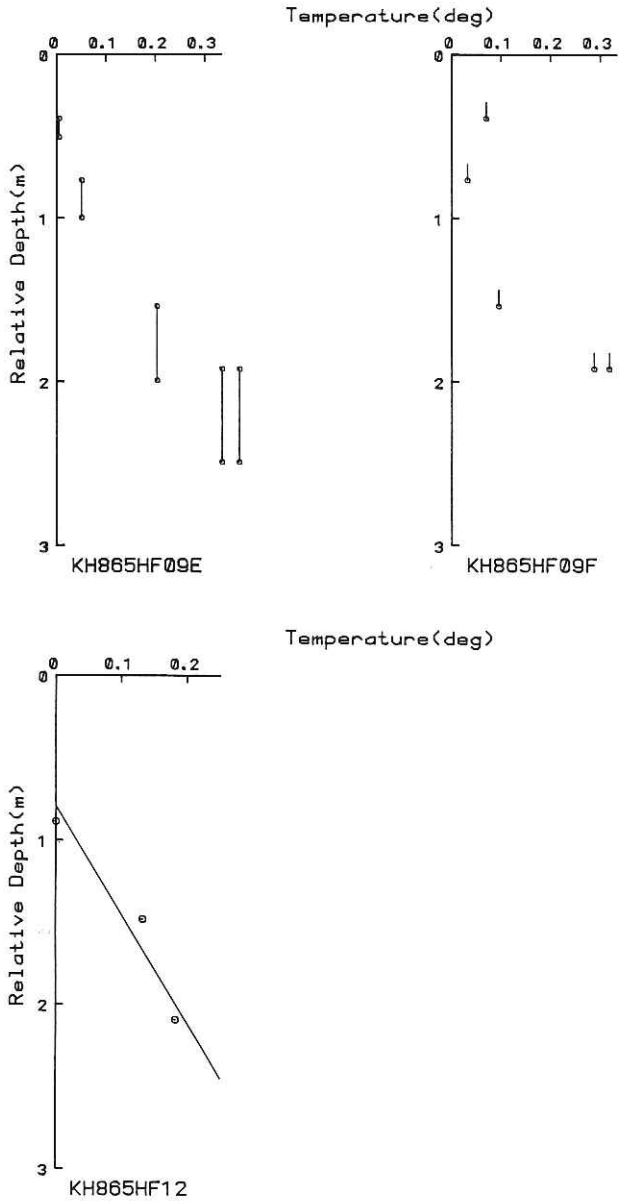
Temperature(deg)
0
0.1
0.2
0.3
Relative Depth(m)
1
2
3
KH865HF09E
KH865HF09F
Temperature(deg)
KH865HF12

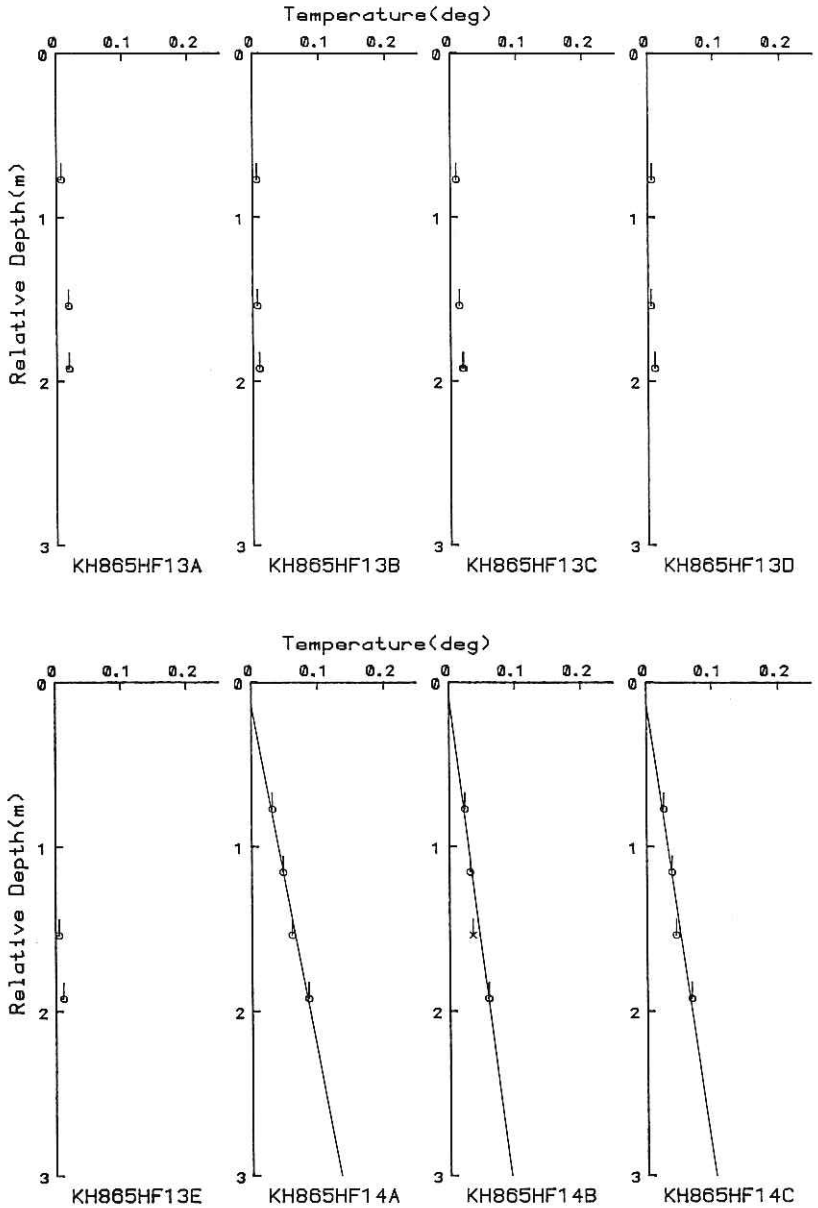
Temperature(deg)
Relative Depth(m)
0
0.1
0.2
1
2
3
KH865HF13A
KH865HF13B
KH865HF13C
KH865HF13D
KH865HF13E
KH865HF14A
KH865HF14B
KH865HF14C

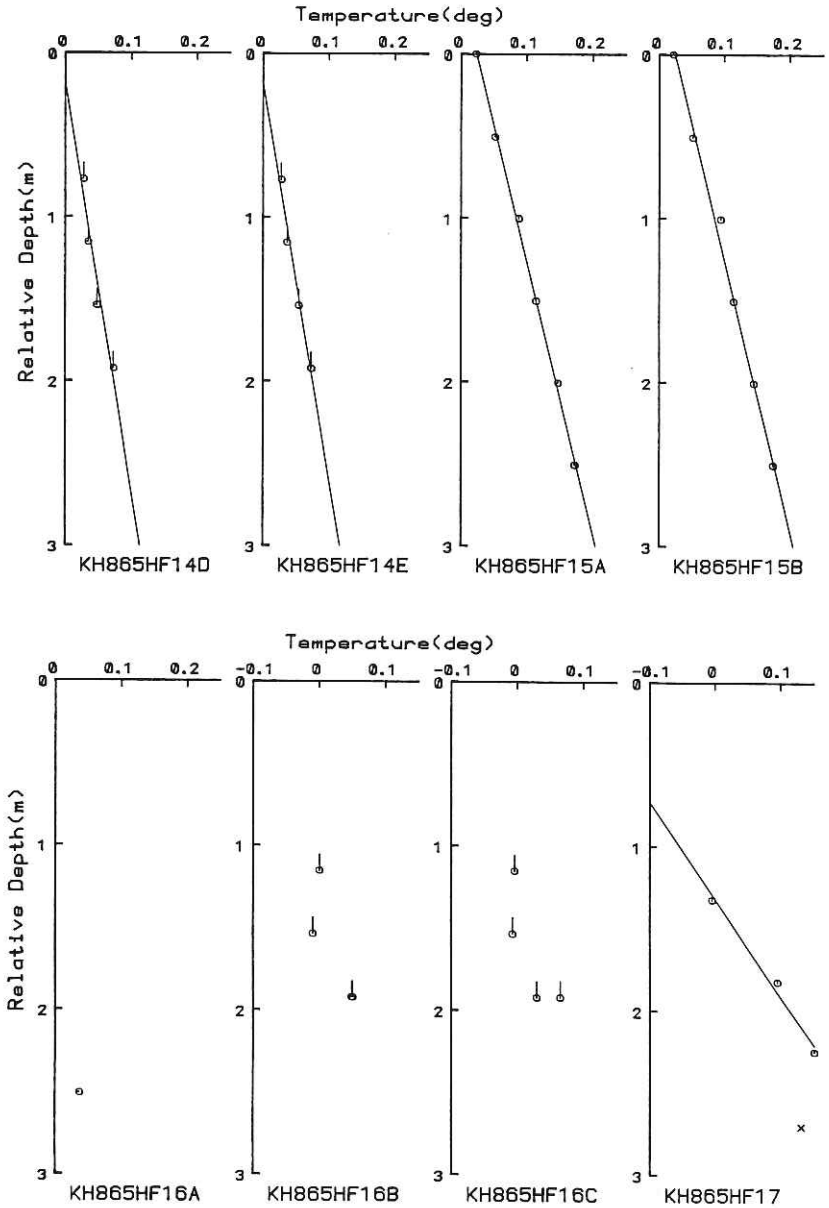
Temperature(deg)
Relative Depth(m)
KH865HF14D
KH865HF14E
KH865HF15A
KH865HF15B
KH865HF16A
KH865HF16B
KH865HF16C
KH865HF17

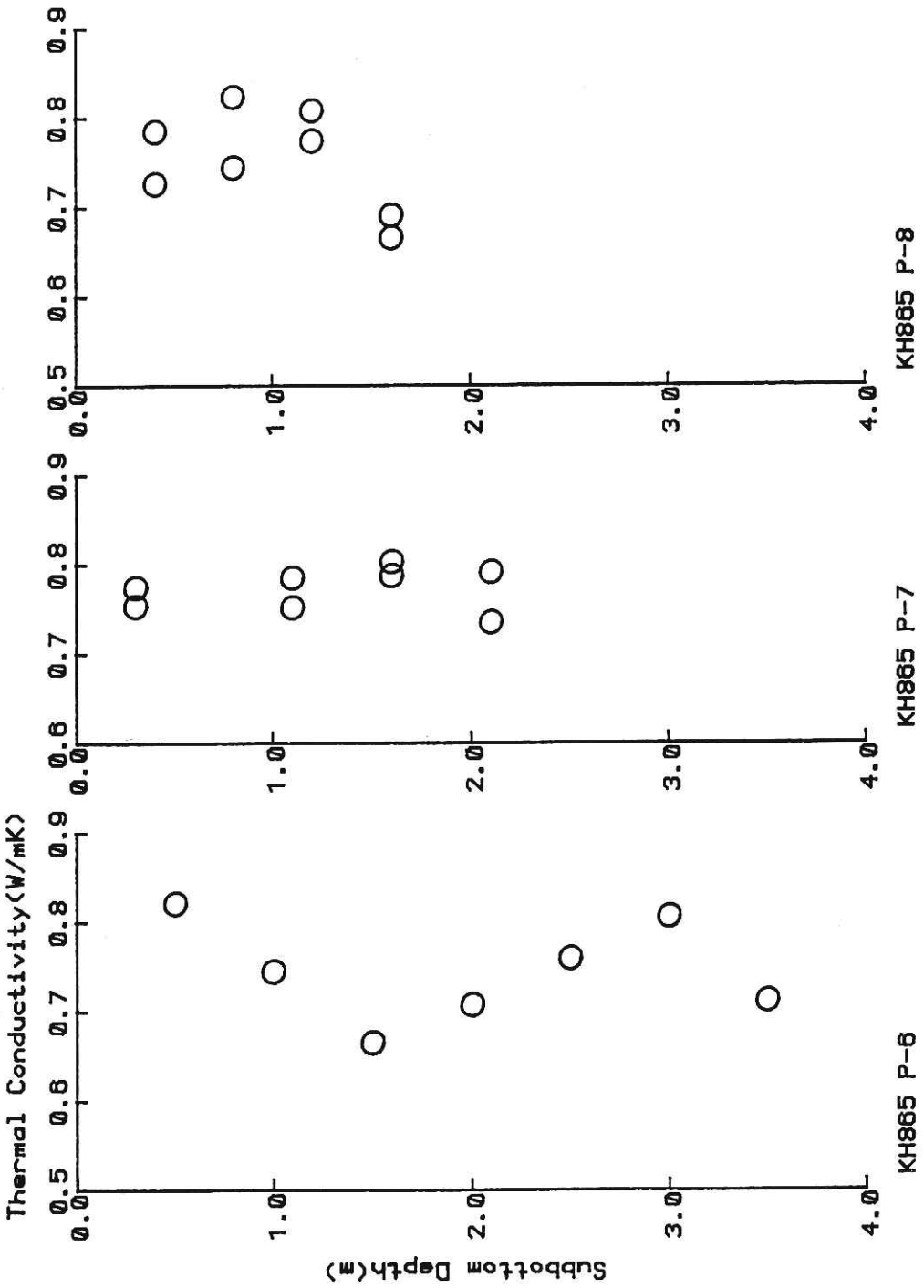

Fig. 5 Thermal conductivity versus depth profiles measured on the samples taken in the Nankai Trough area.

Table 1. Results of Heat Flow Measurements

Station	Latitude (N)	Longitude (E)	Depth (m)	PEN (m)	N	G (mK/m)	K (W/m/K)	Q (mW/m^2)
KH86-5HF01A	32°29.1'	134°54.9'	4380	tilt	(4)	(112-145)	0.92*	(103-133)
01B	32°29.1'	134°55.1'	4380	fell				
HF02A	32°20.4'	134°57.8'	4600	tilt	(3)	(237-308)	0.75*	(178-231)
02B(	32°20.4'	134°57.8')	4600	tilt	(4)	(221-286)	0.75*	(166-215)
02C(	32°20.4'	134°57.8')	4600	tilt	(3)	(199-257)	0.75*	(149-193)
02D(	32°20.4'	134°57.8')	4600	tilt	(2)	(>265)	0.75*	(>199)
02E	32°20.3'	134°58.2'	4600	tilt	(4)	(>181)	0.75*	(>136)
HF03A	32°24.9'	134°54.7'	4370	2.5	5	118	0.92	109
03B	32°24.9'	134°55.0'	4370	tilt	(4)	(>91)	0.92	(>84)
HF04A	32°21.8'	134°56.4'	4500	4.0	6	142	0.75*	107
04B	32°21.9'	134°56.4'	4500	tilt	(4)	(162-210)	0.75*	(122-158)
04C(	32°21.9'	134°56.4')	4500	tilt	(6)	(136-177)	0.75*	(102-133)
04D	32°21.9'	134°56.4'	4500	tilt	(5)	(140-181)	0.75*	(105-136)
HF05A	32°21.5'	134°56.7'	4600	tilt	(3)	(>70)	0.75*	(>53)
05B(	32°21.5'	134°56.7')	4600	tilt	(3)	(>53)	0.75*	(>40)
05C(	32°21.5'	134°56.7')	4600	tilt	(3)	(<-17)	0.75*	(<-13)
HF06A	32°21.1'	134°57.0'	4750	tilt	(2)	(>125)	0.75*	(>94)
06B(	32°21.1'	134°57.0')	4750	tilt	(3)	(145-188)	0.75*	(109-141)
06C(	32°21.1'	134°57.0')	4750	tilt	(2)	(>106)	0.75*	(>80)
06D	32°21.5'	134°57.5'	4750	tilt	(2)	(>177)	0.75*	(>133)
HF07A	32°20.6'	134°57.4'	4750	2.5	4	163	0.75*	122
07B(	32°20.6'	134°57.4')	4750	tilt	(3)	(>105)	0.75*	(>79)
HF08	32°13.2'	135°02.7'	4740	2.5	5	213	0.75*	160
HF09A(	32°19.3'	134°58.4')	4700	tilt	(2)	(>330)	0.75*	(>248)
09B(	32°19.3'	134°58.4')	4700	tilt				
09C(	32°19.3'	134°58.4')	4700	tilt	(5)	(>107)	0.75*	(>80)
09D(	32°19.3'	134°58.4')	4700	tilt	(2)	(>181)	0.75*	(>136)
09E(	32°19.3'	134°58.4')	4700	tilt	(2)	(265-343)	0.75*	(199-257)
09F	32°19.3'	134°58.4'	4700	tilt	(2)	(>499)	0.75*	(>374)
HF10	32°35.4'	134°46.1'	4100	tilt				
	32°35.2'	134°46.5'	4100	tilt				
HF11	32°31.5'	134°49.6'	3800	tilt				
	32°31.4'	134°50.1'	3800	tilt				
	32°31.4'	134°50.2'	3800	tilt				
	32°31.4'	134°50.5'	3800	tilt				
	32°31.4'	134°50.9'	3800	tilt				
	32°31.2'	134°51.5'	3800	tilt				
	32°31.3'	134°51.5'	4150	(end)				
HF12	32°15.7'	135°00.6'	4850	4.0	3	151	0.75	113

Table 1. (continued)

Station	Latitude (N)	Longitude (E)	Depth (m)	PEN (m)	N	G (mK/m)	K (W/m/K)	Q (mW/m^2)
HF13	33°37.4'	137°31.3'	3750	fell				
HF14A	33°46.1'	137°59.7'	3700	tilt	(4)	(>46)	0.75	(>35)
14B	(33°46.1'	137°59.7')	3700	tilt	(3)	(>32)	0.75	(>24)
14C	33°46.3'	137°59.5'	3700	tilt	(4)	(>37)	0.75	(>28)
14D	(33°46.3'	137°59.5')	3700	tilt	(4)	(>40)	0.75	(>30)
14E	(33°46.3'	137°59.5')	3700	tilt	(4)	(>41)	0.75	(>31)
	33°47.4'	137°59.3'	3700	(end)				
HF15A	33°55.3'	138°11.8'	3610	2.5	6	60	0.75*	45
15B	33°55.4'	138°11.8'	3610	2.5	5	61	0.75*	46
HF16A	34°02.8'	138°16.3'	2680	0.5	(2)	(74)	0.75*	(56)
16B	(34°02.8'	138°16.3')	2680	tilt	(2)	(>153)	0.75*	(>115)
16C	34°03.0'	138°16.3'	2680	fell				
HF17	34°03.7'	138°16.9'	2380	1.5	3	(168)	0.75*	(126)
P-6	32°17.9'	135°00.9'	4800	3.5	7		0.75+0.06	
P-7	32°36.2'	134°46.6'	4100	2.0	8		0.77+0.02	
P-8	33°46.2'	138°01.2'	3680	1.5	8		0.75+0.06	

Notes on Table 1.

Depth : Water depth without correction for change in sound velocity.
PEN : Length of the probe in the sediment;
"fell" means that the probe fell without penetration and
"tilted" means that it did penetrated but not vertically.
N : Number of sensors that were used for calculation of dT/dZ.
G : Temperature gradient calculated by the least square method.
The values with inequality sign(>) are the estimates as
minimum values , whereas the ones linked by the slash
indicate the range.
Both are the evalution from the instrument tilt.
K : Thermal conductivity. Asterisk represents values measured
at nearby station.
Q : Heat flow as the product of G and K. Special signs are
the same as the ones used at "G".

SEA SURFACE GRAVITYMETER

H. FUJIMOTO and C.S. YANG
Ocean Research Institute, University of Tokyo, Nakano, Tokyo 164
S. ISEKI
Department of Earth Sciences, University of Chiba, Yayoi, Chiba 260

Sea surface gravimetry was carried out throughout the cruise by use of a Tokyo Surface Ship Gravity Meter (T.S.S.G.). A vibrating-string gravity sensor (No. 68-7-6) was mounted on a vertical gyroscope.

The on-line data processing system is a compact one developed for the Franco-Japanese cooperative project "KAIKO I" in 1984. Period of the string vibration is continuously counted by using two acceleration every some 20 msec. Vertical accelerations caused by ship's motion was removed by use of a digital low-pass filter with a width of a about 10 minutes. Free-air anomaly was calculated in real time on the basis of Loran-C navigation. These gravity data processings were carried out bu use of a board computer Data General MBC/3. The results were recorded in floppy diskettes by using a handy personal computer NEC PC-8201.

Calibration of gravity values was carried out on the basis of the gravity values at Harumi and Kobe Shinkou No. 4 Pier. A LaCoste & Romberg gravimeter (G-124) was used for the gravimetric connection between Kobe Harbor and the gravity station at the Kobe Marine Meteorogic Observatory.

TRIAL EXPERIMENT ON OCEAN BOTTOM PRESSURE MEASUREMENT

S. ISEKI
Department of Earth Sciences, Chiba University, Yayoicho, Chiba 260
H. FUJIMOTO and C.S. YANG
Ocean Research Institute, University of Tokyo, Nakono, Tokyo 164

An ocean bottom pressure meter with an acoustic release was newly developed and its trial experiment was carried out at the Nankai Trough. This instrument aims to measure the absolute value but variation of water pressure at the ocean bottom.

The sensor part is composed of two rooms filled with pure water, and a vibrating-string pressure gauge measures pressure difference between the two rooms (M. Hasiguchi, in prep.). The characteristics of this sensor is that the string vibrates in liquid. When sufficient time has passed after it was deployed on the ocean bottom, the pressure of one room is fixed by closing a valve with a timer. The pressure in the other room is always the same with the outside. In this way this pressure meter is expected to measure pressure variation at any water depth with a high sensitivity. Because the effect of temperature on this pressure gauge is serious, a quartz thermometer is used to monitor the temperature variation. Block diagram of the measuring system is shown in Fig. 1 and the overall appearance of the ocean bottom pressure meter is shown in Fig. 2.

The instrument was deployed on a flat ocean bottom near the Nankai Trough on 30th November, 1986. The location was 32°21' N, 135° 04' E, and 4,800 m in water depth. It stayed on the bottom for about nine days and was recovered on 9th October.

A preliminary result is shown in Fig. 3. Although the meter was deployed under the central part of the instrument, the observed temperature variation is .02°C, and only .004°C for short-time (3 days) fluctuation.

There are some problems in the pressure data. Because both pressure and temperature largely changed during the deployment, it is difficult to make clear the cause and effect. It is scheduled to examine the pressure gauge under varying water pressure and roughly constant water temperature in a water tank.

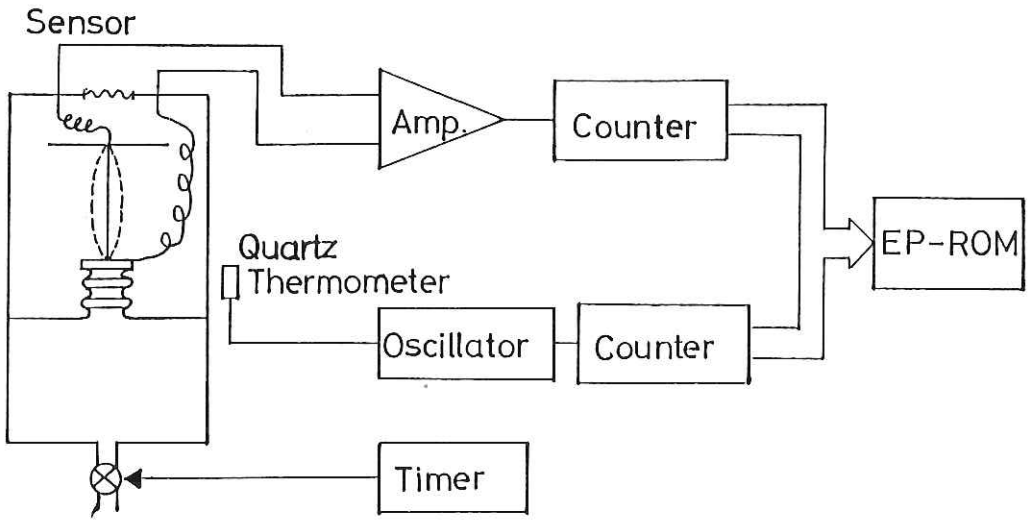

Fig. 1 Block diagram of the measurement system.

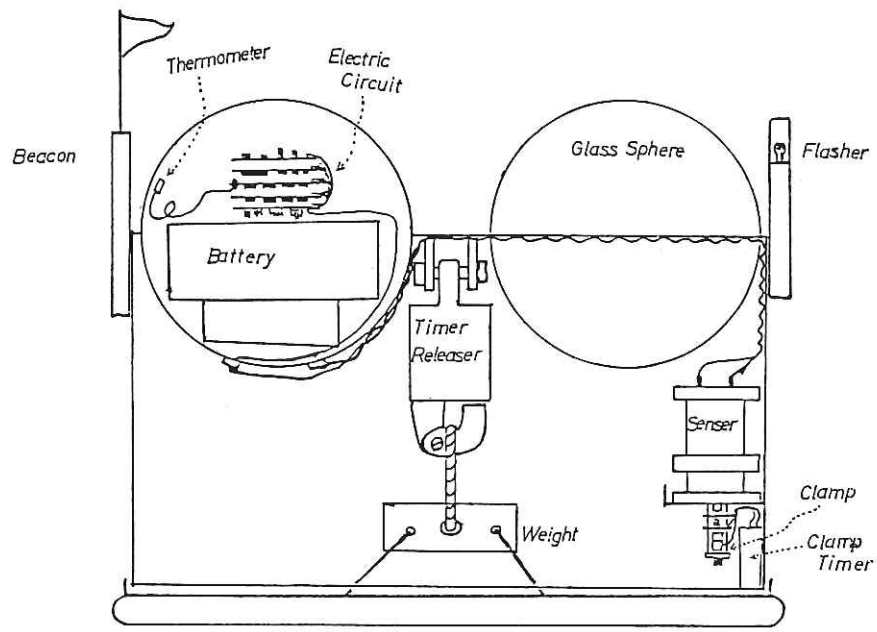

Fig. 2 Overall appeance of the ocean bottom pressure meter.

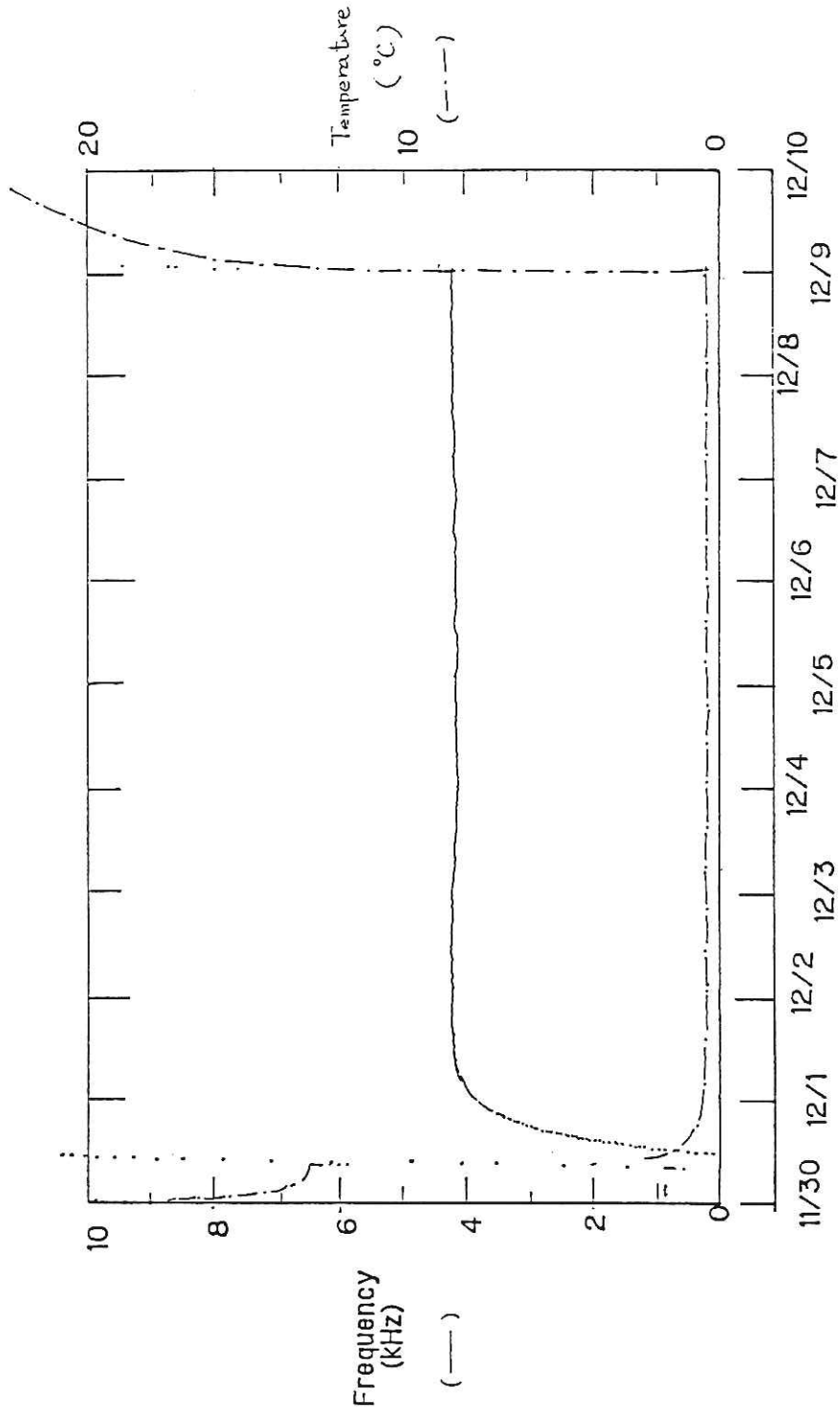

Fig. 3 Preliminary result of pressure and temperature observed on the ocean bottom near the Nankai Trough.

GEOMAGNETIC TOTAL FORCE MEASUREMENT

M. NAKANISHI, T. FURUTA and H. FUJIMOTO
Ocean Research Institute, University of Tokyo, Nakano, Tokyo 164

In order to reveal the tectonic processes of the Nankai Trough and the adjacent area, geomagnetic total field was measured by use of a proton precession magnetometer during this cruise except when the ship was drifting. The magnetometer is ORI-made and consists of the electric circuit, the sensor with a toroidal coil, and the towing cable (200m). An X-T recorder was used for a real-time monitor. The data processing system was used for a real-time monitor. The data processing system was a set of the microcomputer (NEC PC9801F) and its navigation system used Loran-C (JRC JNA760). The sampling interval was 30 seconds and the data were logged in a floppy disk at a interval of a minute. At the same time the data were printed out and transmitted to the microcomputer of Kobe University (Three Component Magnetic Measurement System).

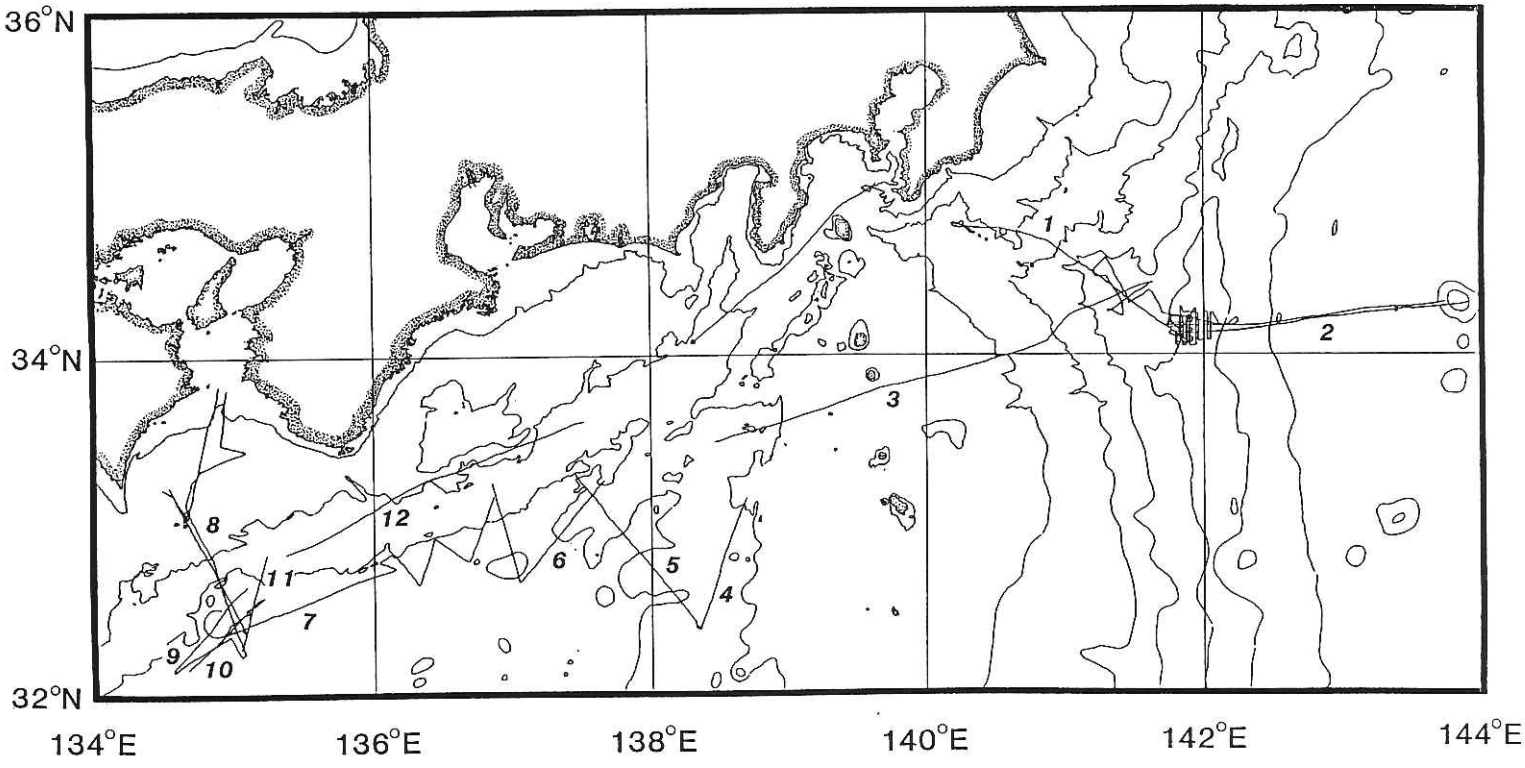

Fig. 1 The tracks of magentic measurements Numerals of lines are cited in Fig.2

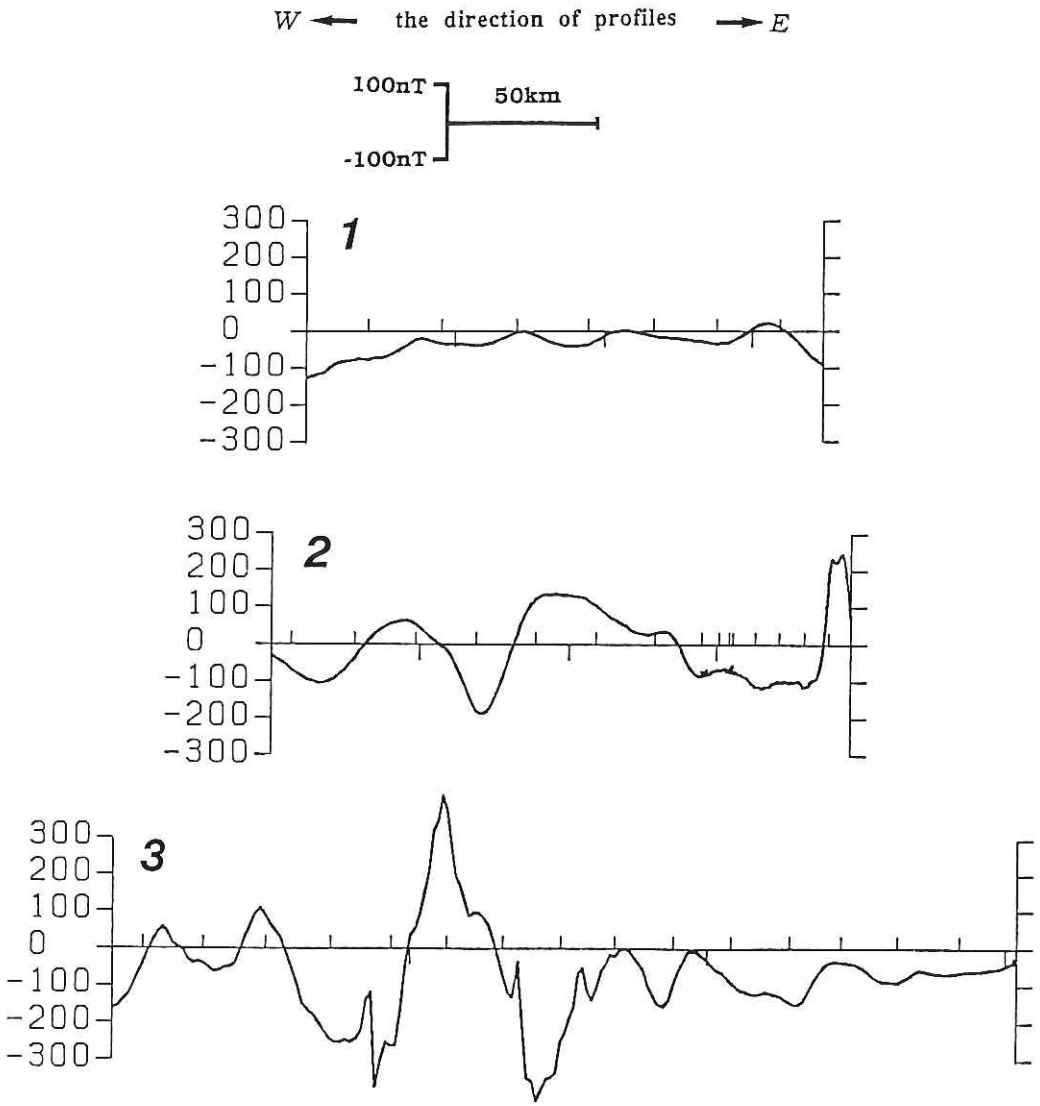

Fig. 2 Several examples of magnetic anomaly profiles (reference field IGRF1985)

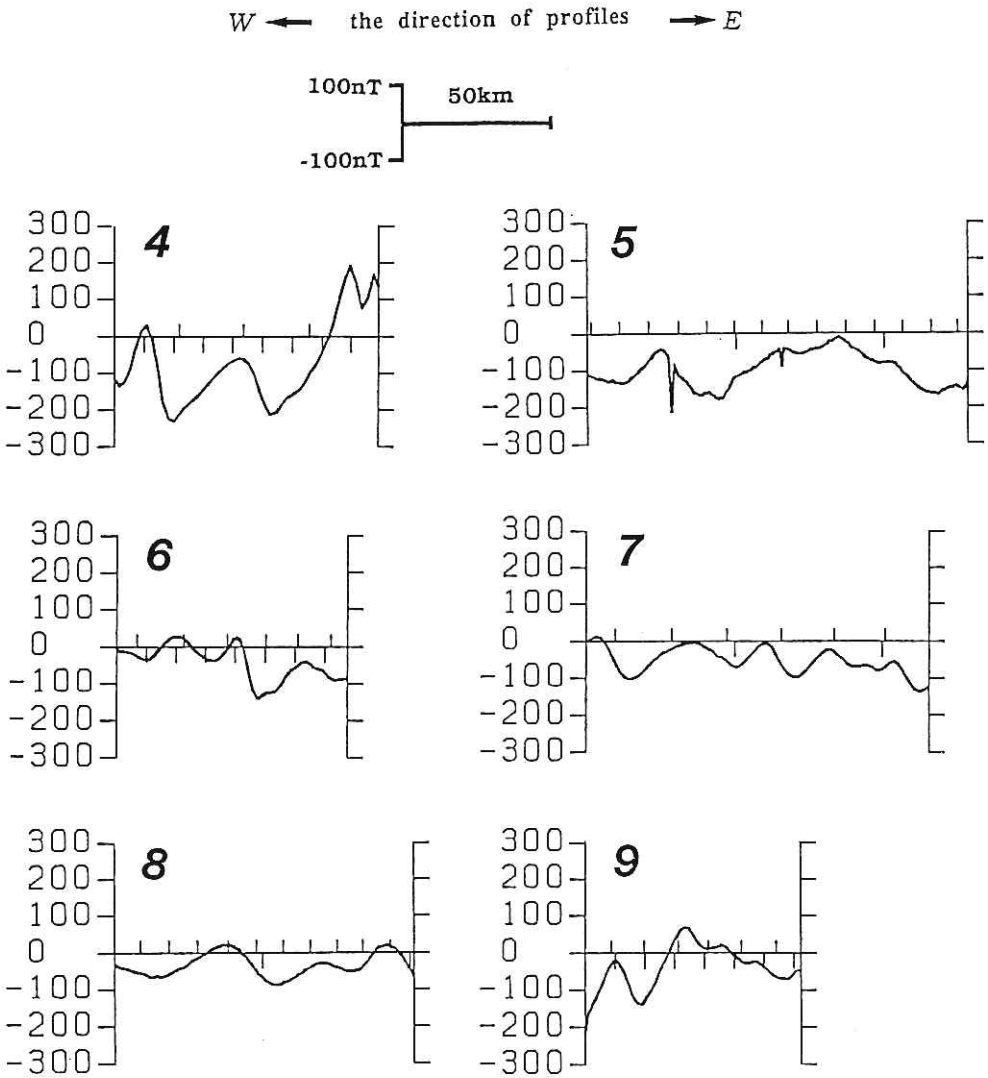
W ← the direction of profiles → E
100nT
-100nT
50km
4
5
6
7
8
9
300
200
100
0
-100
-200
-300

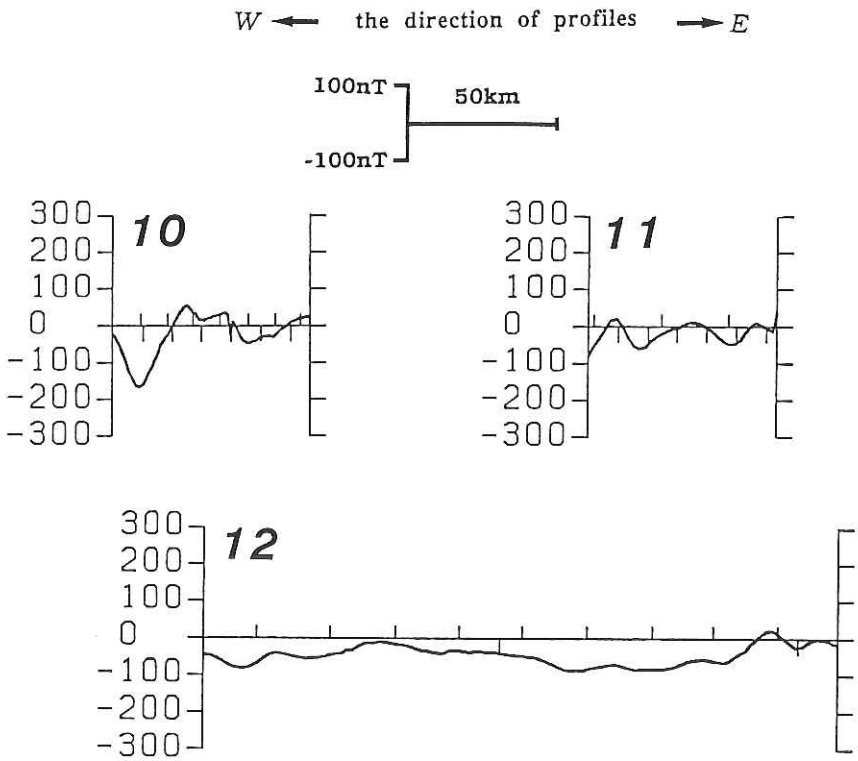
W ← the direction of profiles → E
100nT
-100nT
50km
300
200
100
0
-100
-200
-300
10
11
12

MEASUREMENT OF THE THREE COMPONENTS OF GEOMAGNETIC FIELD

I. UNO

Department of Earth Sciences, Kobe University, Nada, Kobe, 657

INTRODUCTION

Magnetic surveys by STCM (Shipboard Three Component Magnetometer) were carried out in the Nankai Trough area during the KH86-5 cruise. Because of the scarcity of the three component magnetic data in this area, the new data are so precious that we can identify the magnetic anomaly in the Nankai Trough area.

STCM

STCM measures intensity of three components of a geomagnetic field on the shipboard. It should be noted that the observed data consist of both the geomagnetic field and magnetic field induced by the ship's body. For detecting the degree of the induced field, the ship was rotated abruptly on a vertical axis trough 360 degrees. The induced field was removed from the observation data formula of Isezaki (1986). The ship was rotated at 4 points with various values of latitude; (lat.34°15.33'; lon.143°23.25'), (lat. 32°22.46'; lon. 138°21.28'), (lat. 32°29.98'; lon.135°05.53') and (lat. 34°03.99'; lon.138°17.49'), during this cruise.

RESULTS

Track lines of the magnetic survey area are shown in Fig. 1, together with the bathymetric feature of the study area. Geomagnetic anomaly of three components (north, east and downward components) along the track line are shown in Figs. 2-(1), -(2) and -(3), respectively.

North component anomaly : The north component has in general low amplitude (150 nT). The wave length is fairly long (100 Km) on the LINE A, B and C. Higher amplitude more than 700 nT is observed in the trace of the LINE B between the Izu Peninsula and the Oshima Island.

East component anomaly : The east component in anomaly also shows low amplitude except for the LINE B and D. The anomaly on the LINE D has short wave less than 50 Km. Higher amplitude (about 700 nT) is observed on the LINE B.

Downward component anomaly : low amplitude (150 nT) is observed in the downward component anomaly. A short wave length (about 30 km) is observed on the LINE D.

REFERECE

Isezaki, N., 1986, A new shipboard three-component magnetometer: Geophysics, 51, 10, 1992-1998.

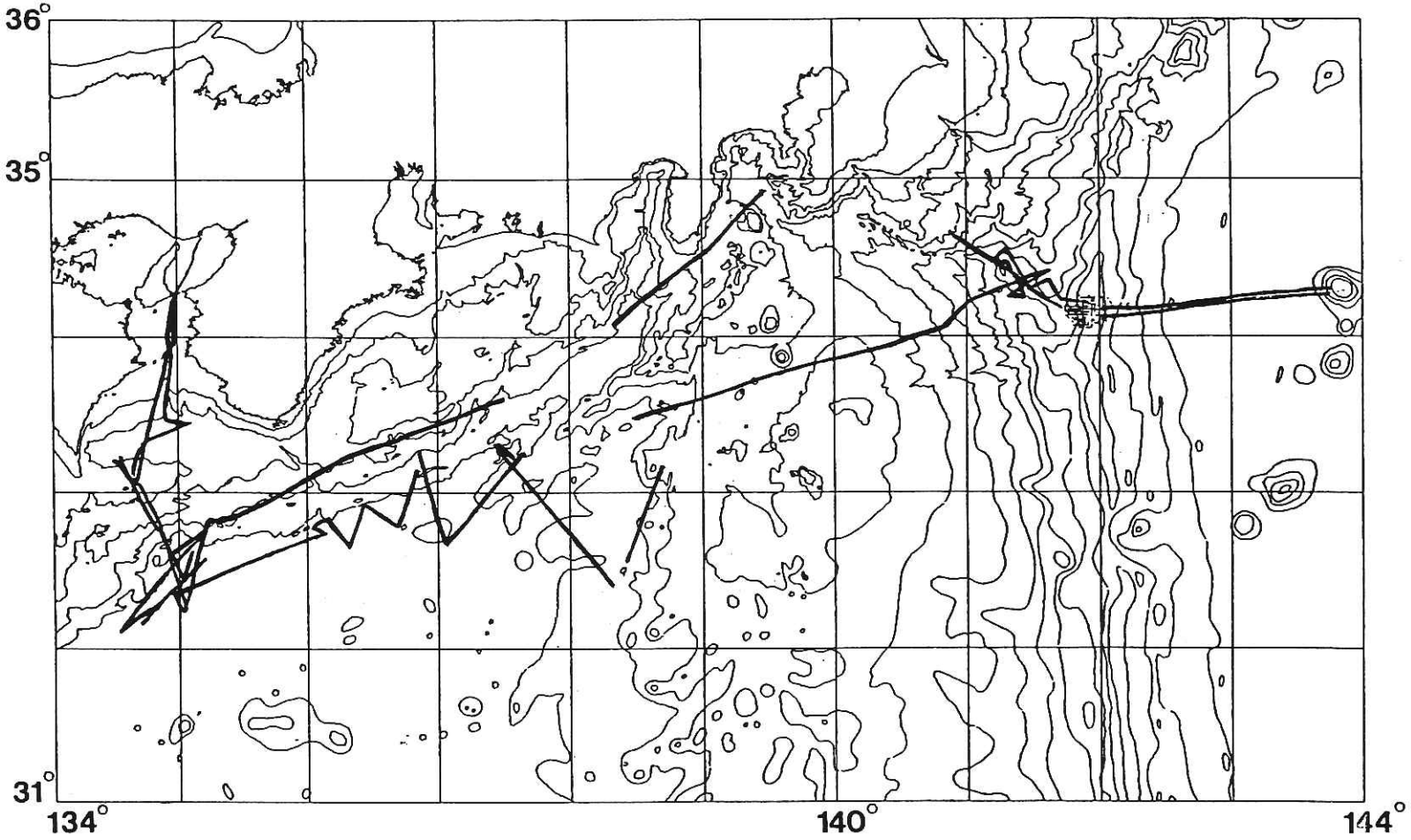

Fig. 1 Track line of the magnetic survey.

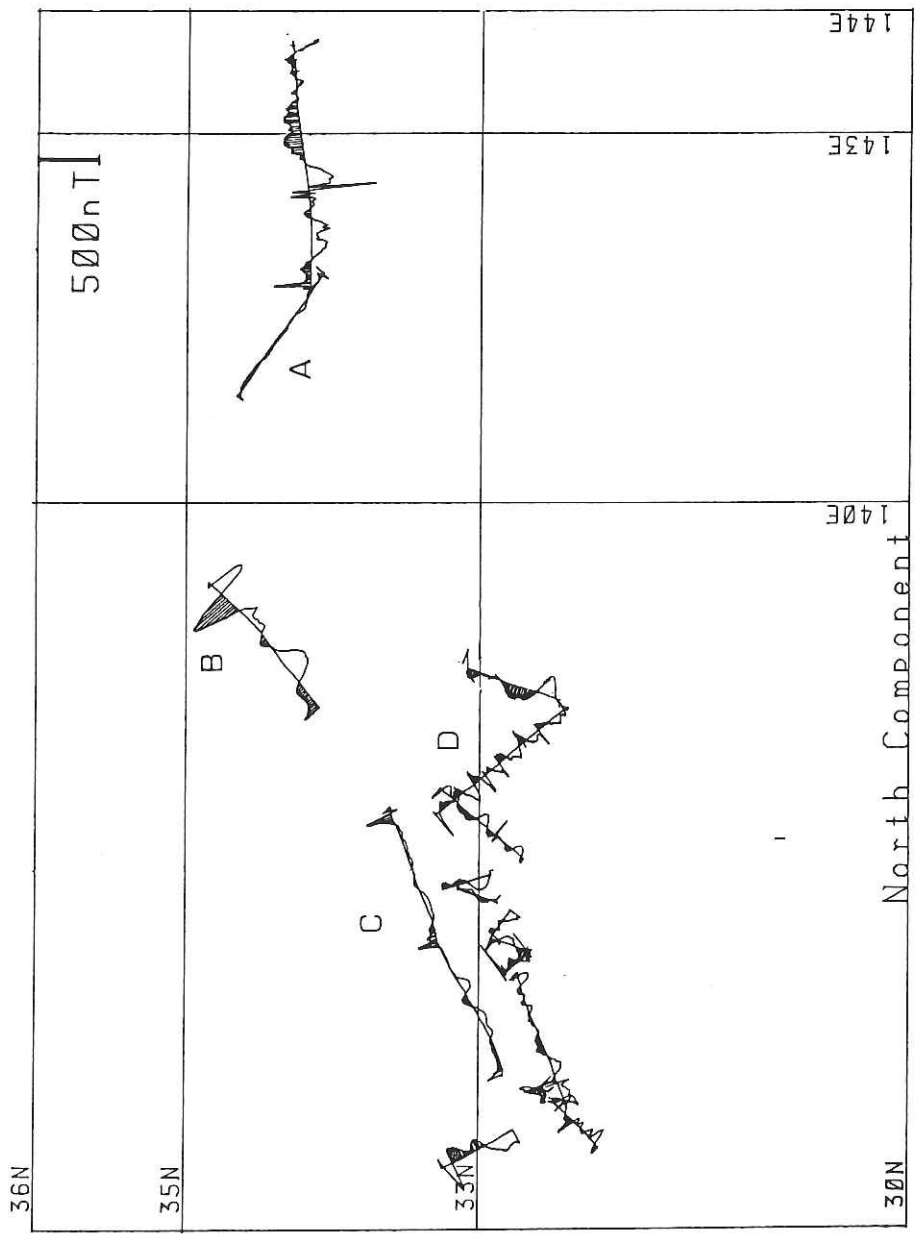

Fig. 2-1 The profiles of north component of geomagnetic anomaly along track lines.

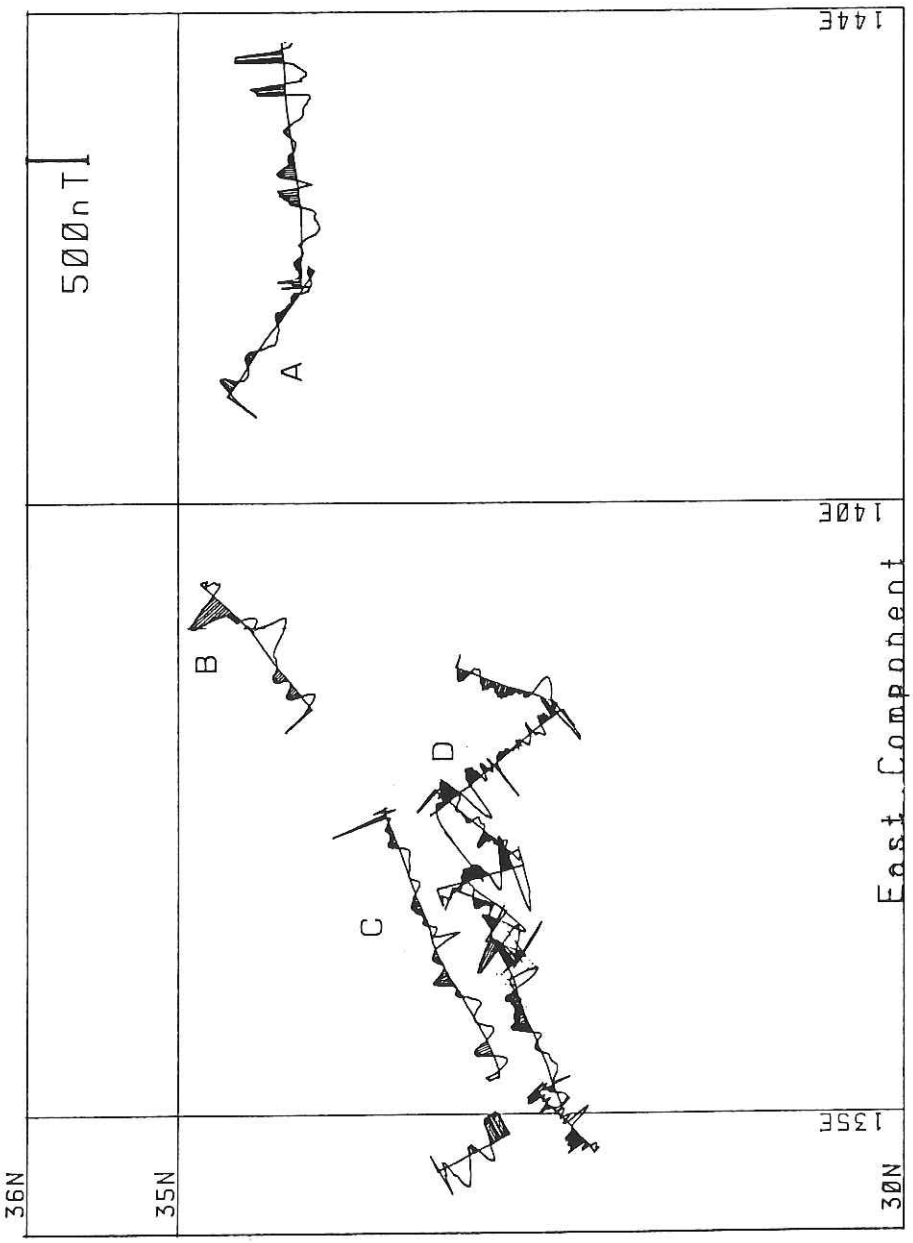

Fig. 2-2 The profiles of east component of geomagnetic anomaly along track lines.

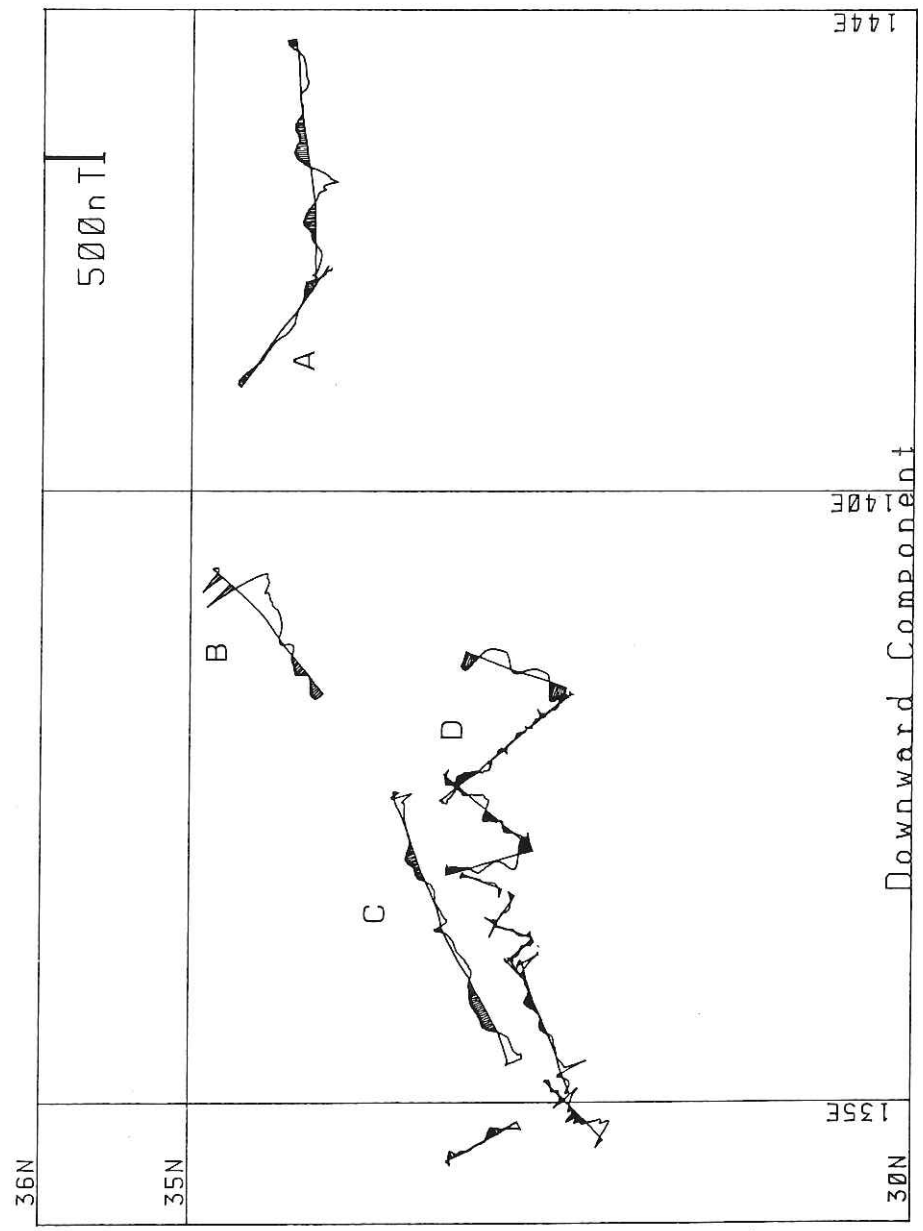

Fig. 2-3 The profiles of downward component of geomagnetic anomaly along track lines.

LBL ACOUSTIC TRANSPONDER NAVIGATION

T. FURUTA and H. FUJIMOTO

Ocean Research Institute, University of Tokyo, Nakano, Tokyo 164

Long base line (LBL) acoustic transponder navigation was carried out at the Nankai Trough area with depth of 4,500 m, to determine the precise ship's and the heat-flow meter's positions. The transponder network was triangular with internal of approximately 3 n.m. and one subnavigation transponder was installed on the heat-flow meter of ERI. Judging from the systematic differences between the Loran-C and the transponders, the ship moved eastward by about 0.4 n.m. after they were dropped from the ship. Mooring configuration of the system is shown in Fig. 1. Anchor weight is about 100 kg, weight of a transponder in water is 11 kg, and total buoyancy is 52 kg. They are connected by nylon ropes and chains as shown in Fig. 1.

The accuracy of position determination of ship and instrument was approximately 5 x 10^{-4} or better, when the physical condition was acoustically good. The relative accuracy obtained from the transponder system is ten times higher than the other navigation systems such as Loran-C, NNSS and GPS. Three dimensional positions of the instruments must be known precisely for the underwater investigations. Because of the acoustic noise generated by propellers of the ship, the position of the heat-flow meter was not always determined. Part of the results is shown in Table 1. Unit D transponder was set on the wire 100 m above the instrument. This trial experiment clearly shows that the positions of the heat-flow meter were horizontally apart from the ship by about 900 m, because of different motions of the ship and the heat-flow meter caused by ocean current and wind.

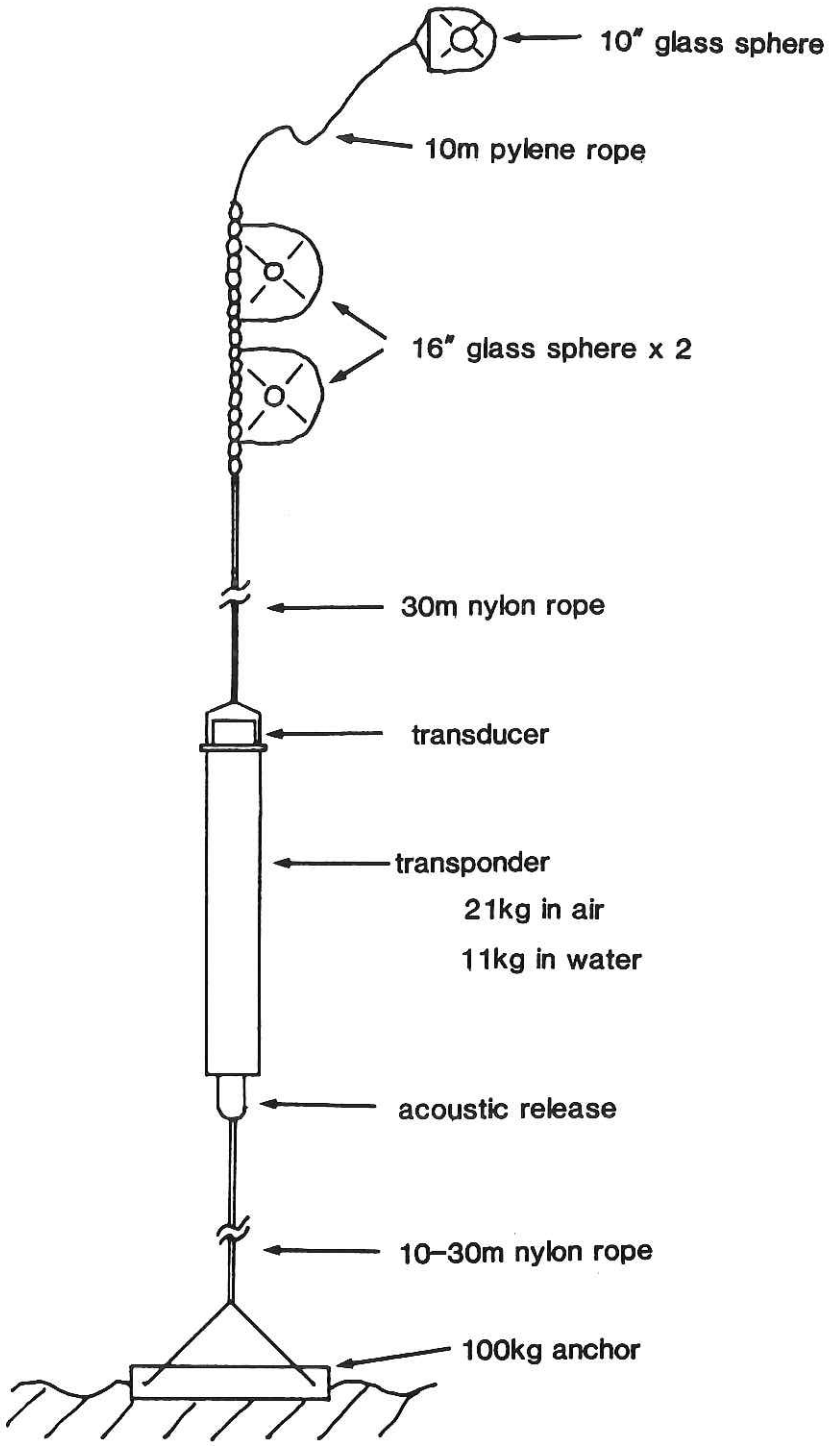

Fig. 1 LBL acoustic transponder navigation system.

Table 1. Positions of the ERI heat-flow meter determined by the LBL transponder system.

Station HF 6. (Nov. 10)

(a) 14:32 (JST) Just after a shift of the ship
ship : 32° 21.06'N, 134° 56.21'E
sub : 32° 21.48'N, 134° 56.49'E

Horizontal distance : 890 m.
Distance : 3970 m

(b) 14:39 (JST) dropping instrument
ship : 32° 21.07'N, 134° 56.24'E
sub : 32° 21.47'N, 134° 56.57'E

Horizontal distance : 900 m
Distance : 4230 m

GLOBAL POSITIONING SYSTEM (GPS)

T. FURUTA, H. FUJIMOTO and M. NAKANISHI
Ocean Research Institute, University of Tokyo, Nakano, Tokyo 164

GPS (Global Positioning System) is a dream for sea-men who are in charge of navigation of a research vessel. In near future, this dream will be realized. If GPS system will be in full operation, we will be able to continuously determine the precise positions of ship at any time and anywhere on the globe.

During this cruise, we used two GPS receivers to test practical operation on board. One of them was provided from Collins (Navcore I) and another from SONY (GTT-3000). Firstly we got data at Harumi to evaluate the accuracy and reliability of the GPS receivers. Data were obtained every individual update intervals and recorded on floppy disk through RS232C interface. Fig. 1 shows the position fluctuation at Harumi. Evaluation of GPS data should be based on the geometry of the satellite arrangement which is presented by GDOP or PDOP. Throughout the cruise, duration of position determination by GPS was approximately three hours per day and GDOP was relatively large (approx. 5), so utilizing of GPS position data to navigation was not efficient. Inspite of low efficiencies, we got many informations of GPS application for onboard operation. For example, the shaking of top of the antenna is one of the serious problems to position fix, because of acceleration of ship's movement. Consequently the GPS positioning is useful for geological and geophysical investigations.

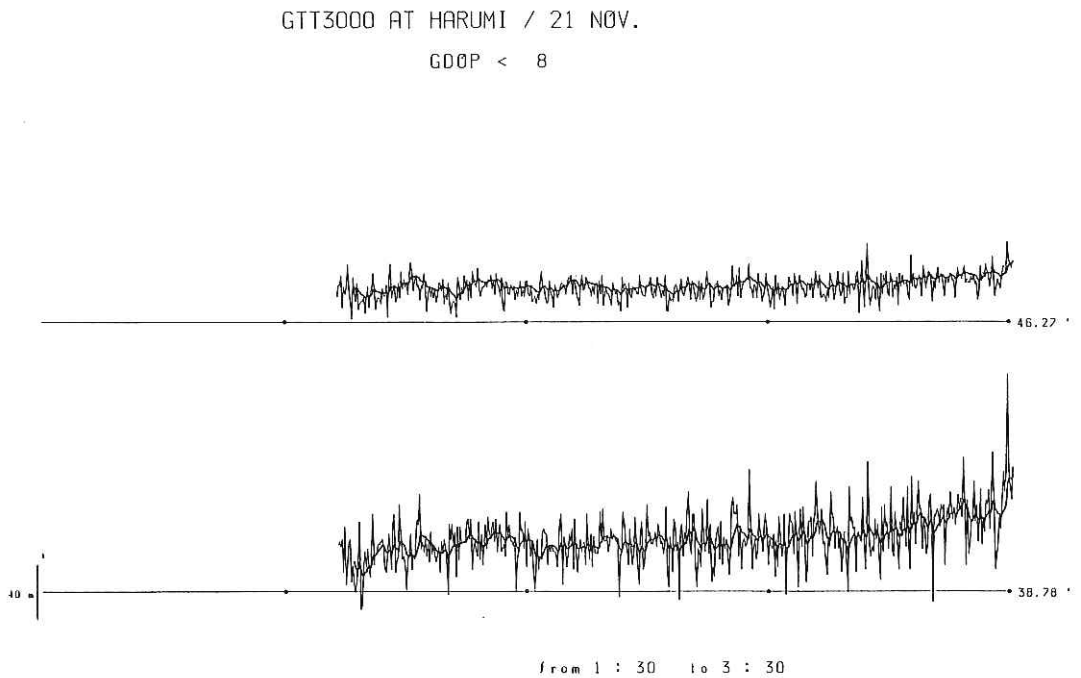

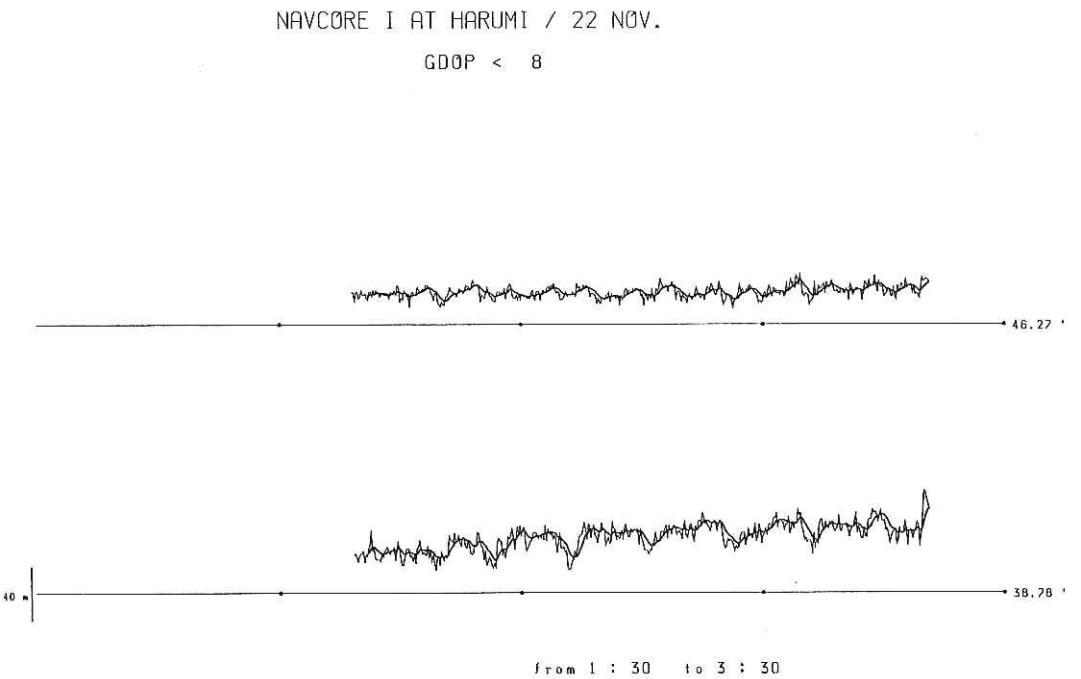

Fig. 1 Position fluctuation at Harumi, Tokyo.

DEEP SEA PHOTOGRAPHY, SYSTEM, OPERATION AND OBSERVATION

M. WATANABE

Ocean Research Institute, University of Tokyo, Nakano, Tokyo 164

DEEP SEA CAMERA SYSTEM

Fundamental constitution of the deep sea camera system used in this cruise was composed of two deep sea cameras, a strobo and a pinger with a compass (Fig. 1). A newly developed specific recorder for the digital compass which has been used since KH86-1 was also deployed in this cruise. This recorder functions as a computer which is able to retrieve the data from RAM in the digital compass and also is capable of sending necessary commands to the RAM. Because the recorder is a hand-held type, the entire operation becomes quite efficient. The data retrieval can be achieved directly from the camera unit in a short time.

OPERATION

Deep-sea photography was carried out at four stations during the cruise and the operation logs of each station are shown in Tables 1 and 2. The data for the orientation and tilt of the camera system, monitored by the compass, are shown in Figs. 2 and 4. The orientation of the camera was recorded as an azimuth between the axis of camera and geomagnetic north-pole. If the camera was an up-light attitude within 5 degrees, a code "OK" was recorded in the memory of the tilt data. Similarly, another code "NG" was memorized in the case that the tilt of the camera exceeded 5 degrees. Using these off-line data of the camera attitude, the spin motion and degree of collision with sea bottom were displayed on board as shown in Figures 2 to 4. The data list of orientation and tilt at each shot time are shown in the same way.

One trouble in the digital compass was happened during the operation at the station KH86-5-C1. The compass data of this station was not memorized in the RAM. It was caused because of a short-circuit in the external I/O port and the signal to the strobe was not generated. The compass data of other three stations was memorized with a command of internal trigger at an interval of every ten seconds.

OBSERVATION

KH86-5-C1(32° 22.7'N, 134° 57.8'E: Water Depth=4780m)

This site is located at the very toe of the deformation front of the Nankai Trough(Fig.5). Muddy substrata with abundant animal traces and current lineations is the characteristic of this site(Fig.7A,B). Trace fossils include feces, feeding tracks and burrows. Photographed animals include brittle star(Ophiuroid) and sea cucumber(*Psychropotes raripes*). Weak current lineations are recognized.

KH86-5-C2(32° 21.4'N, 134° 54.9'E: Water Depth=4530m)

This site was chosen at a small depression of the Nankai prism which is a surface manifestation of a front of a major thrust(Fig.5). An important observation made here is the finding of a possible *Calyptogena* shell(Fig.8A). It is also noted that the density of larger feeding tracks are most abundant among the photographed stations(Fig.8B). This suggest a possibility of high biological activity at this site which may be related to a seepage of fluid near this site. Other photographed animals are brittle stars and deep-sea shrimp(*Plesiopenaeus*). The current lineation is hardly recognized here.

KH86-5-C3(32° 31.0'N, 134 ° 49.0'E: Water Depth=4220m)

The foot of a major slope which is developed due to major thrust dislocation within the prism is the site of this camera station(Fig.5). Rather monotonous muddy substrata changes to an cliff along which layered muddy sediments are exposed. A conspicuous set of fracture trending perpendicular to the cliff(perpendicular to the Nankai Trough axis) is recognized(Fig.9A,B). This may be a set of extensional fractures perpendicular to the NW-SE compression.

KH86-5-C4(33 ° 54.9'N, 138°10.3'E: Water Depth=3420m)

The site is located at the very toe of accretionary prism in the eastern Nankai Trough(Fig.6). Muddy seafloor with abundant worm burrows was photographed(Fig.10). Larger feeding tracks are rare. The current lineations are not recognized.

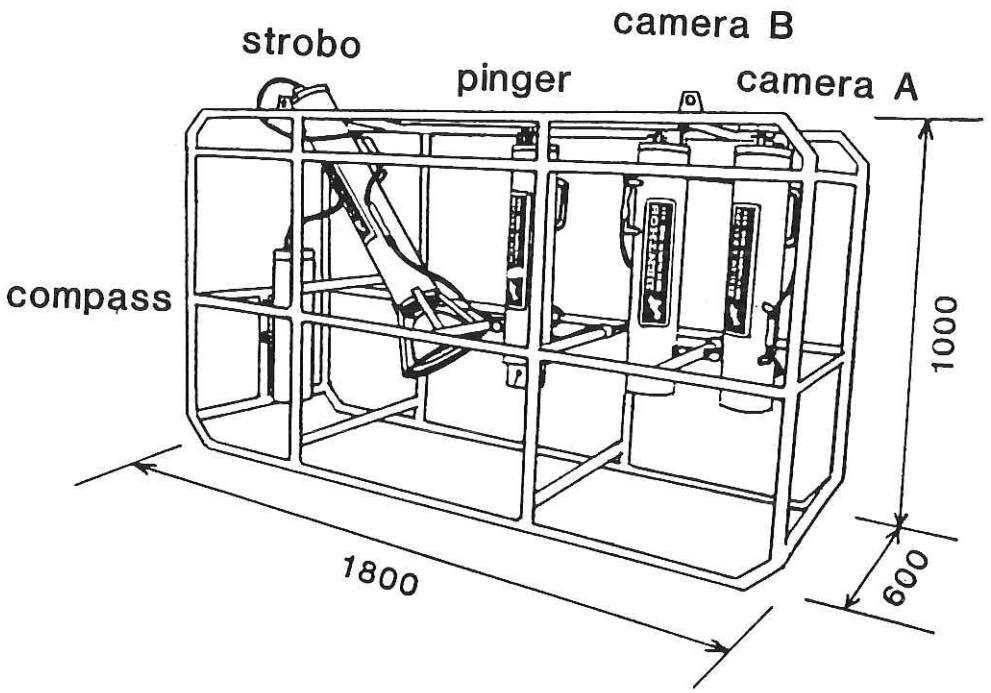

Fig. 1 Overall deep sea camera system

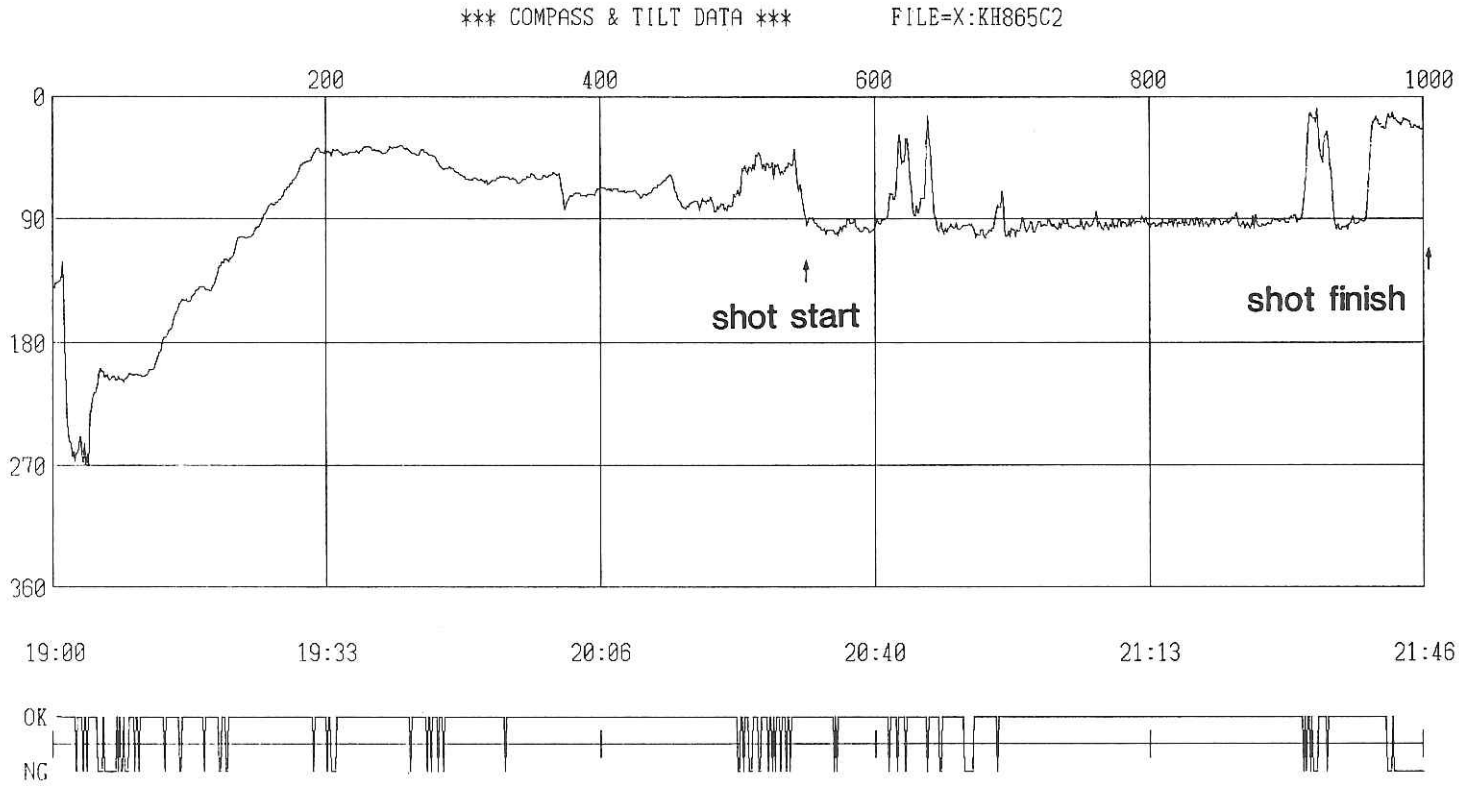

Fig. 2 Direction and tilt data of KH86-5-C2, 4530m deep, Camera unit contacted on the bottom at directly after the start of shot and just before the finish of shot. Bottom current streaned west-east.

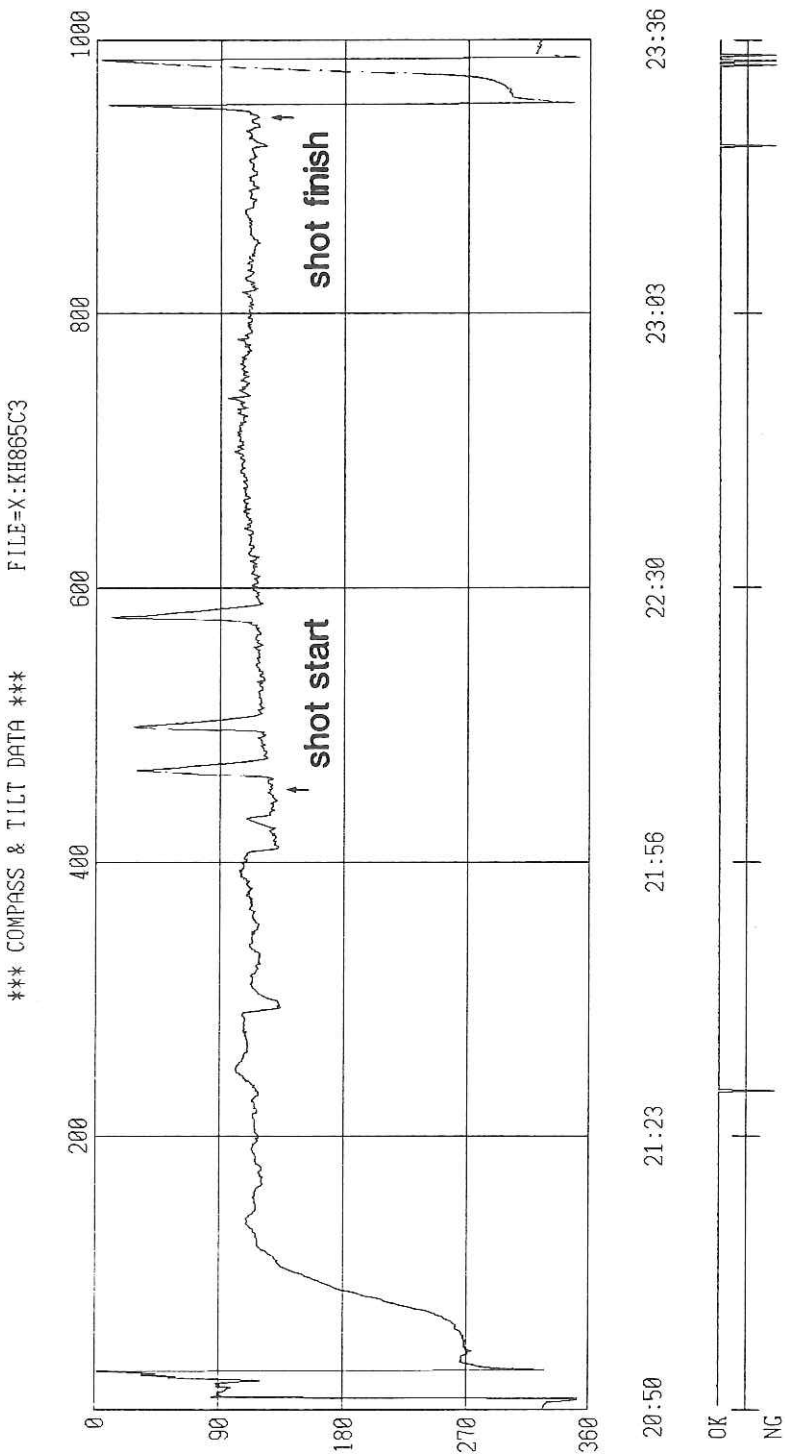

Fig. 3 Direction and tilt data of KH86-5-C3. Water depth is 4220m. Bottom of this station was flat.

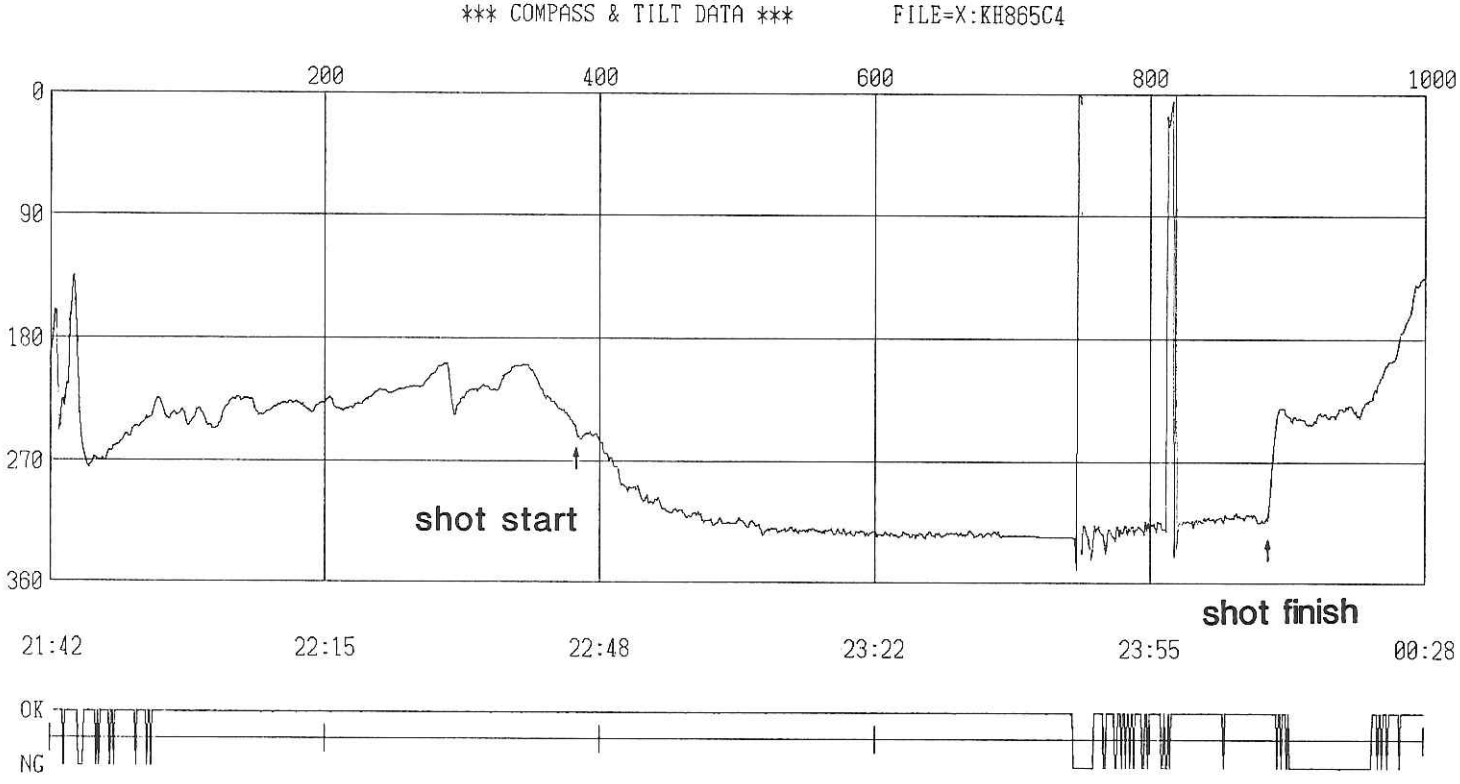

Fig. 4 Direction and tilt data of camera work, KH86-5-C4, 3420m deep. Bottom topography is seen to be flat, and bottom current is NE to SW direction.

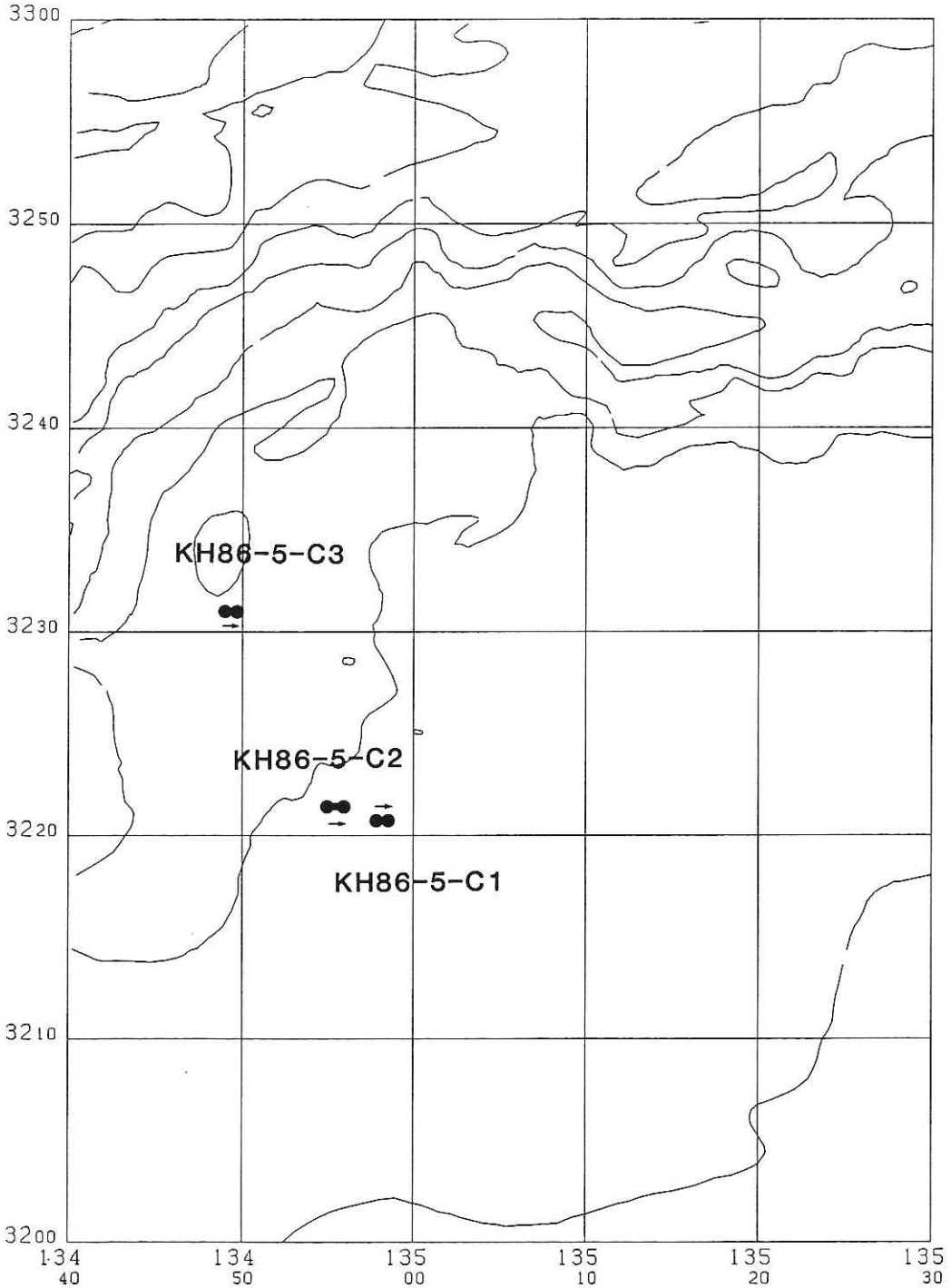

Fig. 5 Operation sites of KH86-5-C1, C2 and C3.

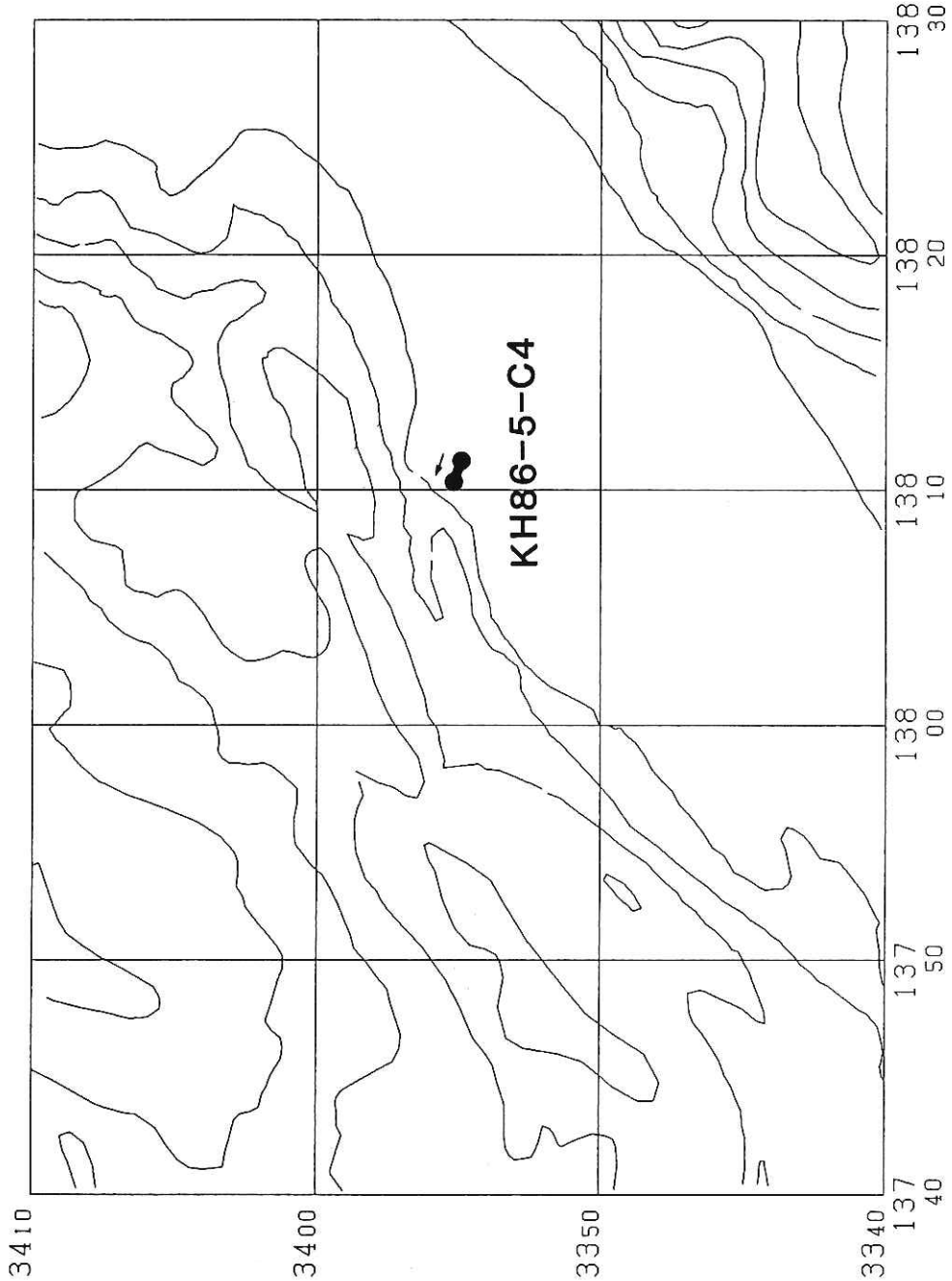

Fig. 6 Location map of operation site, KH86-5-C4.

Fig. 1A. Trace fossils on muddy substrate. Feces at the center. KH86-5-C1.

Fig. 1B. Trace fossils and weak current lineations. KH86-5-C1.

Fig. 2A. Calyptogean shell and trace fossils. KH86-5-C2.

Fig. 2B. Brittle star and feces. KH86-5-C2.

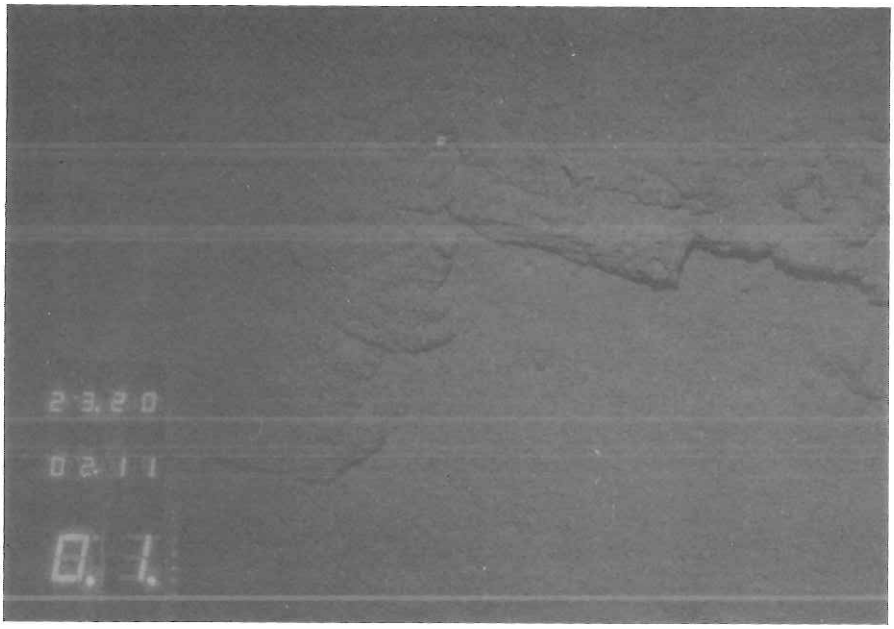

Fig. 3A. Fractured muddy sediments. KH86-5-C3.

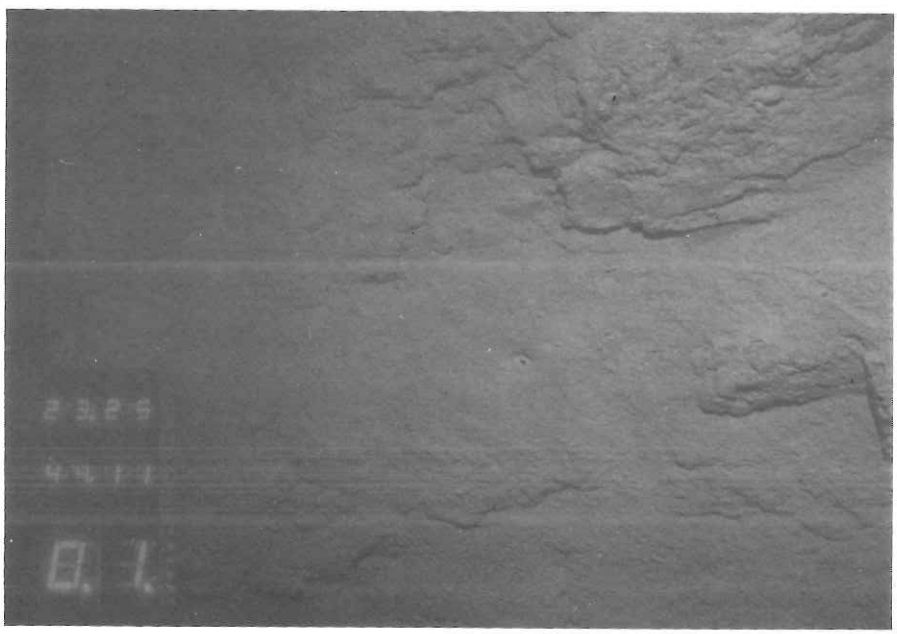

Fig. 3B. Exposure of muddy sediment layer. KH86-5-C3.

Fig. 4A. Trace fossils on muddy substrate. KH86-5-C4.

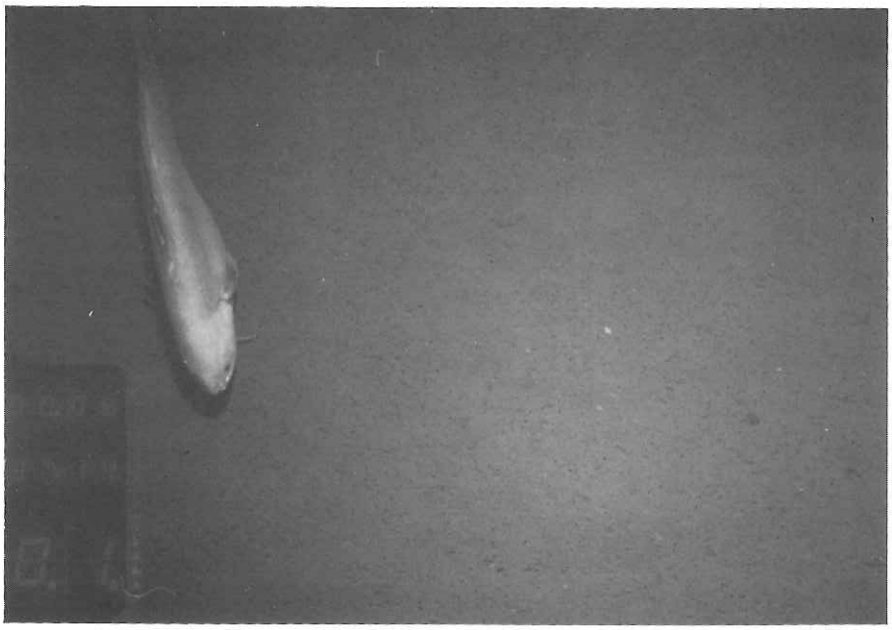

Fig. 4B. A deep-sea fish, *Spectrunculus grandis*. KH86-5-C4.

Table 1. Operation logs of deep-sea photography.

Date	1986.12.10	1986.12.10
Station No.	KH86-5-C1	KH86-5-C2
Location	Nankai Trough off the coast of Muroto	Nankai Trough off the coast of Muroto
Weather	Fine	Fine
Wind	100° 10m/sec	290° 5m/sec
Sea condition	Good	Good
Bottom topography	Flat	Flat
Water depth(start)	4600m	4450m
(finish)	4780m	4530m
Film & Film length	Kodak 5294(100)	Kodak 5294(100ft)
Battery No.	No.81-03	No.86-01
Lens focussed(camera A)	1.2m	1.2m
(camera B)	1.2m	1.2m
Iris(Camera A)	11	11
(Camera B)	11	11
Shoto interval	6sec	6sec
Compass	Ext trigger(6sec)	Int trigger(10sec)
Time lowed	06:20	19:12
& location	32°20.7N 134°55.6E	32°21.1N 134°53.6E
Shot start time	07:40	20:32
& location	32°20.7N 134°57.8E	32°21.4N 134°54.9E
Shot finish time	08:55	21:47
& location	32°20.7N 134°58.5E	32°21.4N 134°55.9E
Time surfaced	09:51	22:48
& location	32°21.1N 134°59.5E	32°21.3N 134°56.9E
Result	Photo.*-4-1, *-4-2	Photo.*-4-3, *-4-4
Remarks	Added to SUB-NAV Transponder	Combine with Heat flow HF-8

Table 2. Operation logs of deep-sea photography.

Date	1986.12.11	1986.12.13
Station No.	KH86-5-C3	KH86-5-C4
Location	Nankai Trough off the coast of Muroto	Nankai Trough off the coast of Yaizu
Weather	Fine	Cloudiness
Wind	350° 2m/sec	180° 5m/sec
Sea condition	Good	Low swell
Bottom topography	Flat & Down slope	Flat
Water depth(start)	4080m	3600m
(finish)	4220m	3420m
Film & Film length	Sakura 400(100ft)	Sakura 400(100ft)
Battery No.	No.81-03	No.81-03
Lens focussed(camera A)	1.2m	1.2m
(camera B)	1.2m	1.2m
Iris(Camera A)	11	11
(Camera B)	11	11
Shoto interval	6sec	6sec
Compass	Int trigger(10sec)	Int trigger(10sec)
Time lowed	20:53	21:44
& location	32°35.1N 134°47.7E	33°54.9N 138°11.9E
Shot start time	22:06	22:47
& location	32°31.0N 134°49.0E	33°54.9N 138°11.2E
Shot finish time	23:26	00:07
& location	32°31.0N 134°49.6E	33°55.2N 138°10.3E
Time surfaced	00:10	00:51
& location	32°30.8N 134°50.0E	33°55.5N 138°10.1E
Result	Photo.*-4-5, *-4-6	Photo.*-4-7, *-4-8
Remarks	Combine with Heat flow HF-10	Combine with Heat flow HF-15

Geological Data

DESCRIPTION OF PISTON CORE SAMPLES OF KH86-5 CRUISE

W. SOH

Ocean Research Institute, University of Tokyo, Nakano, Tokyo 164

INTRODUCTION

The sediment samples taken during KH86-5 cruise are eight piston cores, two dredges and one box core sample. Very small amounts of sediment were also taken from the heat flow equipments. The sample sites are shown in Fig. 4-1 in the data log of the previous section.

OUTLINE OF KH86-5 CRUISE PISTON CORING

To understand the sedimentation in the active margin, we aim to get eight piston core samples from the fore-arc basin, slope basin, trench floor and outer ridge. However, one piston coring, KH86-5 P1, unfortunately failed because of bottom roughness. The two core samples, KH86-5 P4 and P5, were obtained from the Muroto Basin. The core samples are composed of thin-bedded turbidites with ash layers. Two core samples, KH86-5 P3 and P7, were taken from the inner slope basins; they are composed of nannofossil- and diatom-bearing clay with ashy layers and clastic thin-bedded turbidites. The fill sediment of the Nankai Trough axial channel off Shikoku, KH86-5 P6, is thin-bedded turbidites and hemipelagites. The sediment contains a lot of methane in the interstitial fluid, and shows to be anoxic below 70 cm from the sea floor. KH86-5 P8 was obtained from the deformation front of the Nankai Trough off the Tenryu river. KH86-5 P2, is nannofossil-bearing calcareous ooze, and was taken from summit of the Zenisu Ridge, south of Tenryu Submarine Fan.

PISTON CORER AND SAMPLE TREATMENT

We used three types of piston corer of the Ocean Research Institute, University of Tokyo. One is a 8 m-long aluminum pipe sampler with 500 kg weight. The others are 4 m and 6m-long stainless pipe piston core sampler with 600 kg weight. KH86-5 P1, P2 and P5 were performed by the aluminum pipe piston corer. KH86-5 P3, P4 and P7 was

conducted by the stainless pipe corer of 6 m-long. KH86-5 P6 and P8 were done by the stainless pipe corer of 4 m length.

Each core sample was cut into two half-core samples. The one half is preserved in the Ocean Research Institute. We used the other half-core as the working sample for the observation and description, and utilized it for soft x-ray photography. On board, the surface of the working half core sample was first shaved by knife, and well-brushed by a fine misty water-jet. After the treatment, the core samples were observed for description, and photographed. Then, 1 cm thick slices were cut from the surface of the half-cores and used for soft X-lay photography. Microscopic observation using smear slides were also conducted. The classification of the fine-grained sediments in this report is based on Dean et al. (1985).

KH86-5 P2

Location: Lat.:33 38.09'N Water depth 2439 m
Lon.:138 27.89'E Core sample length 343 cm
(Summit of Zenisu Ridge, south of Tenryu Submarine Fan)
Purpose: to investigate sedimentation and paleo-ocean history under the Kuroshiro Current.

The dominant lithology of the sample is diatom-bearing calcareous ooze. The ooze contains large amounts of clay particles. The ooze is mainly composed of sponge spicules, calcareous nannofossils and foraminifers. Some plagioclase and quartz grains are found in the ooze, which are probably derived from the Izu-Bonin volcanic arc, located on the east. The ooze is generally structureless and homogeneous, but burrow structures are commonly observed. *Zoophycus*, *Planolites* and *Scolicia* are found in the clay layers. Especially, *Zoophycus* are well-developed in the core sample. For example, it can be found between 160 to 220 cm below the top of soft X-ray photography of KH86-5 P2.

Five ash layers of volcanic glass, yellowish white in color, were identified between 64 cm to 68 cm, 132 cm to 138 cm, 150 cm to 156 cm, 173 cm to 180 cm and 305 cm to 309 cm below the top. The ash layer, found in 64 cm to 68 cm, are mainly composed of volcanic glass. The refractive index of the glass is 1.4991. Scoria ash layer between 132 to 138 cm is interpreted as fall deposits because it shows a good distribution grading and no distinct sedimentary structure showing sediment gravity flows. Opaque minerals condense the clay zone, between 198 to 205 cm below the top. It is thought to be products from turbid layers of fine-gained volcanic materials with clay particles provided from the Izu-Bonin Ridge.

OCEAN RESEARCH INSTITUTE UNIVERSITY OF TOKYO

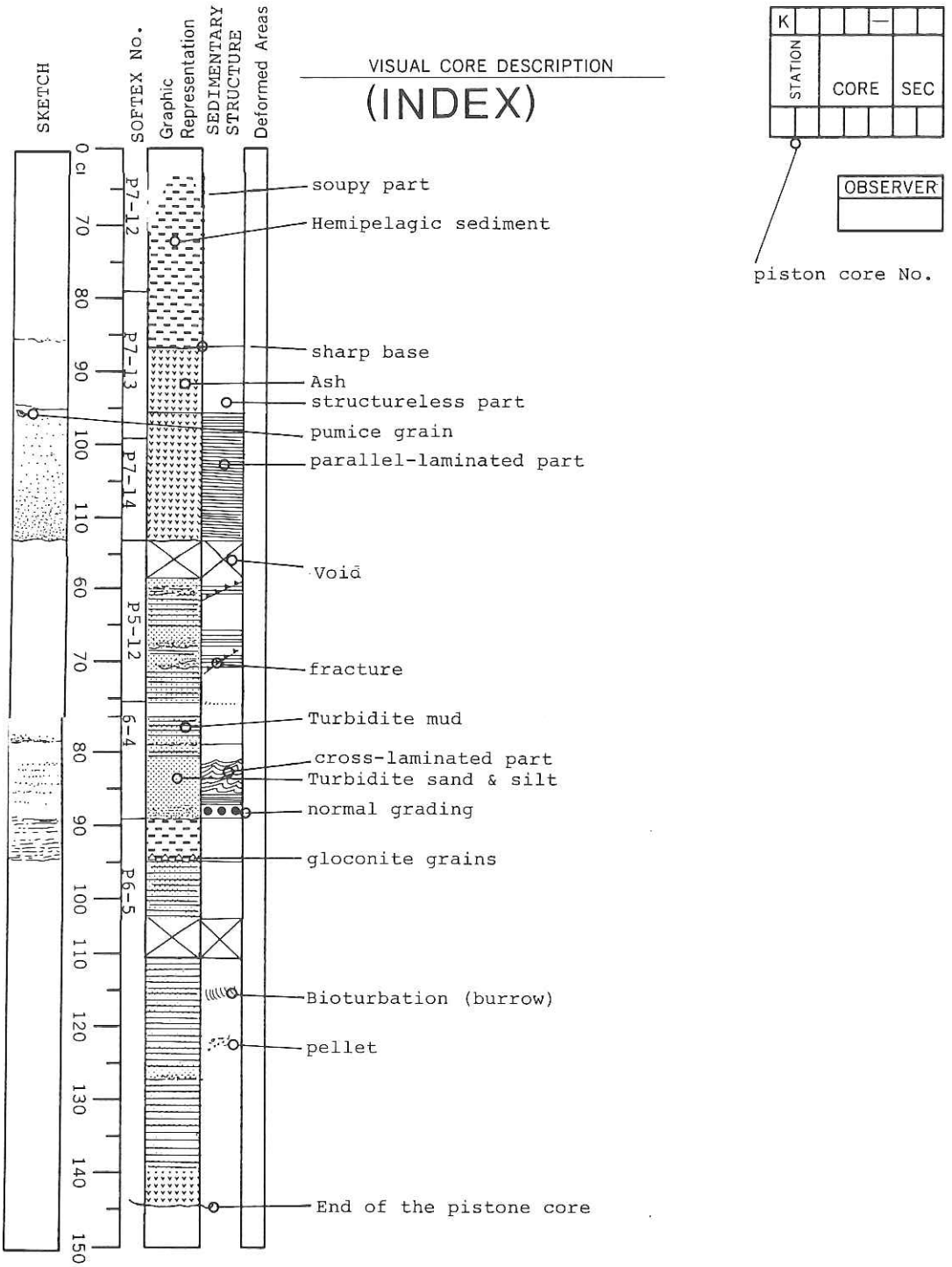

OCEAN RESEARCH INSTITUTE UNIVERSITY OF TOKYO

VISUAL CORE DESCRIPTION

K	H	8	6	—	0	5
STATION		CORE			SEC	
P	2				0	I

OBSERVER

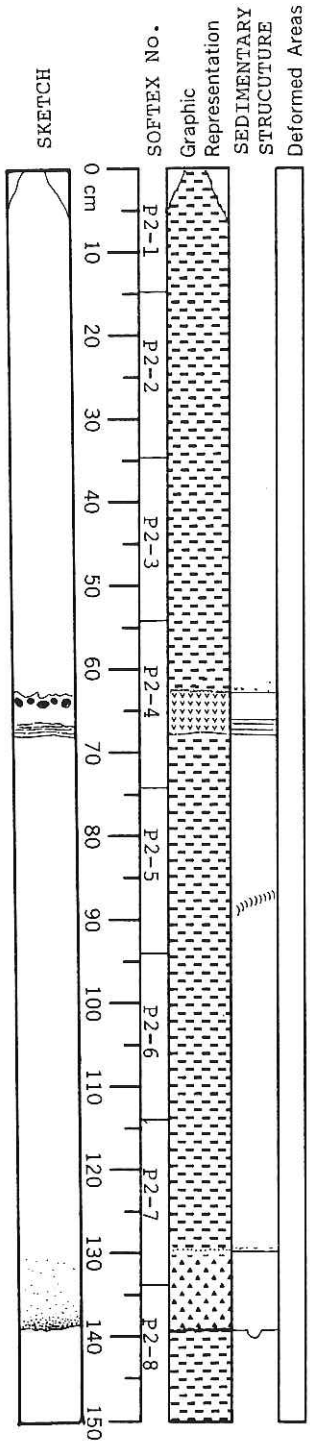

Soupy brown-olive gray, calcareous ooze.

Clayey calcareous ooze (5Y 5/2)
This contains heveay minerals; hyperthene opeque minerals and volcanic glass.
This shows structureless (massive), and is well-develped bioturbation structures; Zoophycus and Condrites so on.

Volcanic ash (5Y 7/2)
The upper portion is structureless, but the lower shows paralell lamination. The base is poorly defined.

Scoricia buurow
Clayey calcareous ooze (5Y 5/2)
Scoria grains are included in the ooze

Scolicia burrow

Scoria bed (5Y 3/2)
This shows distribution grading.
Augites grains are included. The base is well-defined.

OCEAN RESEARCH INSTITUTE UNIVERSITY OF TOKYO

VISUAL CORE DESCRIPTION

K	H	8	6	—	0	5	
STATION			CORE		SEC		
P	2				0	2	

OBSERVER

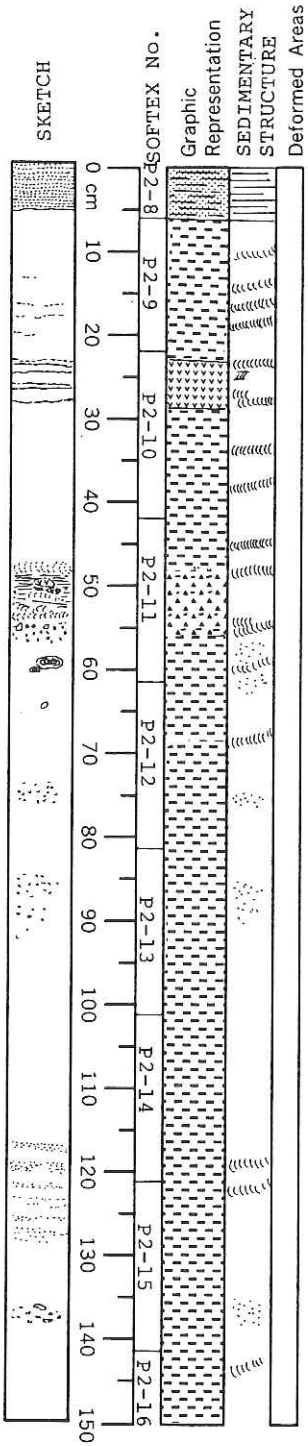

Volcanic sand bed. (fine-grained sand)
This shows crude parallel lamination.
This sand is composed of quartz, plagioclase and mafic minerals.
Zoophycus buurrows.

Calcareous silty mud (5Y 5/2)
In this horizon, Zoophycus is developed.
Volcanic ash, most of them are volcanic glass.
This shows crude parallel lamination, and it is modified by well-developed bioturbation.

Zoophycus burrows

Calcareous silty mud (5Y 5/2)

Volcanic clay with scoria grains with grading.
The clay is mainly composed of opeque minerals.
The base of the bed is blacky scoria ash.
(7.5YR 3/2)
Zoophycus buurows

Calcareous silty mud (5Y 5/2)
The sedimentary structure is modified by well-developed bioturbation.

Scolicia burrow

Zoophycus burrows

Zoophycus burrows

OCEAN RESEARCH INSTITUTE UNIVERSITY OF TOKYO

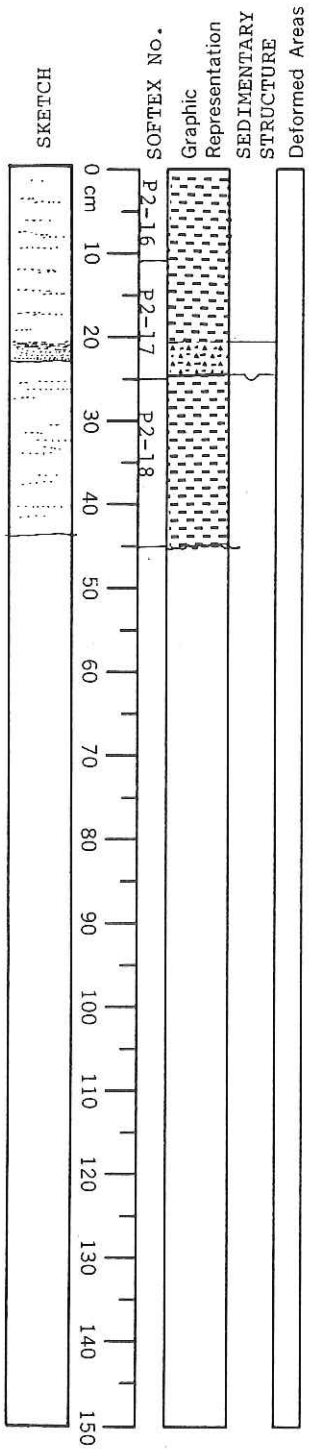

VISUAL CORE DESCRIPTION

K	H	8	6	—	0	5
STATION		CORE			SEC	
P	2				0	3

OBSERVER

Clayey calcareous ooze (5Y 5/2)

Volcanic clay with scoria grains (5Y 3/2)
This shows crude normal grading.

Clayey calcareous ooze (5Y 5/2)

End of this core sample is 343 cm

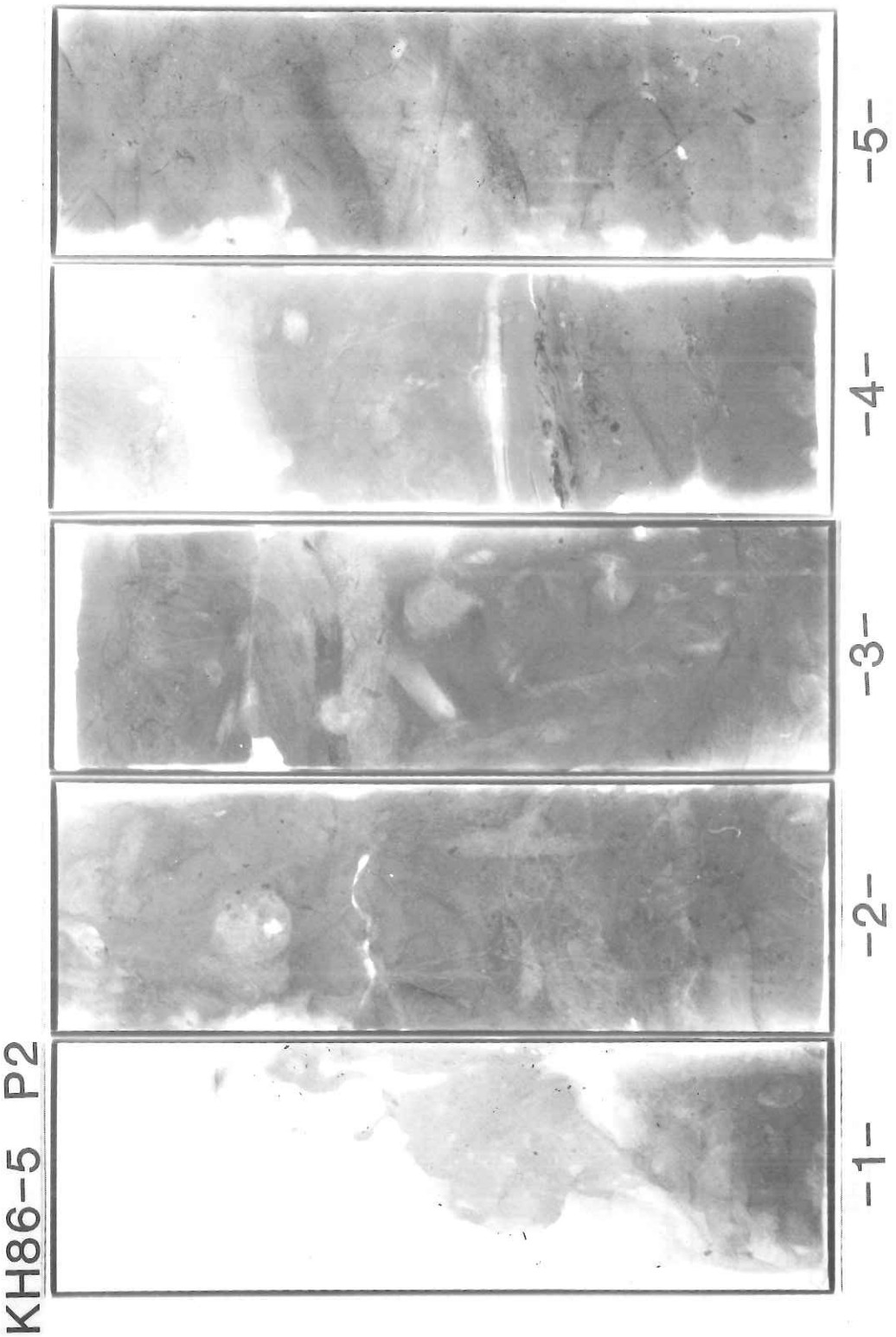
KH86-5 P2
-1-
-2-
-3-
-4-
-5-

KH86-5 P2

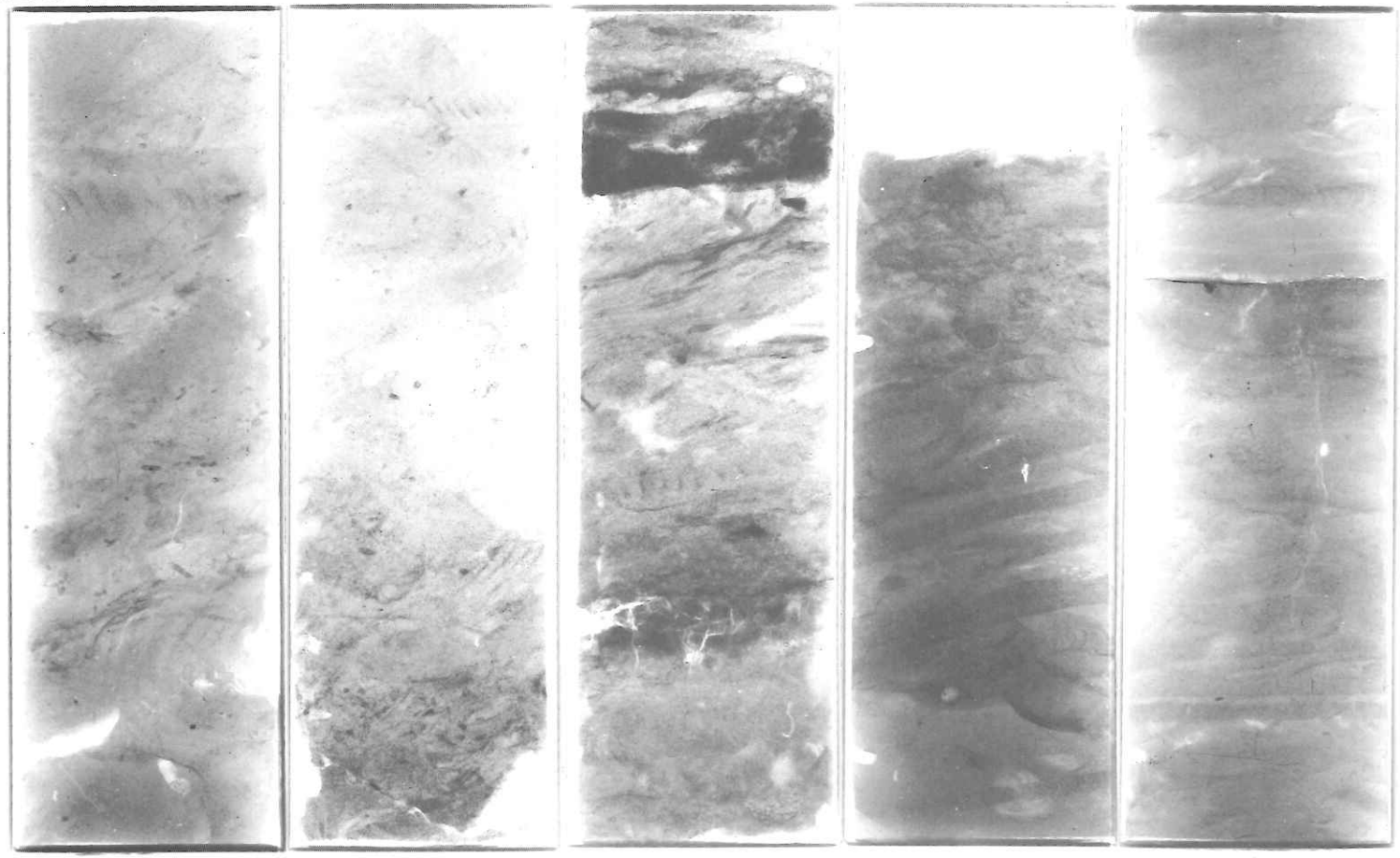

-6- -7- -8- -9- -10-

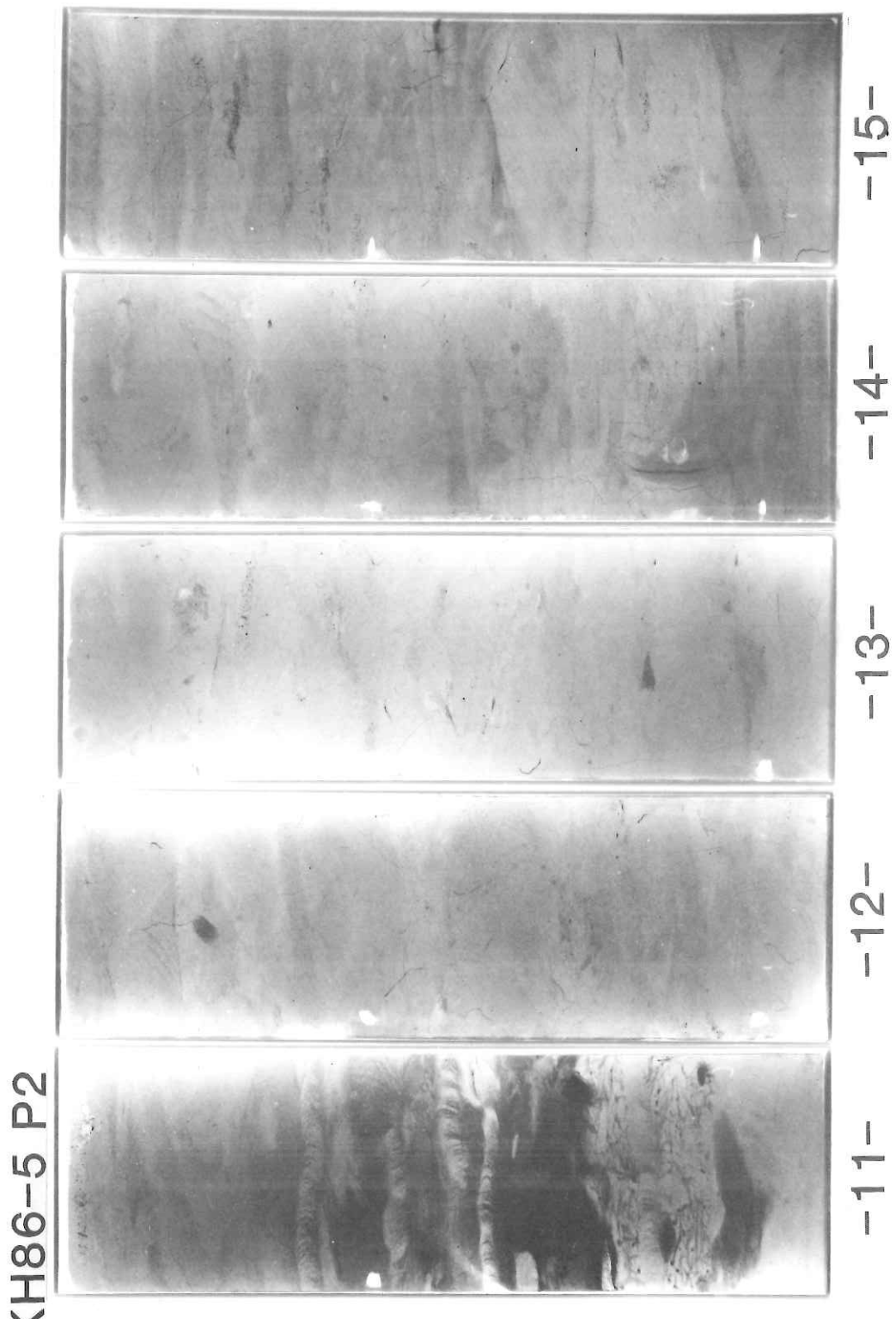
KH86-5 P2
-11-
-12-
-13-
-14-
-15-

KH86-5 P2

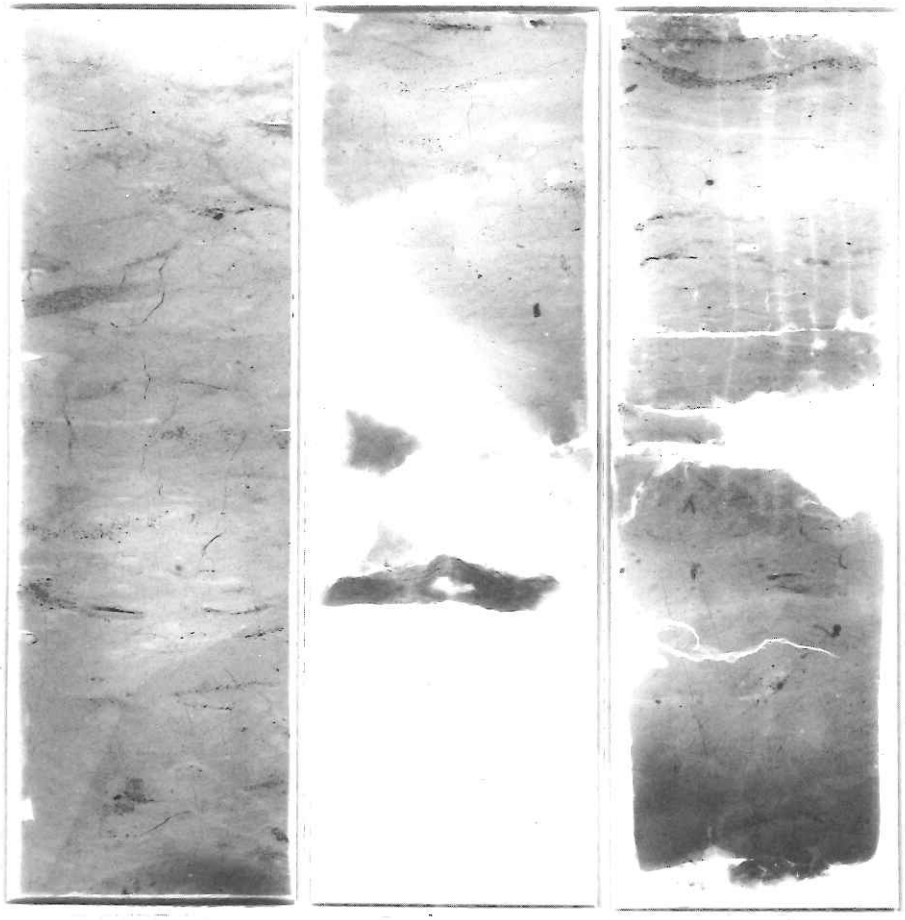

-16- -17- -18-

KH86-5 P3

Location: Lat.:33 11.8'N Water depth 3530 m
Lon.:136 51.4'E Core sample length 634 cm
(the center of unnamed inner slope basin near Daiyon Shima Knoll, off Kumano Trough)

Purpose: to investigate sedimentary structure and biofacies of the typical inner slope basin fill sediment.

The dominant lithology of the core sample is nannofossil-, sponge spicule- and diatom-bearing clay. On the whole, the internal sedimentary structure of core sediment is characterized by being homogeneous and structureless. Relatively harden and fine-grained materials condensed portions are identified in the clay, for example between 47 cm to 52 cm below the top. The layers are not so thick, mostly less than 5 cm in thickness. We tentatively describe it as "clayey mud".

Mafic volcanic ash layers are intercalated between 550 cm to 560 cm and 590 cm to 600 m. Vein-like structures are found in 280 cm below the top. spindle-shape pellets, 3 to 6 mm in longest axis, are commonly included in the uppermost of the clay. The pellets are mantled with a thin transparent membrane. They are thought to be fecal pellets. The pellet with a membrane mantle, however, could not occur below 60 cm from the top. This is probably because diagenesis could dissolve the membrane and make difficult to identify the pellet. Some amounts of different kind pellets could be found from the fillings of the burrows, and the microfossil tests are commonly condensed in the pellet.

OCEAN RESEARCH INSTITUTE UNIVERSITY OF TOKYO

VISUAL CORE DESCRIPTION

K	H	8	6	−	5
STATION			CORE		SEC
P	3				0 I

OBSERVER

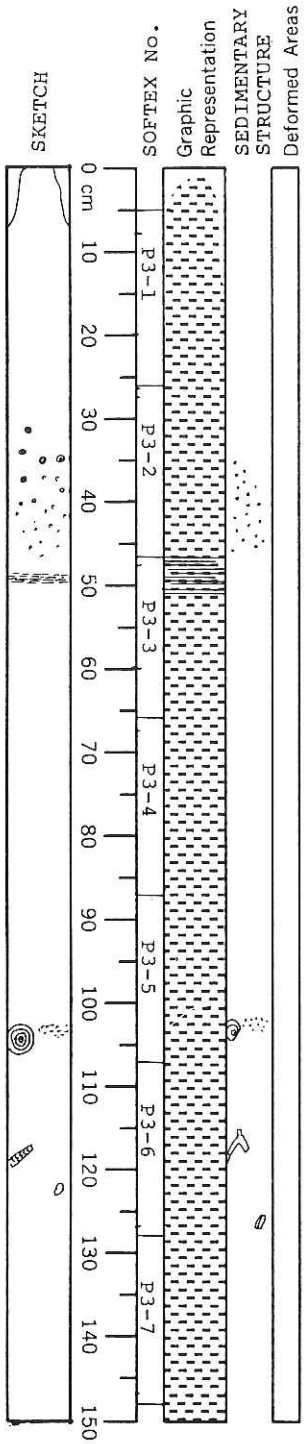

Soupy Nannotossil-, sponge spicule- and diatom-bearing clay and with foraminifers. (2.5GY 5/1)

Burrow-densed zone.
Silty mud (5GY 4/1)
There are many silty pellets in the mud.
The pellets, 1 to 0.5 mm, are spindle shape.

"Clayey mud" (2.5GY 5/1)
Maximum depth for preservation of silty pellets

Nannofossil-, sponge spicule- and diatom-bearing clay (5GY 4/1)
Structureless due to severe bioturbation.

Burrow of concentric shape. In the center, silty pellets are contained.

In the burrow, there are many pellets.
Foraminifers and diatoms are contained in the pellets.
Pumice grain
Nannofossil-, sponge spicule- and diatom-bearing clay

OCEAN RESEARCH INSTITUTE UNIVERSITY OF TOKYO

VISUAL CORE DESCRIPTION

K	H	8	6	—	0	5
STATION			CORE		SEC	
P	3				0	2

OBSERVER

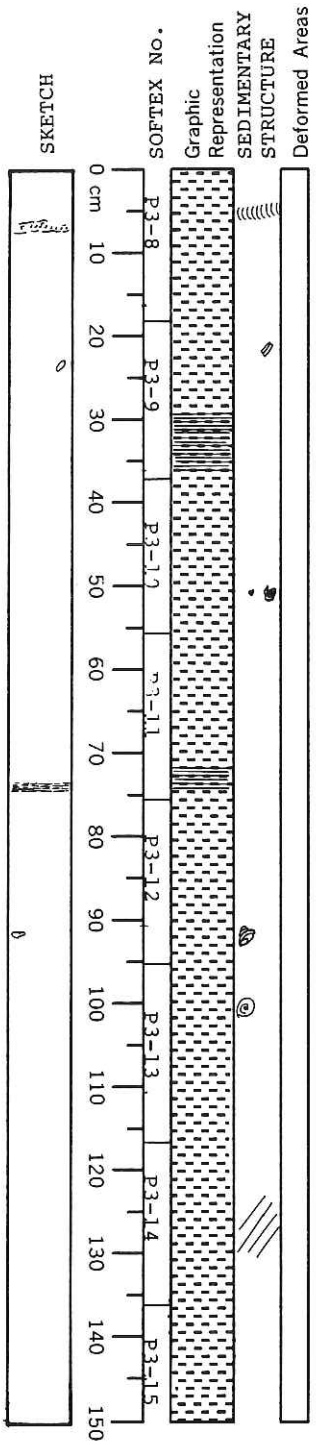

Many pellets, spindle-shape, are contained in the burrow.

Nannofossil-, sponge spicule- and diatom-bearing clay (5GY 4/1), structureless.

Pumice grain

"Clayey mud" (2.5GY 3/1)
Structureless

Nannofossil-, sponge spicule- and diatom-bearing clay

Scoria grains are contained.

"Clayey mud", silt particles less than 10%
(2.5GY 3/1)
Structureless, homogenous.

Nannofossil-, sponge spicule- and diatom-bearing clay
(5GY 4/1)

Shell fragment, 3 mm in diameter.

Nannofossil-, sponge spicule- and diatom-bearing clay

Planolites (?) burrow

Vein-like structure

OCEAN RESEARCH INSTITUTE UNIVERSITY OF TOKYO

VISUAL CORE DESCRIPTION

K	H	8	6	—	0	5
STATION		CORE			SEC	
P	3				0	3

OBSERVER

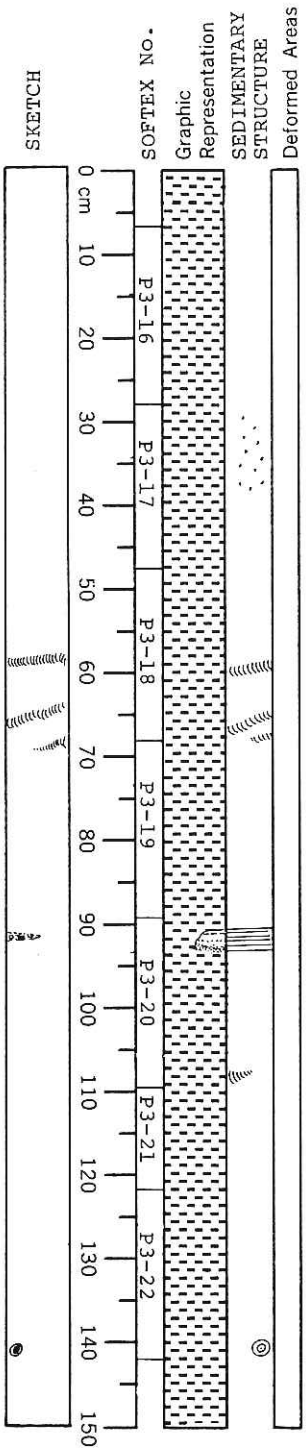

Nannofossil-, sponge spicule- and diatom-bearing clay (5GY 4/1)

Condrites (?) condensed zone

Zoophycus burrows

Burrow with the pellets

Scoria-bearing silt
Sponge-condensed bed, showing crude parallel lamination. The lower contains Sponge sp. and carbonate materials, 2 to 3 mm in diameter.
The upper is free of sponge spicule.
Nannofossil-, sponge spicule- and diatom-bearing clay (5GY 4/1)
Condrites (?) condensed zone.

2 mm in diameter burrow. Foraminifers are condensed in the filling of the burrow.

OCEAN RESEARCH INSTITUTE UNIVERSITY OF TOKYO

K	H	8	6	—	0	5
STATION		CORE			SEC	
P	3				0	4

OBSERVER

VISUAL CORE DESCRIPTION

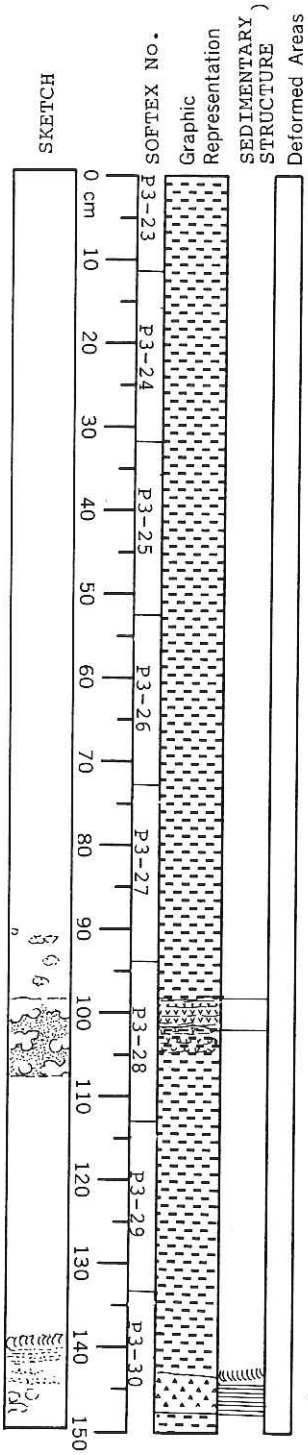

Planorites (?) condesnsed zone

Nannofossil-, sponge spicule- and diatom-bearing clay (5GY 4/1)
Homogeneous

Planorites (?) condensed zone

Structureless

Ashy clay
Burrow developed and condensed zone.
The filling of the burrows is slightly dark in color. (2.5GY 3/1)

Nannofossil-, sponge spicule- and diatom-bearing clay (5GY 4/1)

Planorites (?) condensed zone.
Structureless

Volcanic ash and ashy clay, showing parallel lamination. The ash contains mafic minerals (eg.px)

OCEAN RESEARCH INSTITUTE UNIVERSITY OF TOKYO

K	H	8	6	—	0	5
STATION			CORE		SEC	
P	3				0	5

OBSERVER

VISUAL CORE DESCRIPTION

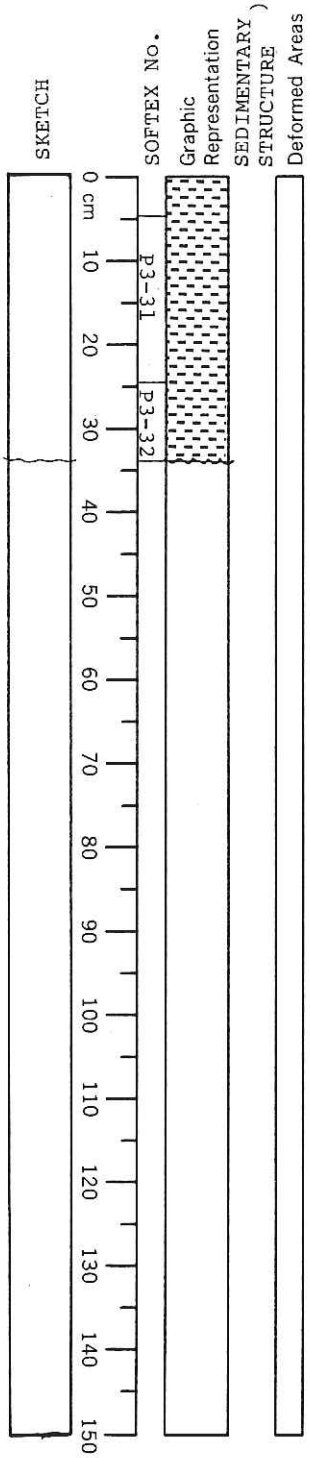

Nannofossil-, sponge spicule- and diatom-bearing clay (5GY 4/1)
Structureless with burrows.

End of the core sample is 634 cm.

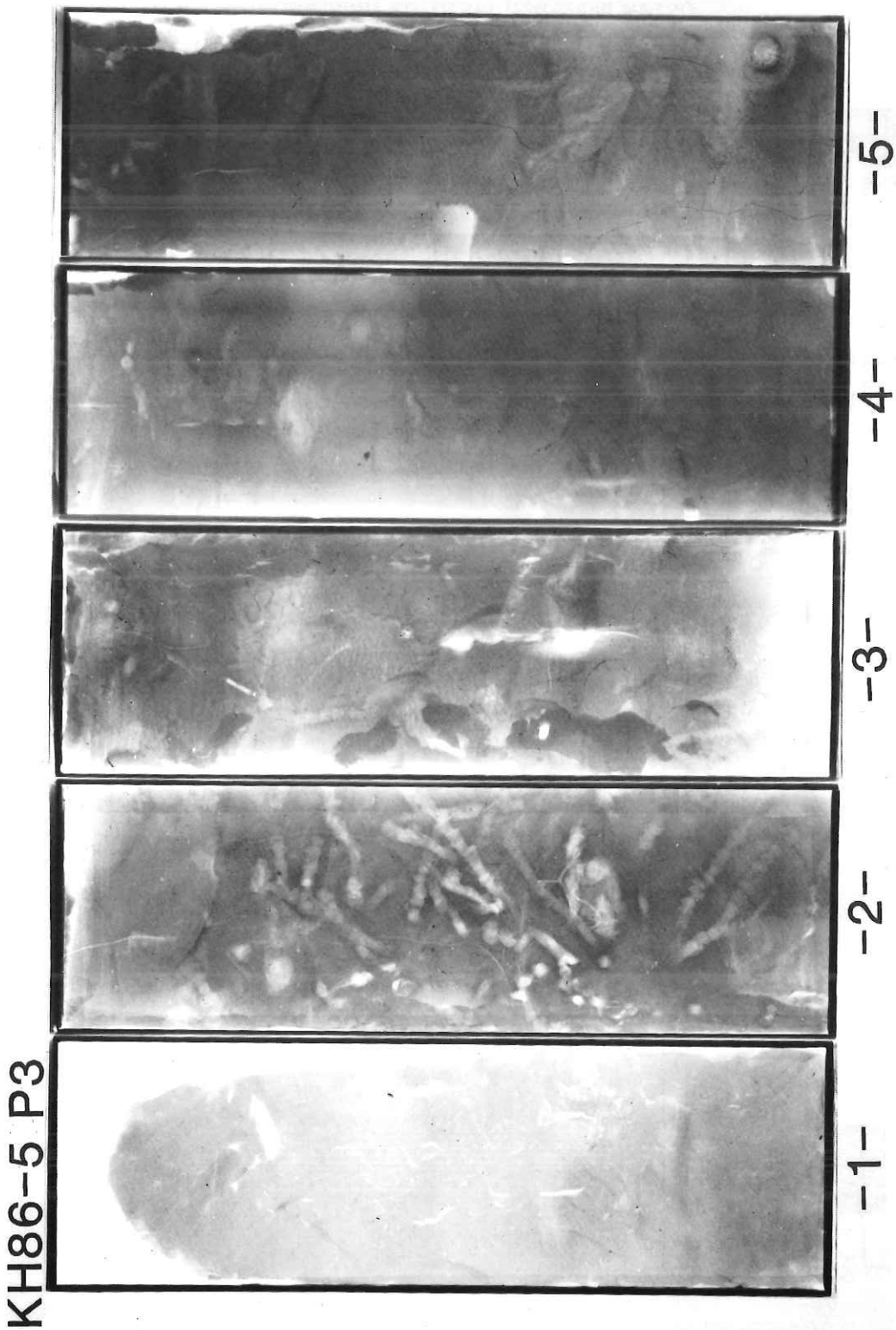
KH86-5 P3
-1-
-2-
-3-
-4-
-5-

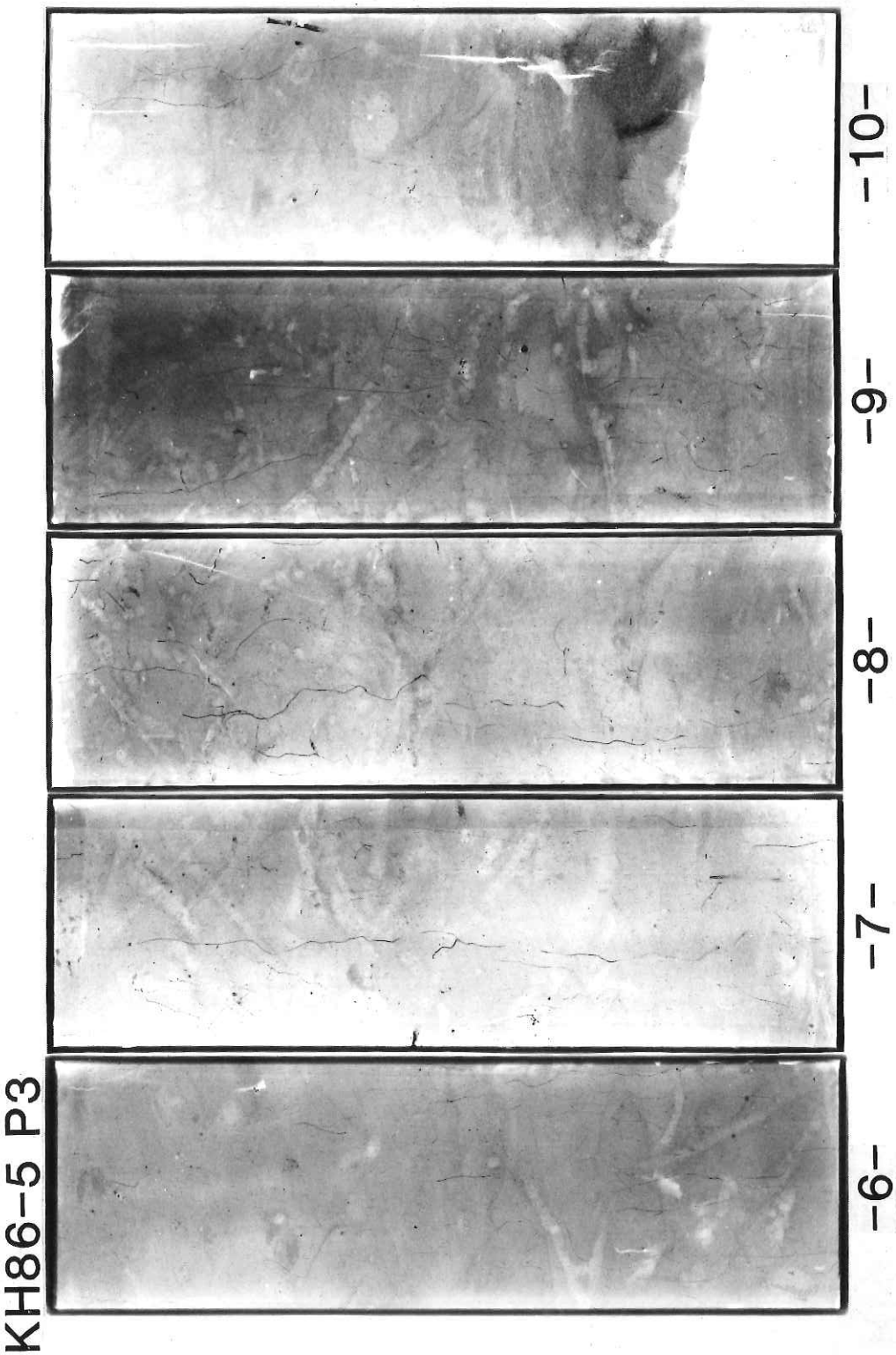
KH86-5 P3
-6-
-7-
-8-
-9-
-10-

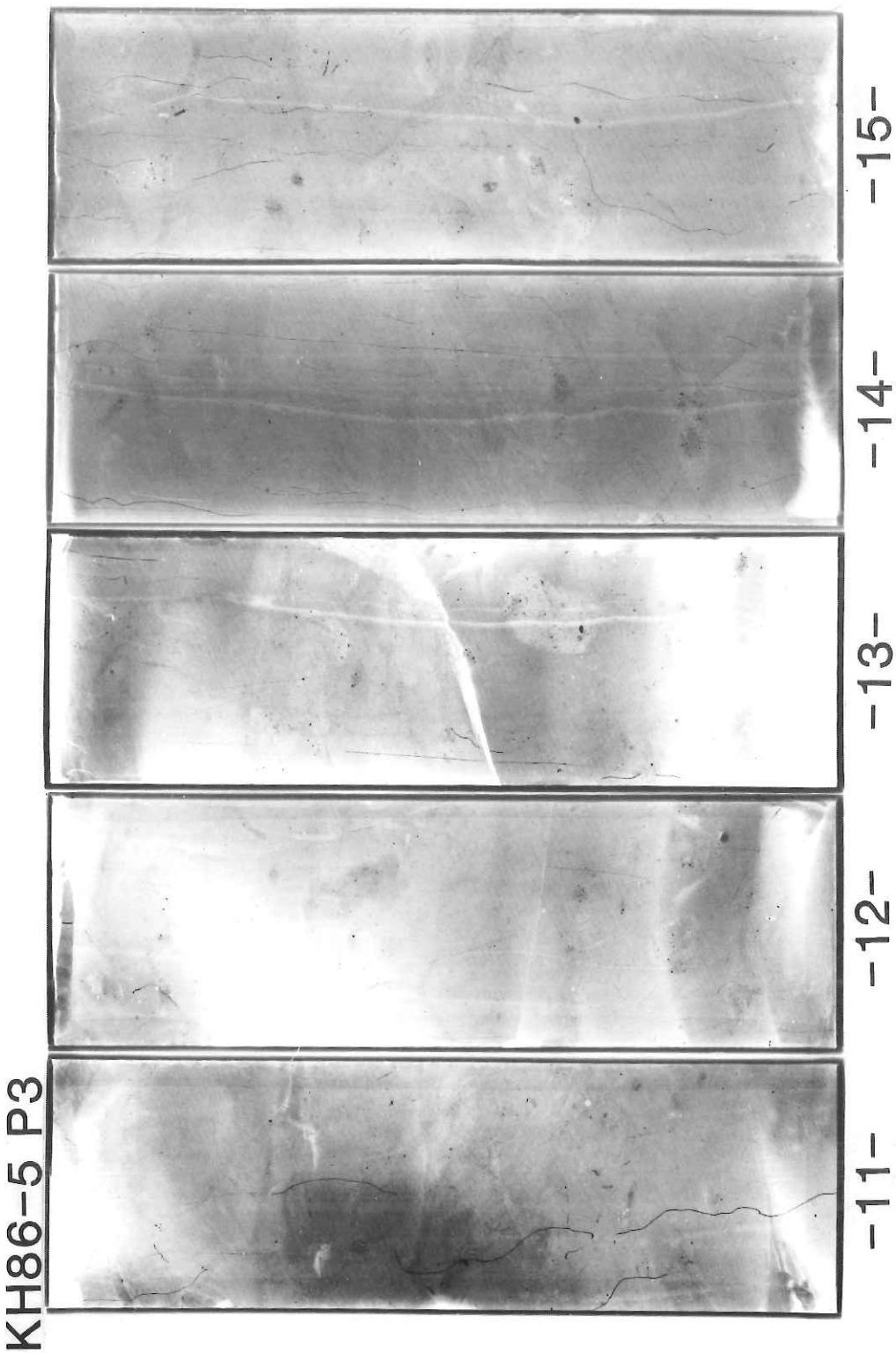
KH86-5 P3
-11-
-12-
-13-
-14-
-15-

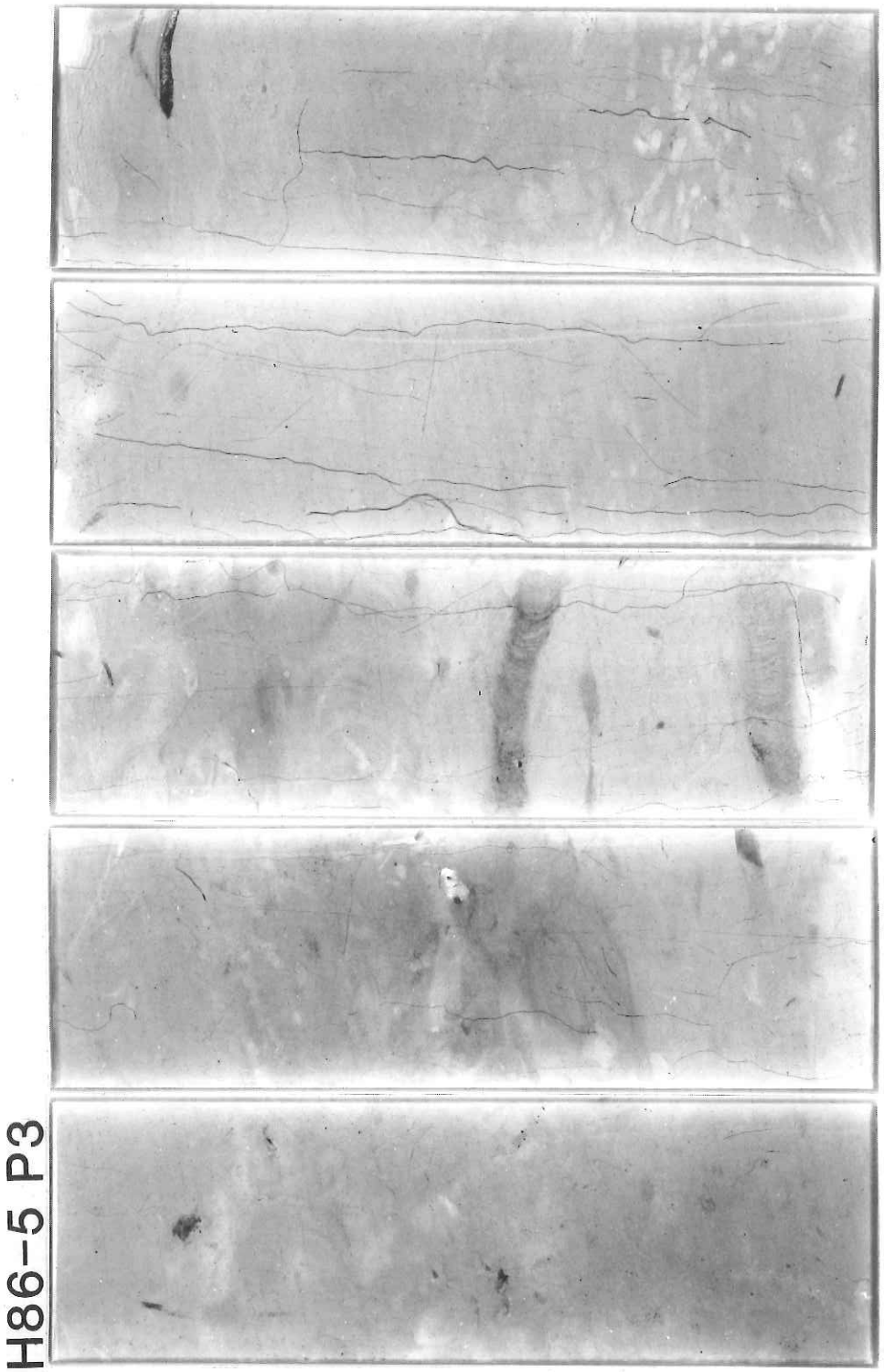
KH86-5 P3
-16-
-17-
-18-
-19-
-20-

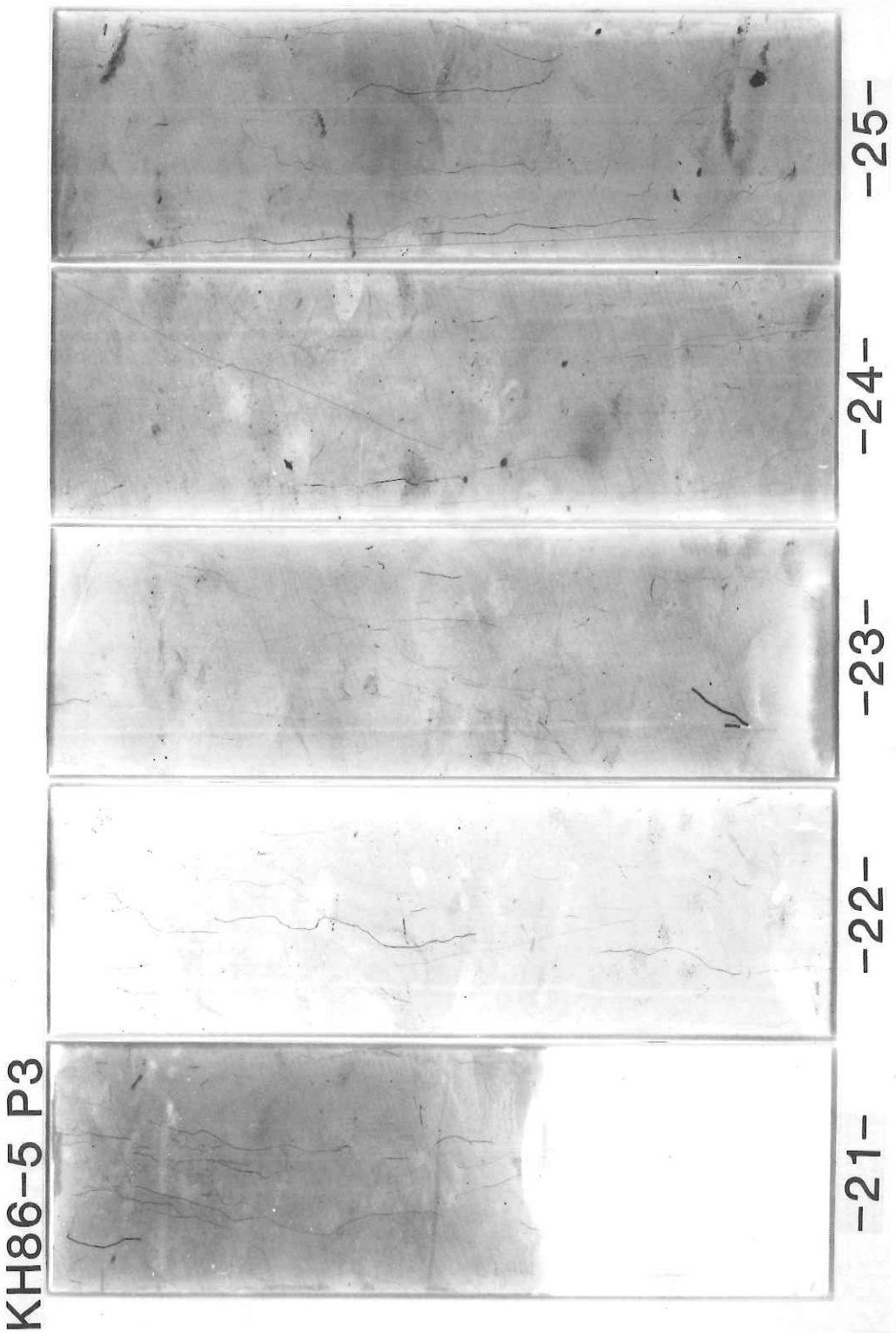
KH86-5 P3
-21-
-22-
-23-
-24-
-25-

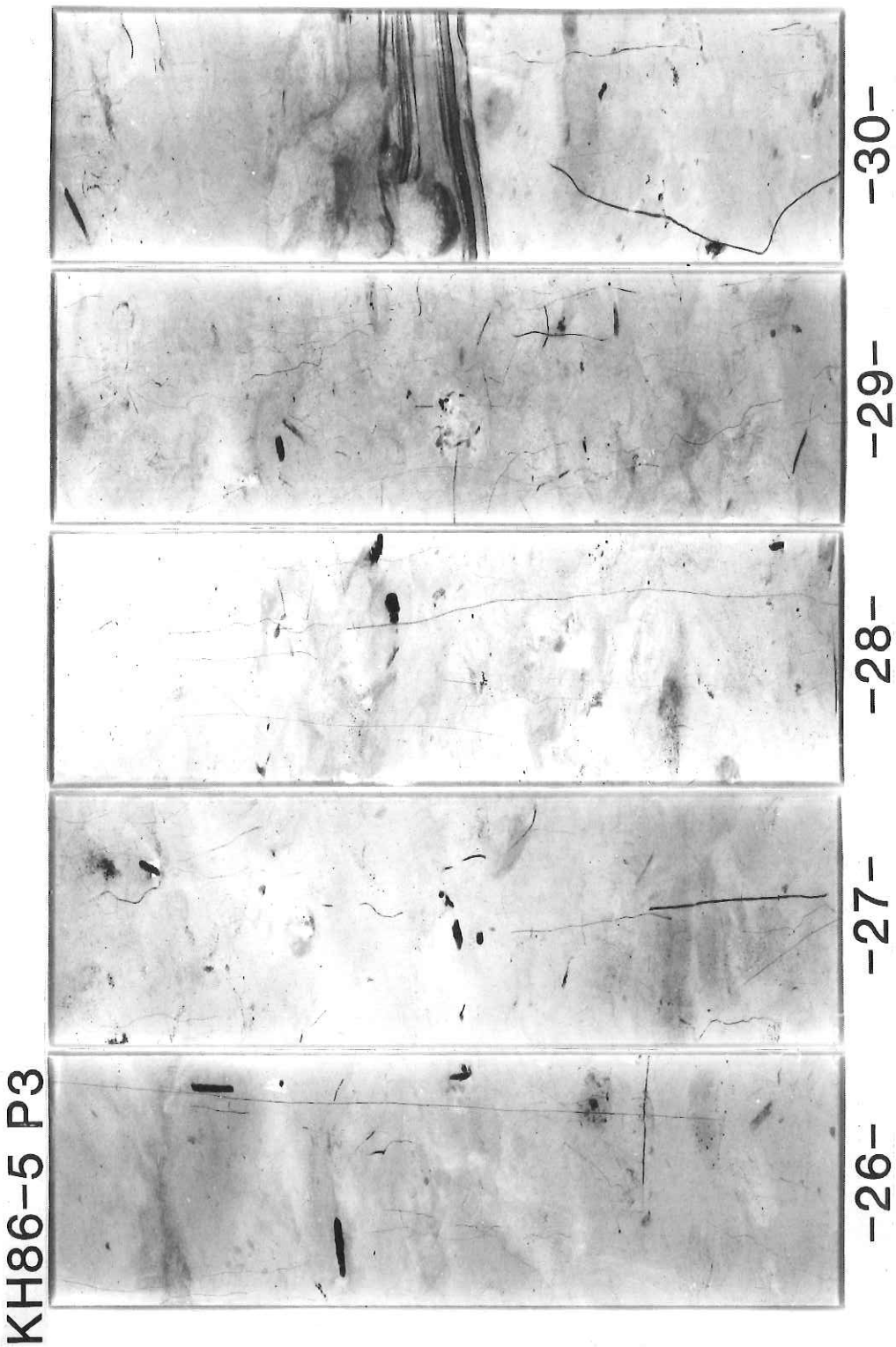
KH86-5 P3
-26-
-27-
-28-
-29-
-30-


KH86-5 P3

KH86-5 P4

Location: Lat.:3314.9'N Water depth 1270 m
Lot.:134 31'E Core sample length 331 cm
(South slope of the Muroto Basin; north of Tosa Bae Embayment)
Purpose: to investigate sedimentary- and bio-facies of the typical fore-arc basin.

The core sample is composed mainly of thin-bedded turbidites. Small amounts of volcanic ash are also contained in this core sample. For example, thick-layered ash is found at the base of the core sample. The turbidites are Tbc and Tb type of sequence. Cross-laminated division (c-division) is usually modified by the bioturbation. 29 turbidites layers could be identified in 331 cm core sample. The other layer consists of ashy clay brown in color, being between 290 to 293 cm below the top. Average thickness of the turbidites is approximately 10 cm. Among them, the sand portion of turbidites is about 2 cm and the mud portion is 8 cm on an averages. The turbidite sand is mainly composed of quartz grains and lithic fragments of shale. Small amounts of plagioclase and volcanic glass, and of foraminifers are also contained in the turbidite sand. The turbidite mud consists of nannofossil- and diatom-bearing clay. The clay contains benthic and planktic foraminifers too. Two distinct ash layers of bubble-walled shard could be identified between 79 to 80 cm, and 310 to 331 cm below the top. The former is intercalated with turbidite sand layer, that is interpreted as a derived ash layer. The latter is thickly bedded and structureless. It should be identified as Kikai-Akahoya Ash (Machida & Arai, 1978), judging from the similarity of the refractive index and mineral composition. Plant debris, up to 5.1 cm in the longest axis, are included in the turbiditic sand, at 273 cm below the top. According to 14C analysis, the depositional age of plant debris would be 5260 +90 yrs B.P. (Suk et al., in this report). *Scolicia* (burrow) is well developed in the upper surface of the turbidite sand. So, the upper portion of the sedimentary structure of sand layer is usually modified after deposition. The other burrow such as *Zoophycus*, seem to be poorly developed.

OCEAN RESEARCH INSTITUTE UNIVERSITY OF TOKYO

VISUAL CORE DESCRIPTION

STATION	CORE	SEC
K H 8 6 — 0 5		
P 4		0 I

OBSERVER

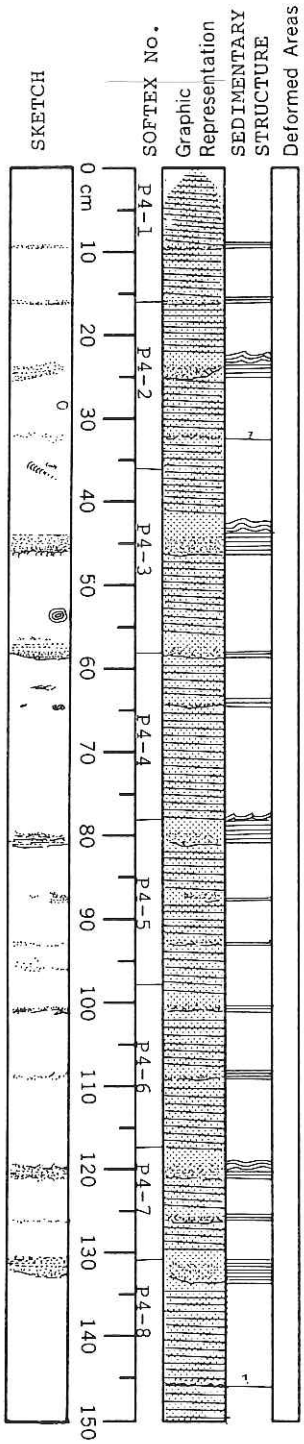

Soupy nannofossil- and diatom-bearing clay

Very fine-grained sand

Nannofossil- and diatom-bearing clay (5GY 3/2)
Structureless
Fine-grained sand, cut-and-fill structure.
Parallel lamination to cross lamination (Tbc type)

Crude laminated sand (Tbc type)

Parallel-laminated sand (very fine- to fine-grained sand)

parallel-laminated ash layer interbedded with sand (resedimented ash)

Scolicia burrow

Tb type; base cut the underlying clay

Tbc type; the upper is modified by Scolicia burrow

OCEAN RESEARCH INSTITUTE UNIVERSITY OF TOKYO

VISUAL CORE DESCRIPTION

K	H	8	6	–	0	5
STATION			CORE		SEC	
P	4				0	2

OBSERVER

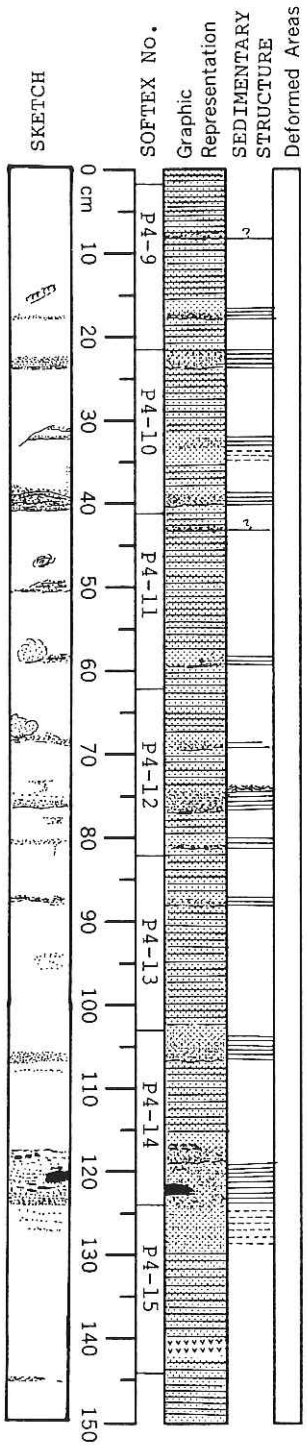

Nannofossil- and diatom-bearing clay
(5GY 3/2)

The layer can be divided into two portion.
The upper one is composed of fine-grained sand-and-silt layer, that shows parallel lamination. The lower is composed of foraminifer-and-silt layer.
The lower boundary is not well-defined.

Nannofossil- and diatom-bearing clay
Structureless

Crude parallel-laminated sand
Very fine-grained sand .

Parallel-laminated and cross-laminated sand (Tbc)
The upper is modified by Scolicia burrow.

Nannofossil- and diatom-bearing clay.
Structureless

Plant debris

large fragment of plant debris
Crude parallel-laminated sand and silt

Crude parallel-laminated foraminifers and silt.
The base is not well-defined.

Ashy clay (?)

OCEAN RESEARCH INSTITUTE UNIVERSITY OF TOKYO

K	H	8	6	–	0	5
STATION			CORE		SEC	
P	4				0	3

OBSERVER

VISUAL CORE DESCRIPTION

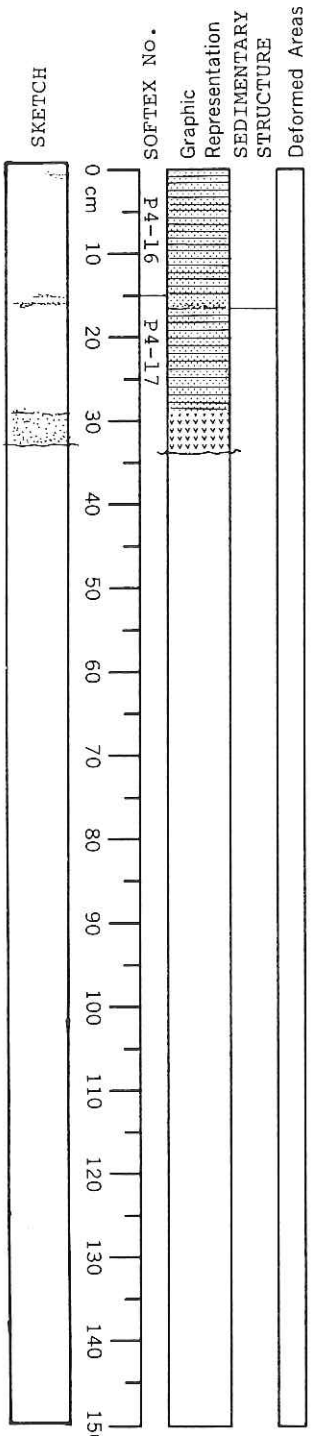

Nannofossil- and diatom-bearing clay
(5GY 4/2)

Volcanic glass, structureless

End of the core sample (331 cm)

KH86-5 P4

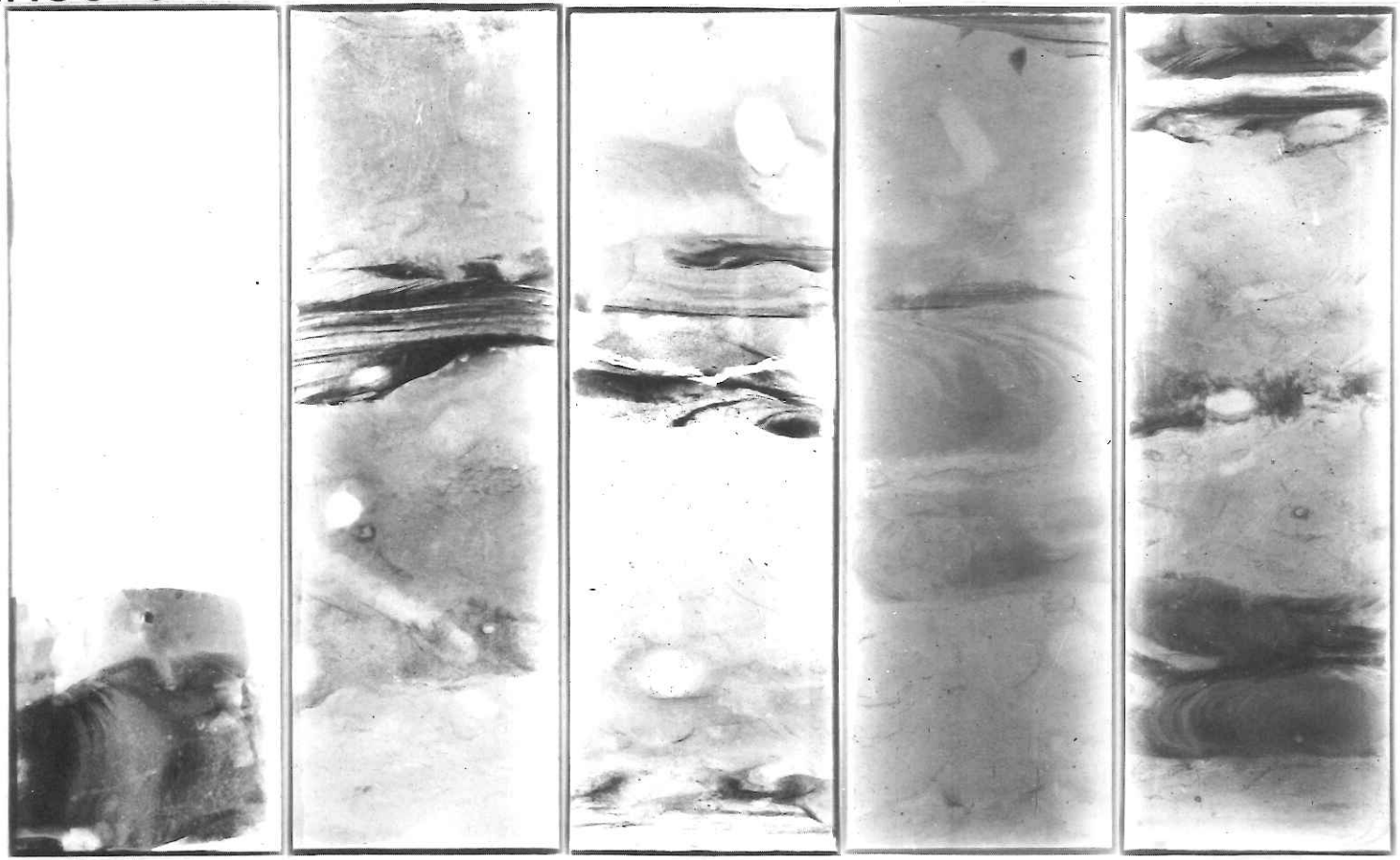

-1- -2- -3- -4- -5-

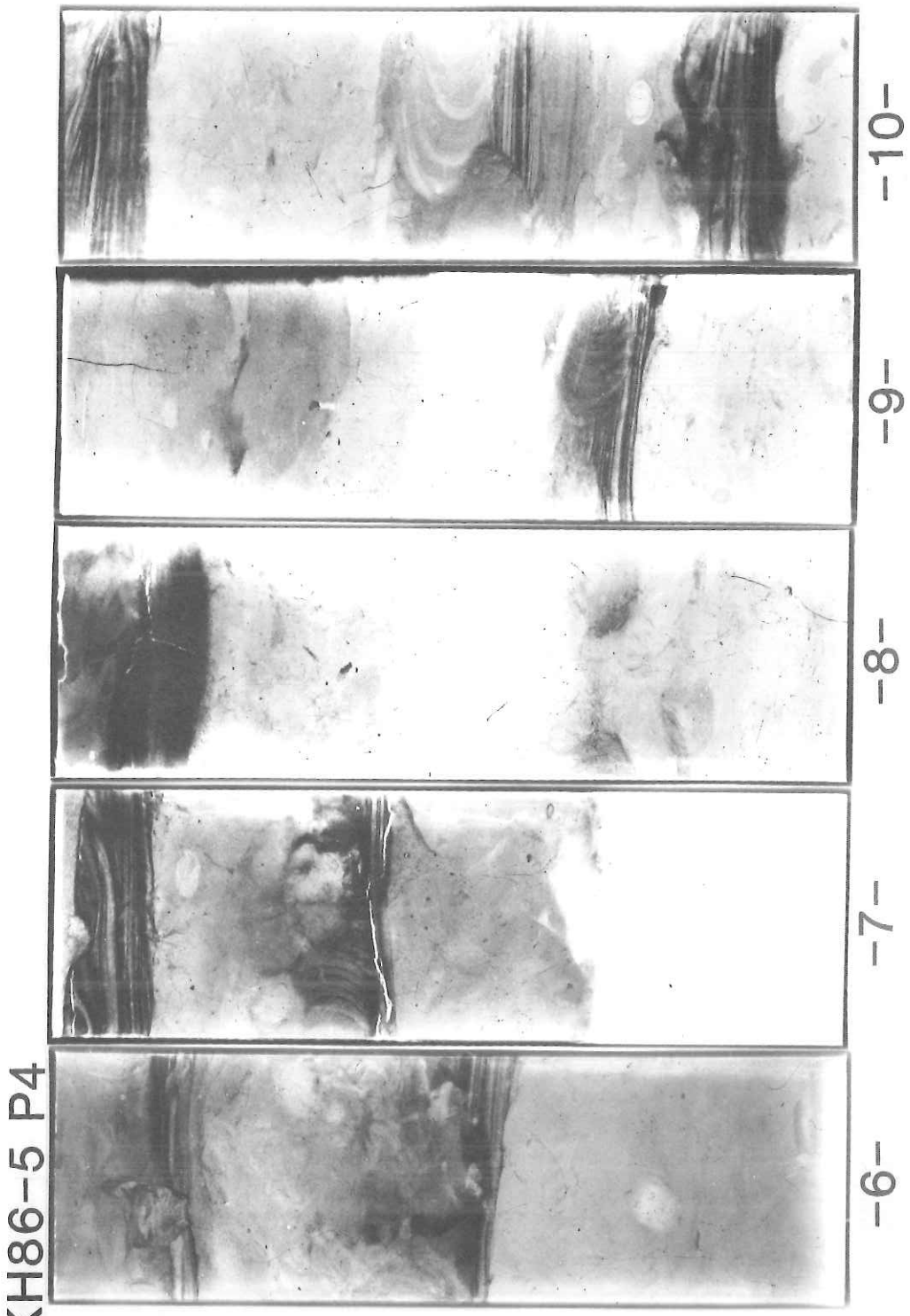
KH86-5 P4
-6-
-7-
-8-
-9-
-10-

KH86-5 P4

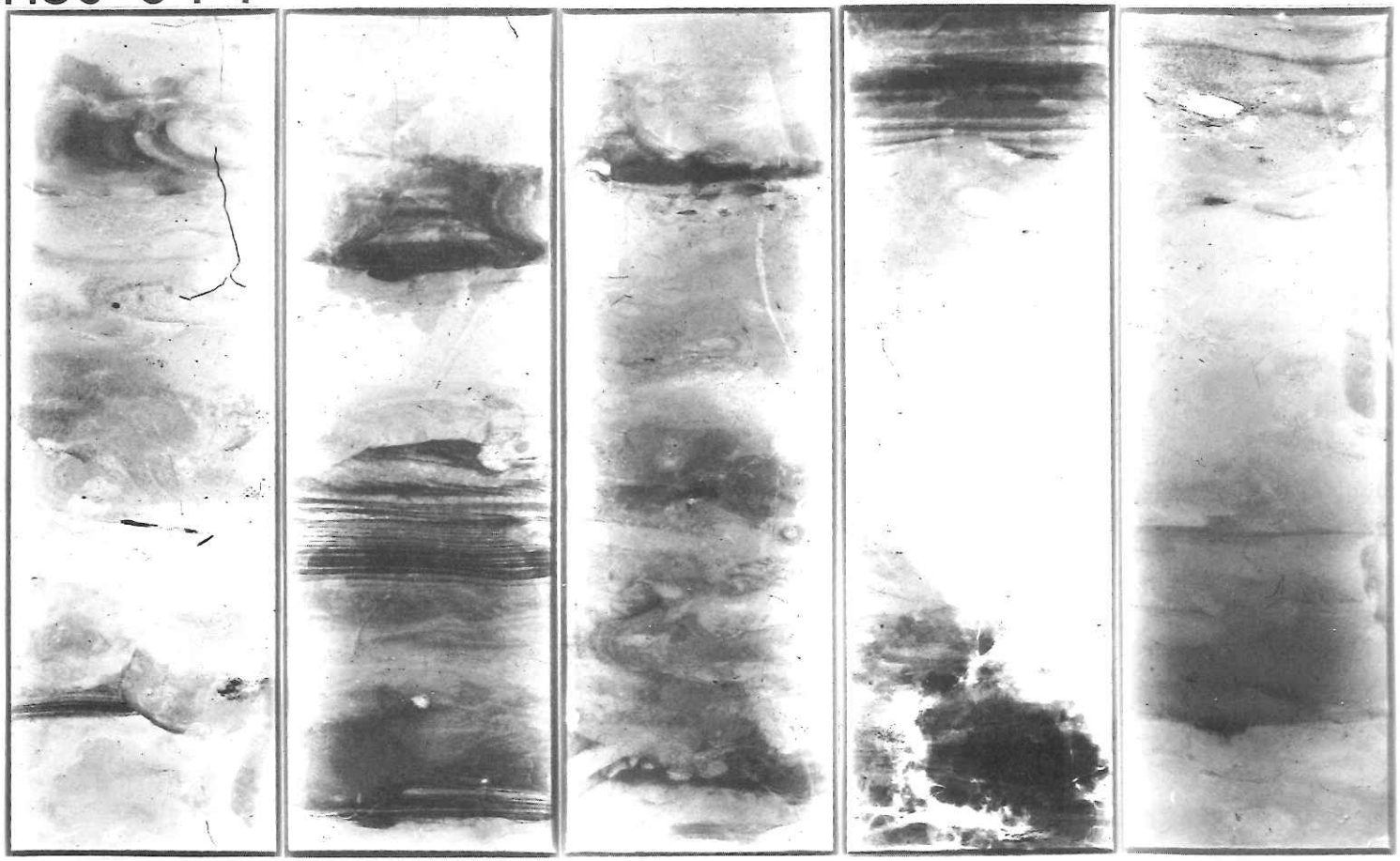

-11- -12- -13- -14- -15-

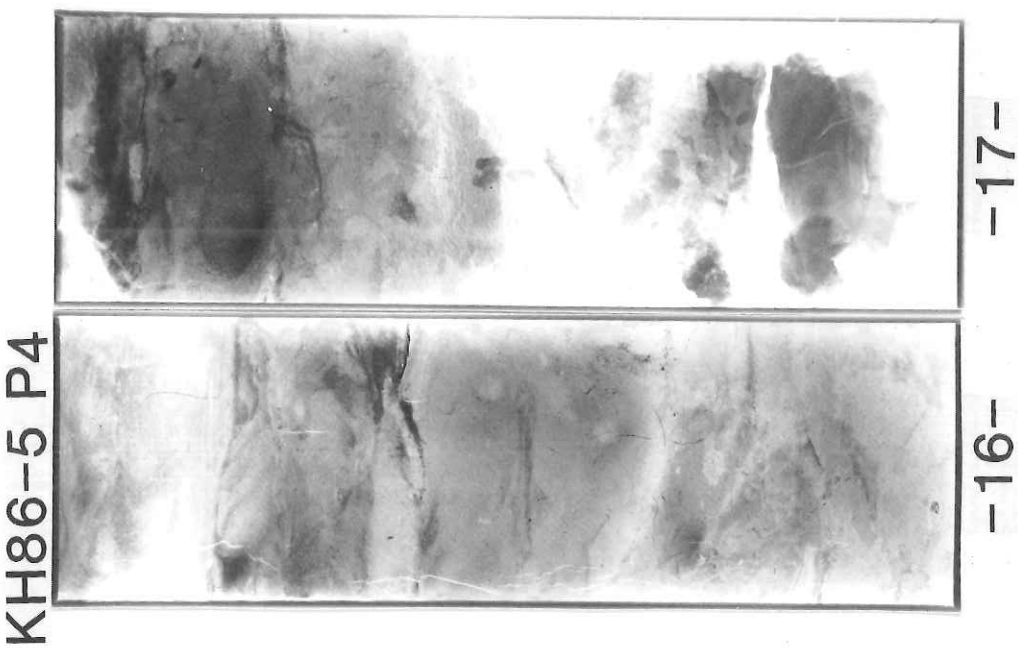
KH86-5 P4
-16-
-17-

KH86-5 P5

Location: Lat.:33 13.74'N Water depth 1240 m
Lon.:134 28.95'E Core sample length 339 cm
(South slope of the Muroto Basin; north of Tosa Bae Embayment)
Purpose: to investigate sedimentary- and bio-facies of the typical fore-arc basin.

The dominant lithology of the core sample is composed of thin-bedded turbidites with thick, layered volcanic ash at the base. The main lithology of this core sample is quite similar to that of P4 as mentioned above. And thick layered ash is also found in the base of the core sample. The turbidites are Tbc and Tb types of turbidite sequence. Cross-lamination of the turbidite (c-division) is usually modifies by the bioturbation, mainly of *Scolicia* burrow. 38 turbidite layers could be identified in 339 cm core sample. The sand consists of quartz, plagioclase, lithic fragments of shale and volcanic glass. The sand composition is quite similar to that of P4. The mud is composed of nannofossil- and diatom-bearing clay. Some amounts of foraminifers also found. The detail comparison between P4 and P5 in lithology and grain size were done by P. Blum (in this report).

OCEAN RESEARCH INSTITUTE UNIVERSITY OF TOKYO

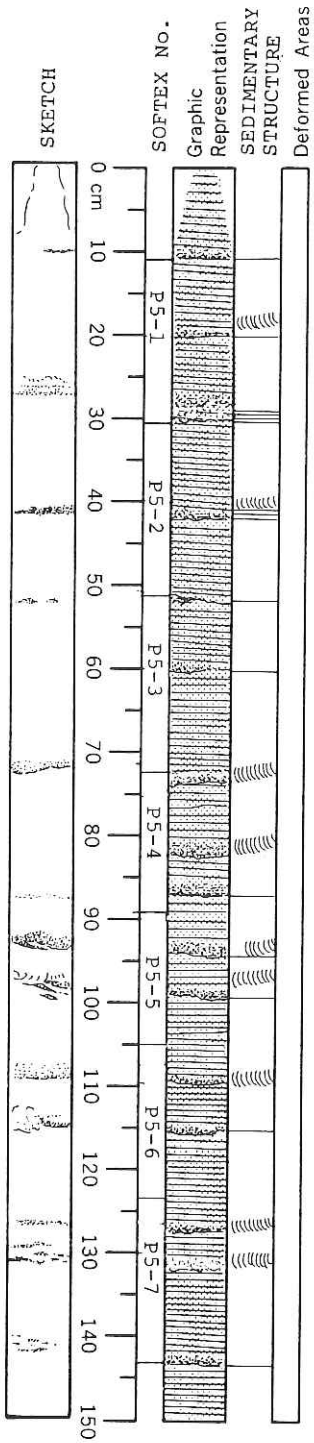

VISUAL CORE DESCRIPTION

K	H	8	6	—	0	5
STATION			CORE		SEC	
P	5				0	1

OBSERVER

Soupy nannofossil-, sponge spicule- and diatom bearing clay (7.5Y 4/2)

Very fine-grained sand (shale frag. & qtz ect.)

Nannofossil- and diatom bearing clay (5GY 4/2)

Very fine-grained sand

Nannofossil- and diatom bearing clay
(Plagioclase, volcanic glass, foraminifer and sponge.)

Very fine-grained sand, crude parallel lamination

Within the sand, derived foraminifers are contained.

Pinched-out sand

Planolites (?)

Nannofossil- and diatom bearing clay
(plagioclse, sponge spicule and foraminifer)

Crude cross laminated-sand with mud drapes

Crude parallel-laminated sand

Parallel-laminated sand (Very fine-grained sand)

Parallel-laminated sand (Very fine-grained sabd)

OCEAN RESEARCH INSTITUTE UNIVERSITY OF TOKYO

K	H	8	6	–	0	5
STATION			CORE		SEC	
P	5				0	2

OBSERVER

VISUAL CORE DESCRIPTION

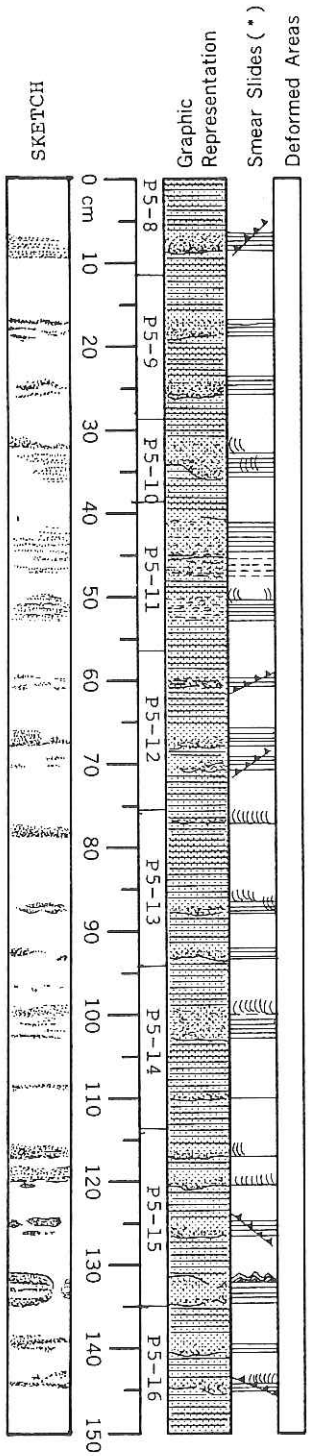

Nannofossil- and diatom-bearing clay

Crude parallel-laminated sand
(sedimentary structure is cut by fractures)

Crude parallel-laminated sand

Parallel- to wavy-laminated sand

Nannofossil- and diatom-bearing clay

Crude parallel-laminated sand
(qtz, shale frag. and foraminifer with green horblende and biotite)

Upper portion shows well-developed parallel lamination
(fine-grained sand and mud drape)
Lower portion shows crude parallel lamination.
(Silt, foraminifers and mud drape)
Parallel-laminated sand with a drop stone.
Nannofossil- and diatom-bearing clay

Very fine-grained sand with fracturing.

Sheared sand layer

Nannofossil- and diatom-bearing clay
(clay mineral, nannofossil, diatom, sponge spicule plagioclase etc.)

Parallel-laminated sand

Structureless sand due to bioturbation.

Structureless sand due to bioturbation.

Tbc type turbidite
In sand layer foraminifers are condensed.

OCEAN RESEARCH INSTITUTE UNIVERSITY OF TOKYO

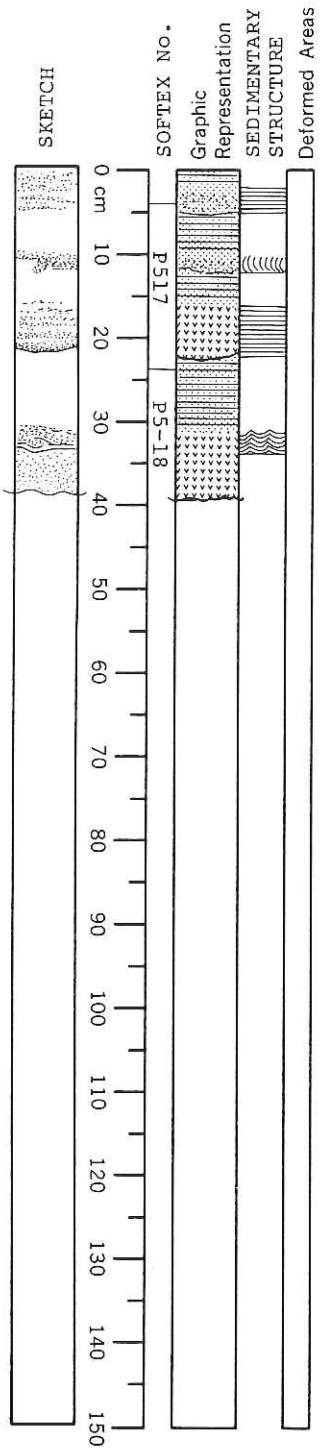

VISUAL CORE DESCRIPTION

K	H	8	6	—	0	5
STATION			CORE		SEC	
P	5				0	3

OBSERVER

Parallel laminated sand
(fine-grained sand)

Parallel-laminated volcanic glass
(resedimented ash layer)

Volcanic glass, upper portion shows cross lamination.
LOwer portion indicates structureless.
End of the core sample (339 cm)

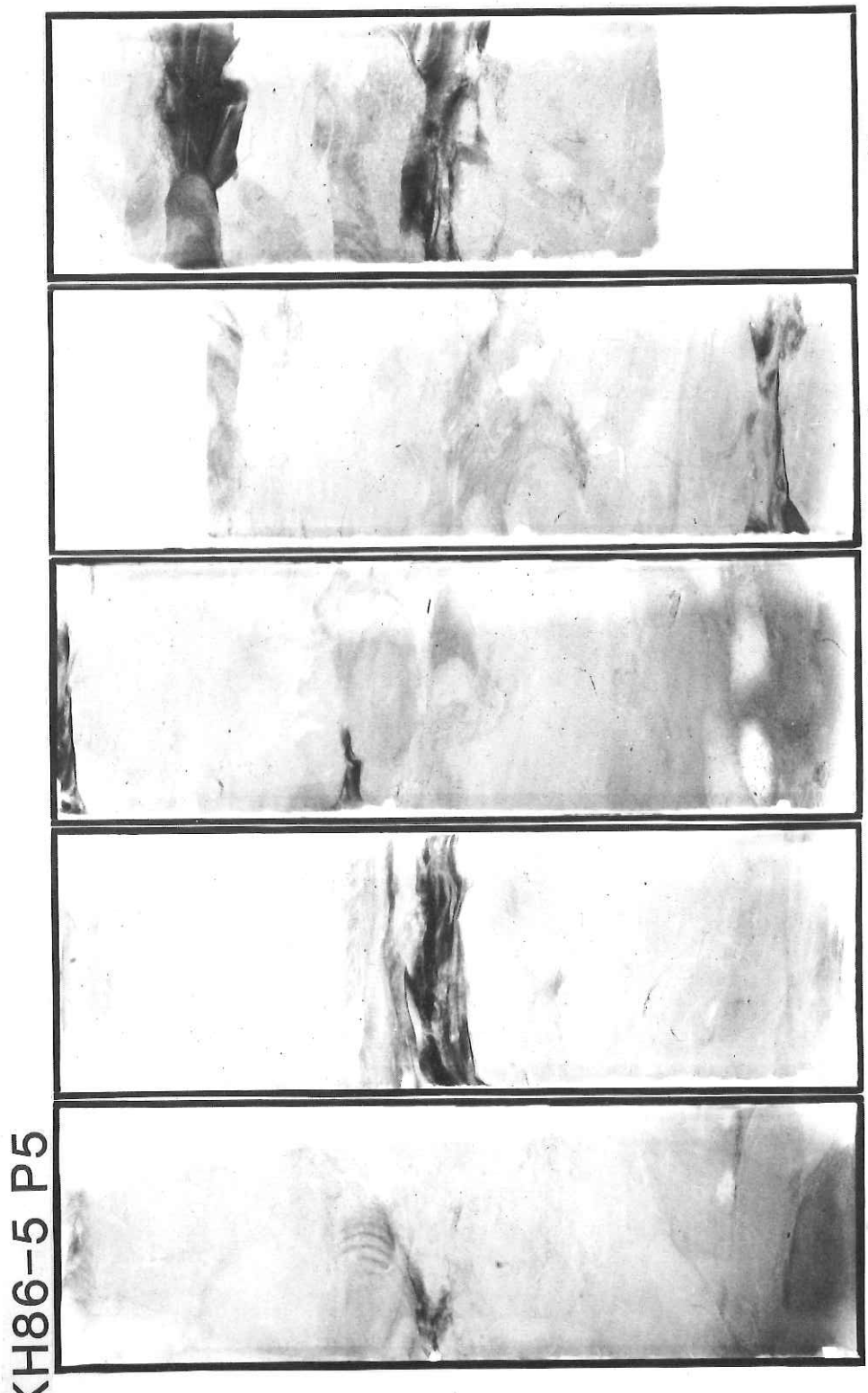
KH86-5 P5
-1-
-2-
-3-
-4-
-5-

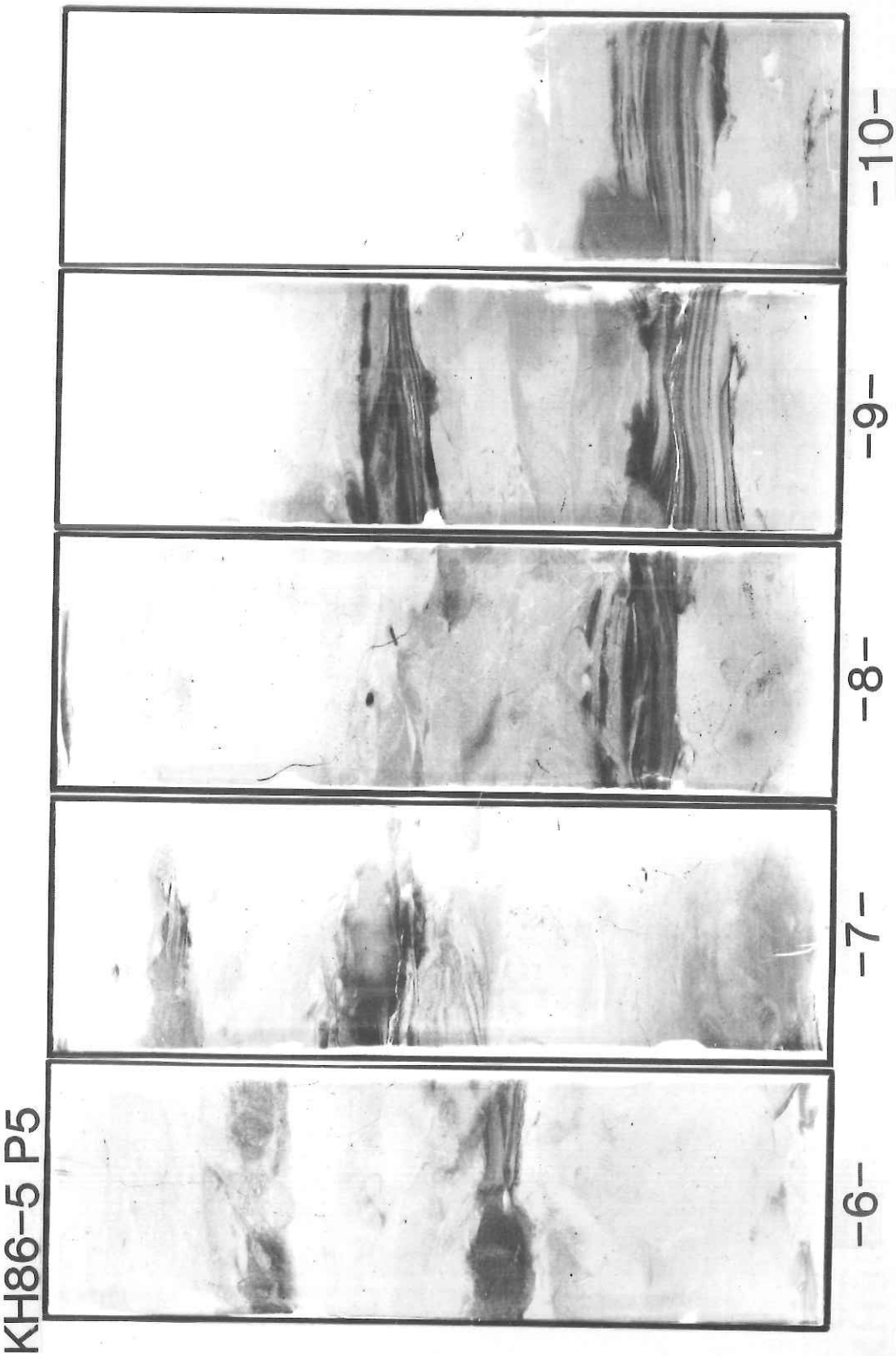
KH86-5 P5
-6-
-7-
-8-
-9-
-10-

KH86-5 P5

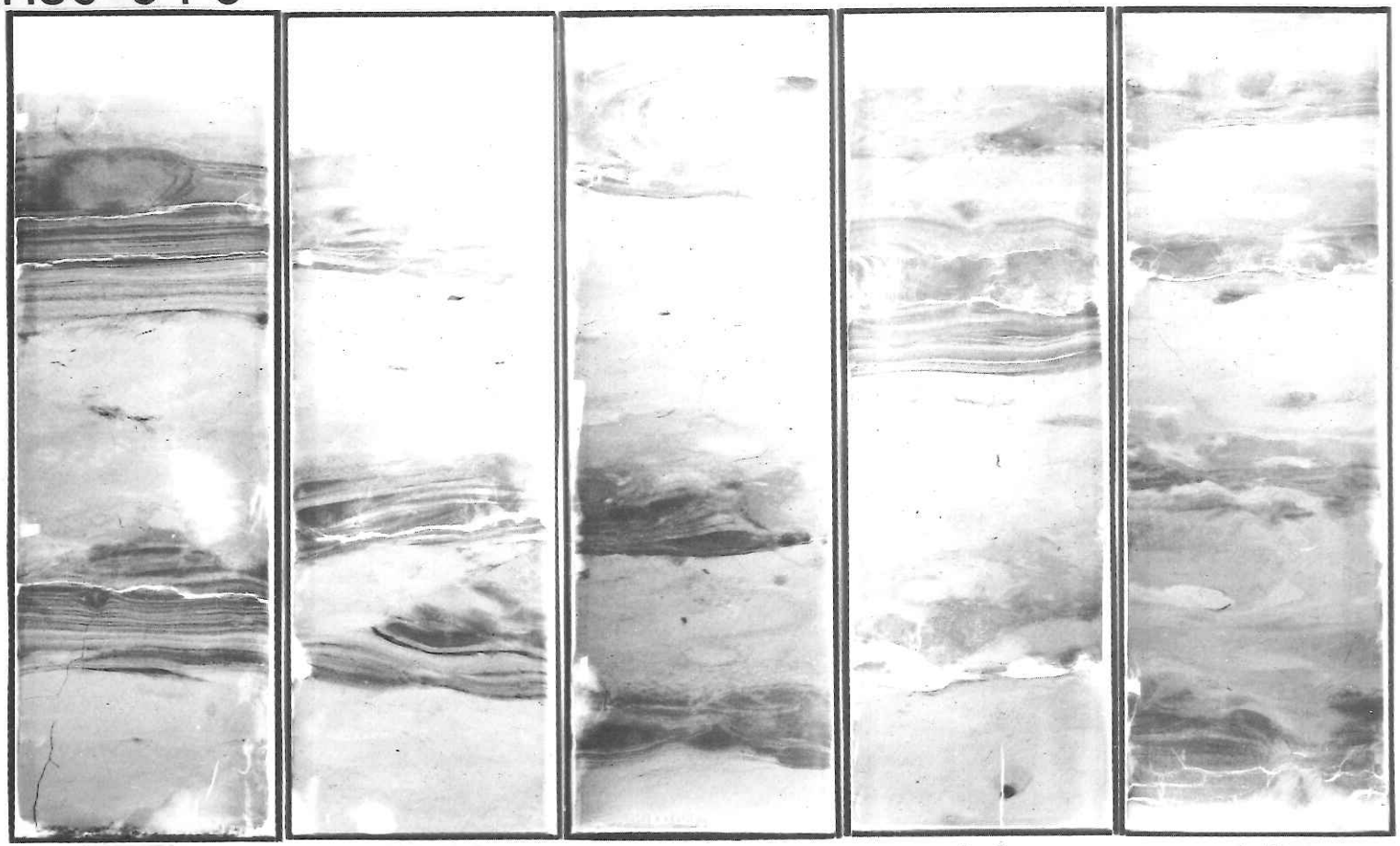

-11- -12- -13- -14- -15-

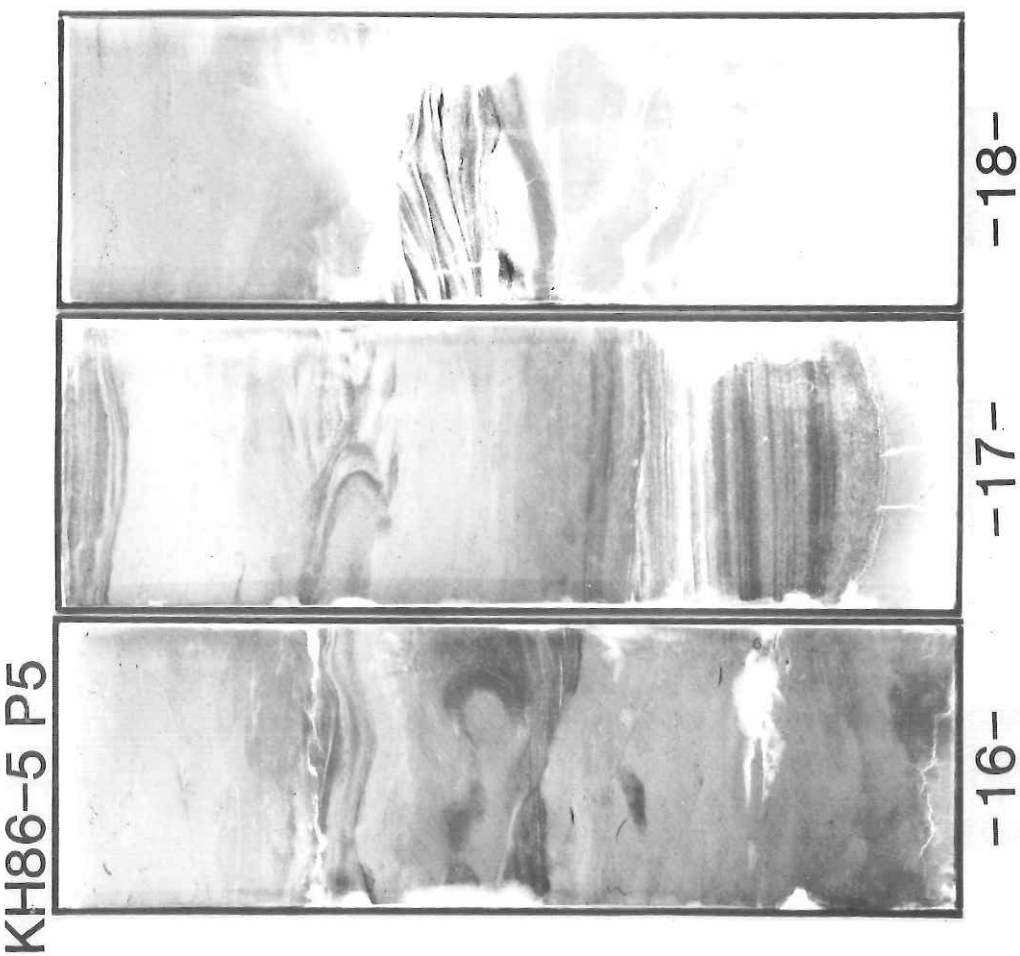
KH86-5 P5
-16-
-17-
-18-

KH86-5 P6

Location: Lat.:32 17.9'N Water depth 4800 m
Lon.:135 00.9'E Core sample length 440 cm
(South slope of the Muroto Basin; north of Tosa Bae)
Purpose: to investigate sedimentary- and bio-facies of the typical distal trench channel fills.

P6 is mainly composed of thin-bedded distal turbidites, and the composition is carbonate-free siliceous clay. The turbidites consists mainly of turbiditic mud with some amount of fine-to very fine-grained turbiditic sand. Most of them show Tbc sequences. The turbiditic mud consists of nannofossil-bearing siliceous clay with little amount of foraminifers and carbonate debris. The turbiditic sand is mainly composed of quartz, plagioclase, lithic fragments such as shale and volcanics. The mineral composition is similar to that of trench axis channel fill off Tenryu submarine fan reported by Taira & Niitsuma (1986) and Soh (1986). It means that the turbidite is provided from the drainage basin of Fujikawa River, the Izu collision zone. The carbonate-free siliceous clay is composed of diatom, sponge spicule and clay minerals with little amount of volcanic glass. Carbonate materials such as nannofossils or foraminifers are not included in the siliceous clay. Glauconite grains are found near the base of the carbonate-free siliceous clay layers, for examples, at 36 cm and 94 cm below the top. Judging from the detailed observation of grain morphology under microscope, we interpret that the glauconite is a authigenic mineral formed as a infilling of foraminifer, and that the test of foraminifer had been already dissolved as a result of accumulation below CCD.

The most striking fact is that the core sample contained a large amount of natural gasses. The gasses are thought to be mostly composed of methane with little amount of sulfate gasses such as hydrogen sulfide. The boundary between the oxidic and anoxidic (sulfate-reducing) zones can be identified at 50 cm to 60 cm below the top. The core samples were redolent of sulfide. Pyrites were found in the anoxidic zone. However, they disappeared as soon as oxidation took place. Authigenic calcite is not found. As shown in soft X-ray photograph, there are much vacant space in the core sediments. This is thought to be caused by gas expansion chiefly on board, because we on board large amounts of natural gasses were abruptly released from the core sample. Bioturbation, such as burrows, seems to be less developed in the core sample. This is likely to be as a result of the anoxidic environment. That is small animal activity making the burrows could not be so active, but the bacteria should be more active in the anoxidic environment.

OCEAN RESEARCH INSTITUTE UNIVERSITY OF TOKYO

VISUAL CORE DESCRIPTION

K	H	8	6	—	0	5
STATION			CORE		SEC	
P	6				0	I

OBSERVER

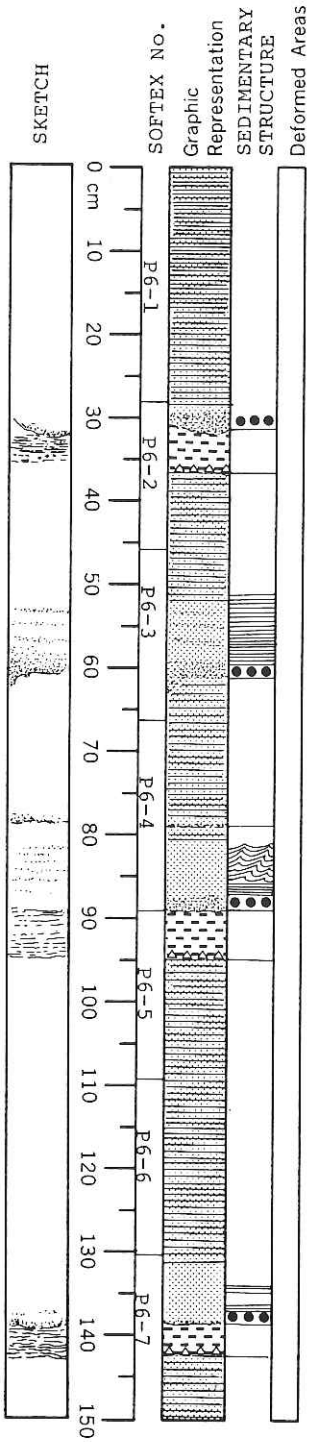

Soupy nannofossil-bearing siliceous clay (2.5GY 4/1)

Fine-grained sand (N 1.5/0)
Nannofossil-free siliceous clay
Glauconite grain in the base

Nannofossil-bearing siliceous clay (2.5GY 4/1)

Reduction patches are dotted.

Silt (2.5GY 4/1)

Fine-grained sand (2.5GY 2/1)

Nannofossil-bearing siliceous clay (5GY 2/1)

Reduction patches are increased toward the base of the clay layer.

Silt to very fine-grained sand (N 1.5/0)

Very fine-grained to fine-grained sand
Siliceous clay (N 1.5/0; after oxidation: 5Y 4/2)
(Calcareous material-free)
Glauconite grains at the base

Nannofossil-bearing siliceous clay
(N 1.5/0; after oxidation: 5Y 4/2)
Structureless

Silt (N 1.5/0; after OX.:N 2/0)

Siliceous clay (N 1.5/0; after OX.: 5Y 4/2)

Nannofossil-bearing siliceous clay
(N 1.5/0; after oxidation: 2.5GY 4/1)
Spindle-shape pelletsare contained.

OCEAN RESEARCH INSTITUTE UNIVERSITY OF TOKYO

K	H	8	6	—	0	5
STATION			CORE		SEC	
P	6				0	2

OBSERVER

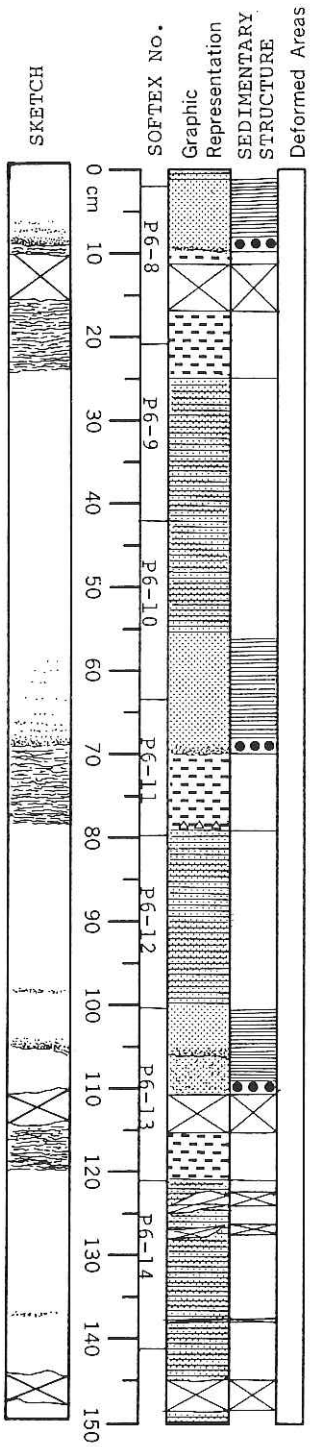

VISUAL CORE DESCRIPTION

Silt (N 1.5/0)

Fine-grained sand (N 1.5/0)

Siliceous clay (N 1.5/0; after OX.;5Y 4/2)

Nannofossil-bearing siliceous clay, structureless
(N 1.5/0; after oxidation; 2.5GY 4/1)

Silt and silty mud (N 1.5/0; after OX.:N 2/0)

Silt to very fine-grained sand

Siliceous clay

Glauconite grains are contained near the base.

Nannofossil-bearing siliceous clay, structureless
(N 1.5/0; after oxidation; 2.5GY 4/1)

Silt to very fine-grained sand

very fine-grained sand

Siliceous clay (N 1.5/0; after OX.: 5Y 4/2)

Nannofossil-bearing siliceous clay, structureless
(N 1.5/0; after oxidation; 2.5GY 4/1)

OCEAN RESEARCH INSTITUTE UNIVERSITY OF TOKYO

K	H	8	6	–	0	5
STATION		CORE			SEC	
P	6				0	3

OBSERVER

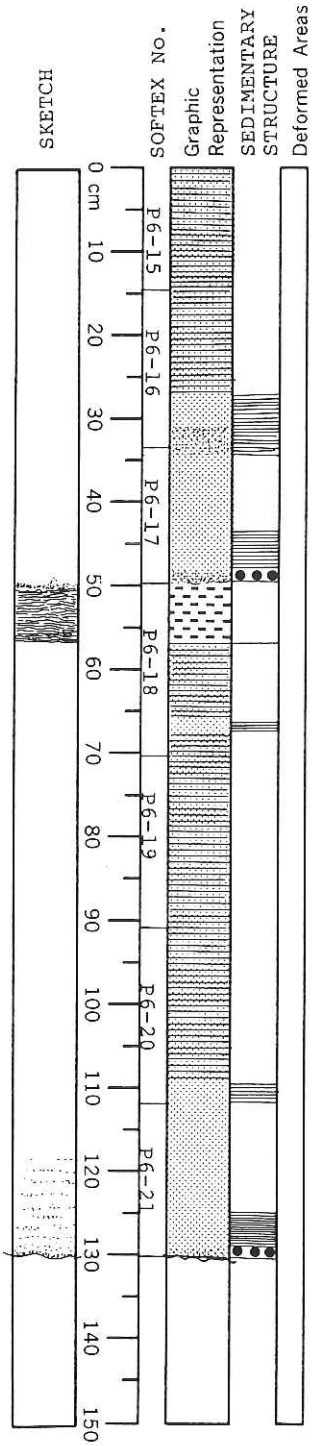

VISUAL CORE DESCRIPTION

Nannofossil-bearing siliceous clay,
(N 1.5/0; after oxidation: 2.5GY 4/1)

Silt to very fine-grained sand

Very fine-grained sand

Siliceous clay (N 1.5/0; after OX.: 5Y 4/2)

Nannofossil-bearing siliceous clay
(N 1.5/0; after oxidation: 2.5GY 4/1)

Silt to very fine-grained sand

Nannofossil-bearing siliceous clay
(N 1.5/0; after oxidation: 2.5GY 4/1)

Silt

Nannofossil-bearing siliceous clay
(N 1.5/0; after oxidation: 2.5GY 4/1)

Fine-grained sand

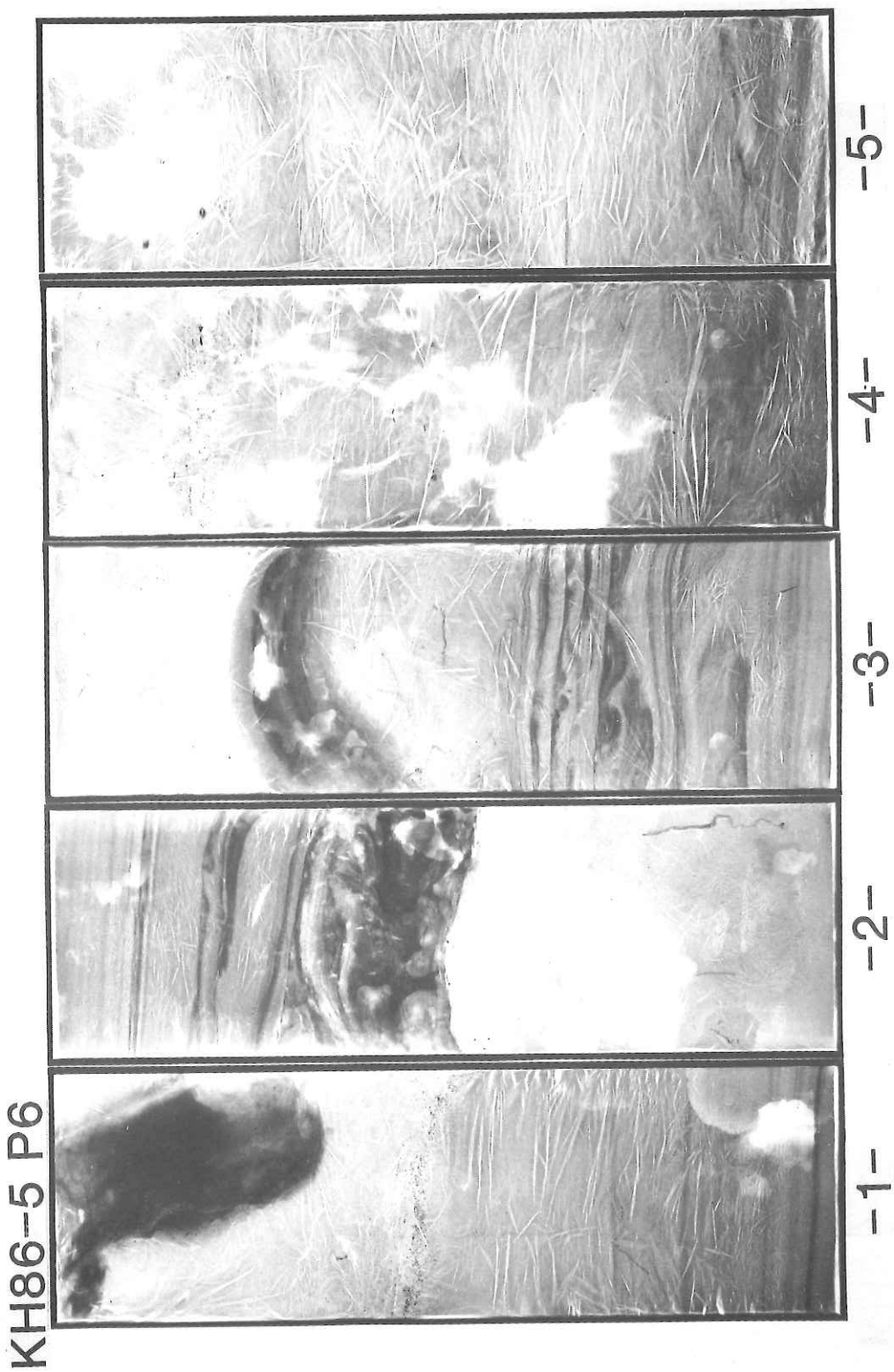
KH86-5 P6
-1-
-2-
-3-
-4-
-5-

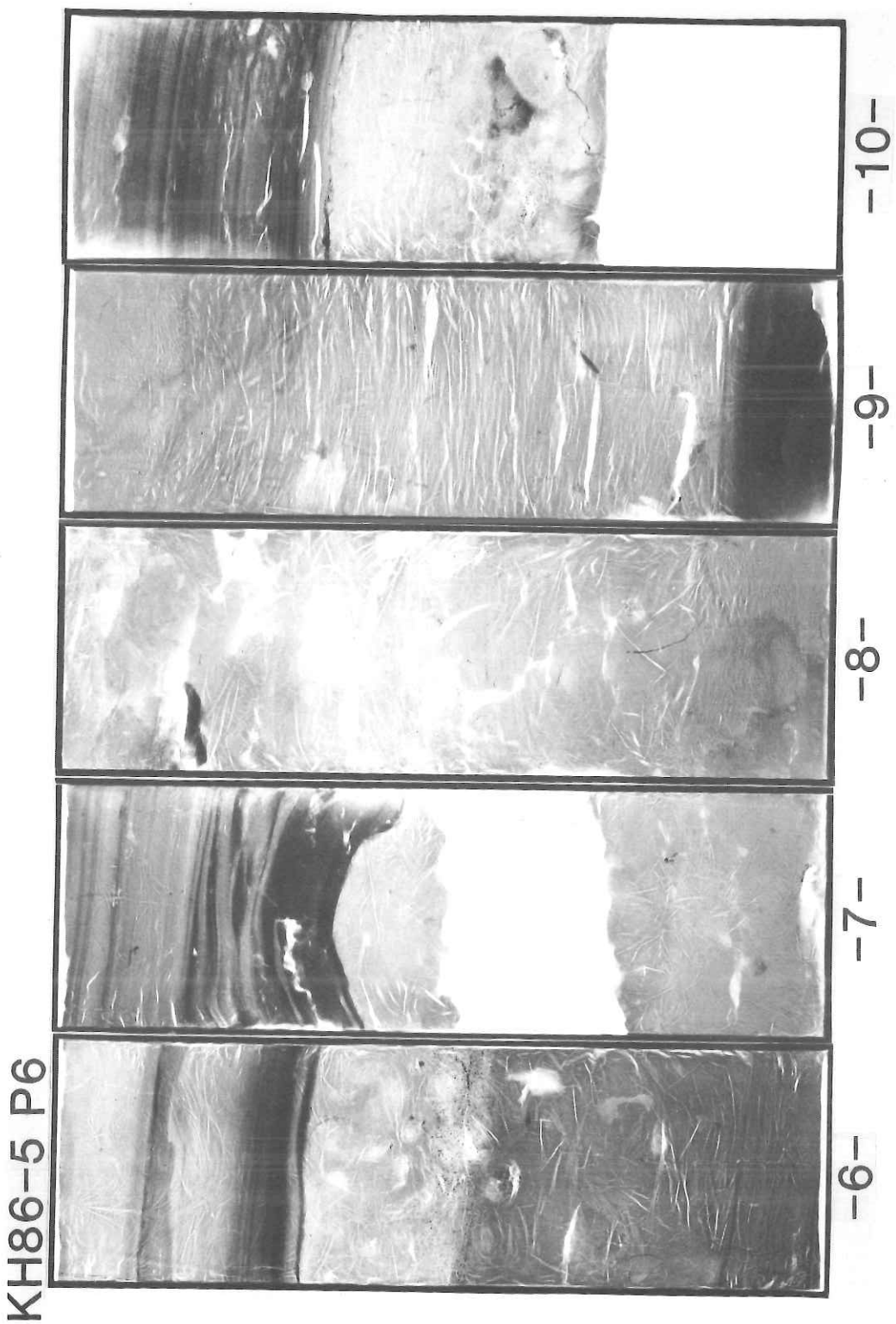
KH86-5 P6
-6-
-7-
-8-
-9-
-10-

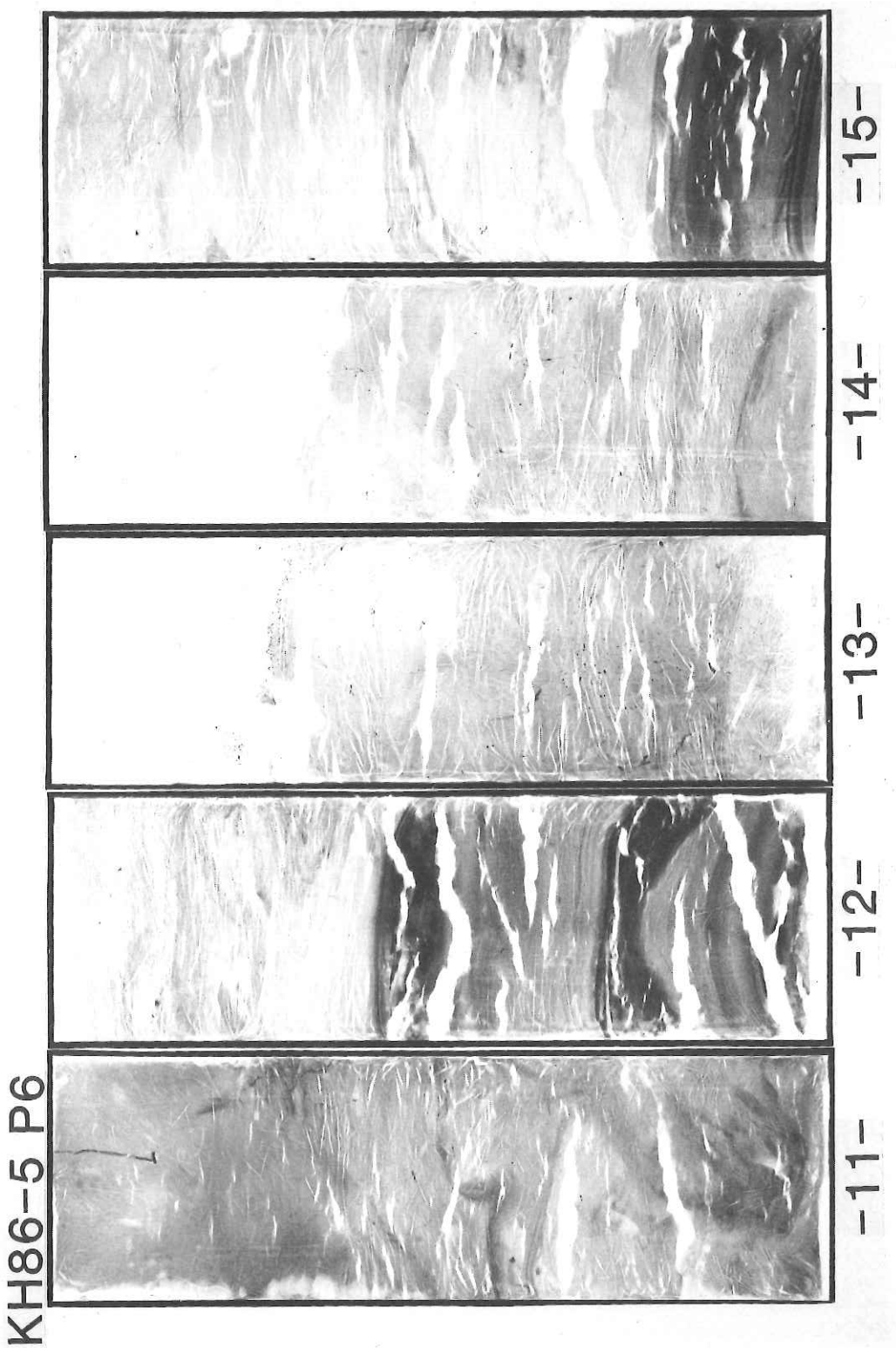
KH86-5 P6
-11-
-12-
-13-
-14-
-15-

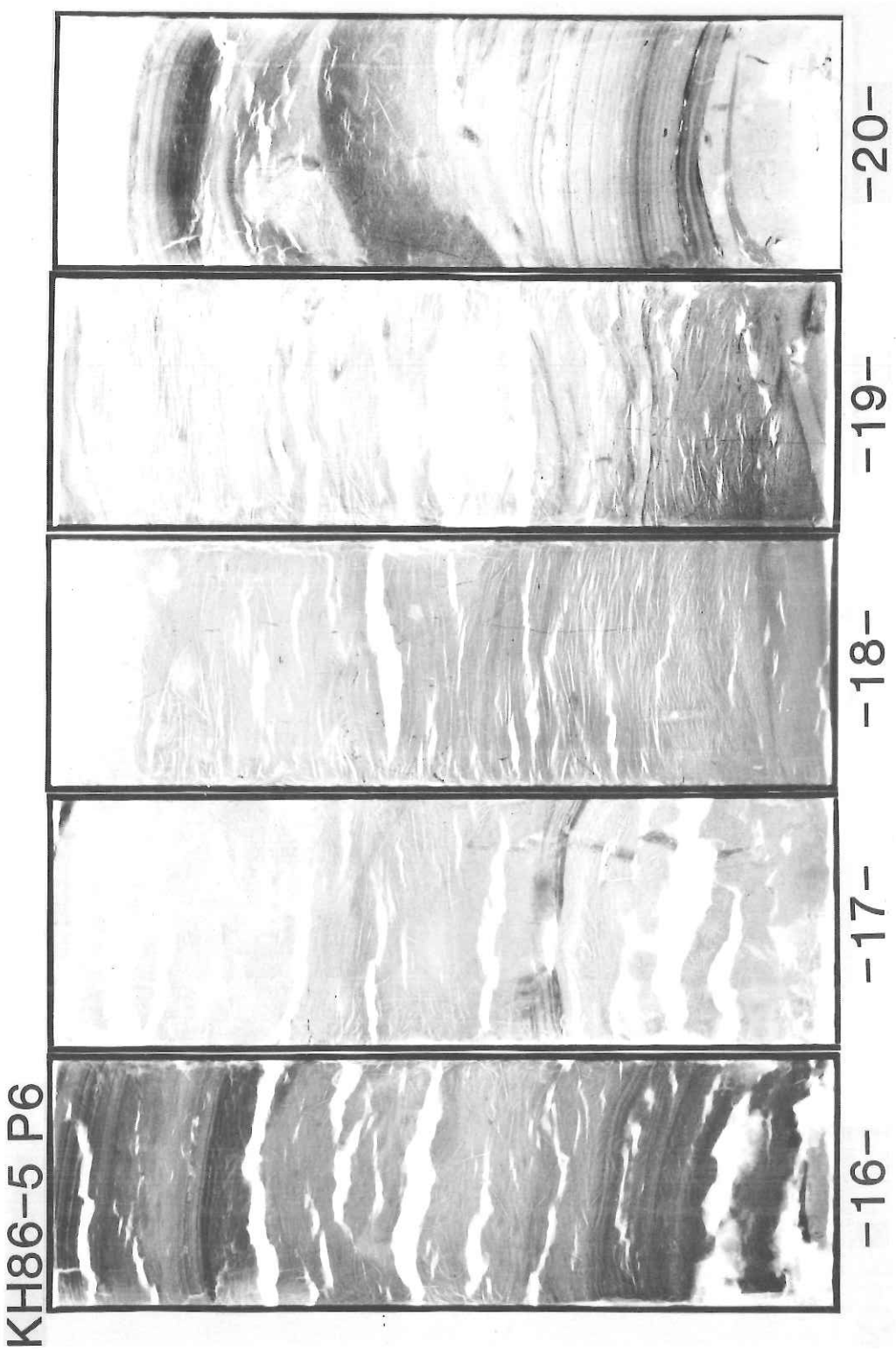
KH86-5 P6
-16-
-17-
-18-
-19-
-20-

KH86-5 P7

Location: Lat.:32 36.2'N Water depth 4100 m
Lot.:134 46.6'E Core sample length 263 cm
(Unnamed slope basin off the Muroto Basin; north of Tosa Bae Embayment)
Purpose: to investigate sedimentary facies and biofacies of typical slope basin fills.

The dominant lithology of the core sample, KH86-5 P7, is nannofossil-and diatom-bearing clay with turbiditic sand of 18 cm thick. The nannofossil- and diatom-bearing clay is homogeneous and structureless with lots of burrows from the bottom to the top. The structure and lithology of the clay is likely to be similar to that of KH86-5 P3, as mentioned before. The two ash layers consist of coarse- to fine-grained ash. One. the top ash layer, is included in 7 cm to 26 cm below the top. The top ash layer is homogeneous and structureless through the layer, and mostly composed of volcanic glass. The refractive index of the volcanic glass is 1.5027. The base of the core sample, 237 cm to 263 cm below the top. The base ash layer consists mostly of volcanic glass of bubble-wall shard. Some amount of pumice particles, for example, 2 cm in the longest axis, are contained in the upper part of the ash layer. The upper part of the ash layer between 237 cm to 245 cm, is mixed zone with very fine-grained ash and clay. The base ah layer shows good grading. Judging from the refractive index of the volcanic glass; 1.5089, and from mineral composition, it is likely to be fall deposit of Kikai-Akahoya Ash (Arai & Machida, 1978). The turbidite bed is intercalated during 38 cm to 47 cm below the top. The turbidite shows Tbc turbidite sequence with erosional base. The turbidite sand is composed mainly of fine- to very fine -grained grains. The pellets, spindle-shape of a few mm in diameter with a thin transparent membraine mantle, can be identified in the upper sediments of the core, 50 cm below the top. The another type of the pellet is microfossil test condensed one. This tends to be condensed in the filling of burrows.

OCEAN RESEARCH INSTITUTE UNIVERSITY OF TOKYO

VISUAL CORE DESCRIPTION

STATION	CORE	SEC
KH86-05		
P7		01

OBSERVER

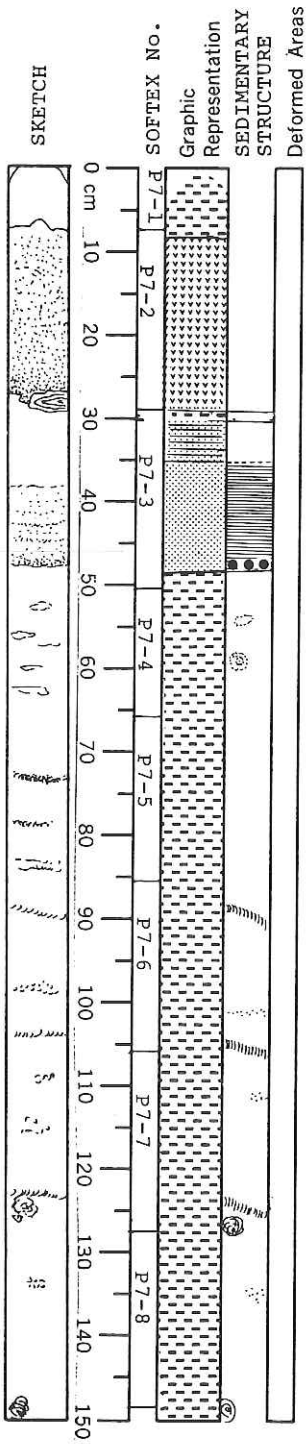

Soupy nannofossil- and diatom-bearing clay (5GY 3/2)

Coarse-grained volcanic ash (5GY 5/2)
This shows structureless. The ash is composed mainly of volcanic glass.

The thin silty mud layer (5YR 4/4)

Turbidite, showing normal grading form the base to top that is silty mud.
The lower consists of fine-grained sand with parallel lamination. The base is shape, seems to be erosional.

Nannofossil- and diatom-bearing clay (5GY 4/1)
Structureless with burrows

Pellet-condensed zone.

Zoophycus burrows

Pellet-condensed zone.

The pellet is spindle-shape, and condensed in the burrow.

Pellet-condensed zone.

OCEAN RESEARCH INSTITUTE UNIVERSITY OF TOKYO

K	8	6	–	0	5
STATION		CORE		SEC	
P	7			0	2

OBSERVER

VISUAL CORE DESCRIPTION

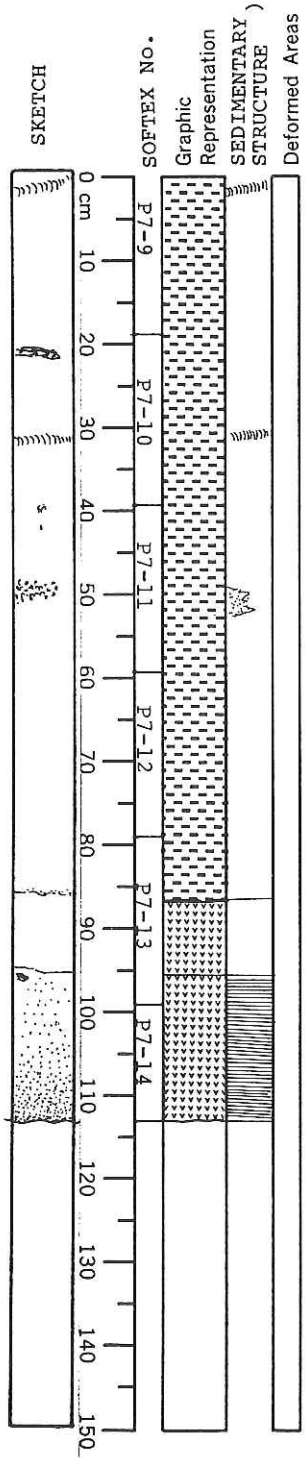

Pellet-condensed zone (Burrow)

Nannofossil- and diatom-bearing clay (5GY 4/1)
Structureless with burrows

Pellet-condensed patch (burrow?)

Pellet-condensed patch (burrow?)

Mixed zone of volcanic ash and tuffaceous clay.
This zone shows crude parallel laminations.

Pumice; 2 cm in diameter.

Volcanic ash (7.5GY 5/1)
This shows wavy to parallel-laminations.

End of the core sample is 263 cm.

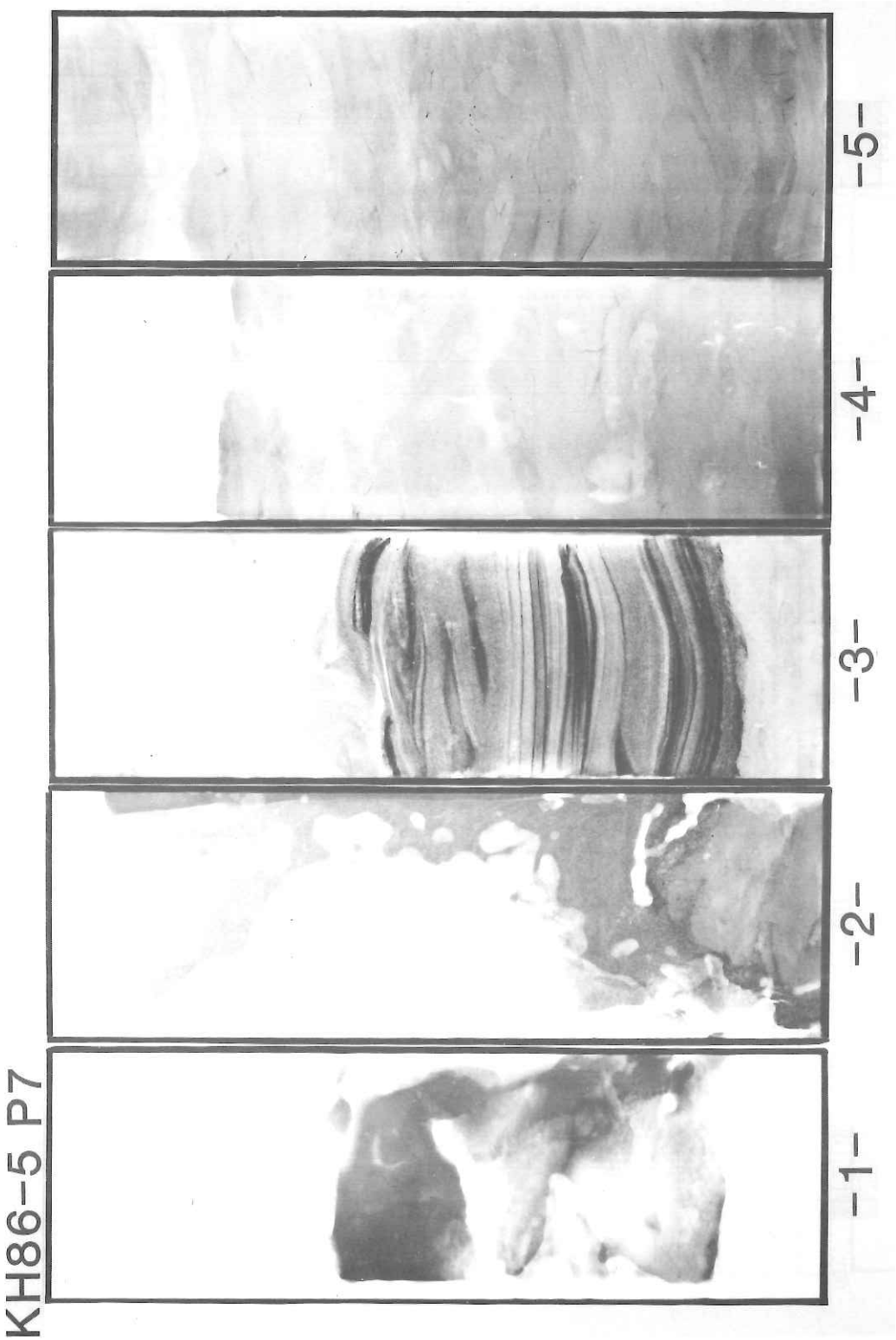
KH86-5 P7
-1-
-2-
-3-
-4-
-5-

KH86-5 P7

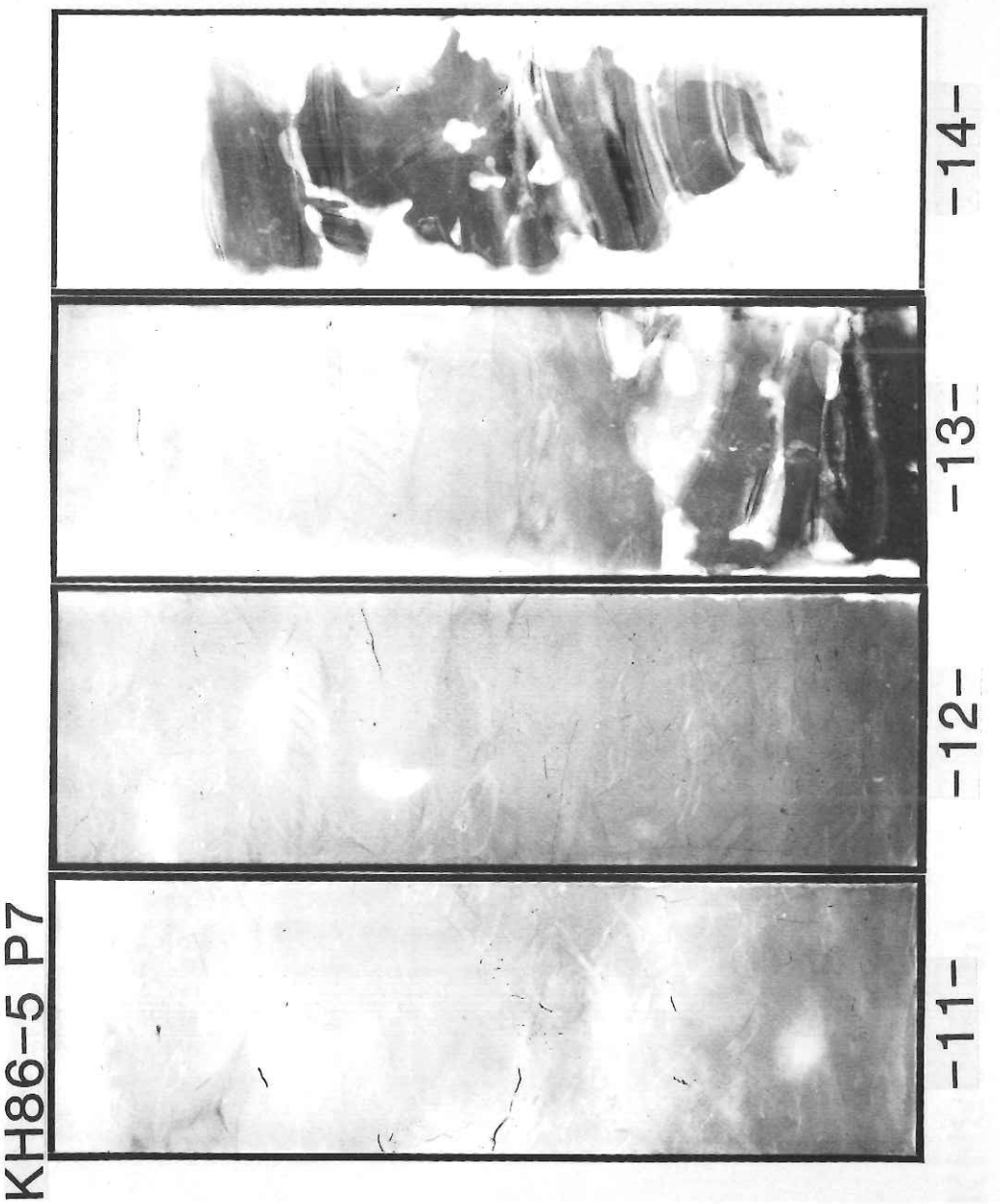
KH86-5 P7
-11-
-12-
-13-
-14-

KH86-5 P8

Location: Lat.:33 46.22'N Water depth 3680 m
Lon.:138 00.12'E Core sample length 263 cm

(Near deformation front of Nankai trough off the Daisan Tenryu Knoll)
Purpose; to investigate sedimentary facies and biofacies of Nankai trough fill sediments deposited alone the deformation front scarp, and in levee setting off the axial channel.

P8 seems to be a turbidite sequence. Unfortunately, the core sample below 24 cm from the top completely suffered the strong dewatering modification as a result of flow-in. The modified graded sand layers are dotted in the core sample. The turbidites are likely to be mud-dominant turbidites shown Tbc sequence.

REFERENCE

Dean, W.E., Leinen, M. and Stow, D.A.V., 1984: Classification of Deep-sea, fined-grained Sediments. Jour. Sedim. Petrol., 55, 250-256.

Machida, H. and Arai, F., 1978: Akahoya ash - a Holocene widespread tephra erupted from the Kikai caldera, south Kyushu, Japan. Quaternary Res. (Daiyonki-Kenkyu), 17, 143-163.

Taira A. and Niitsuma, N., 1986: Turbidite Sedimentation in Nankai Trough as interpreted from magnetic fabric, grain size and detrital model analysis, DSDP-IPOD Leg 87, DSDP Initial Rep., Leg. 87, 611-632

Soh, w., 1986: Sedimentation pattern of the Nankai Trough Turbidite (preliminary report), Clastic Sediments (Saisetubutsuno Kenkyu), 4, 61-72.

OCEAN RESEARCH INSTITUTE UNIVERSITY OF TOKYO

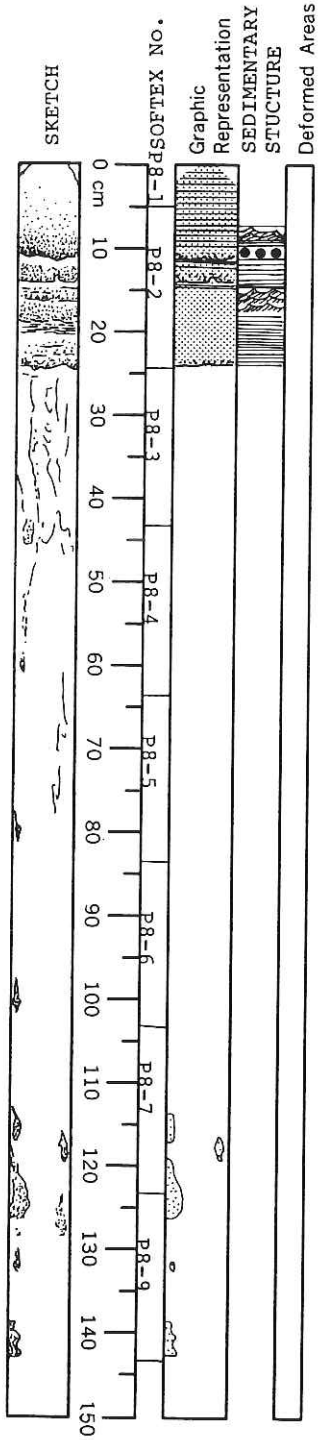

VISUAL CORE DESCRIPTION

KH86-05		
STATION	CORE	SEC
P8		01

OBSERVER

Soupy nannofossil-bearing siliceous silt (5GY 5/2)

Very fine- to fine-grained sand (Tbc type) (10G 2/1)

Fine-grained sand (10G 2/1)

Flow-in structure

Silty clay, poor-sorted materials (10Y 3/2)

Sand patch (10G 2/1)

OCEAN RESEARCH INSTITUTE UNIVERSITY OF TOKYO

VISUAL CORE DESCRIPTION

STATION	CORE	SEC
KH86-05		
P8		02

OBSERVER

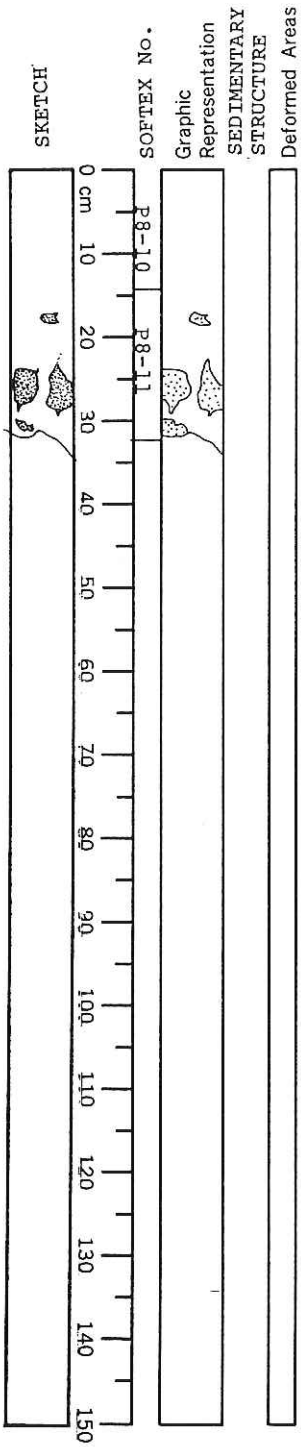

Flow-in structure

Silt and mud, poor-sorted materials
(10Y 3/2)

Fine-grained sand patch

End of the core sample

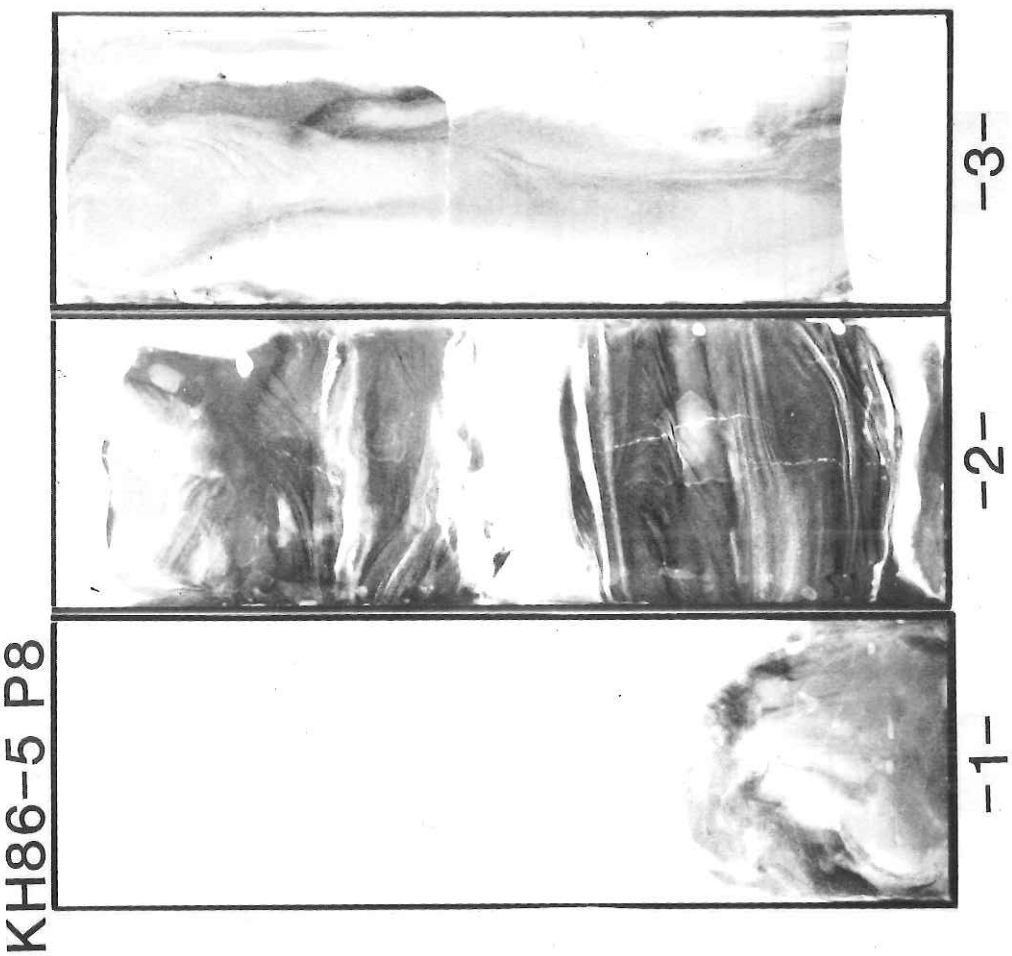
KH86-5 P8
-1-
-2-
-3-

MINERAL COMPOSITION OF SANDS AND SANDY SEDIMENTS OBTAINED FROM KH86-5 CRUISE

K. YAGISHITA

Ocean Research Institute, University of Tokyo, Nakano, Tokyo 164

Mineral composition of sands and sandy sediments from three piston cores of KH86-5 cruise has been estimated under the binocular scope. Most of these sediments, as noted in the lithologic description of cores, shows a grading.

P-4 CORE SAMPLE

The sampled locality of P-4 core is located on the southern slope of the Muroto Basin. Because of the sample location, most of sediments of P-4 core may not have been directly derived from the land mass, like "Shikoku" or "Kyushu". Rather, they are probably reworked, secondary deposits of turbidites, of which source was to the south and upper slope of the Muroto Trough Basin. Two-types of turbidites are recognized from the P-4 core; One consists of medium- to fine-grained, subangular to subrounded sand-sized sediments without any volcanic glass. The other consists of medium- to fine-grained, subangular to subrounded sand-sized quartz and lithic fragments together with coarse to very coarse volcanic glasses.

P-5 CORE SAMPLE

The sampled locality of P-5 core is farther south of P-4 core. It is rather curious, however, that two types of sediments in P-4 core (i.e., sediment with volcanic glasses, and sediments without volcanic glasses) cannot be recognized in this P-5 core. Sediments with volcanic glasses are observed only in the very bottom part of the core (more than 300 cm depth). A tuff layer at 355 cm is characterized by broken fragments of bubble-walled glasses.

P-2 CORE SAMPLE

The P-2 core was sampled from the southern slope of the Suruga-Nankai Trough. Grain size of observed sediments is mostly silt-size. Tuff and tuffaceous sediments

generally contain minor amount of clino-pyroxene, of which source is probably basic to intermediate volcanoes. Scoria layers consist of dark-brown devitrified glasses.

Length of core	Sediments	Composition(with roundness)	
16 cm	f.gr.sds.	qtz(subangular to subrounded)	50%
		plg	5%
		lithic frgmnt	42%
		biogenic frgmnt	3%
18 cm	silts	qtz(subangular to subrounded)	20%
		foram.	2%
32 cm	c.gr.silts	qtz (angular)	20%
		lithic frgmnt	20%
		foram.	2%
46 cm	m.gr.sds.	qtz(angular)	20%
		volc.glasses(v.c.gr.sd.size)	45%
		lithic frgmnt.	30%
		fossils	5%
57 cm	m-c.gr.sds.	qtz(subrounded)	20%
		lithic frgmnt(mostly shale)	40%
		volc.glasses(c.gr.sd.size)	35%
		spicule	5%
136 cm	m-f.gr.sds.	qtz(subangular)	60%
		lithic frgmnt	30%
		volcanic glasses	10%
219 cm	v.f.gr.sds.	qtz(subrounded)	60%
		lithic frgmnt	32%
		plgcls	3%
		fossils	5%
255 cm	f-m.gr.sds.	qtz(subangular)	51%
		lithic frgmnt	40%
		plgcls	2%
		foram	7%
272 cm	f-m.gr.sds.	qtz(subangular)	30%
		lithic frgmnt	60%
		fossils	10%
331 cm	silts	volcanic glasses	40%
		qtz	5%

Fig. 1 Mineral composition and roundness of KH86-5, P-4.

Length of core	Sediments	Composition	
10 cm	v.f.gr.sds.	qtz	50%
		lithic frgmnt	20%
		silts	30%
41 cm	v.f.gr.sds.	qtz.	50%
		lithic frgmnt	20%
		silts	30%
94 cm	v.f.gr.sds.	qtz	50%
		lithic frgmnt	20%
		silts	30%
99 cm	f.gr.sds.	qtz(mostly subrounded)	75%
		lithic frgmnnt(mostly shale)	25%
		fossils	5%
115 cm	v.f.gr.sds.	qtz	30%
		lithic frgmnt(shale)	20%
		fossils	10%
		silts	40%
133 cm	v.f.gr.sds.	qtz(subangular-subrounded)	70%
		fossils	15%
		lithic frgmnt	15%
150 cm	silts	qtz	7%
		lithic frgmnt(shale)	3%
		silts	90%
159 cm	m.gr.sds.	qtz	70%
		fossils	10%
		lithic frgmnt	15%
		others(plgcl etc.)	5%
200 cm	f.gr.sds.	qtz(subangular)	65%
		foram.	25%
		lithic frgmnt(shale)	10%

Fig. 2 Mineral composition and roundness, KH86-5, P-5.

250 cm	v.f.gr.sds.	qtz(angular)	60%
		fossils	20%
		lithic frgmnt	20%
316.5 cm	f-m.gr.sds.	qtz(v.f.gr.sd.size)	50%
		volc.glasses(c.gr.sd.size)	30%
		fossils	20%
320 cm	m.gr.sds.	qtz	50%
		lithic frgmnt(shale)	30%
		fossils	10%
		clino pyroxene	5%
321 cm	m.gr.sds	qtz(v.f.gr.sd.size)	20%
		lithic frgmnt(shale)	30%
		foram	20%
		volc.glasses(c.gr.sd.size)	20%
		silts	10%
335 cm	tuff	volcanic glasses	95%

Fig. 2 continued.

Length of core	Sediments	Composition	
20.5 cm	silts	qtz	3%
		fossils	3%
		augite & hypersthene	1%
65.5 cm	tuff	volc.glasses(v.f.gr.sd.size)	40%
		augite & quartz	1%
90 cm	silts	lithic frgmnt(shale)	2%
123 cm	silts	fossils	3%
		others(augite & qtz)	1%
138 cm	scolia	scolia(c-m.gr.sd.size)	45%
		augite	10%
		silts	45%
150 cm	sds	lithic frgmnt(shale)	20%
		fossils	2%
155 cm	silts	qtz	5%
		augite	7%
		fossils	1%
173 cm		volc.glasses(silt size)	97%
		others(spicule & augite)	3%
177 cm	tuff	volc. glasses(silt size)	50%
		foram	15%
205 cm	scolia	scolia(v.f.gr.sd.size)	90%
		augite & others	10%
274 cm	silts	qtz	5%
		fossils	5%

Fig. 3 Mineral composition and roudness of sand and sandy materials, KH86-5, P-2.

DESCRIPTION OF SAMPLES FROM TAKUYO-DAINI SEA MOUNT AND ZENISU RIDGE, DURING KH86-5 CRUISE

Y. TAMURA
Department of Geology, University of Tokyo, Bunkyou, Tokyo 113
T. ISHII
Ocean Research Institute, University of Tokyo, Nakano, Tokyo 164

During the Hakuho Maru Cruise KH-86-5, samples were dredge from two sites, Takuyo-Daini Sea Mount (KH86-5-D1), and a small seamount on the Zenisu Ridge (KH86-5-D2). They are all igneous rocks and Mn-nodules, and do not contain limestone as well as sedimentary rocks. Precise positions, depth of each station, and other informations are given in the operation logs of the dredge hauls. Dredge samples were classified by lithology and numbered in the order of size, and the diameter (L, M and S), roundness, weight and the thickness of Mn-coating estimated by similar manner to Ishii et al. (1975).

Glasses made of several dredge igneous rocks were prepared by the direct fusion method of Nicholls (1974) for the bulk chemical analysis. Chemistries of bulk rocks and minerals were estimated by a JEOL electron microanalyzer Model JCXA-733 of the Ocean Research Institute, and shown Tables.

TAKUYO-DAINI SEAMOUNT

About 50 boulders, cobbles and gravels of altered basalts and hyaloclastites were dredge from the Takuyo-Daini Sea Mount. Basalts are vesicular and some cavities are filled with secondary minerals such as carbonates and submicroscopic apatite. They consist of primatic laths of plagioclase phenocrysts and microphenocrysts. Though mafic minerals have been completely altered, pseudomorphs of olivine can be observed. Groundmass of these basalts shows intersertal texture. All basalts (D1-01 to -10) are poor in MgO, on the other hand, they are rich in CaO, P_2O_5, NaO and K_2O. Bulk chemistries of dredged basalts from sea mounts are usually affected by the alternation and especially by the vesicule filling apatite (Naka, 1985). As feldspars are fairly fresh in comparison with mafic minerals. It is excepted that alkali contents did not relatively changed through the alteration. If so, they are thought to be alkali olivine basalt affinities, but the conclusion

alteration. If so, they are thought to be alkali olivine basalt affinities, but the conclusion contains so big uncertainty that more investigations (for example REE geochemistry etc.) are requested.

ZENISU RIDGE

About 20 boulders, cobbles and pebbles of hornblend dacites and Mn-nodules were dredged from a small sea mount on the Zenisu Ridge, north of Enshunada Sea Mount. Hornblende dacites are monolithologic and consist of phenocrysts of plagioclase (1-2 mm) and green hornblende, magnetite and glass. Rarely biotite is contained in hornblende phenocryst.

Based on the bulk chemical compositions (D2-01-05), they are thought to be calc-alkalic dacite of an island are origin. Further investigations should be done to reveal the origin of the Zenisu Ridge and the volcanism on it.

REFERENCE

Ishii, T., Kobayashi, K., Shibata, T., Naka, J., Jonhson, K., Ikehara, K., Iguchi, M., Konishi, K., Wakita, H., Zhang, F., Nakamura, Y. and Kayane, H., 1985, Description of samples from Ogasawara Fore-arc, Ogasawara Plateau and Mariana Trough, During KH84-1 Cruise. Preliminary Rep. Hakuho Maru Cruise KH84-1, Ocean Res. Inst. Univ. Tokyo, 89-168.

Naka, J., 1985, Volcanic Rocks dredged from the Ogasawara Plateau, ibid. 196-201.

Nicholls, I. A., 1974, A direct fusion method of preparing silicate rock glasses for energy dispersive microprobe analysis. Chem. Geol., 14, 151-157.

Powers, M. C., 1853, A new roundness scale for sedimentary particles. Jour. Sedim. Petrol., 23, 117-119.

List of dredged materials during KH 86-5

Sample No.	Diameter(mm) L	M	S	Round-ness*	Wt.(g)	Mn-coat-ing(mm)	Lithology & Remarks
D1-01	138	105	91	0.50	1221	F-1	basalt (pl,ol)
02	116	97	88	0.50	1058	F	"
03	115	65	61	0.40	456	F	"
04	97	72	56	0.40	316	F	"
05	86	73	62	0.60	342	F	"
06	82	67	36	0.40	146	O-2	"
07	76	58	41	0.40	208	F	"
08	63	52	35	0.50	81	F	"
09	64	46	36	0.30	66	F	"
10	54	43	32	0.40	69	F	"
11	47	45	36	0.60	65	F	"
12	54	36	27	0.50	42	F	"
13	52	44	36	0.40	34	F-2	"
14	45	42	24	0.50	31	F	"
15	40	29	27	0.40	29	F	"
16	39	35	27	0.60	32	F	"
17	42	33	28	0.40	34	F-4	"
51	111	77	39	0.50	334	F	hyaloclastite
52	112	72	59	0.40	335	F	"
53	113	61	55	0.40	317	F	"
54	100	64	31	0.40	185	F	"
55	95	64	46	0.30	213	F	"
56	62	50	33	0.50	85	F	"
57	64	36	28	0.60	74	F	"
58	52	45	31	0.50	60	F	"

Sample No.	Diameter(mm) L	M	S	Round-ness *	Wt.(g)	Mn coating(mm)	Litology & Remarks
59	52	38	35	0.40	69	F	"
60	58	37	29	0.50	52	F	"
61	56	39	24	0.20	48	F	"
62	48	36	25	0.70	40	F	"
63	48	35	29	0.30	38	F	"
100							others
D2-01	200	190	140	0.60	8800	5	dacite(hb, pl, mt)
02	150	100	80	0.60	1850	1-10	"
03	105	68	63	0.30	965	F	"
04	104	68	62	0.40	1170	F	"
05	91	58	47	0.30	280	2-8	"
06	52	38	11	0.30	30	4	"
11	105	84	47	0.50	370		Mn-nodule
12	89	85	28	0.30	255		"
13	74	55	34	0.30	115		"
14	75	44	17	0.40	67		"
15	73	52	15	0.40	64		"
16	65	48	18	0.30	59		"
17	65	45	18	0.30	54		"
18	38	35	25	0.30	34		"
19	38	20	15	0.40	13		"
50					26		others

* after Powers' system (Powers, 1953)
0.10 = very angular, 0.20 = angular, 0.30 = subangular,
0.40 = subrounded, 0.60 = rounded and 0.85 = well-rounded

Bulk Chemical Compositions of Volcanic Rocks

Sample No.	Takuyo-Daini SMt. D1-01	D1-02	D1-03	D1-04	D1-05
SiO2	45.15	39.45	42.87	46.51	38.83
TiO2	2.39	2.19	2.33	2.60	2.16
Al2O3	15.98	14.62	15.35	17.31	14.23
FeO	8.56	6.92	7.89	9.61	7.27
MnO	0.06	0.08	0.10	0.11	0.11
MgO	1.81	1.45	1.58	1.63	1.60
CaO	16.61	26.24	16.57	10.60	26.40
Na2O	3.25	2.79	2.94	3.28	2.57
K2O	2.25	1.80	1.78	1.72	1.84
Cr2O3	0.02	0.03	0.02	0.03	0.02
V2O3	0.00	0.00	0.00	0.00	0.00
NiO	0.05	0.06	0.04	0.05	0.05
P2O5	1.77	2.35	6.67	4.27	3.06
Total	97.91	97.95	98.14	97.71	98.15

Sample No.	D1-06	D1-07	D1-08	D1-10	D1-11
SiO2	47.12	45.04	37.07	35.89	40.10
TiO2	2.68	2.19	2.30	1.86	2.21
Al2O3	16.54	15.68	13.20	12.77	14.76
FeO	9.30	7.35	8.36	7.03	7.98
MnO	0.08	0.09	0.14	0.08	0.14
MgO	2.46	2.17	1.55	1.31	1.72
CaO	13.88	18.21	26.87	23.47	23.68
Na2O	2.17	2.42	1.58	2.31	2.62
K2O	2.53	1.78	2.30	1.32	1.62
Cr2O3	0.04	0.01	0.01	0.01	0.01
V2O3	0.00	0.00	0.00	0.00	0.00
NiO	0.06	0.06	0.06	0.03	0.06
P2O5	1.00	3.20	4.03	12.37	2.73
Total	97.85	98.22	97.47	98.45	97.62

Sample No.	Zenisu Ridge D2-01	D2-02	D2-03	D2-04	D2-05
SiO2	66.80	66.89	66.88	66.79	65.87
TiO2	0.34	0.34	0.34	0.36	0.34
Al2O3	16.68	16.63	16.74	16.60	16.90
FeO	2.93	2.88	2.93	2.91	3.24
MnO	0.23	0.28	0.23	0.18	0.34
MgO	1.25	1.25	1.27	1.28	1.31

CaO	4.29	4.31	4.35	4.24	4.36
Na2O	3.93	4.08	4.06	4.08	4.02
K2O	2.30	2.30	2.32	2.33	2.15
Cr2O3	0.01	0.01	0.02	0.00	0.02
V2O3	0.00	0.00	0.00	0.00	0.00
NiO	0.03	0.03	0.02	0.03	0.04
P2O5	0.32	0.35	0.34	0.33	0.34
Total	99.10	99.34	99.49	99.12	98.93

Research Paper

INTERPRETATION OF SEISMIC REFLECTION PROFILES IN THE NORTH BASIN OF THE BOSO-OKI TRIPLE JUNCTION OFF HONSHU

T. SENO

International Institute of Seismology and Earthquake Engineering, Building Research Institute, Tsukuba, Ibaraki 305

H. TOKUYAMA

Ocean Research Institute, University of Tokyo, Nakano 164

Y. OGAWA

Department of Geology, Kyushu University, Hakozaki, Fukuoka 812

E. NISHIYAMA and A. TAIRA

Ocean Research Institute, University of Tokyo, Nakano 164

Lines B-B' and C-C' cross the North Basin (NB) and the western edge of the North Nose (NN) in a WSW-ENE direction (Fig.1). In profile C-C', the basement at shotpoints 4050-4180 looks cut by normal faults at both sides (Figs.2c). In profile B-B', the numerous diffractions at the western edge of NN suggest normal faults here (Figs.2b). The deformation of the sediments seen in Lines B-B' and C-C', in its deeper part below11 sec (two-way travel time), is consistent with this normal fault interpretation. The depocenters are located above the basement cut by the normal faults. However, the shallower part of the sediments does not show simple sagging in the above depocenters and suggests that the mode of deformation has changed. For example, though the sediments between 10.25 and 11 sec in profile C-C' are still thickest in the eastern part of the basin, it is upheaved at its eastern end with respect to the western part. Furthermore in the portion shallower than 10.25 sec, the depocenter has migrated to the western half of the basin. In profile B-B', this migration of depocenter cannot be seen because this line covers only the eastern half of NB. In this profile, an anticlinal structure is slightly seen around shotpoint 1900. However, this should not be taken as it appears; the two-way travel time beneath the terrace is shorter by as much as 0.1 sec than that of the west of it. Thus this produces an artificial uplift of the part beneath the terrace. Also note that the track line changed to the north shortly after shotpoint 1900 and the basement of NB is known to be dipping to the north (Renard et al., 1987). Thus the anticline is exaggerated. Although Huchon and

Labaume (1987) interpreted a similar anticline in one of the KAIKO profiles as an indication of compression and suggest thrusts dipping to the east, we do not agree with their opinion. This apparent anticline was seen in only one KAIKO profile (Line 85) which crosses NB at almost the same location of Line B-B' and none of the other KAIKO profiles show such features of sediment deformation. Note that the lines in which the anticline appears are crossing the steepest portion of the scarp of the terrace (KAIKO I Research Group, 1986), on which the travel time difference effect would be most pronounced. We thus believe that the anticline is apparent one and the deformation of the sediments in Line B-B' would not essentially be different from that seen in Line C-C'; that is, NN has been uplifted with respect to the west of it during the deposition of the sediments above 11 sec, though the sagging around shotpoint 1800 between 10 and 11 sec indicates that subsidence due to normal faulting also continued during the sedimentation of this part. We suggest that this uplift of NN has probably been caused by the accretion at the eastern base of NN. In the profile crossing the northernmost part of the Bonin Trench (profile A-A', Fig.2a), we can see the deformation of the trench wedge sediments at the tow of NN. Apparently accretion is curently taking place there. The start of this accreton is likely to be the time when a vast amount of sediments was started to be supplied into the trench. This should also be the time of the major sediment supply to NB. Consistently we observe the above change in mode of deformation of the sediments at the base of the major turbiditic portion of NB. We suggest that this might be around 0.5 Ma, when a vast amount of turbidites started to be supplied into the Nankai Trough (Taira and Niitsuma, 1985) due to the collision of Izu with central Honshu around this time (Koyama, 1986). This is also coincident with the time when the relative motion between NEJ and PHS has changed from the EUR-PHS motion to the NA-PHS motion (Seno, 1985). The component of the crustal separation at the eastern end of NB would have diminished significantly by this change in motion. This explains why the subsidence in the eastern half of NB became minor in the upper part of the sediments. In conclusions, the deformation of the basement seen in the seismic profiles suggests the stretched basin origin for the North Basin, which was caused by the westward retreat of the Philippine Sea plate with respect to the Eurasian plate (Seno et al., 1987). we believe that it may hold only during the period before 0.5 Ma. This conjecture on timing, however, should be tested by the deep-sea drilling in NB in the future and knowing directly the age of sedimentaion. The more complete discussion of the evolution of the triple junction is treated in the separate paper (Seno et al., 1987).

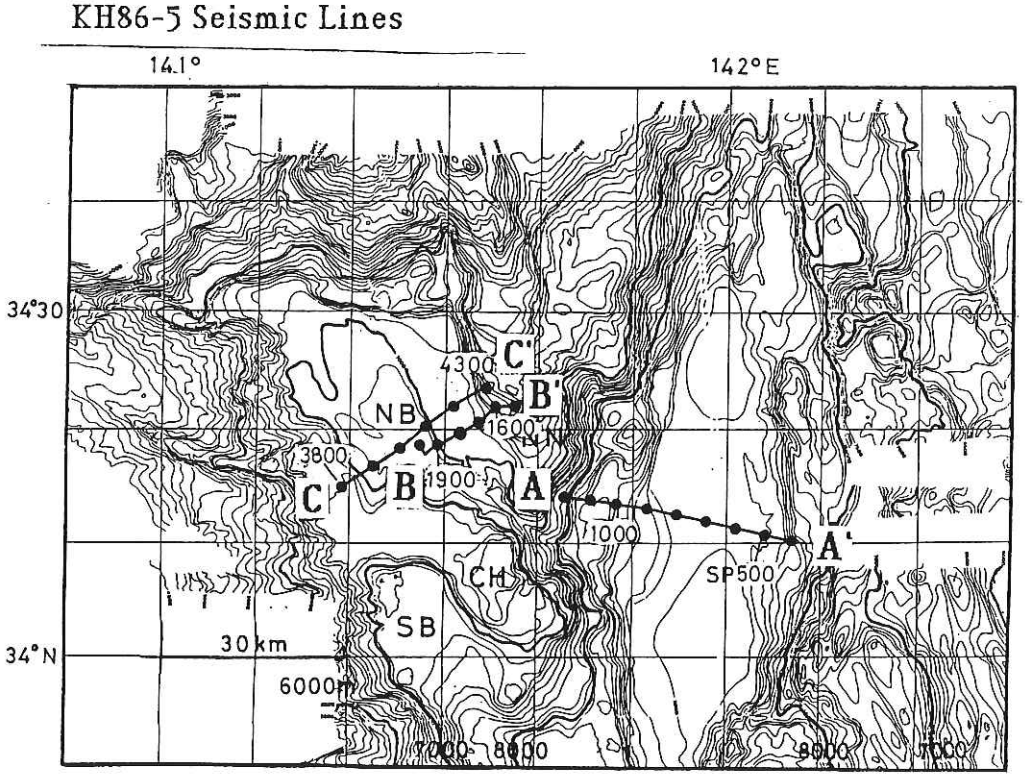

Fig. 1 Track lines of the multi-channel seismic reflection survey in the Hakuho-maru cruise KH86-5. The solid circles indicate the shotpoint at every 100 shots.

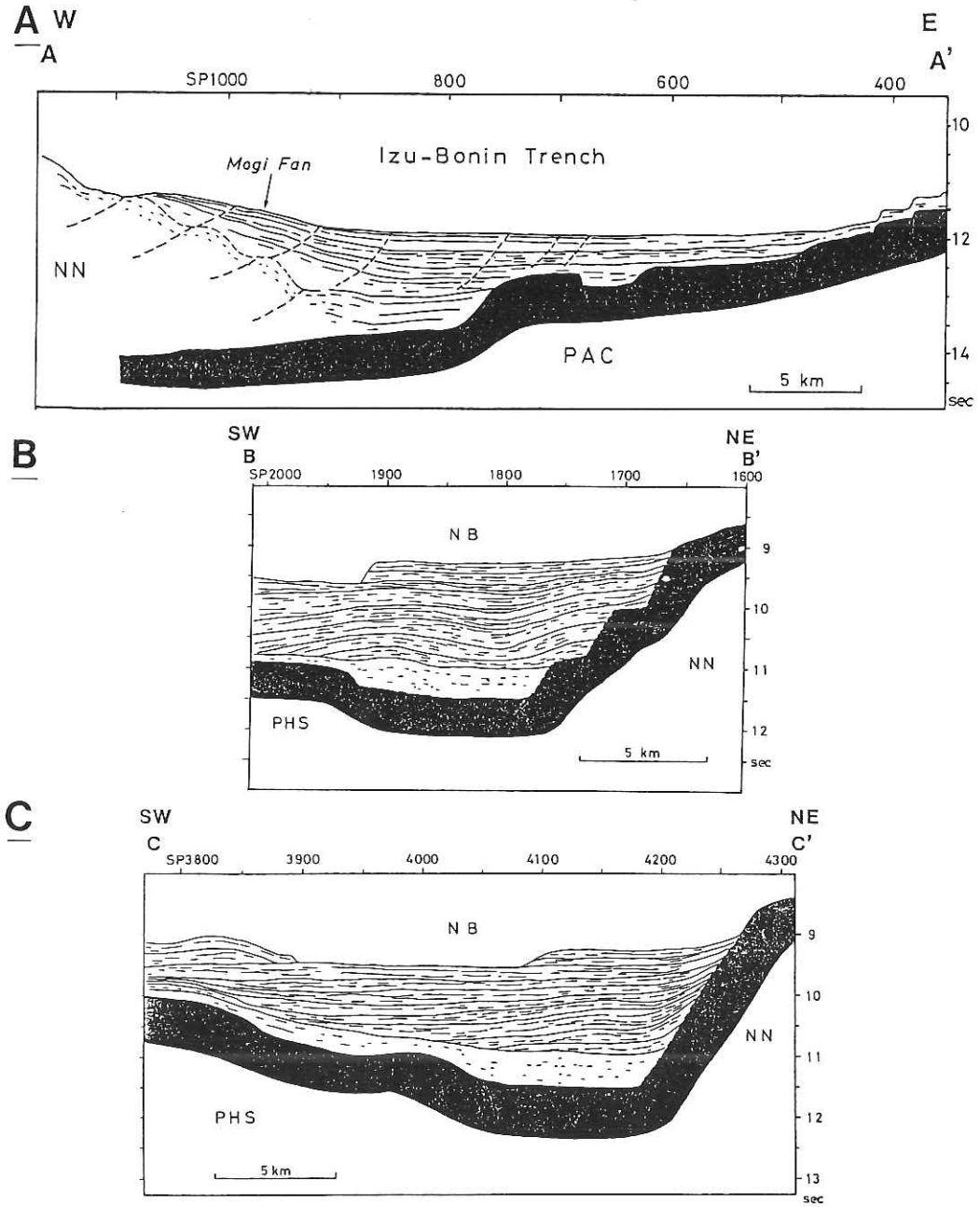

Fig. 2 Interpretation of the seismic profiles. (a) Line A-A' across the Izu-Bonin Trench. The PAC oceanic basement is dipping to the west, and at the base of NN, accretion is currently taking place. (b) Line B-B' and (c) Line C-C' across the North Basin (NB). The basement of NB is cut by normal faults; however, the shallower part of the sediments (above 11 sec) shows an uplift of NN with respect to the basement to the west.

ACOUSTIC IMPEDANCE LOGS OF THE ACCRETIONARY PRISM

E. NISHIYAMA

Ocean Research Institute, University of Tokyo, Nakano, Tokyo 164

TRACK LINE AND PROCEDURES

Synthetic acoustic impedance logs of the sedimentary layer of the Nankai Trough were obtained over through the analysis of the seismic reflection data of Line 6-1 and Line 6-2. Line 6-1 was traced from the offshore of the Muroto Peninsula to the axis of the Nankai Trough, oriented normal to the trough axis. Line 6-2 was recorded to the southwest of Line 6-1 and was a southeastern extension of JAPEX Line 55-2 (Fig. 1). Reflection signals were recorded digitally with twelve fold CDP coverage, twelve traces per shot and 50 meter between traces. Conventionally processed seismic sections of both lines are shown in Figs 2 and 3.

DATA PROCESSING

Initially, the reflection signals were processed carefully not to distort the amplitude distributions. Initial processing contains mainly 600% CDP stacking and deconvolution filtering with a filter length of 400 ms.

Acoustic impedance logs were reconstructed from the initially processed seismogram using one of the exact methods with concept of seismic inversion(Newton,1981). Derivation of basic equation of this inversion method was introduced to determine vocal-tract shape from impulse response at the lips(Sondhi and Gopinath,1971) and developed in the field of geophysical signal processing(Sarwar and Rudman,1985 ; Sato and Saito,1987). In this study the algorithm of Sarwar *et al.* was applied to the filed data for the first time.

Fig. 4 shows an example of the inversion result. In this, initial processed trace are shown as deconvolved seismogram. Synthetic seismogram calculated from the recovered impedance series are traced also. The synthetic seismogram shows a good relation to the original deconvolved trace.

ACOUSTIC IMPEDANCE LOGS

Calculation of absolute values of the acoustic impedance have not been achieved, however, relative changes of the impedance could be used to discuss acoustic characters of sediments which consist of accretionary prism.

Fig. 5 shows a profile of line 6-2 superimposed by several acoustic impedance

logs. Line 6-2 runs across the trough axis from the southeast to the northwest. The reflector which can be traced around 7.3 second in two-way travel time indicates the top of the oceanic layer 2 and the reflector identified around 6.9 second can be correlated to the sandy layer of Pliocene age. The outer margin of trench turbidite is near shot point (SP) 2200. Between SP 2100 and 2360, the impedance values of sedimentary layer increase with depth. Logs of SP 2400, 2450 and 2470 have nearly constant zone of impedance value below the sandy layer.

Fig. 6 is a part of the section of line 6-1. In this section, the trench fill sediments are slightly deformed to show folding and faulting. At SP 1650 a first major thrust which cuts through the upper sedimentary layer is observed. The impedance logs show a nearly constant zone of impedance values within the lower part of accretionary prism. Then it appears to show a low impedance zone in the sandy layer. Figs 7 and 8 are part of line 6-1. This section extends in the imbricate thrust zone. The impedance logs are characterized by a zone of nearly constant value.

REFERENCES

Newton, R. G., 1981, Inversion of reflection data for layered media, : a review of exact methods, Geophys. J. R. astr. Soc., 65, 191-215.

Sarwar, A. K. M. and Rudman, A. J., 1985, Inversion of a normally incident reflection seismogram by the Gopinath-Sondhi integral equation, Geophys. J. R. astr. Soc., 81, 551-562.

Sato, J. and Saito, M., 1987, Inversion of Reflection Data through the Gopinath-Sondhi Integral Equation, in proceedings of the 76th SEGJ Conference, 63-66.

Sondhi, M. M. and Gopinath, B., 1971, Determination of vocal-tract shape from impulse response at the lips, J. acoust. Soc. Am., 49, 1867-1873.

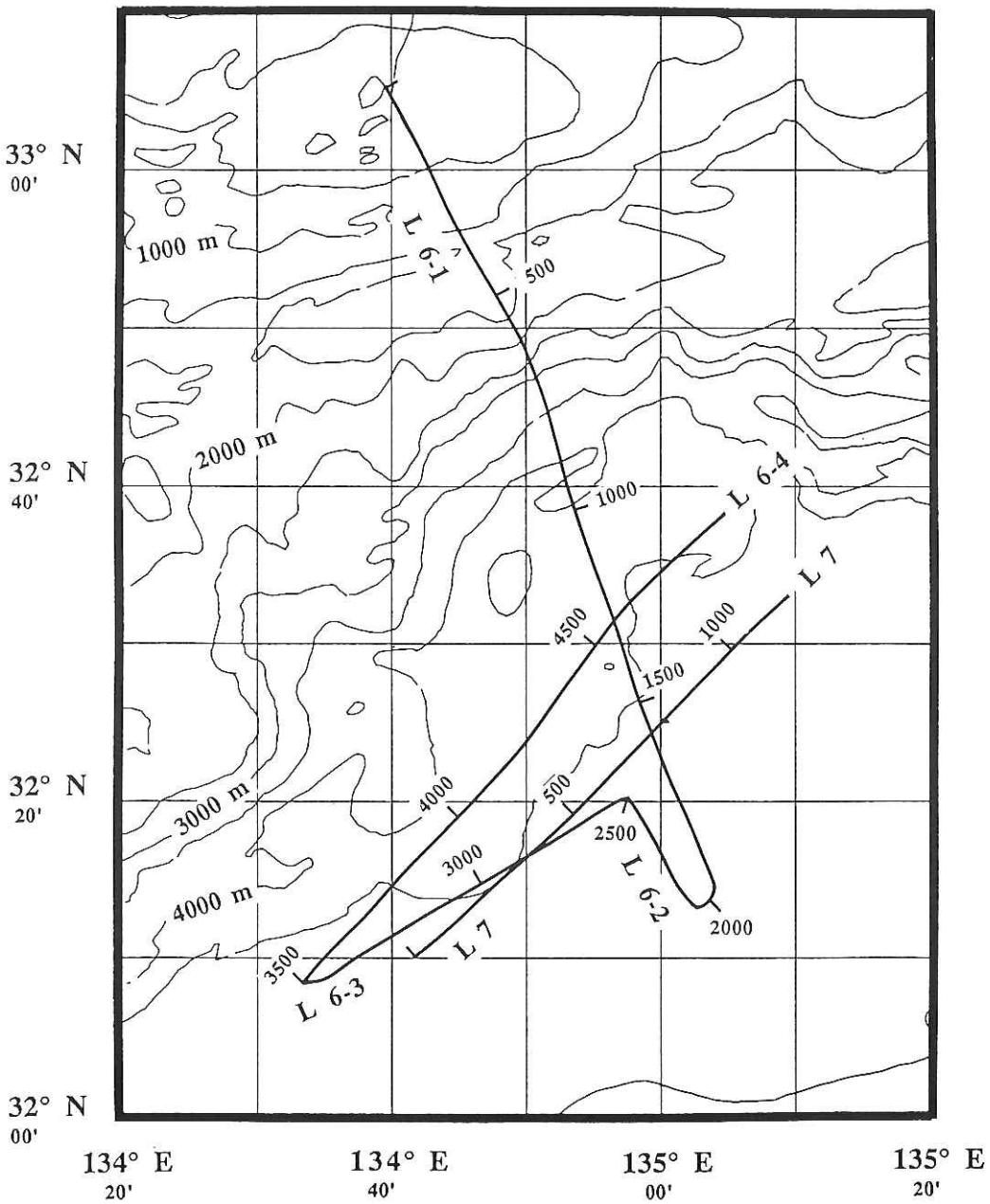

Fig. 1 Track lines of seismic profile lines 6-1 and 6-2.

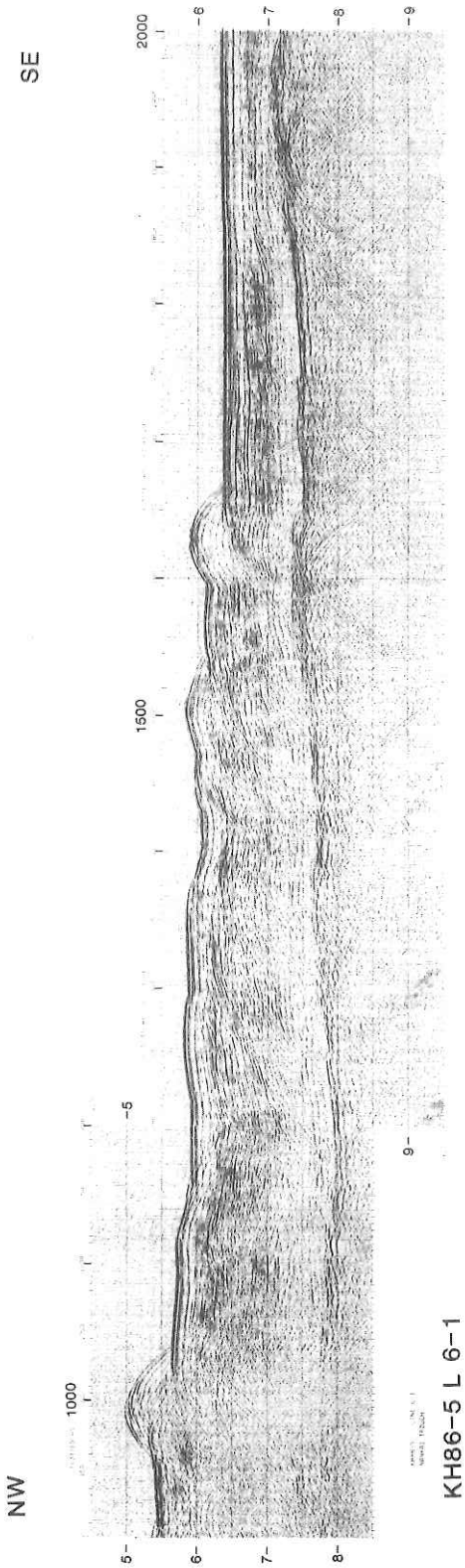

Fig. 2 Conventionally processed seismic section of line 6-1.

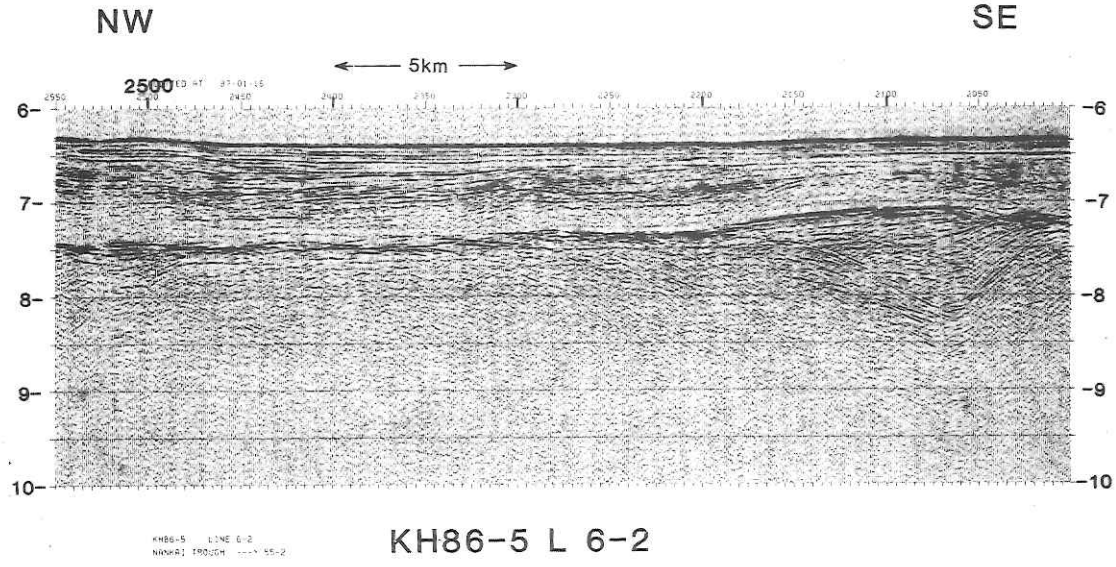

Fig. 3 Conventionally processed seismic section of line 6-2.

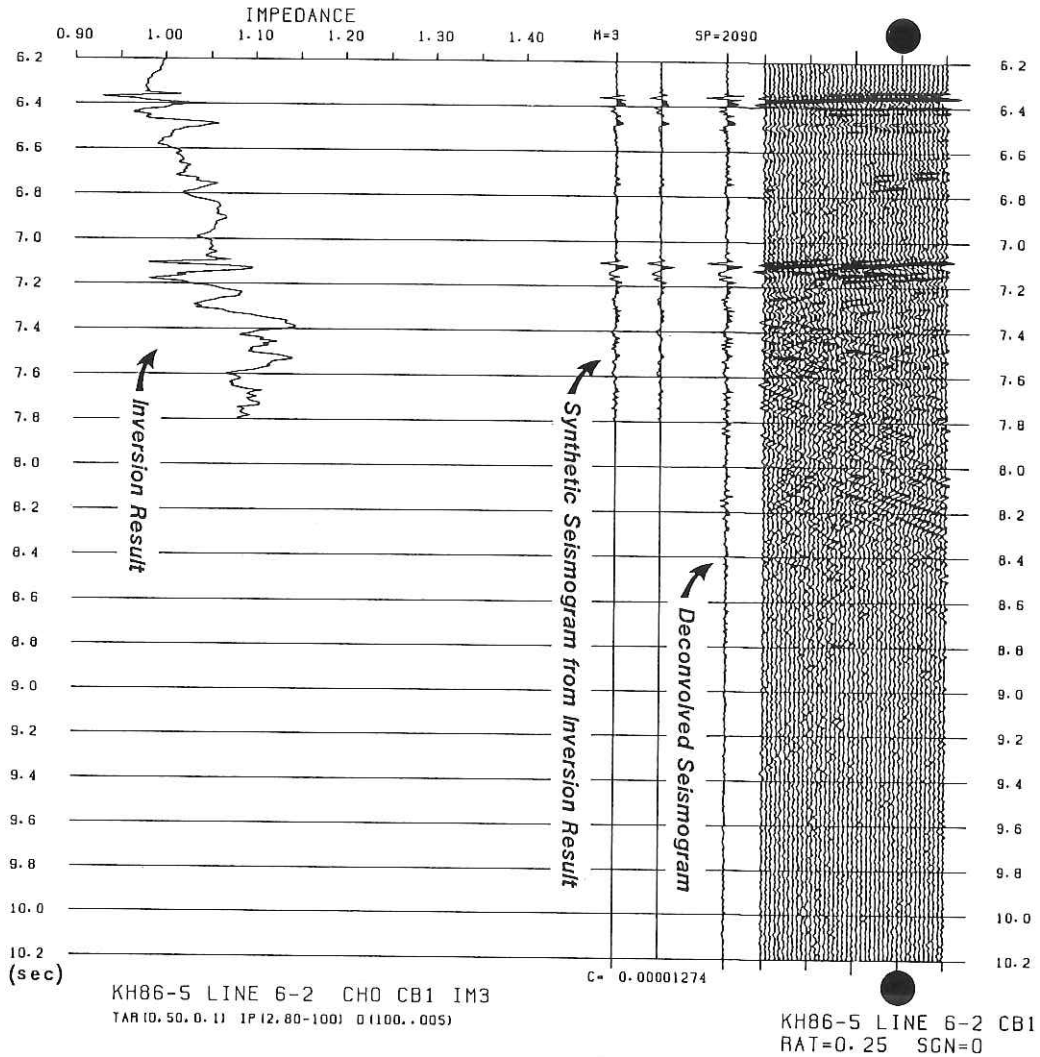

Fig. 4 An example of the inversion result.

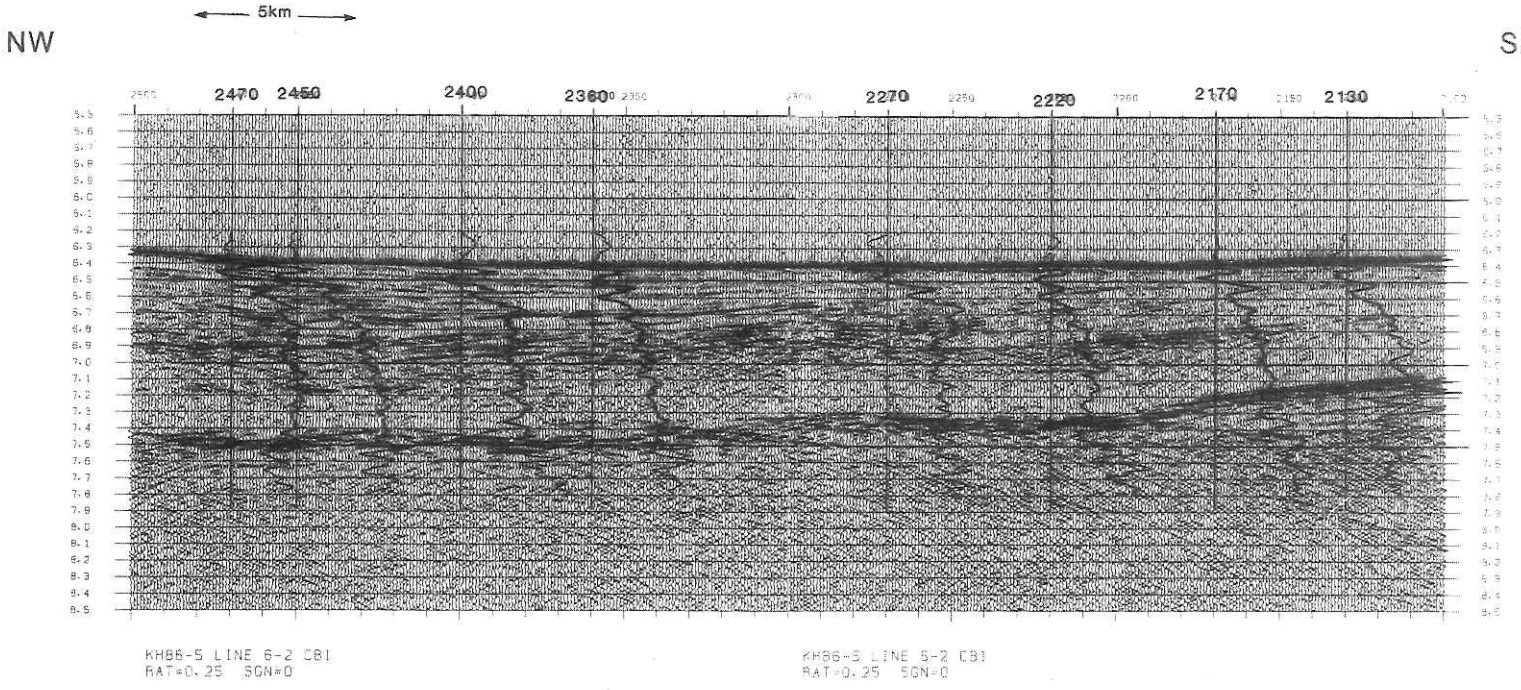

Fig. 5 A profile of line 6-2 superimposed by several acoustic impedance logs.

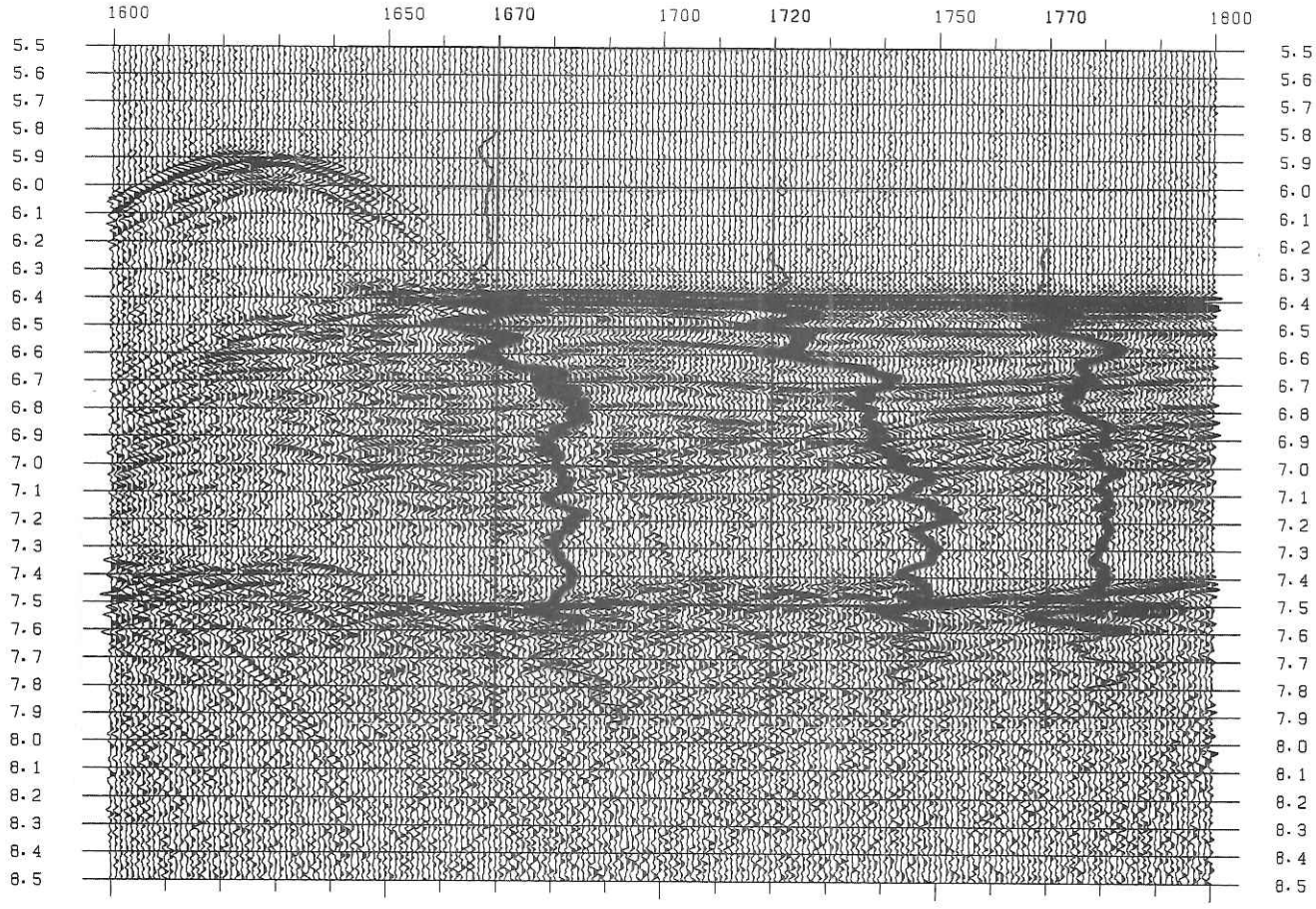

Fig. 6 A profile of line 6-1 and acoustic impedance logs shot points between1600 and 1800.

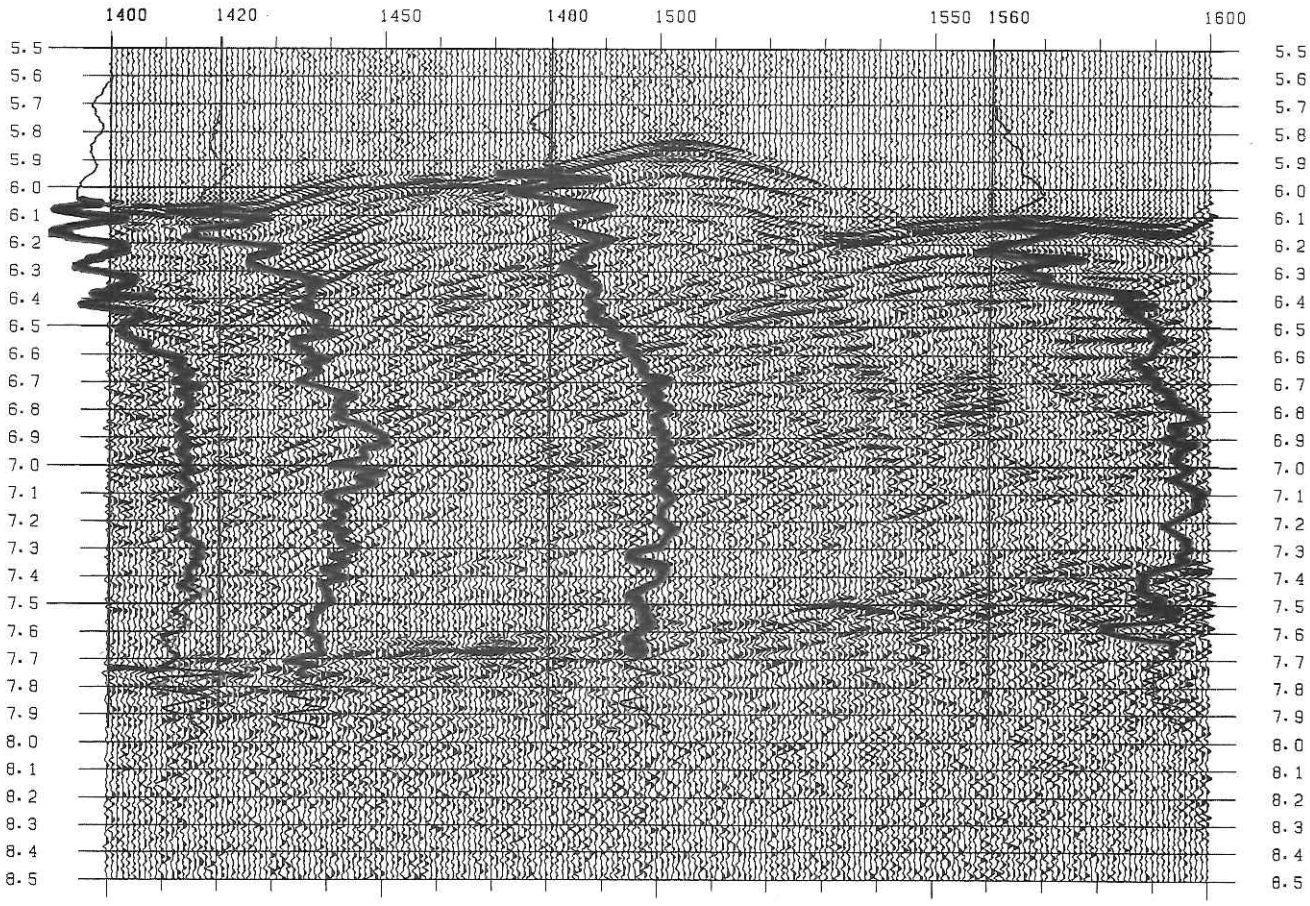

Fig. 7 A profile of line 6-1 and acoustic impedance logs shot points between1400 and 1660.

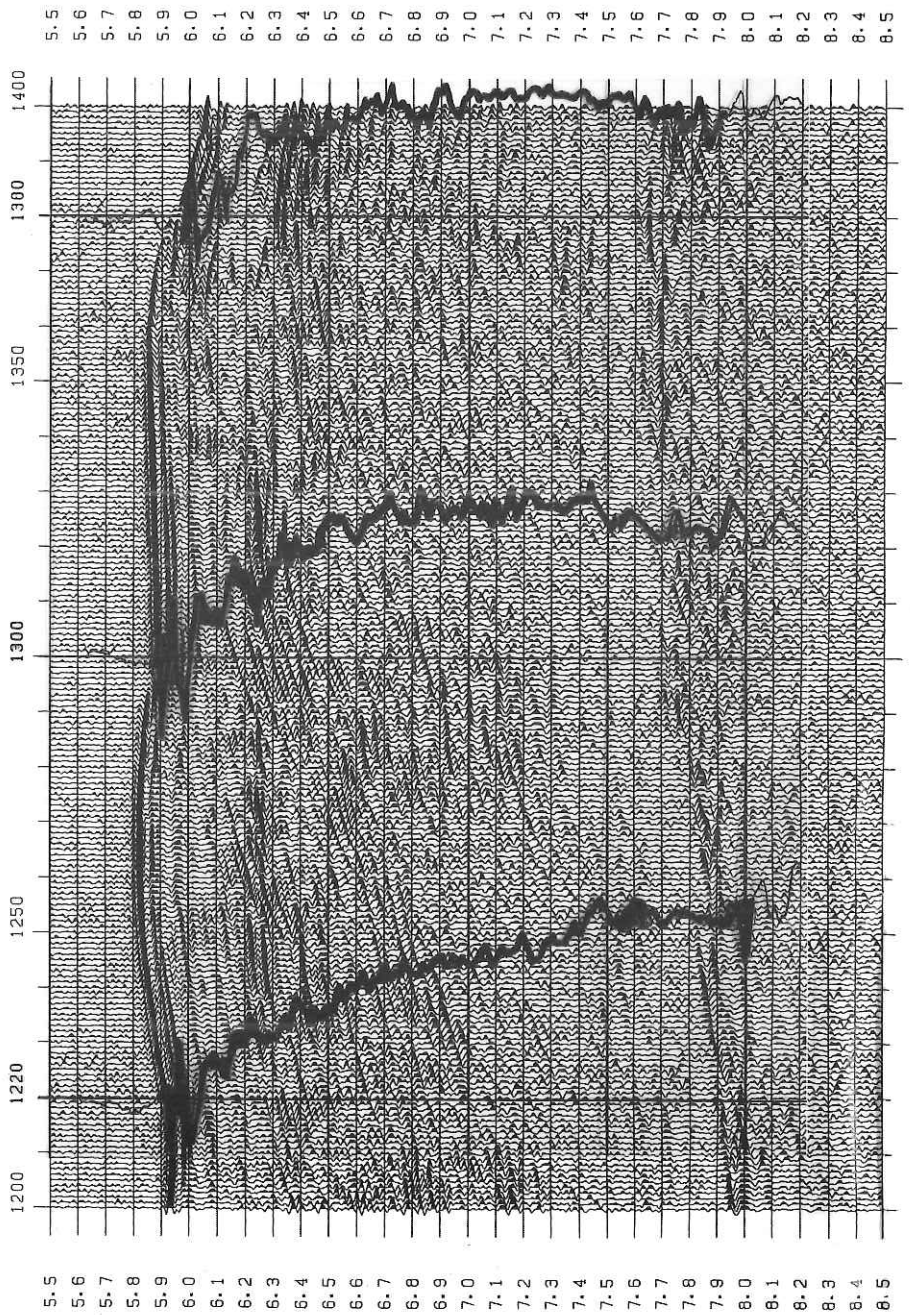

Fig. 8 A profile of line 6-1 and acoustic impedance logs shot points between 1200 and 1400.

A NEW APPARATUS FOR AZIMUTH DETERMINATION OF OCEAN BOTTOM SEISMOGRAPH

A. NISHIZAWA and S. NAKAO

Observation Center, Earthquake Prediction, Tohoku University, Sendai 980

INTRODUCTION

Recently, a lot of investigations about detailed crustal and upper mantle seismic structures have been performed by the experiments using OBSHs (Ocean Bottom Seismograph and Hydrophone). If we know the azimuthal variation of the seismic wavespeeds, we are able to deduce the tectonic evolution at the corresponding area. One of effective methods to know an anisotropy is detection of poralization anomaly of S wave. However, we could not know the horizontal seismeter orientation, since the pop-up types OBSHs fell freely to the ocean bottom. In this paper, we report a new apparatus for determination of the horizontal sensor orientation at the ocean bottom and the results from the experiment using that.

APPARATUS

A block diagram of the new apparatus is shown in Fig. 1. We used a magnetic needle to measure the azimuth and put it in a glass container filled with paraffin of a low viscosity and of a low melting point. In the container there is a nichrome time at the bottom. The magnetic needle rotates freely in the fluid paraffin and points to the north. After the electric current on the nichrome wire is shut at the other programmed time, the needle is fixed. Therefore we are able to know the horizontal sensor orientation at the ocean bottom.

Two apparatuses were placed in the one of the two glass sphere of OBSH system developed at Chiba University (Matsuda et al., 1086). These were tested for three OBSH systems in the KH86-5 cruise at the Nankai Trough.

RESULTS

Fig. 2 shows the orientation of the horizontal seismometers obtained from the magnet needles and the particle motions calculated for the direct water waves which were generated by the airgun shots. The orientation obtained from the apparatus shows consistency with that from the particles motion. We could determine the azimuth the

inclination of the seismometer from the slope of the paraffin surface. In the next step, we will investigate wavespeed variation for the circle airgun profile in this cruise based of the orientation of the OBSH.

ACKNOWLEDGEMENT

We thank Prof. H. Kinoshita, Miss N. Matsuda, Mr. Y. Kasumi and the scientists involved in the KH86-5 cruise for their cooperation during the experiment. We are also grateful to Drs. K. Suyehiro, T. Kanazawa and Y. Kuwahara for their valuable seggestions.

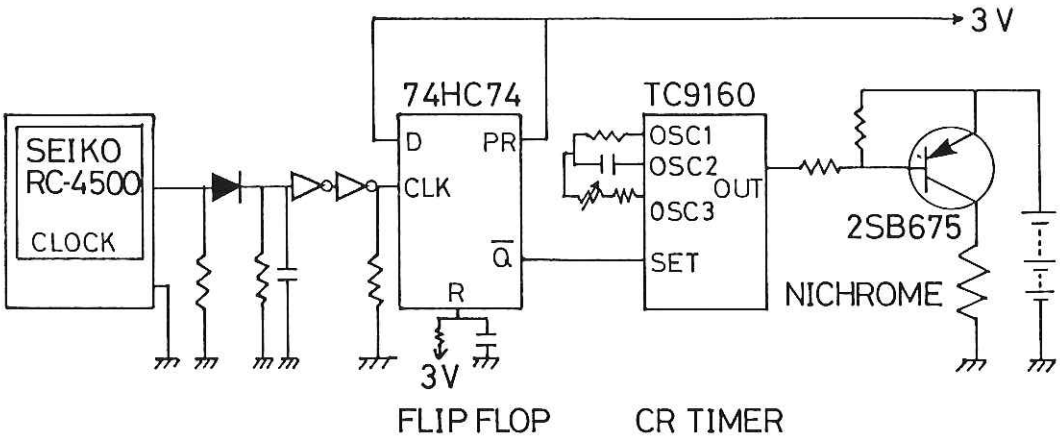

Fig. 1 Block diagram of the apparatus.

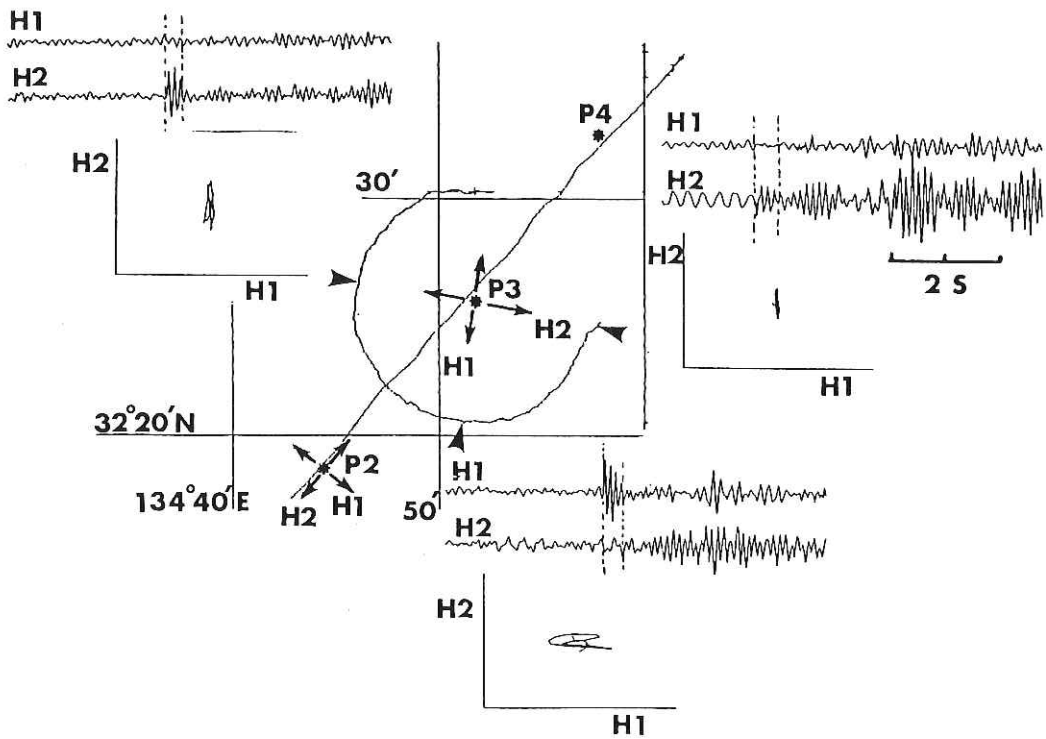

Fig. 2 Locations of OBSH(asterisks). Solid lines show the airgun profiles. Arrows at the P1 and P2 indicate the horizontal sensor orientation of each OBSH obtained from the magnet needles. Particle motions of the direct water wave from the airgun were calculated for the position shown by solid triangles.

HEAT FLOW MEASUREMENTS IN THE NANKAI TROUGH AREA

M. KINOSHITA
Earthquake Research Institute, University of Tokyo, Bunkyo, Tokyo 113
Y. KASUMI
Department of Earth Sciences, Chiba University, Yayoi, Chiba 260

INTRODUCTION

The Nankai Trough shows some peculiar features as a subduction zone (e.g. Sugimura, 1978; Yoshii & Kobayashi, 1981). First, it is not so deep (about 4,500 m at deepest) as compared with the normal subduction zones. Second, there is no deep earthquake (deeper than 70 km). Third, accretion structure is extremely developed on the landward slope.

The heat flow profile shows a strange feature. On the floor of the trough the heat flow is higher (130-150 mW/m^2) than either in the Shikoku Basin or on the landward slope (Yamano et al., 1984). In this study, therefore, a detailed survey across this "transitional" zone (boundary between the high heat flow on the trough floor and lower one on the landward slope) was made off Cape Muroto where the landward slope is not so steep as those in other similar parts of the trough. Furthermore, it has been tried to explain the high heat flow anomaly by pore water advection through the sediment (Yamano et al., 1984; Kinoshita and Yamano, 1986). To clarify this mechanism was one of the objectives of this study. Additionally, in relation to this mechanism, detection of dewatering along the thrusts by discovering high heat flow peaks was expected.

Five heat flow measurements were made along the main thrust in the easternmost part of the Nankai Trough. This area includes the southern end of the Tenryu Canyon, where biological colonies were discovered accompanied by thermal anomalies of 0.4 deg/10cm beneath the seafloor by the dives of the submersible Nautile (Le Pichon et al., 1987). Therefore, it was also planned to re-examine or to catch any sigh of the thermal anomaly along the main fault.

RESULTS

1. Off Cape Muroto

In Fig. 1, heat flow values around this area are shown. The results of measurements are plotted in Fig.2. (the area corresponds to the hatched area in Fig.1) on the Seabeam map obtained by the KAIKO project Phase I (KAIKO I Research Group, 1986) together with previous heat flow was measured.

The heat flow profile along the 55-2 line is shown in Fig.3 together with the interpretation of the 55-2 line by A. Taira (personal communication). Values with error bars represent the estimation by the gas hydrate method developed by Yamano et al. (1982). Plotted values are taken from the area enclosed in Fig.1 in other area is not plotted.

First, gradual decrease of heart flow from 100mW/m^2 near the deformation front to 30-40W/m^2 on the upper part of the slope is clearly recognized. Second, the high heat flow (about 150mW/m^2) seems to be confined on the seaward side of the deformation front i.e. on the trough floor, through the number of data is not enough. Third, at HF2 which is located on the deformation front, quite high heat flow (around 190mW/m^2) was observed. At this station none of five trials were successful and the probe stood tilted. However, their temperature profiles were linear and obviously the sensors were in the mud. Furthermore. estimated values (HF2A-HF2E) in consideration of the instrument tilt are in good agreement with each other. Therefore, the high heat flow at HF2 is rather reliable. A much more detailed heat flow profile near the deformation front is shown in Fig.4, in which all the data including less reliable ones due of the instrument tilt are plotted.

2. The Easternmost Part of the Nankai Trough

The results is shown in Fig.5. As is seen, very few heat flow measurements have been performed so far around this area.

Unfortunately, the position of HF13 was a few miles north of the biological communities at the end of the Tenryu Canyon (Fig.6-a, Seabeam map). The probe did not penetrate at all and heat flow value could not be determined. No thermal anomalies were found in the seawater.

At HF14 and HF15 located slightly seaward of the main thrust (Fig.6-b), rather low heat flow values were observed, which seem to be consistent with the previous values along the eastern part of the Nankai Trough. This indicates that the high heat flow anomaly in the Nankai trough is at least limited to the area west of 137° E.

DISCUSSION

First of all, we try to explain the gradual decrease of heat flow on the landward slope of the Nankai Trough as the cooling effect of the subducting Philippine Sea plate and the topographic effect by the landward thickening of the slope sediment due to accretion. For

this purpose, a simple two dimensional steady state model is constructed and its thermal structure is numerically calculated. The model is depicted in Fig.7-b, together with the values of the convergent velocity and thermal conductivity for each block. In the steady state, thermal structure is described in the next formula :

$$\rho c\left(u\frac{\partial T}{\partial x} + v\frac{\partial T}{\partial z}\right) = \frac{\partial}{\partial x}\left(k(x,z)\frac{\partial T}{\partial x}\right) + \frac{\partial}{\partial z}\left(k(x,z)\frac{\partial T}{\partial z}\right)$$

were T is the temperature, (u,v) the converging velocity in the direction of (x,z), k(k,z) the thermal conductivity, the density and c the specific heat. In this case, the term ρc is determined from the thermal diffusivity, κ(8/0*10-^{7}m /s), which is assumed to bae constant, as k(x,z)/κ.

The boundary conditions are :

T=0(C) at surface

lateral heat flux=0 at both sides

basal heat flux=Q(mW/m^2) (treated as a parameter)

As the value of Q, either 150mW/m^2 that was observed on the trough axis or 110mW/m^2 estimated from the age of the Shikoku Basin (Kobayashi and Nakada, 1978), was attempted.

The calculated surface heat flow is shown in Fig.7-a together with the model configuration. As is recognized, the calculated values corresponding to Q=110mW/m seem to fit rather well with the observation on the landward slope, while the Q=150mW/m^2 curve are too high. However, the Q=110 curve does not fit the observation on the trough floor. This means that the model is too simple and needs some supplementary heat transfer mechanism.

As one of these possible mechanisms, the dewatering process was suggested (Yamano et al., 1984). Trough fill sediment (turbidite and the Shikoku Basin hemipelagite) is, as it is accreted landward, deformed and compacted. This causes warm pore water included in the sediment to well up and carry heat together, which consequently causes high heat flow at the surface. However, this mechanism is quantitatively not preferred by the same authors because unrealistically large amount of warm water at depth is necessary to explain the high heat flow on the trough, assuming basal heat flux as 110mW/m^2. Kinoshita and Yamano (1986) in turn suggested and alternative mechanism that, instead of this large scale dewatering, the water is supplied somewhere on the landward slope.

Here, the result of our measurements is qualitatively interpreted in view of the dewatering process on trial. One possible interpretation is schematically drawn in Fig.8. The basal heat flux is assumed to be 110mW/m^2. The higher heat flow on the trough is considered to be caused by upwelling of the pore water, which comes from the sediment

deformed on the accretionary complex through the channel of the "megathrust" (decollemant) that bounds two plates. This upwelling process may be supported by the nonlinear (convex upward) temperature versus depth profile of HF12, which can be caused when the upward advective heat transfer exists. At the deformation front, water may come up more rapidly than on the undeformed floor, which causes the higher heat flow at HF2. However, judging from that the temperature profile of HF2 are linear, the flow rate of the upwelling water can not be so large as to generate nonlinear temperature profiles. On the landward slope, in turn, lower heat flow than is expected from the cooling model should be caused by the downgoing of the pore water or the injection of sea water downward. However, if the flow rate is slow enough, this decrease may not be recognizable. The heat flow obtained by this study seems to indicate that the upwelling of water does not occur landward of the deformation front at all. The upwelling may be occurring along the thrusts in the accretionary prism and it could be observed as a local high heat flow anomaly, through it was not detected in this survey.

However, the explanation presented here is extremely crude, and it still lacks the quantitative basis and may not overcome the problem of the amount of water to be squeezed out and to carry enough heat for the anomaly. To explain the heat flow anomaly completely, more detailed survey is absolutely necessary.

Next, we discuss about the nonlinear temperature profiles at HF9 and HF12 in relation to the change in the thermal conductivity.

At P-6 and P-7, thermal conductivities were measured (Fig.2). The change in the thermal conductivity with depth prevails at P-6 (Fig.5), which may have an influence on the temperature profile and give nonlinear profiles as in HF-9 and HF-12. We estimate the magnitude of the change in temperature profiles affected by the nonlinear distribution the thermal conductivity with depth.

Suppose that the sedimentary layer consists of N layers of thickness equal to z (Fig.9-a). Tn, the temperature at the bottom of the N-th layer, is approximately given the next from:

$$Tn = Q \cdot \Delta Z \cdot \sum_{i=1}^{n} \frac{1}{Kn} + T_0$$

where Q is the heat flow which is constant throughout the sedimentary layer, Kn the thermal conductivity assumed to be constant in the N-th layer, and T_0 the surface temperature.

The temperature profile is obtained on the assumption as follows:

(1) The distribution of the thermal conductivity at P-6 is given in Fig. 9-b, based on the measurement;

(2) $T_0 = 0$ (C);

(3) Q=110 (mW/m^2)

The temperature profile at P-6 obtained in this manner is shown in Fig. 10.

The influence of the nonlinear change in the thermal conductivity on the temperature profile does not seem to be significant. It seems likely that the temperature profiles at HF-9 and HF-12 (Fig.4-e) may be influenced by some other factors.

By the way, we consider whether acceptable heat flow value can be obtained using the average value of thermal conductivities which actually with depth. In this case, the temperature gradient is decided from the temperature profile in Fig. 10 by the least square fit and the heat flow value is simply estimated as the product of this temperature gradient and the average thermal conductivity at P-6. The heat flow estimated in this manner should be different from the true value 110mW/m^2 to some extent.

The temperature gradient is calculated as 151mK/m^2 and the average thermal conductivity at P-6 as 0.75W/mK, which give the heat flow as 113mW/m^2. This value is within the limit of error of observation in the present technique. It seems that the true heat flow may safely be obtained using the average thermal conductivity, if the magnitude of its variation with depth is as small as in the case of P-6.

CONCLUSIONS

Heat flow was measured at the accretion toe off Cape Muroto in the Nankai Trough to investigate the thermal structure around the deformation front in detail. On the landward slope., heat flow gradually decreases landward, which can be explained by the cooling effect of subduction. The high heat flow anomaly is confined on the non-deformed through floor,and just at the deformation front was observed much higher heat flow. These features may result from the dewatering process of the pore water, though it is not quantitatively inspected.

Heat flow measured along the main thrust in the eastern part of the Nankai Trough was lower than those in the western part, which, together with previous results, limits the high heat flow area west of 137 E.

REFERENCES

Kaiko I Research Group, 1986, Topography and structure of trenches around Japan -Data atlas of Franco-Japanese Kaiko Project, Phase I-, Ocean Research Institute (University of Tokyo), Institute Francais de Recherche pour 1' Exploitation (IFREMER), and Centre National de la Recherche Scientifique.

Kobayashi, k. , and Nakada, M. , 1978, Magnetic anomalies and tectonic evolution of the Shikoku inter-arc basin, J. Phy. Earth 26, Suppl.: S391-S402.

Le Pichon, S. , Iiyama, T. , Boulegue, J. , Charvet, J. , Faure, M. , Kano, K. , Lallemant, S, Okada, H. , Rangin, C. , Taira, A. , Urabe, T. , and Uyeda, S. , 1987, Nankai Trough and Zenisu Ridge : A Deep-Sea Submersible Survey, Earth Planet. Sci. Lett. 83, 199-213.

Sugimura, A. , 1978, in " The Earth Science " vol. 10, pp.159-181, (in Japanese).

Yamano, M. , Uyeda, S. , Aoki, Y. , and Shipley , T. H. , 1982, Estimates of heat flow derived from gas hydrates, Geology 10:339-343.

Yamano, M. , Honda, S. , and Uyeda, S. , 1984, Nankai Trough: A hot trench?, Marine Geophys. Res. 6:187-203.

Yoshii, T., and Kobayashi, K. , 1981, Geophysics of Subduction Zones, in " Kagaku" , 51: 472-478 (in Japanese).

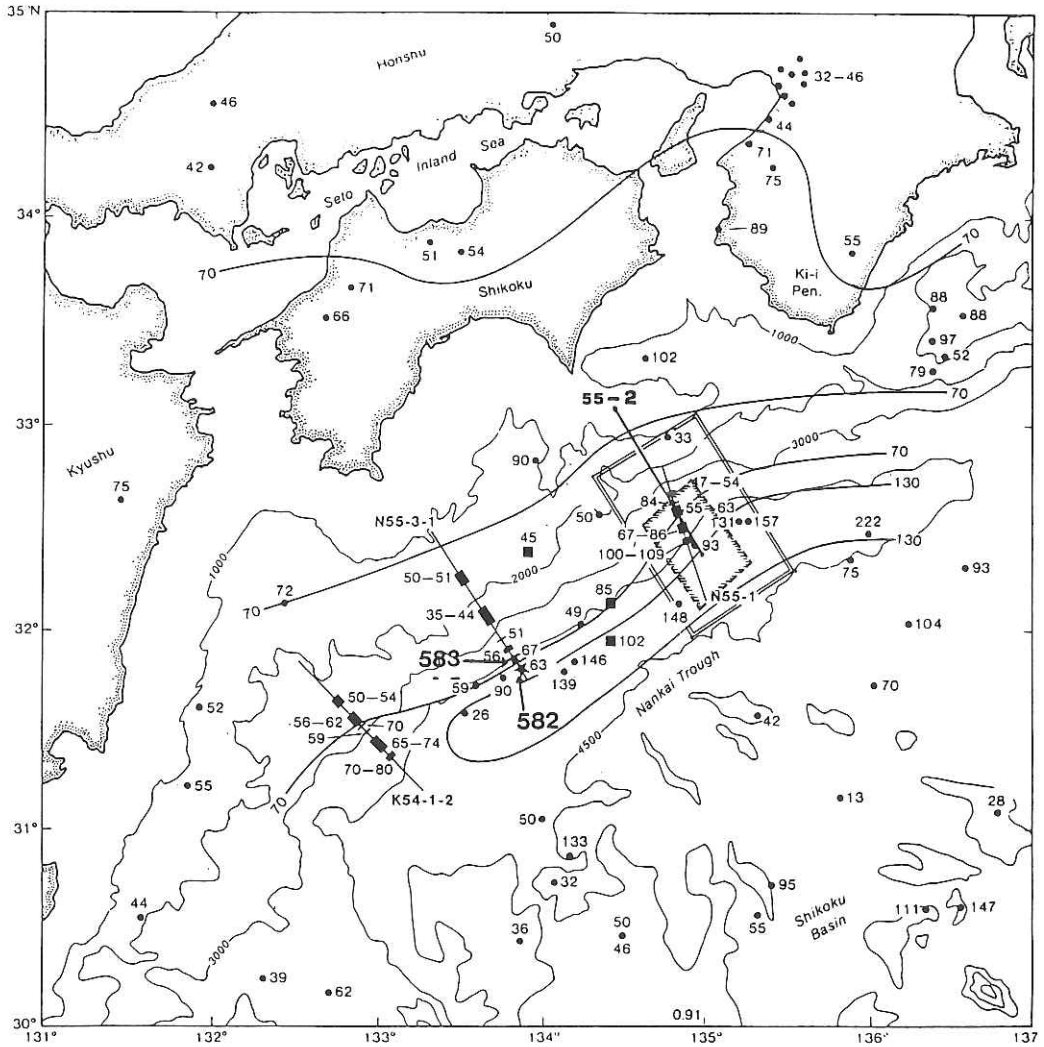

Fig. 1 Index map of the Nankai Trough area together with previous heat flow vales (from Kinoshita and Yamano, 1986). The area enclosed by the hatched square is the measured area. Heat flow value within the area enclosed by the double square are used for the interpretation of this area. The "55-2" line is the multichannel seismic line by JAPEX.

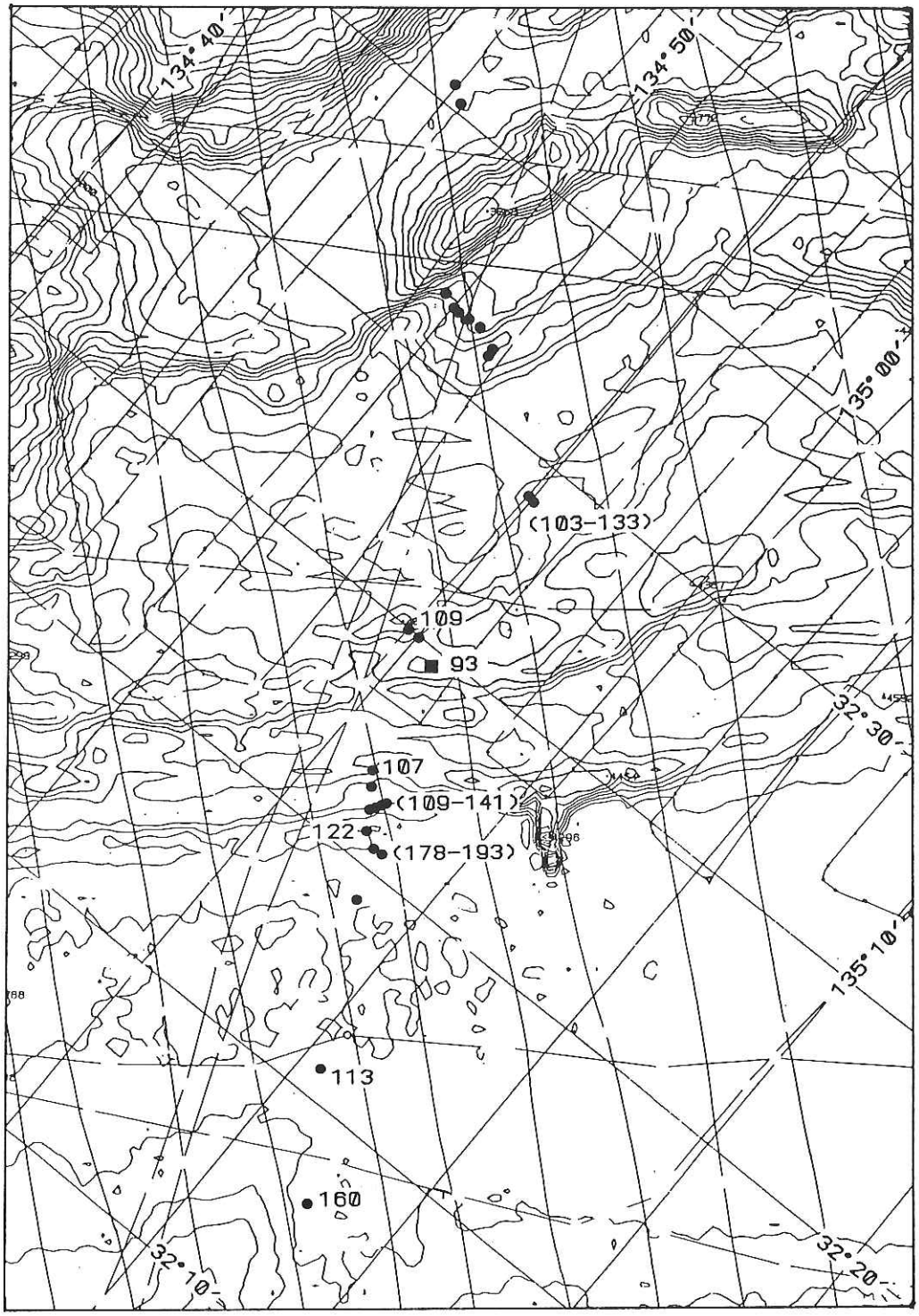

Fig. 2 Results of heat flow measurements in the Nankai Trough off Cape Muroto (solid circles) together with previous one (solid square). Unit: mW/m^2. Values in parentheses are less reliable due to the tilt of the probe.

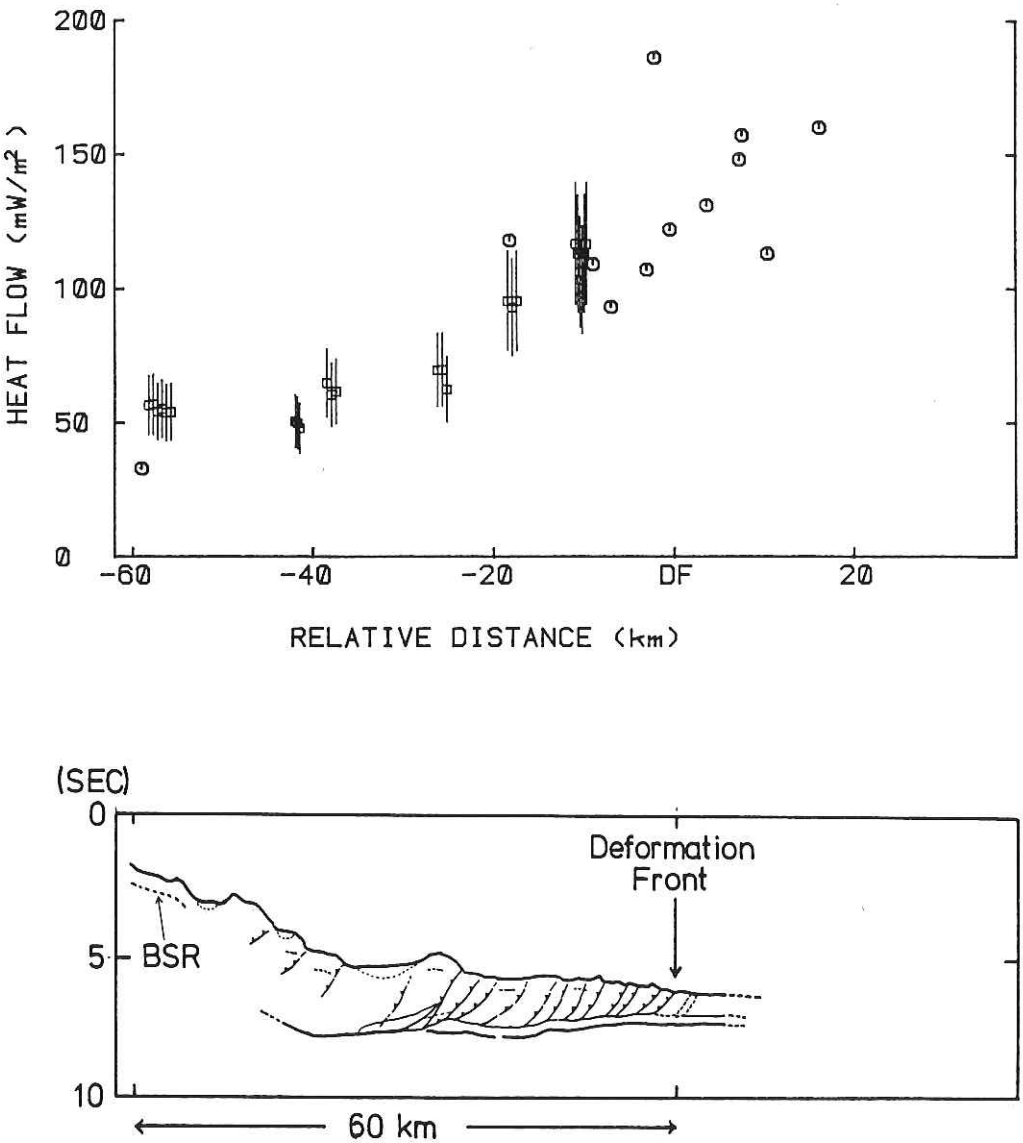

Fig. 3 The heat flow cross section in the Nankai Trough off Cape Muroto together with the interpretation of the seismic profile "55-2". Solid circle: this study, open circle: previous ones, open square with error bar: estimation by the gas hydrate method. These data are taken within the area enclosed by the double square in Fig. 1. In the lower part is shown the interpretation of the "55-2" line by Taira (personal communication).

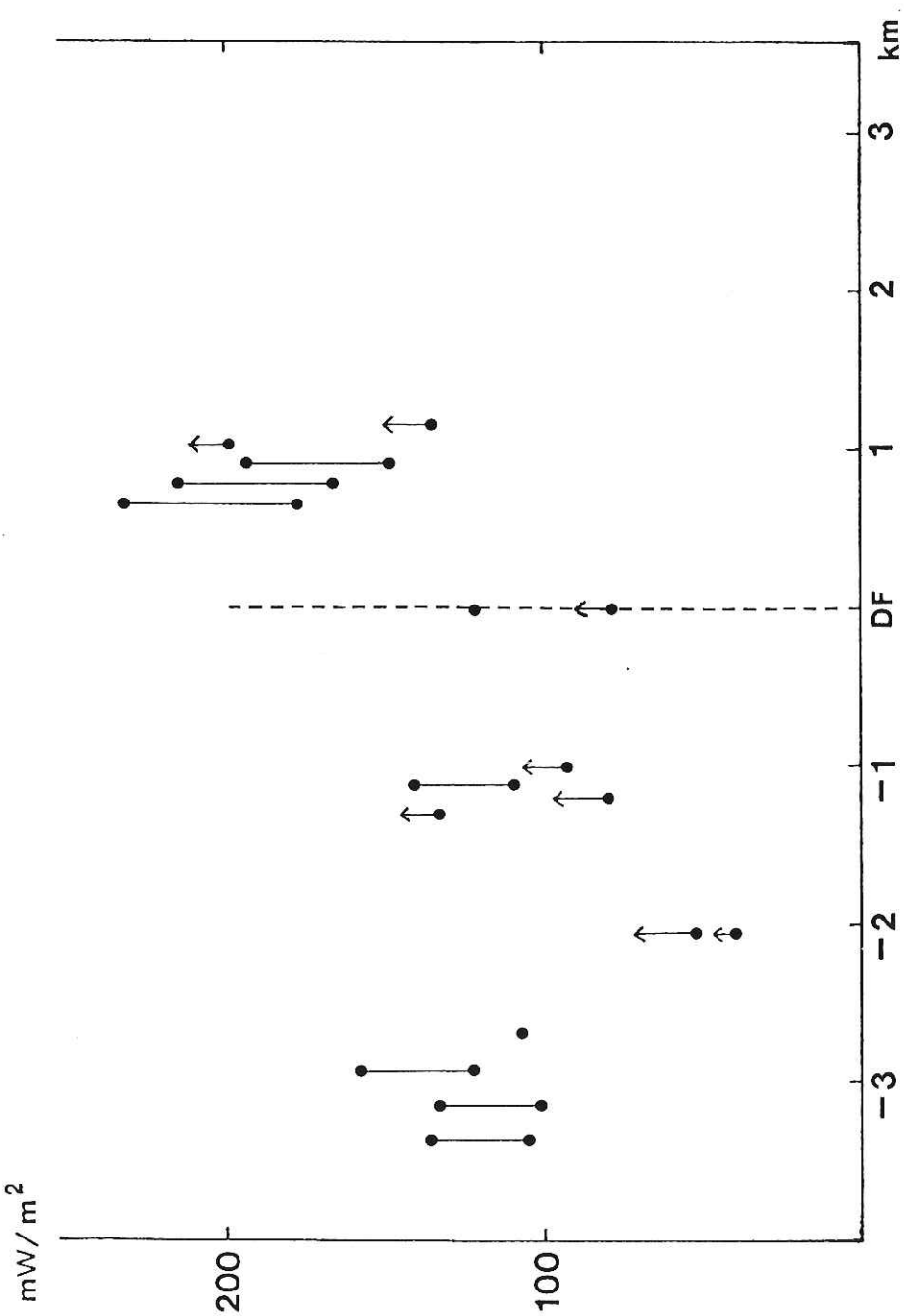

Fig. 4 The detailed heat flow cross section near the deformation front (DF) of the Nankai Trough off Cape Muroto. In this figure, all the data including tilted trials are plotted. The data which have two dots linked by a line is the estimation in case of tilted penetration. The lower dot corresponds to 7° tilt, and the upper 40° tilt. The data with the arrow upwards indicates the minimum estimate in case of tilt of more than 40°.

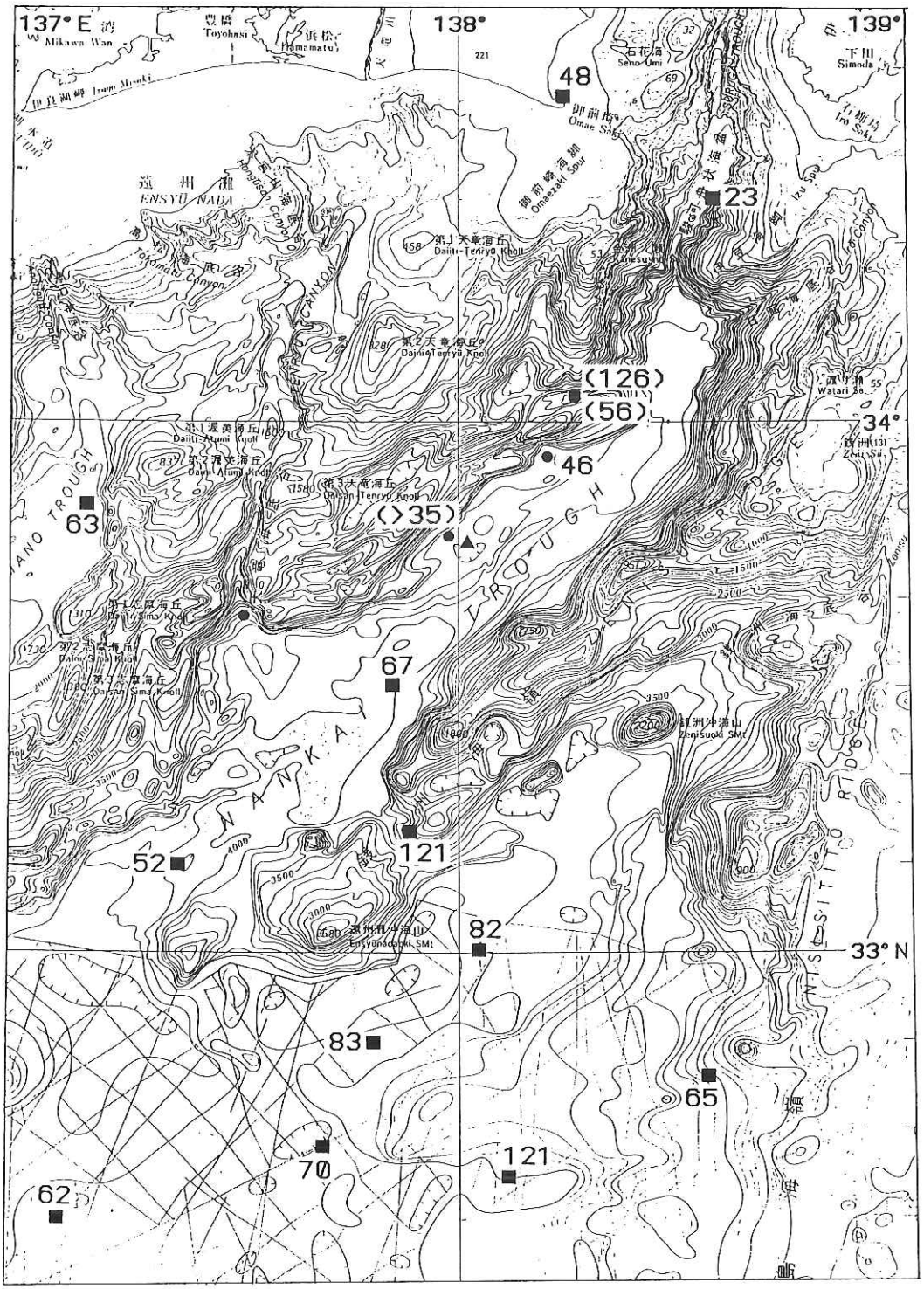

Fig. 5 Results of heat flow measurements (solid circle) in the eastern part of the Nankai Trough, together with previous values (solid square). The data with parentheses are less reliable due to the tilt of the probe.

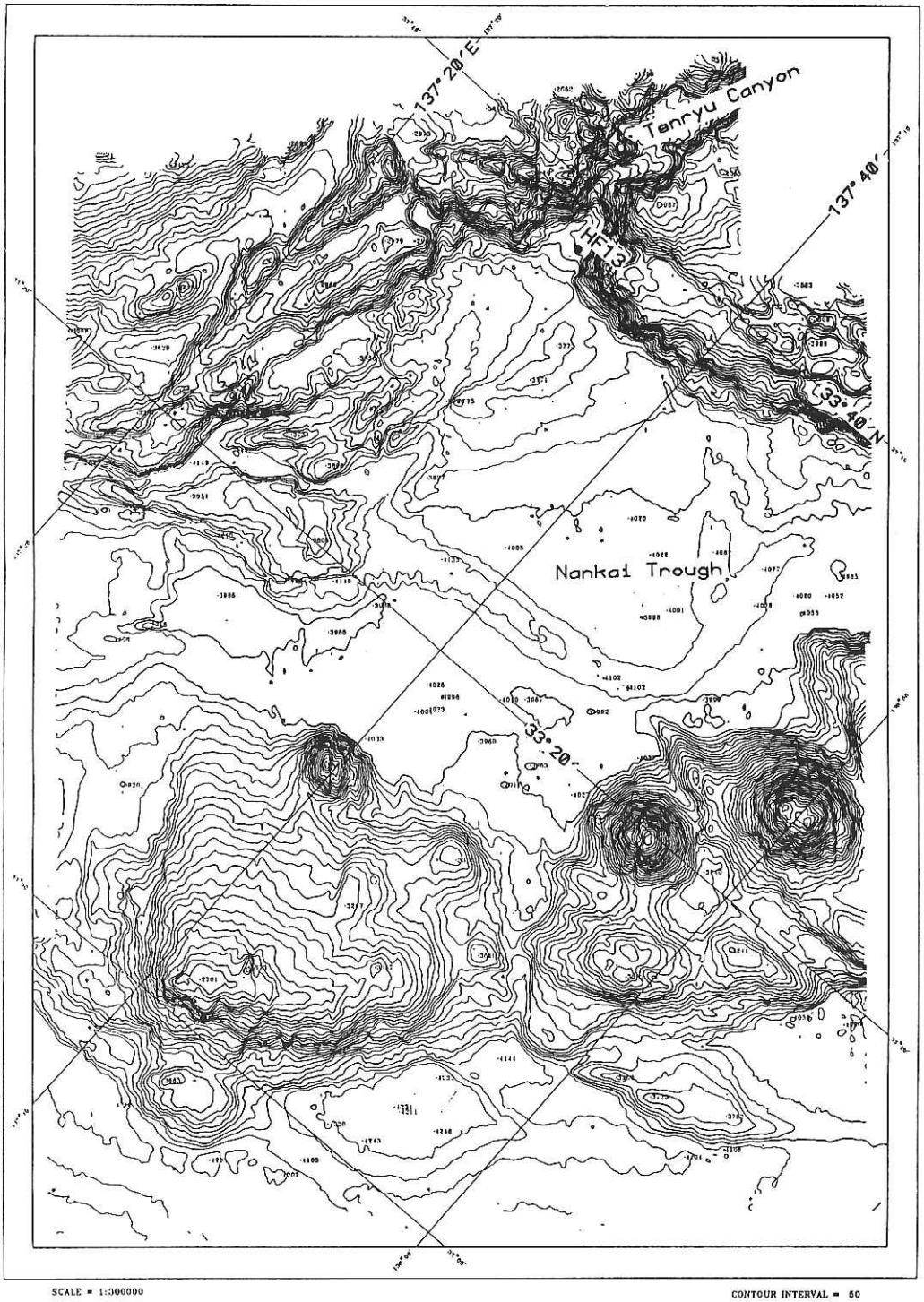

Fig. 6 (a) The detailed Seabeam map near the end of the Tenryu Canyon and the heat flow station HF13.

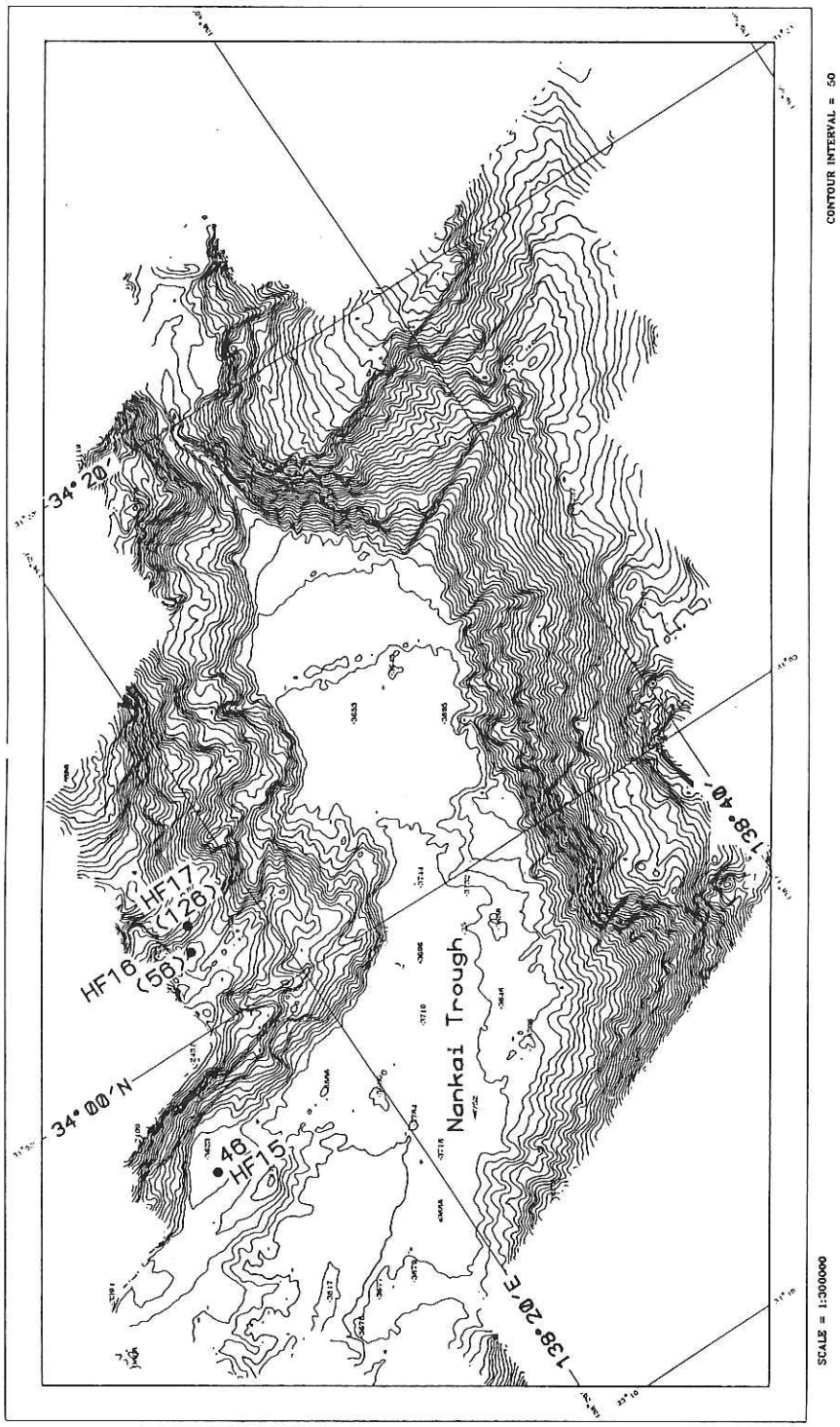

Fig. 6 (b) The seabeam map in the eastern end of the Nankai Trough, including the heat flow stations and values.

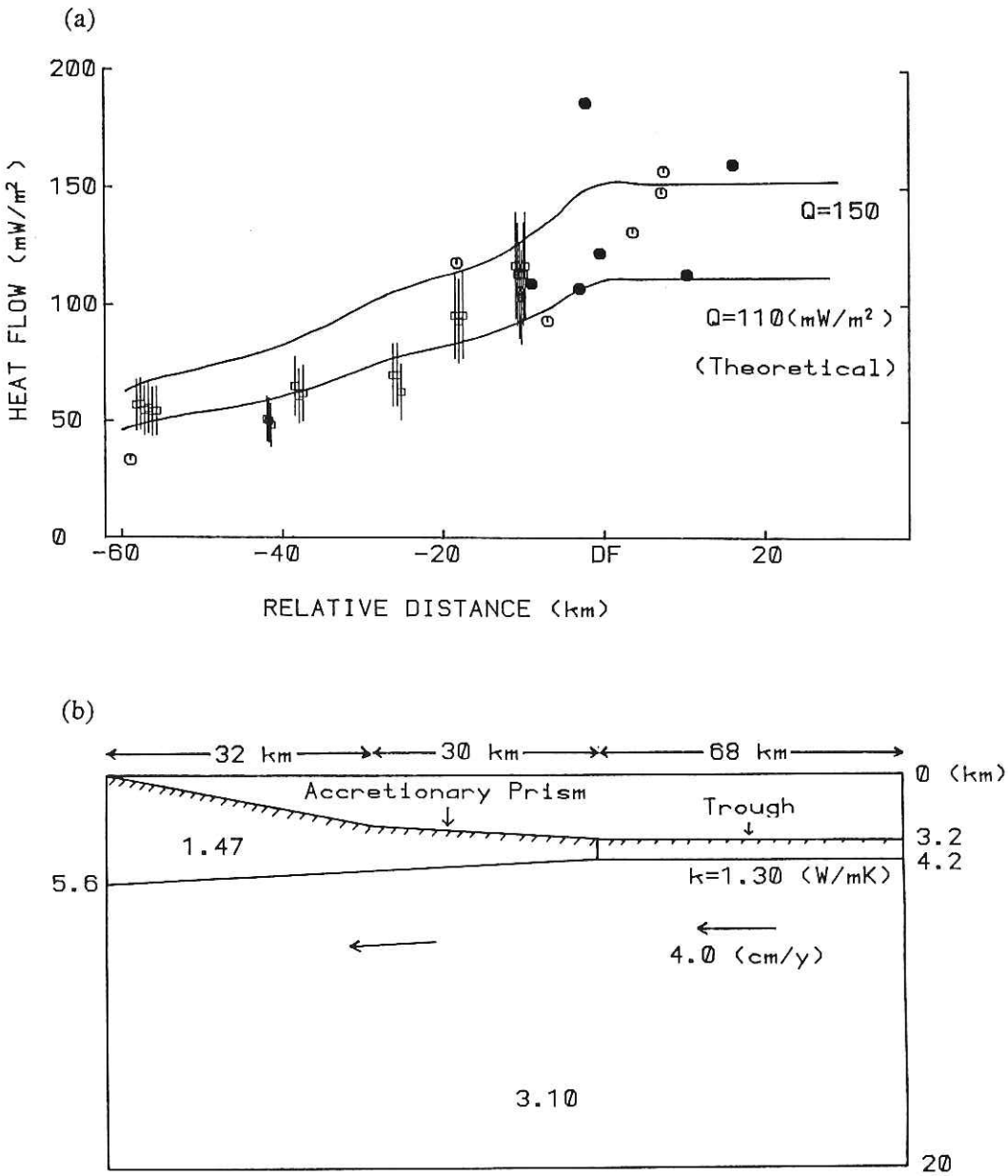

Fig. 7 (a) Calculated surface heat flow according to the steady state model described in (b). (b) The steady state subducting model simulating the Nankai Trough. The notation k is the conductivity.

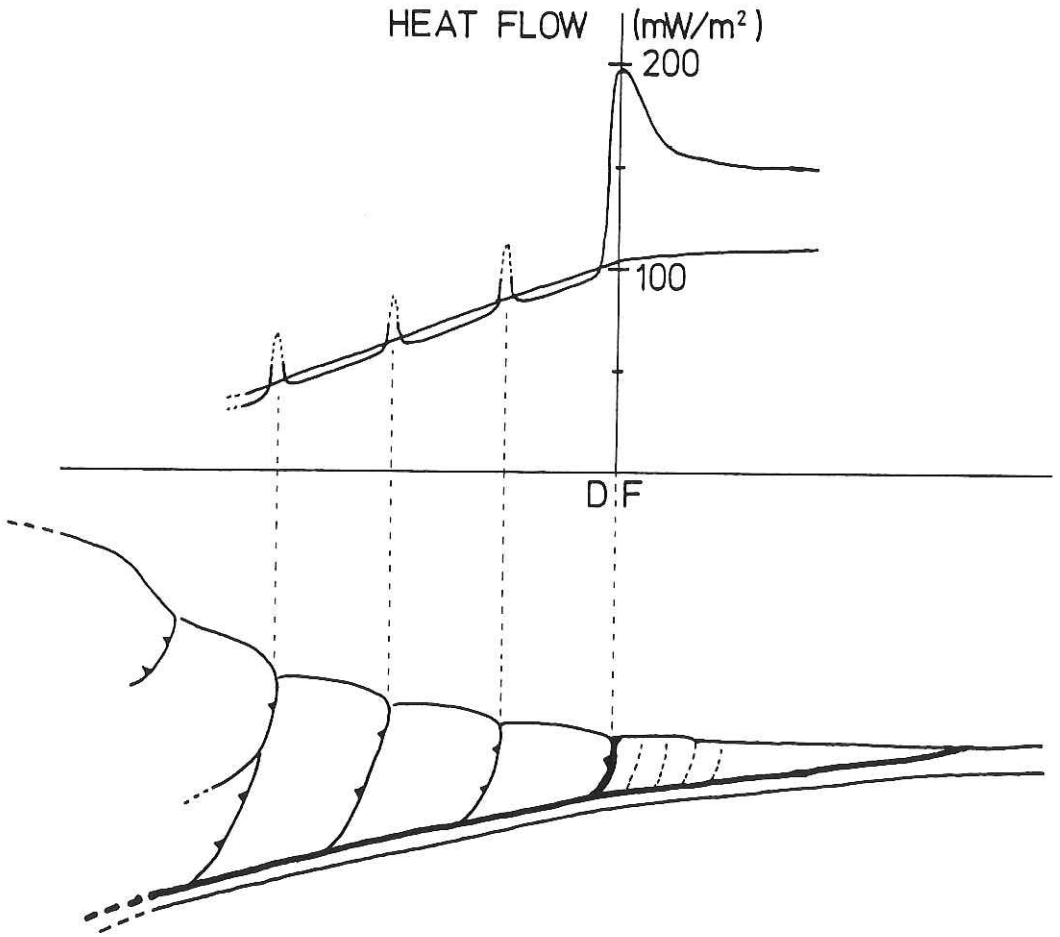

Fig. 8 Schematic drawing that shows the flow of pore water quantitatively, and the heat flow profile expected from this model.

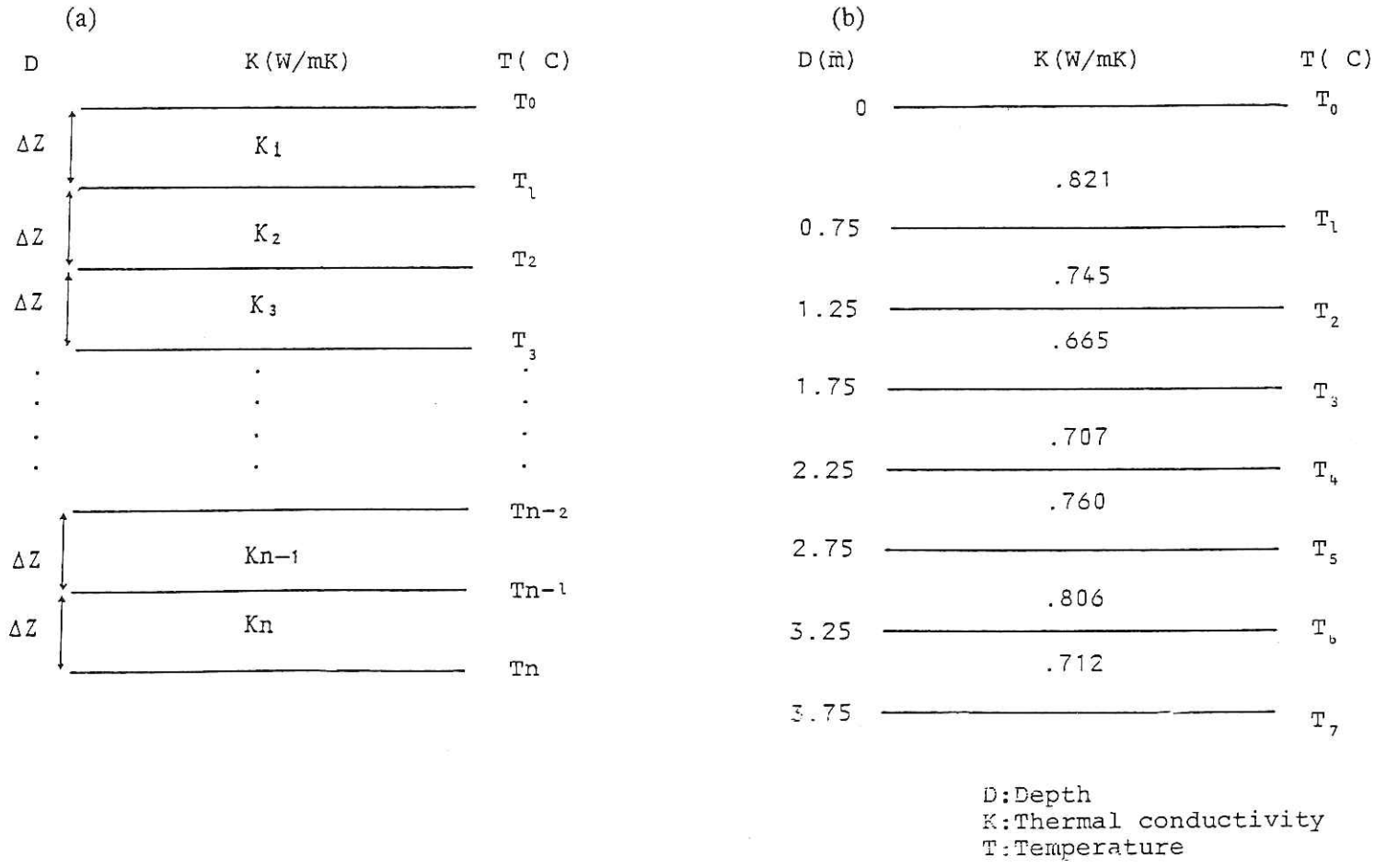

Fig. 9 (a) Sedimentary layer supposed consists of N layers of thickness equal to Z, Tn is the temperature at the bottom of the N-th layer. (b) Sedimentary layer supposed at P-6, thermal conductivity is constant within one layer.

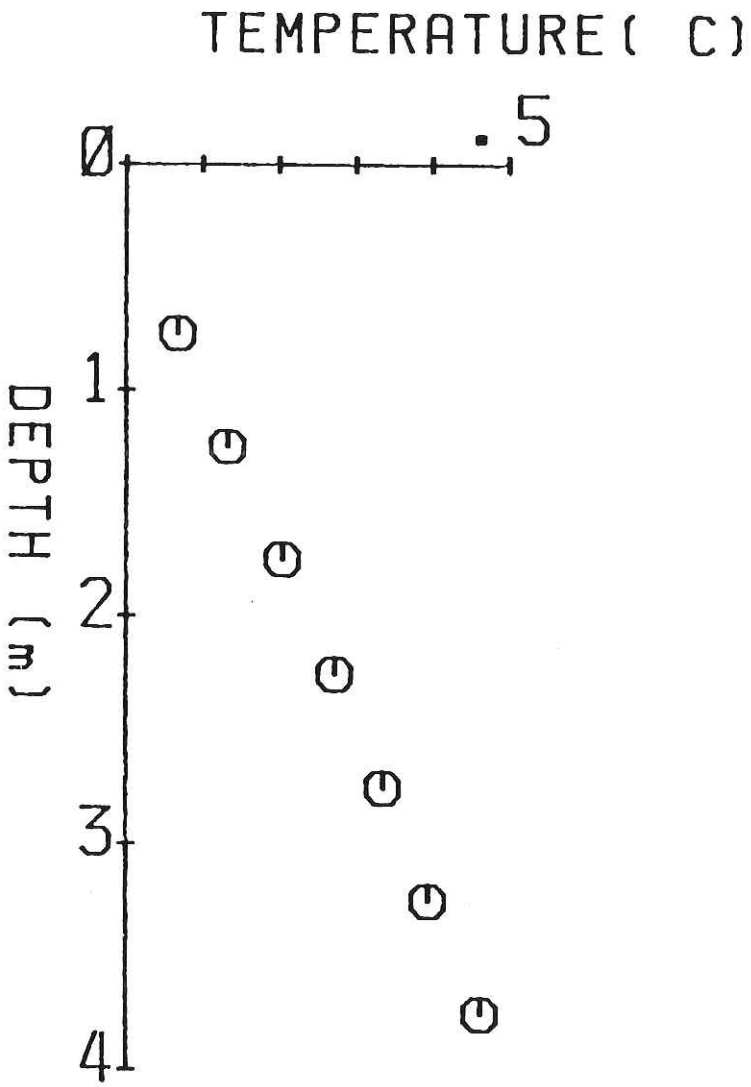

Fig. 10 Calculated temperature profile at P-6 assuming that sedimentary layer is given as in Fig. 9-b. To is 0°C and Q is 110mW/m^2.

HYDROGEOLOGIC FRAMEWORK OF THE NANKAI TROUGH ACCRETIONARY PRISM

A. TAIRA, E. NISHIYAMA and H. TOKUYAMA
Ocean Research Institute, University of Tokyo, Nakano, Tokyo 164
M. KINOSHITA
Earthquake Research Institute, University of Tokyo, Bunkyo, Tokyo 113
W. SOH and J. ASHI
Ocean Research Institute, University of Tokyo, Nakano, Tokyo 164

INTRODUCTION

Deformation of sediment at the toe of landward slope of trench and subsequence accretion of sediment are the initial processes of crustal evolution and mountain building. Freshly deposited sedements usually contain high percentage (80 to 50%) of interstitial water. The deformed and accreted sediments on land usually show very low porosity values normally less than 10 per cent. Therefore, it is expected that a remarkable reduction of porosity takes place within accretionary prism. Because the structual styles and fabrics of accretionaly prisms are controlled by physical properties of the sediments, it can be inferred that the hydrogeology of accreted sediments is a key factor for understanding the initial tectono-diagenetic evolution of orogenic belts.

The Nankai Trough is an impotant field in this aspect for several reasons:

1. It is a coarse-grained, clastic dominated trench similiar to most ancient accretionary complexes.
2. It has been surveyed by various means including most of geophysical and geological techniques. Thus, a large data base will allow us to constrain our scientific interpretation.
3. An ancient example of an accretionary prism which was formed in a quite similiar setting is exposed onshore directly to the nortth. The Cretaceous-Tertiary Shimanto accretionary prism is a direct analogy to the Nankai accretionary arism.

One of the main objectives of the KH86-5 cruise by the R/V Hakuho-Maru was to investigate the hydrogeologic framework of accretionary prism at the Nankai Trough to the south of Island of Shikoku. This report presents a preliminary interpretation of the results.

At the same time, we present a brief account for an comparision of Nankai vs. Barbados, i.g. sand- vs. mud-dominated prism hydrogeology.

STRUCTURE OF THE TROUGH ACCRETIONARY PRISM

The structual style of the Nakai Trough trench and accretionaty prism of the surveyed area can be interpreted based on the seismic reflection data (Fig. 1). At the trench, seismic stratigraphy shows three distinctive layers: horizontally layered upper sequence, inclined lower transparent sequence and acoustic basement. The resuots of the DSDP Legs 31 and 87 (Karig and Ingle et al.,1975; Kagami and Karig et al,. 1986) showed that these layers correspond with the upper turbidite layer and the lower hemipelagic layer respectively. The acoustic basement are considered as the oceanic crust. There is a highly reflective horizon within the hemipelagic layer which has been interpreted as the Pliocene sandy layer.

The accretionary prism is characterised by a series of folded and thrusted turbidite sediments. Underneath, the hemipelagic layer continues to subduct without being doformed for a distance of some 30 kilometers. Then the acoustic image of the structure becomes unclear substituted by vague landward dipping reflectors. The boundary between the upper deformed turbidite and the lower horizontal hemipelagic layer should be a fault zone because of structual discontinuity. We call this horizontal fault decollement hereafter.

In the more landward portion of the prism, It is inferred that there is a series of late thrusts (out-of-sequence thrust) cross-cutting the initial imbricate thrust system. This was judged based on the details of seismic structure and vertical thickening characteristics of the prism. Figure 2C summarizes the main structural feature of the Nankai accretionary prism.

It is also noteworthy that there is a bottom simulating reflector throughout the prism which is a good indicator of geothermal gradient.

FLUID CIRCULATION AS INFERRED FROM HEAT FLOW

Heat flow transect obtained during the cruise was analyzed by M. Kinoshita (see Kinoshita, 1987MS; also Kinoshita and Kasumi,this report). The result indicates the following important implications to the hydrogeology (Fig. 2).

1. There is a general landward decrease of heat flow value.
2. A sharp rise of heat flow is recognized at the toe of deformation front.
3. Fluctuation of heat flow values is a characteristic feature of the landward slope.

Taking a value of 110W/m^2 as a theoretical basal heat flow from oceanic crust. It was found that the heat flow value observed at the trench was higher than general trend (Fig. 2A). We suggest that this anomalous heat flow trend is due to fluid circulation. The high peak at the deformation front can be related to the concentrated seepage along the fault. At the landward slope, the fluctuation pattern of heat flow seems to correspond to the structure of prism; high at the fault zone and low in between. We

propose upwelling and downwelling circulation within the prism.

SEEPING RELATED ANIMAL COMMUNITIES

One of the direct evidences for fluid circulation and related fluid venting is the existence of unusual animal communities. During the Japan-French KAIKO Project, seepage related animal communities mainly composed of clam(*Calyptogena*) and tube worm were found through the observation using the submersible Nautile in the region of Tenryu deep-sea fan (Le Pichon and Iiyama et al, 1987). *Calyptogena* and tube worm have been also found in the trend landward slope region of offshore of the Island of Shikoku by means of dredging and the submersible Shinkai 2000 diving (Fig. 3).

During the KH86-5 cruise, underwater photography was carried out in order to detect the evidence of seepage. The result was that we have found a single shell of *Calyptogena* at the toe of the accretionary prism (Fig. 4) . Although this is not an eye-opening discovery, it is quite significant that this result almost ensure that there is an active and extensive seepage system from the toe region to the upper slope of this area.

ACOUSTIC IMPEDANCE ANALYSIS

Physical properties and seismic characteristics of accretionary prism is a key to the understanding of the structual development of accretionary prism. The air-gun seismic reflection data obtained during the cruise was analyzed by E. Nishiyama in order to study such objectives. The method deployed was the analysis of acoustic impedance using an inversion method (see Nishiyama, this volume). Because the details of this study will be published elsewhere, we present an essence of the result relevant to this report.

Acoustic impedance is a property which is defined by:

Acoustic Impedance = Density x Seismic Velocity

Because the material which composes the Nankai accretionary prism is mostly terrigenous sand and mud, the density variation of the strata is within 1.5 to 2.8 g/cm^3. Therefore it is expected that the acoustic impedance of the Nankai accretionary prism relates closely to the seismic velocity.

The results of acoustic impedance structure can be summerized as follows (Fig.2B).

1.Outside of the trench, the acoustic impedance structure within the hemipelagic layer shows a normal increasing trend with depth. But at the axis of the trench, htere is an abnomal trend below the trench tirbodote where the acoustic impedance increases very little with depth. This suggests that the development of elevated pore pressure under the trench turbidite probably is related to overpressuring of the hemipelagic layer due to sudden overburden, as a result of rapid turbidite deposition.

2. The acoustic impedance structure within the accretionary prism shows further evidence for the existence of overpressured porewater.
The acoustic impedance reaches a constant value at about half a second (two way time) depth from the seabottom surface. In some of the seismic traces, the value show a dereasing trend just above the boundary between sedimentary column and oceanic crust.

Therefore, considering the above evidence, we have inferred that there is a widely developed over-pressure horizon within the trench and landward slope of the Nankai Trough.

The seismic velocity (P wave) analysis obtained by ocean bottom seismometers indicates that the velocity reaches 3 to 3.5 km/sec at the base of prism (Fig.2B). This suggests that dehydration and consolidation of prism take place rapidly. The consolidated sediments are then repeatedly stacked by faults separated by a side overpressured horizons producing a homogeneous acoustic impedance structure.

HYDROGEOLOGIC FRAMEWORK

Based on the above, we have constructed a model showing the hydrogeologic framework and structural style of the Nankai Trough (Fig. 2). We interpreted that there is a conduit of porewater flow along the decollement primary based on the fact that there is a polarity reversal of the seismic wave and decreased acoustic impedance value. The analysis of heat flow indicates the existence of a convection fluid circulation system in the more landward portion of the prism. The elevated heat flow value in the trench indicates an upwelling system within the trench turbidite wedge.

NANKAI vs BARBADOS

Leg 110 of the ODP drilled the trench and accretionary prism of the Barbados (Moore and Muscle et al. , 1987). The result has given an important comparison between mud-dominated system vs sand-dominated system (Fig. 5). In the northern Barbados, the incoming sediments are primary pelagic-hemipelagic in nature being high in porosity and underconsolidated (upper 400m). In the Nankai, the incoming sediments include a thick sequence of sand-rich turbidite. The muddy sediments of the Nankai are overconsolidated and low in porosity compared with Barbados.

Two fluid circulation systems are identified within the Barbados prism: methane-bearing fluid along the decollement and methane-free fluid in the upper portion of prism. It is suggested that the fracuture porosity along the fault zone is a primary fluid conduite within the Barbados system. Active mud-shale diaprism is also a prominant feature of the Barbados hydrogeology and is dominated by confined aquifers controlled by fracture porosity. On the contrary the Nankai system shows more diffused fluid

circulation systems; upwelling at the trench, convection in the prism and flow along the decollement. So far no prominant diapir structure was found in the Nankai area (except the possible ones within the trench turbidite wedge). Therefore, it can be pointed out that in the Nankai hydrogeologic system, both fracture and granular porosity are impotant. Sand layers soak fluid expelled from the finer-grained sediments during the initial phase of compaction. Thus, at the toe of prism, we expect that sand-diking is more important as adjusting mechanism of over porepressure than mud diaprism in the case of the Nankai system.

REFERENCES

Kagami, H. , Karing, D.E. , et al. , 1986, Intial Report of DSDP, Leg 87: U.S.Goverment Printing Office, Washigton,D.C. .

Karig, D.E. , and Ingle,J.C. , et al. , 1975, Intial Report of DSDP, Leg, 31: U.S. Gevernment Printing Office, Washigton, D.C. .

Kinoshita , M. , 1987MS, Heat flow measurements in some western Pacific trench-arc-backarc systems and their interpretation: Master's thesis submitted to Earthquake Res. Inst. , Univ. of Tokyo.

Le Pichon, X.and Iiyama, T., et al., 1987, Nankai trough and Zenisu Ridge: a deep-sea submersible survey: Earth Planet. Sci. Letters, v. 83, p.285-299.

Shipboad Scientist of Leg 110, in press, Structural and hydrologic framework of the Northern Barbodos Ridge complex: Nature.

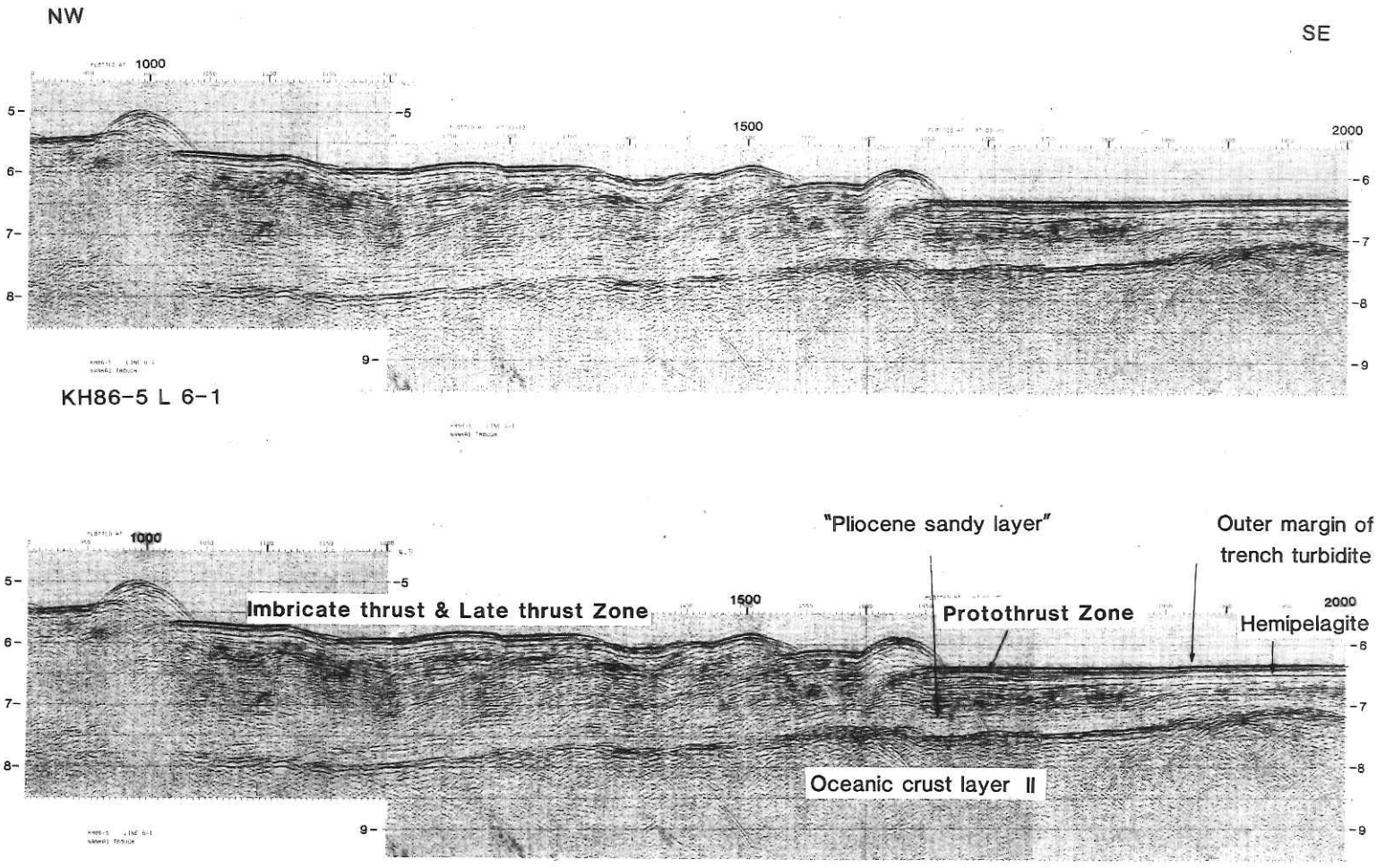

Fig. 1 Seismic reflection profile of the Nankai accretionary prism offshore of the Island of Shikoku (see Nishiyama et al. this volume).

Nankai Trough Hydrogeologic & Structural Interpretation

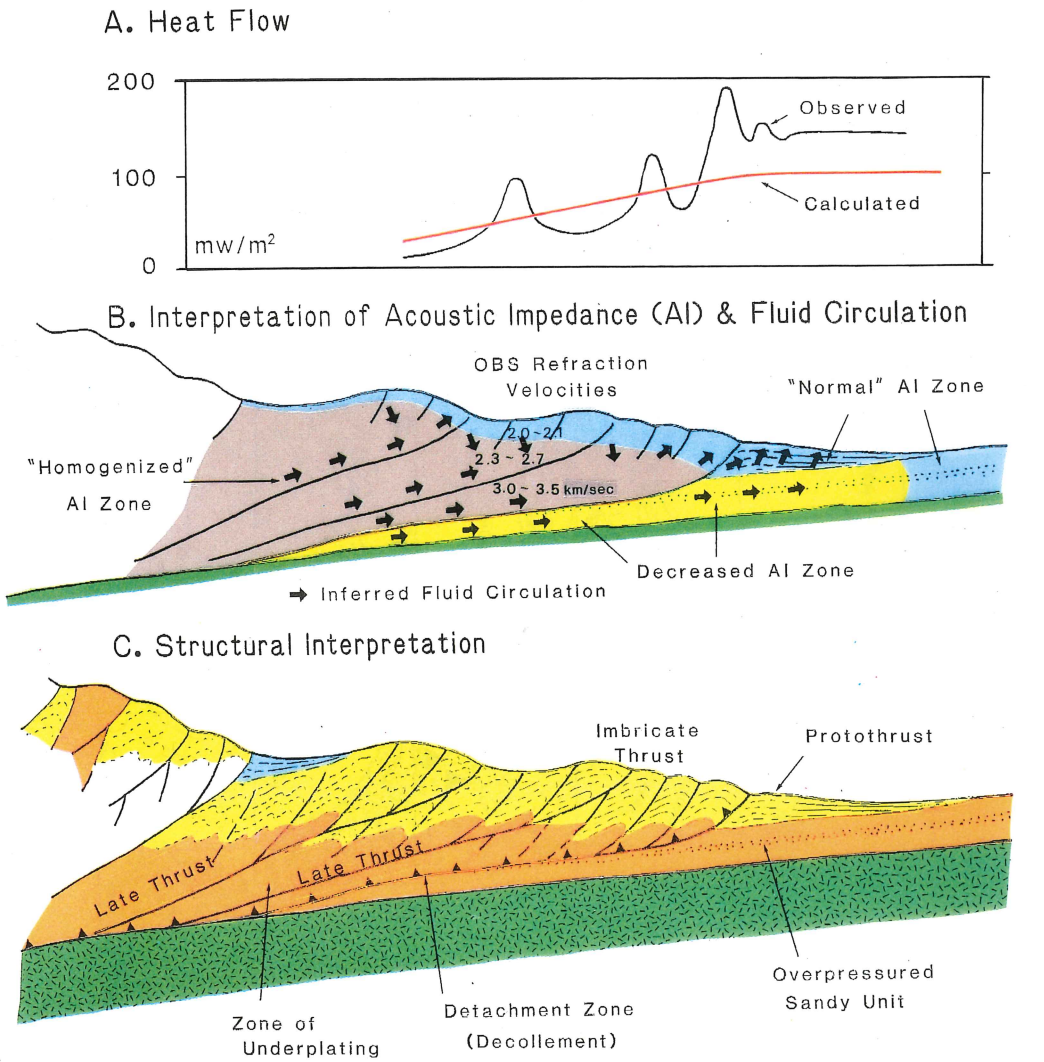

Fig. 2 Summary of heat flow, acoustic impedance characteristics and structural style of the Nankai Trough accretionary prism.

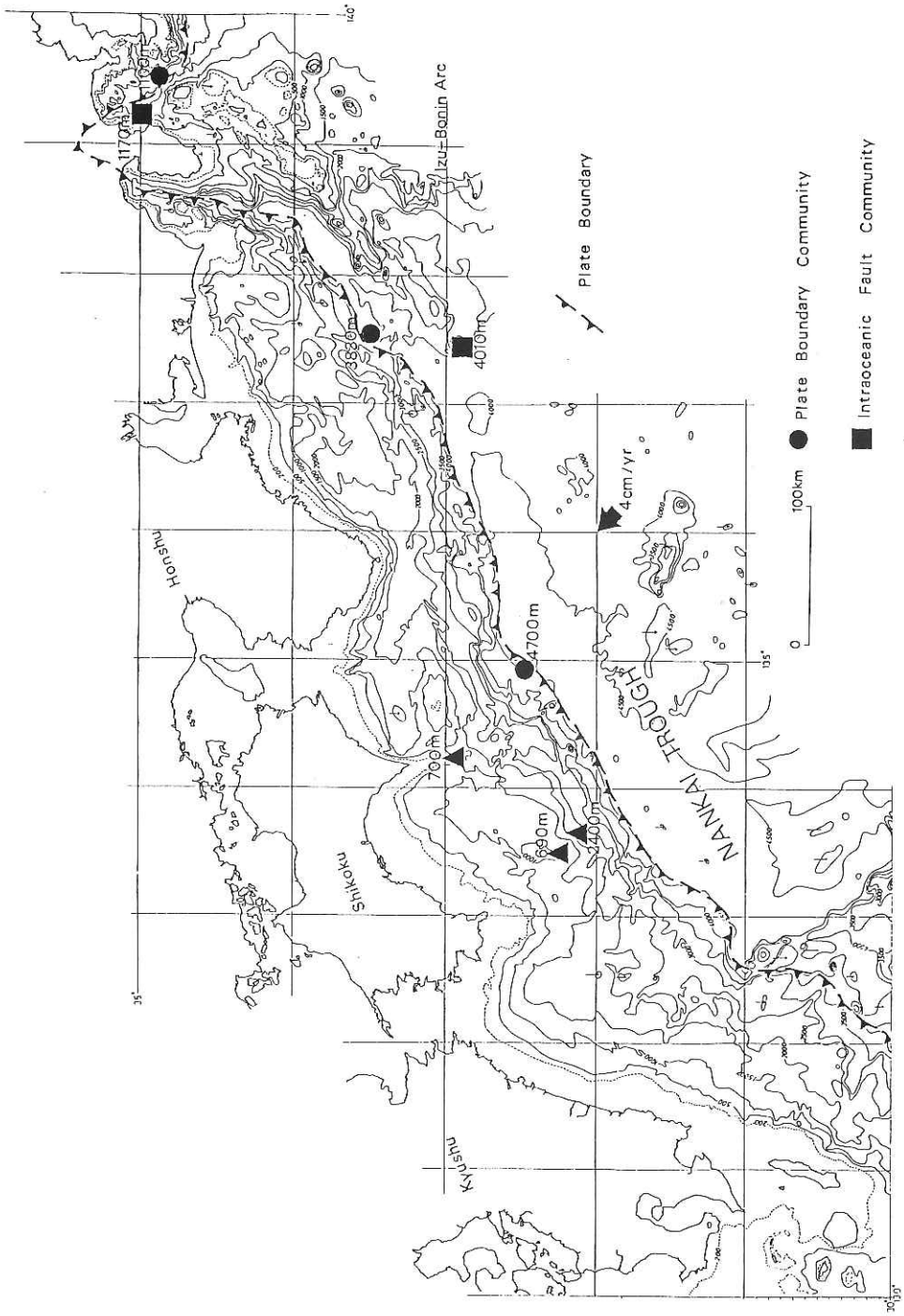

Fig. 3 Location of fluid seepage related animal communities off shore of southwest Japan.

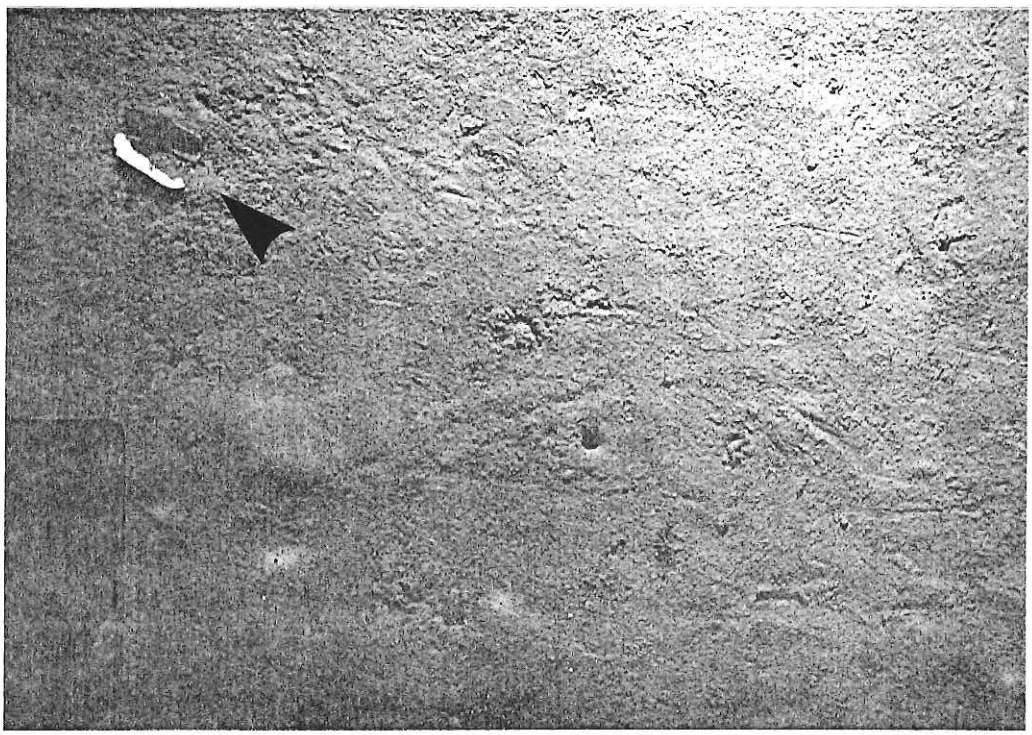

Fig. 4 A shell of *Calyptogena* found at the toe of the prism.

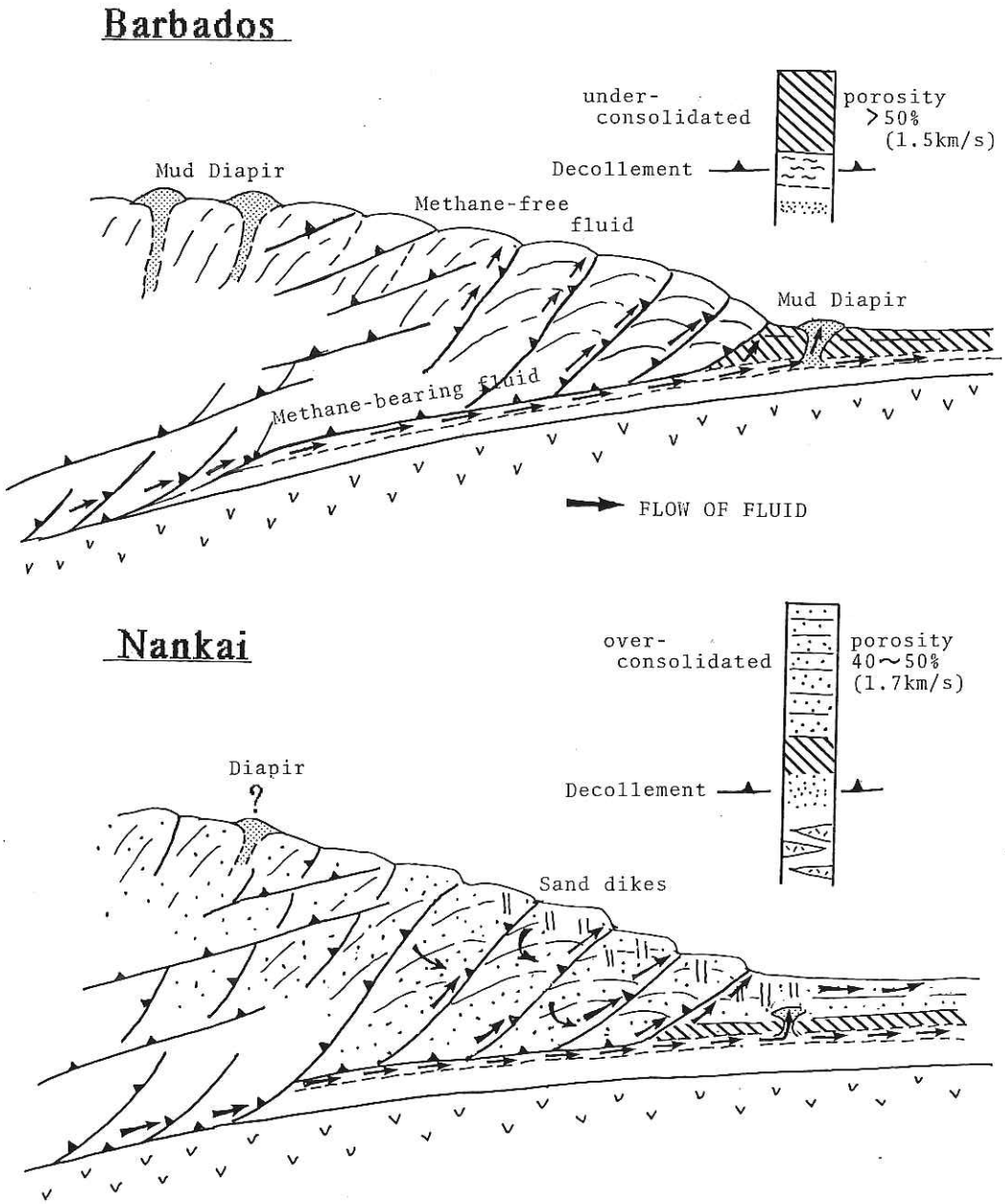

Fig. 5 Comparison of hydrologic framework between Barbados and Nankai accretionary prism.

CLAY MINERAL COMPOSITION OF THE KH86-5 SAMPLES COLLECTED FROM THE NANKAI TROUGH AREA

J. YIN and K. OTSUKA

Department of Earth Sciences, Shizuoka University, Shizuoka 422

INTRODUCTION

In oder to clarify dispersal patterns of clay minerals and their dispersal mechanism along the shelf margins, we have carried out clay mineral analysis of slope sediments collected from the Nankai Trough area.

SAMPLES AND PROCEDURES

The materials used for this study were obtained on board R/V Hakuho Maru, Ocean Research Institute, University of Tokyo by piston coring at five sites, by box coring at one site, and by dredging at one site (Fig. 1 and Table 1). Samples from piston cores were collected from the top 5 cm.

The procedures undertaken for the qualitative and quantitative analyses of clay minerals are described in detail in Yin et al. (1987), which are followed in this study.

RESULTS

All the samples examined are composed of such clay minerals as illite, chlorite, kaolinite and montmorillonite, as shown in Table 1.

Illite is most abundant of all the clay minerals, varying in amount from 33 % for KD1 sample to 41 % for KP6 sample. Both illite and chrorite are almost constant in abundance in their horizontal distribution. The montmorillonite content is small, only a little more than 10 %. Kaolinite is neglegibly small in amounts in all the samples.

As far as the examined samples are concerned, clay mineral compositions are characterized by the suite of illite and chlorite.

DISCUSSION AND CONCLUDING REMARKS

Chamley et al. (1986) stated from the study of clay minerals from DSDP Sites 582 and 583 cores that major constituents illite and chrorite were derived from igneous, metamorphic and older sedimentary rocks now widely exposed in Southwest Japan. Our

study also confims his conclusion from the results that the surface sediments not only of the Nankai Trough axis (KP6) but also of the trench landward slope are characterized by illite and chrolite. This fact has also been supported by Aoki and Oinuma (1981) in the Suruga Bay sediments and by Sakae and Maeda (1984) in the Tosa Bay sediments off Shikoku.

The above mentioned fact suggests that turbidity currents and related gravity flows are most important for the dispersal mechanims of illite and chrolite in the studied area. It is because the landward side of the Nankai Trough is excaved frequently by submarine canyons and troughs on a large scale, through which turbidity currents must have flown forming turbid plumes (Shipley, 1978; Moore, et al., 1982), by which fine clay particles are suspended.

On the other hand, surface sediments in the East China Sea show much higher illite contents than in neighbouring areas (Aoki et al., 1983; Yin et al., 1987). Accoding to Yin et al. (1987), montmorillonite is a major consituent in the sediments off the east coast of Northeast Japan, whereas illite is very scarce in amounts in that area (Fig. 2). Another interesting fact is that the KD1 sample from the top of the Takuyo Daiichi Seamount off Boso Peninsula is characterized by large illite content. Such an occurrence of illite strongly suggests that some amounts of illite were dispersed by the Kuroshi Current from the East China Sea area.

It is concluded that clay minerals in the sediments off the south coast of Southwest Japan are characterized by illite and chlorite. Most of them must have been derived from adjacent land areas mainly by turbidity currents and some were brought into the Kuroshio Current from the East China Sea.

ACKNOWLEDGEMENT

We wish to express our sincere thanks to Prof. A. Taira, cheif scientist for the KH86-5 cruise, and the captain and crew aboard R/V Hakuho Maru.

REFERENCE

Aoki, S. and Oinuma, K., 1981, Distribution of clay minerals in surface sediments of Suruga Bay, central Japan. Jour. Geol. Soc. Japan, 87, 429-438.

Aoki S., Oinuma, K., Okuda, K. and Matsuike, K., 1983, Clay mineral composition in surface sediments and the concentration of suspended matter of the East China Sea. Proceeding Intern. Symposium Contin. Shelf, with Spec. Ref. East China Sea, 1, 473-582.

Chamley, H., Cadet, J. P. and Chavet, J., 1986, Nankai Trough and Japan Trench Late Cenozoic Paleoenvironmenta deduced from clay mineralogic data. Init. Rept. DSDP, 87, 633-642.

Moore, J. C., Watkins, J. S., McMillen, K. J., Bachman, S. B., Leggett, J. K., Lundberg, N., Shipley, T. H., Stephan, J. F., Beghtal, F. W., Butt, A., Didyk, B. M., Niitsuma, N., Shepard, L. E. and Strandner, H., 1982, Facies belts of the Middle America Trench and forearc region, south Mexico, Results from Leg 66 DSDP. In. Leggett, J. K. (ed.): Trench forearc geolog. Geol. Soc. London, Spec. Publ., 10, 77-94.

Otsuka, K., 1985, Processes and facies of active trough filling up sediemts - Geology of Upper Quaternary sediments in the northernmost areas of the Sagami and Suruga Troughs-. Geosci. Repts. Shizuoka Univ., 11, 57-117.

Sakae, T. and Maeda, S., 1984, Grain size distributions of sediments in Tosa Bay, south of Bungo Strait and Hyuga-nada and clay mineral composition of sediemts in Tosa Bay, Unpub. Graduation Thesis, Coll. Marine Sci. Tech., Tokai Univ., 112 pp.

Shipley, T. H., 1978, Sedimentation and echo characteristics in the abyssal hills of the west-central North Atlantic, Geol. Soc. Amer. Bull., 89, 397-4-8.

Taira, A. and Niitsuma, N., 1986, Turbidite sedimentation in the Nankai Trough as interpreted from magnetic fabric, grain size, and detrital modal analysis. Init. Repts. DSDP., 87, 611-632.

Yin, J. Okada, H. and Labeyrie, L., 1987, Clay mineralogy of slope sediments around the Japanese Islands, Geosci. Repts. Shizuoka Univ., 13, 41-65.

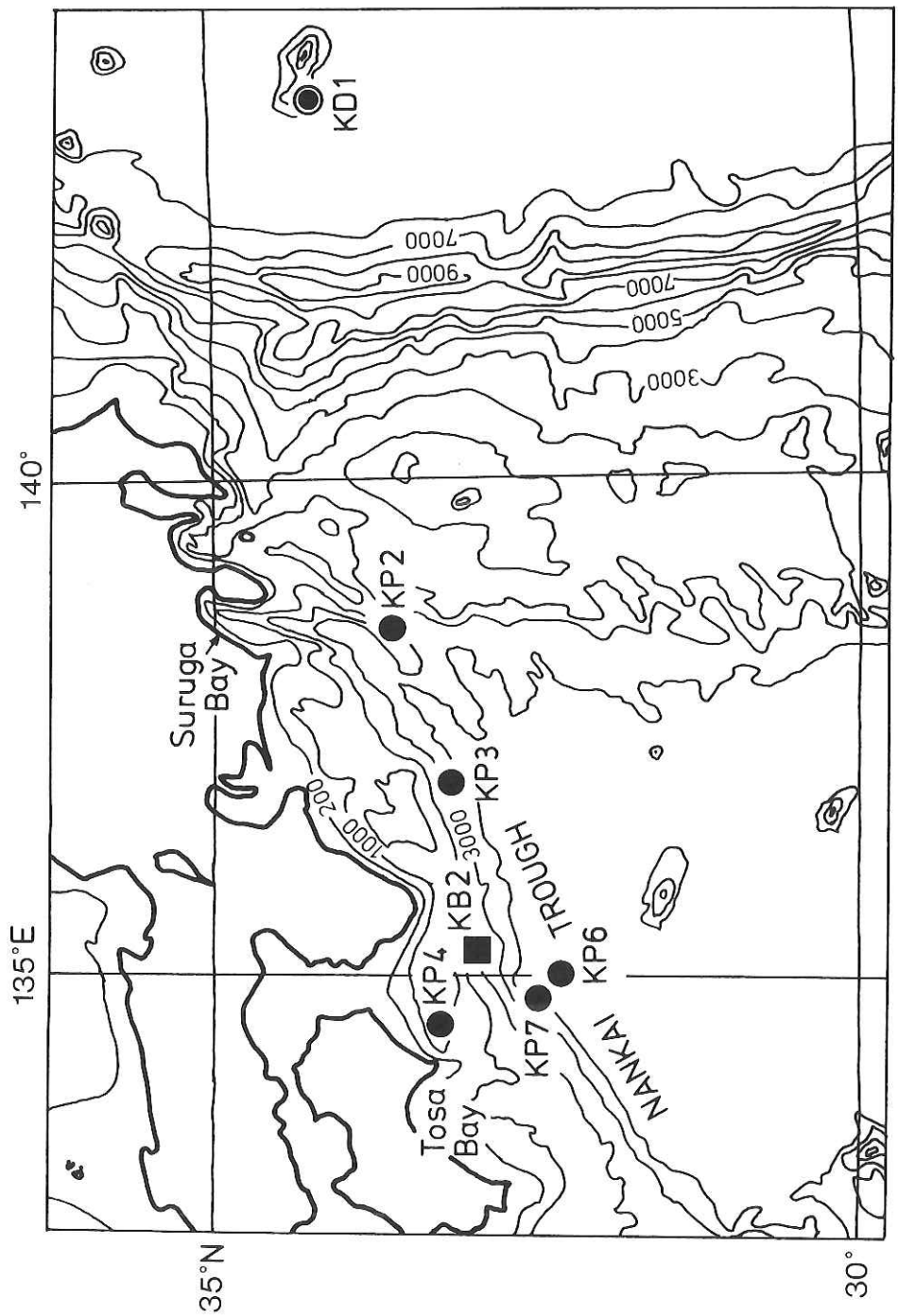

Fig. 1 Locations of the samples used. P of the prefix of the sampling site numbers: piston-core samples, B: box-core sample, D: dredged sample.

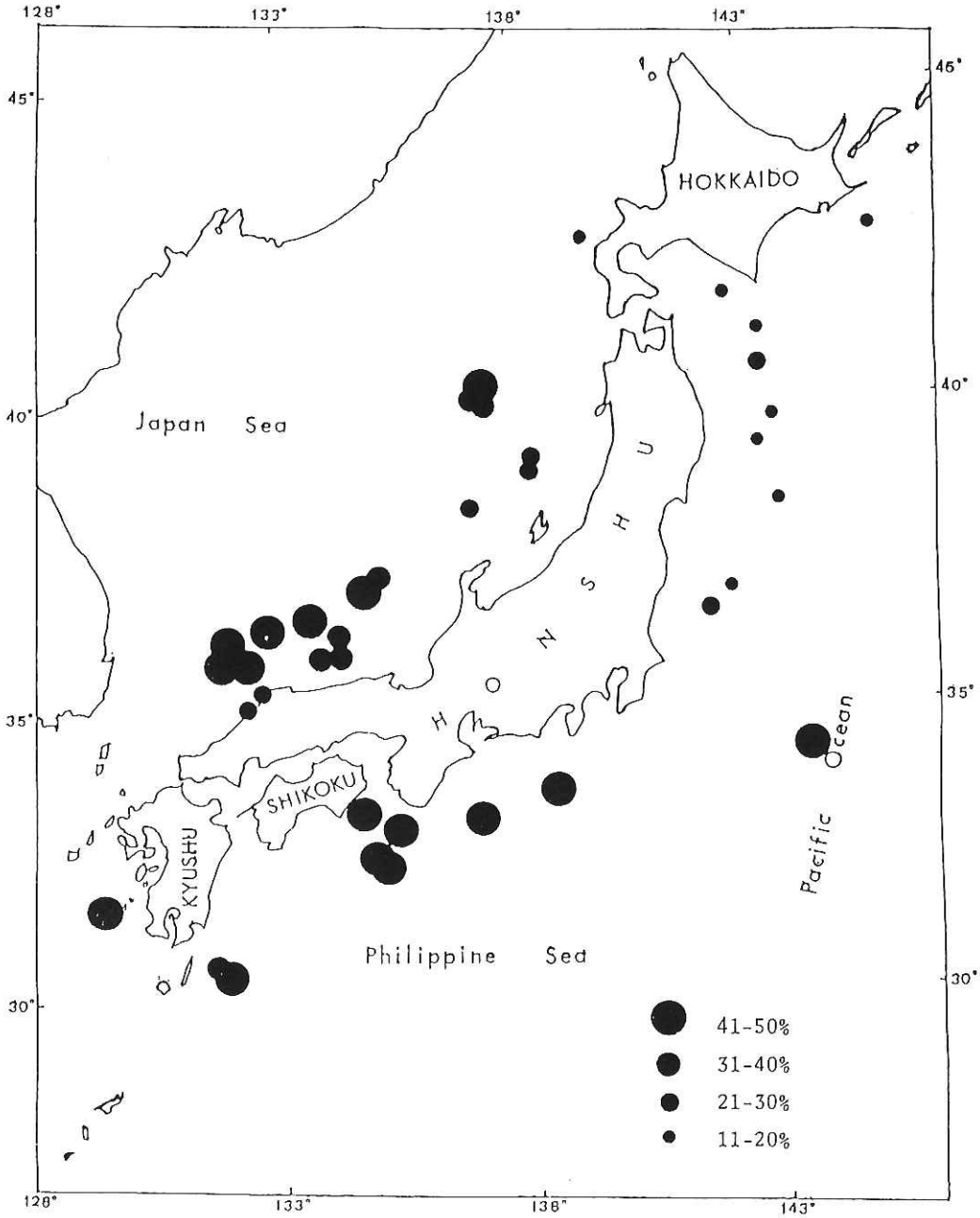

Fig. 2 Illite concentrations in the <2μm size fraction of surface sediments around Japan. The other data are owing jto samples collected by ESTASE I cruise by the Jean Charcot (from Yin et al 1987).

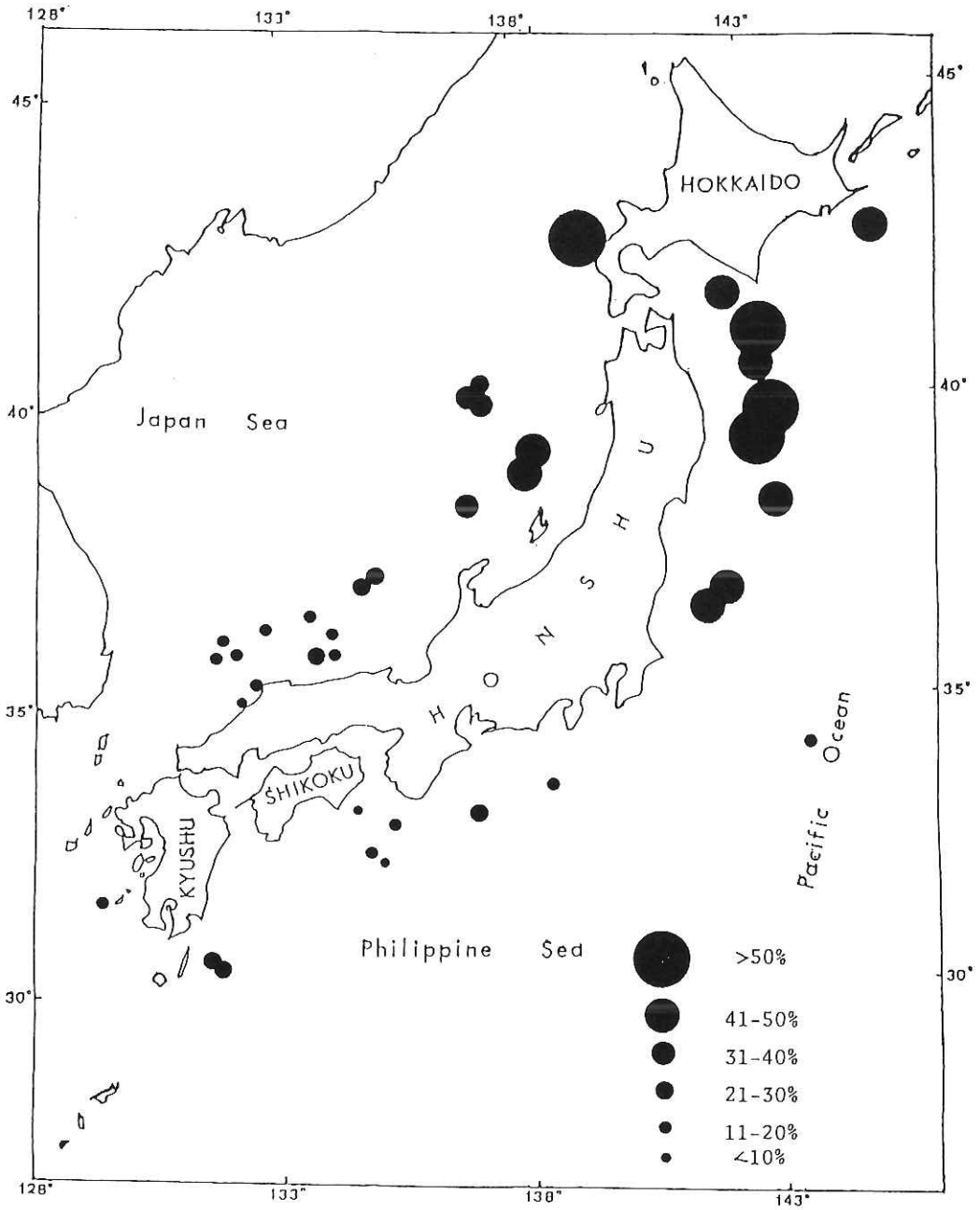

Fig. 3 Montmorillonite concentrations in the <2μm size fraction of surface sediments around Japan. The other data are owing to samples collected by ESTASE I cruise by the Jean Charcot (from Yin et al., 1987).

Table 1. Clay mineral compositin of the surface sediments obtained by the KH86-5 cruise

SAMPLES	DEPTH(m)	KAOLINITE	ILLITE	CHLORITE	MONT.
KP2	2430	3	44	36	17
KP3	3518	2	41	34	23
KP4	1265	3	49	40	8
KP6	4800	2	47	41	10
KP7	4100	3	43	36	17
KB2	2450	3	46	38	12
KD1	2640	7	41	33	20

PISTON CORES P4 AND P5 FROM THE MUROTO TROUGH

P. BLUM

Department of Geology & Mineralogy, Kyoto University, Sakyou, Kyoto 606

INTRODUCTION

Two piston cores were taken in the western Muroto Trough, at the base of the Tosa Bae structural high (Fig. 1) in order to clarify the possibility of comparing and correlating sedimentary facies and depositional events. The sites are 5 km apart from each other, with locations and water depths as follows: P4: 33° 14.90N/134° 30.99E, 1279m; P5: 33° 13.74N/134° 27.94E, 1240m. At 3.3 meters below sea bottom both cores hit volcaniclastic sediments which prevented from further penetration.

In part I of this report the sediment composition, sedimentary and biogenic structures and texture are described based on smear slide estimations, x-radiographs and settling analysis respectively. The sedimentation rate is estimated based on the identification of the Kikai-Akahoya ash layer. In part II some aspects of the bioturbation in the cores are discussed.

I. ANALYSIS OF CORE SEDIMENTS

SEDIMENT COMPOSITION

Cores P4 and P5 are composed mainly of alternations of mud and laminated or bioturbated, fine-grained sand layers (Fig. 2). The lowermost 7-10 cm of each core consist of light colored volcanic ash.

The mud layers, usually 5-10 cm thick, build up about 70% of the core length and were determined as "nannofossil-diatom-bearing muds" (Dean et al.,1985) in several smear slides. Minor components (less than 10% in the smear slides) are commonly planktonic and benthonic foraminifers, sponge spicules, pellets (100-200 micron) and occasionally fishbones.

The intercalated sand layers, usually 1 to 5 cm thick, build up about 25% of the core length. Their composit lamination consists of (silty) fine-grained sand alternating with mud-laminae of the same composition as the mud layers (Fig. 3). Altered and fresh volcanic glass shards and pumice make up 30-60% of the sand composition. Within some of the sand layers are several millimeter thick laminae, consisting entirely of well sorted, fresh volcanic ash (e.g. P4, 80cm, Fig. 3). Planktonic and benthonic foraminifers, usually moderately fragmented, present 10-50% of the sand composition.

The ash layers at the base of the cores consist generally to more than 90% of

fresh, transparent or rarely brown bubble-wall type glass shards in the silt to fine-grained sand range. Within the ash layers are only small lenses containing up to 50% mud and diatoms (Fig. 3).

The 10 cm thick muddy sand layer rich in coarse plant debris in core P4 (270-280 cm) contains pieces of wood with dimensions more than 1 cm, fishbones and many foraminifers. It has no equivalent in core P5.

SEDIMENTARY AND BIOGENIC STRUCTURES

The bedding planes at the base of the sand layers are sharp to transitional, and distinct to transitional at the top of the sand layers, depending on the degree of bioturbation.

The sand layers are usually laminated, but the lamination is often partly or completely destroyed by bioturbation. If well preserved, it is usually recognized as heterogeneous small-scale trough cross-lamination. Wavy to parallel laminated sand is also observed, but these may as well represent transversely cut cross sets. There is neither a significant change in sedimentary structure nor grain size grading in the sand layers, suggesting constant flow conditions during the deposition of the sand and the subsequent migration of ripples, leading to the formation of cross-lamination. The lower bedding planes are often gently undulating (1 cm in amplitude, about 8 cm in wavelength, estimated from trough-crest distances of 4 cm), which probably represents ripple troughs formed just prior to the deposition of the sand onto the old mud surface.

More consistent "parallel" lamination (upper stage plane bed) is only developed in sand layers consisting mainly of fresh volcaniclastic material, i.e. near the base of the cores (e.g. core P5, 320 cm).

In the entirely volcaniclastic, lowermost parts of the cores, no distinct structures are visible in the x-ray images. This seems to be due to the composition of those units, because in the smear slides we find variations in the maximum grain size of about 1 phi grade as well as lenses of sandy mud.

In Fig. 2, two types of biogenic structures are distinguished:
1) biodeformational structures which are recognized on the radiographs, but show no sharp contours or distinctive shape ("bioturbation") and
2) biogenic traces with more or less distinct shape. Three types of traces are identified and marked in Fig. 2 (compare with x-radiograph prints in W. Soh, in this volume): (S) Scolicia, (P) Planolites and (T) Teichnichus?. Planolites is a straight to gently curved, inclined or horizontal tube with various types of cross section (max. 1cm diameter). Teichnichus? is recognized as a sharply bounded, subrectangular vertical section with concave top (tube). Planolites and Teichnichus? are usually preserved in the mud layers, and only rarely found in strongly bioturbated sand layers.

Scolicia is the most conspiceous trace observable in the x-radiographs: more than 50% of the sand layer sections in the cores are slightly to drastically disorganized by tube-like burrows with diameters of 2-3 cm. The longitudinal sections are characterized by internal sand/mud laminated curved menisci. Often the horizontal burrows appear and disappear within the 6.5 cm core section given, showing their cross section and indicating the meandering character of Scolicia. Well preserved cross sections are found in core P4 at 101 cm, 108 cm, 125 cm, and in core P5 at 191 cm depth below sea bottom.

SEDIMENTATION UNITS AND BEDDING

Based on sediment composition and structures a sedimentation unit (or bed) can be defined from the base of a sand layer to the top of the overlying mud layer (Fig. 2). 31 units and 40 units are recognized in P4 and P5 respectively. Figure 4A shows a compilation of these units from the coloumns in Fig. 2. Apparent similarities and differences between the sequential pattern of the units in P4 and P5 are clarified in fig. 4B, where bed thickness is plotted against bed number.

A comparable sequence is found in both core for the upper 25 units (2.3 m below sea bottom), with a unique bed thickness peak for the 15th and 18th unit respectively (1.5 m below sea bottom). If we assume a correlation for the two peaks, depositon of two corresponding beds out of one current or during one event is implied. The difference of three unit numbers would in this case represent the error range for recognizing sand layers in the x-radiographs, i.e. three sand layers (and therefore 3 units) might not be recognizable anymore in core P4 due to complete bioturbation (e.g.P4, 157cm).

Between the 26th unit and the ash layer at the bottom of the cores, which is taken as a time correlation, only five relatively thicker units in P4.contrast with 14 units of average thickness in P5. The lower parts of the cores therfore suggest either 1) deposition out of different currents or during different events, or 2) differentiation of the deposits out of one current due to the effect of the "microtopography" (bedforms).

SEDIMENTATION RATE

The sedimentation rate can be estimated based on the identification of the partly penetrated ash layer at the bottom of the cores. The abundant bubble wall type glass and relatively rare pumice are characteristic for both important most recent tephras in and off SW Japan, the Kikai-Akahoya (K-AH) ash and the Aira-Tn ash. Even though refraction indices could not be determined for the differentiation, the occurence of 1-5 % brown couloured glass and the lack of hornblende in the samples are clear evidence for the K-Ah ash after K. Takemura (oral comm.). K-AH ash is an airfall ash from

Kyushu with radiocarbon dates between 6000 and 6500 y.B.P. (Machida & Arai, 1978). Assuming that the recovered ash represents the main ash deposit, we arrive at a sedimentation rate of more than 50 cm/1000ys, and a turbidite frequency of 1/200ys in core P4 and 1/160ys in core P5.

SETTLING-VELOCITY DISTRIBUTIONS

Settling-velocity distributions of the particles of some sedimentation units from cores P4 and P5 are presented in figures. 4-6 as psi-plotts, where psi-intervals represent a logarithmic scale for the settling velocity (at 22°C), analogous to the phi-scale for grain-sizes. For comparison with grain-size values, a scale bar with the major size classes is illustrated as well, where "ideal" indicates that the sizes correspond to the settling velocities for smooth, spherical particles with densities 2.65 g/cm^3, settling alone in distilled water at T=22°C, the size being computed after Gibbs et al. (1971).

Sample: Settling analysis was carried out on three samples of each core. The six samples represent sedimentation units as defined above, from three approximately corresponding levels of the two cores; P-4-1 35-48 cm (Su4), P-4-2 182-194 cm (SU19), P-4-3 317-321 cm (only sand layer of SU31, sampling error); P-5-1 31-42 cm (SU4), P-5-2 182-196 cm (SU22), P-5-3 311-322 cm (SU39).

Procedure: After cutting 5-10 g sample slices vertically through the sedimentation units ("channel samples"), organic material was oxidated with hydrogene peroxide and solubles were washed out with distilled water to ensure dispersal of the clay minerals. The bulk sample was sieved through a 46 micron mesh in order to get a "coarse fraction" for analysis by the settling tube method, and a fine "fraction" for analysis by the pipette method.

Only moderate accuracy was achieved by the procedure due to the following practical limitations: 1) the separation into "coarse" and "fine" fraction was done by sieving, the physical principal of which contrasts with the principle of sttling; and 2) the available settling tube was not in full accordance with the accuracy limitations given by Gibbs (1972).

Results and discussion: The distributions are presented as conventional cumulative weight plots in Fig. 5. In Fig. 6A, the graphic dissection of the log-probability cumulative curve after Spencer (1963) is attempted, but it is shown, that the straight line for the "clay" population can hardly be estimated because 1) the distribution of the finest 10 % of the population is (as usually) not known, and 2) we really do not know, weather the assumed individual log-normal distributions are mixed or truncated or both.

Visher's approach (Visher, 1969), which relates "log-normal segments" of the distribution curves to depositional processes (Fig. 6B) is more practical in terms of a

basic interpretation: a sand population is transported in a turbulent suspension for a certain distance and deposited by a final "saltation (traction) transport", forming ripples and cross-lamination, whereas the mud population is subsequently deposited out from the suspension.

Another approach to recognize characteristics features and possible differences between the samples is presented in Fig. 7, where the results of the analyses are plotted individually as arithmetic cumulative weight percentages vs settling velocity in psi units, together with the graphically constructed frequency histograms. To visualize the distribution of the individual modes in the samples, the average histogram (mean percentage for each interval) was calculated and plotted together with the sample histograms. Additionally the mean and standard deviation values of the bulk populations, graphically determined after Fork & Ward (1957) are given.

It is apparent from the histograms, that the samples from cores P-4 and P-5 have a polymodal distribution. A first order mode for a psi-value around 0 (fine-grained sand) is found in all samples. A secondary mode of the average histogram is around a psi-value of 4 (coarse to medium silt). In the individual frequency distributions, however, this mode varies, being dominant, moderate or not pronounced. Subordinate modes vary strongly among the samples between psi-values of 10 and 15 (coarse to medium clay) and therefore disappear in the average histogram. This variation is partly attributed to the limited accuracy mentioned above, which requires an approximate connection between the data sets obtained by the two analysis methods.

It can be concluded that the velocity distribution of the analyzed samples are characteristic for turbidites as shown by Visher (1969), but a polymodal pattern which reflects the complex character of turbulent suspensions can neither sufficiently be represented by the graphical percentile measures nor by straight line segments in log-probability plots. To visualize the limitation of log-probability plots, a hypothetical "rectangular distribution" (RD) is shown to closely approximate a measured distribution in Fig. 6.

SUMMARY

Based on the sedimentary structures and the results of settling analysis, it is suggested that the sedimentation units defined above and shown in Figs. 2 and 4 were deposited by turbidity currents. A (hemi-) pelagic layer at the top of the units has not been preserved. The facies of the core sediments can be summarized as thinly-bedded fine-grained T_{bc} or T_{cd} turbidites rich in volcaniclastic debris and with abundant bioturbation in sand and mud layers. This type of sediment can represent distal levee or lobe deposits in a fan setting, or basin fringe or distal lobes of downslope gravity flows in a "normal slope" environment (e.g. Stow, 1985).

Topographically there are two major possibilities for the source of the sediment at the two core sites: 1) from the northern, narrow shelf via None Canyon, and 2) from the Tosa Bae structural high and/or from the shelf down the slopes. The sediment facies does not favour one of the two possibilities.

II. SPECIAL NOTES ON THE PRESERVATION OF THE TRACE SCOLICIA

As mentioned in the core description, Scolicia traces occur frequently within or, more often, just at the base of the sand layers. Some considerations about the relationship between burrowing and depositional process are expressed here.

The relationship between Scolicia and echinoids as trace markers has been well established during the past 15 years by approaches from different disciplines. Even though the burrowing behaviour of sea urchins is known for many decades, there still exist many opinions about the burrowing and/or ploughing behaviour of various types and species of echinoides (e.g. Reineck, 1968; Goldring & Stephenson, 1970; Higgins, 1974; Broomley & Asgaad, 1975; Smith & Crimes, 1983). Identification of this behaviour in the sediment record is dependent on the type and degree of preservation of the trace, and therefore also a function of the sedimentary processes. An example for a possible relationship between animal behaviour and depositional process is given here.

Scolicia is often reported from mud-sand interfaces as it is the case in cores P5/P4. It is suggested here, that this type of burrow may not represent the normal behaviour of the spatangoid, but rather an escape structure of the animal, which normally lives mainly on the sea floor ploughing it. A possible vertical escape trace can be observed only once in the limited core sections (P-5, 327-330 cm), but upward trends may be recognized in some sand layers. The interpretation of a normal ploughing behaviour is suported by the deep-sea photographs from Hollister et al. (1975), showing irregular echinoids producing strongly meandering ridge-like furrows in the mud of the south-east Indian Ocean as well as in the sandy continental shelf off Nova Scotia. Assuming a ploughing and/or very shallow burrowing behaviour plus an adaption of the animal to a wide grain-size spectrum, the deposition turbidites presents the key to the question of the excellent preservation of the traces at the mud/sand interfaces. In a hemipelagic setting, where sedimentation takes place slowly and continuously, spatangoid traces are expected to be almost completely bioturbated by other, deep burrowers, or ill preserved because of the fine texture of the sediment. In an environment however, where occasionally turbidity currents of limited thickness (no Scolicia in beds thicker than 8cm after Hallam (1975) cover the sea floor, the preservation potential of spatangoid (escape) traces increases drastically.

The scenario can be sketched as follows: sea urchins ploughing through the muddy sea bottom are covered with a thin sand layer from a seismically triggered turbidity current, and the sandy cover is "sealed" by a mud layer during the folllowing hours or days. The spatangois,being adapted to sand as well as to mud, start crawling through their disastrous cover towards the sediment-water interface, producing texturally well recognizable traces in and near the sand layers. Other burrowers, which are restricted to mud (e.g. , Planolites) establish themselves in the new mud layer and are never tempted to disorganize the spatangoid traces in the sand-layer beneath.

REFERENCES

Broomley, R. G. & Asgaad, U. (1975) : Sediment stuructures produced by a spatangoid echinoid: a problem of preservation. Bull. Geol. Soc. Denmark. 24, 261-281.

Dean, W. E. , Leinen, M. & Stow, D. A. V. (1985) : Classification of deep-sea, fine-grained sediments. Jour. Sed. Petrology, 47, 650-656.

Folk, R. L. & Ward, W. C. (1957) : Brazos river bar : a study in the significances of grain size and setting velocity. Jour. Sed. Petrology, 27, 7-18.

Gibbs, R. G. , Mathews, M. D. , & Link, D. A. (1971) : The relationship between sphere size and settling velocity. Jour. Sed. Petrology, 41, 7-18.

Gibbs, R. J. (1972) : The accuracy of particle-size analysis untilizing settling tubes. Jour. Sed. Petrology, 42, 141-145.

Goldring, R. & Stephenson, D. G. (1970) : Did Micraster burrow? In: Crimes, T. P. & Happer, J. C. (eds.) : Trace Fossils. Geol. J. Spec. Issue 3, 179-184. Seel House Press, Liverpool.

Hallam, A. (1975) : Preservation of trace fossils. In: Frey, R. W. ed. The Study of Trace Fossils, 55-63, Springer Verlag.

Higgins, R. C. (1974) : Specific status of *Echinocardium cordatum, E. australe* and *E. zealendicum* (Echinoidea: Spatangoida) around New Zealand, with comments on the relation of morphological variation to environment. Jour. Zool., London, 173-451-475.

Hollister, C. D., Heezen B. C. and Nafe, K. E. (1975) : Animal traces on the deep-sea floor. In Fray, R. W. (ed.) The Study Of Trace Fossils, 493-510. Springer-Verlag.

Machida, H and Arai, F. (1978) : Akahoya ash - a Holocene widespread tephra erupted from the Kikai Caldera, south Kyushu, Japan. The Quaternary Res. (Daiyonki-Kenkyu), 17, 143-163 (in Japanese with English abstract).

Reineck, H. E. (1968) : Lebensspuren von Herzigeln. Senckenberg. Leth., 49, 311-318.

Smith, A. B. and Crimes, T. P. (1983) : Trace fossils formed by heart urchins - a study of *Scolicia* and related traces. Lethaia,16,79-92.

Spencer, D. W. (1963) : The interpretation of grain size distribution curves of clastic sediments. Jour. Sedim. Petrol.,33, 180-190.

Stow, D. A. V. (1985) : Deep-sea clastics: where are we and where are going? In: Brenchley, P. J. & Williams B. P. J. (eds.), Spec. Publ. Geol. Soc., 18, 67-93.

Visher, G. S. (1969) : Grain size distribution and depositional processes. Jour. Sedim. Petrol., 39, 1074-1106.

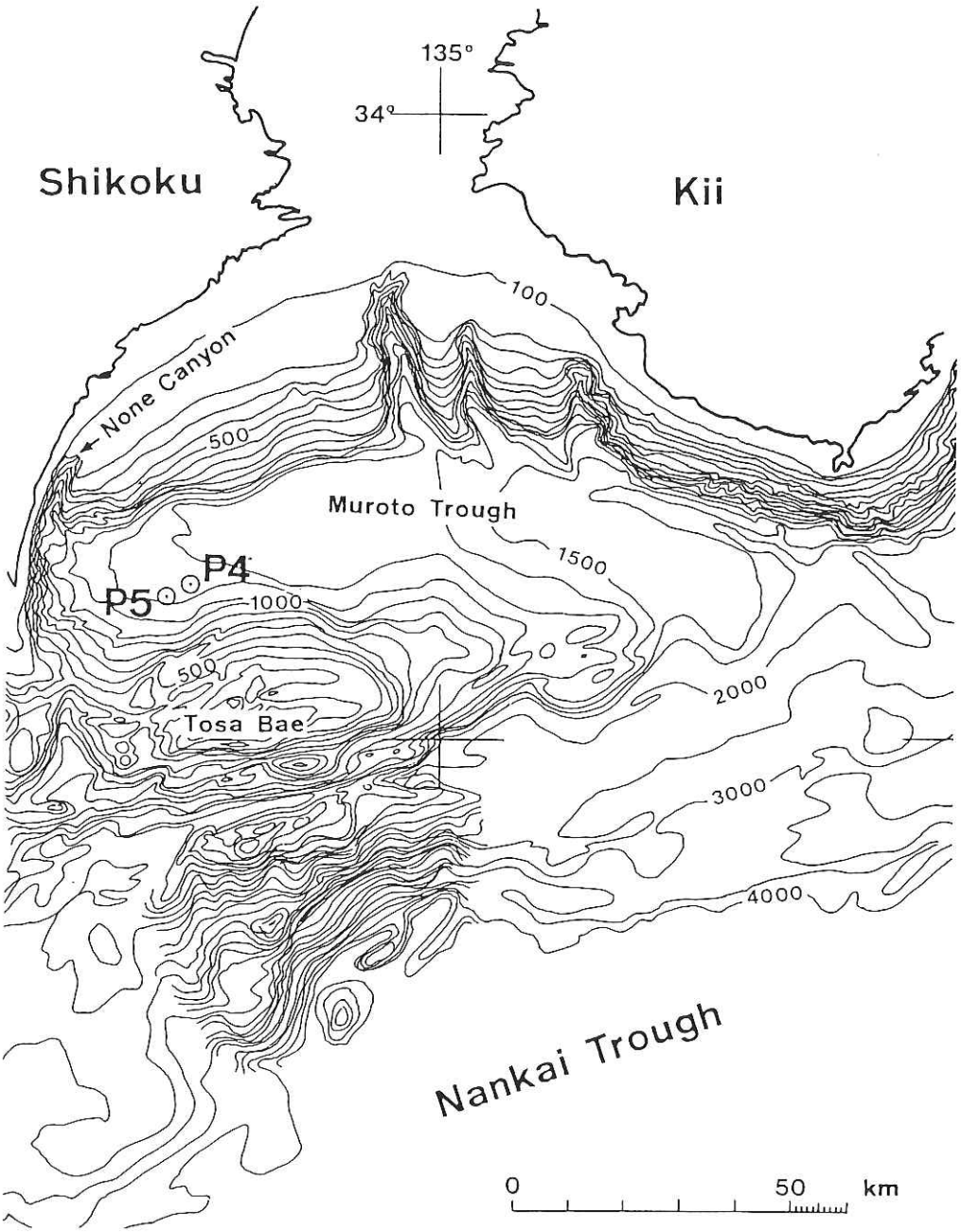

Fig. 1 Locations of piston cores P4 and P5.

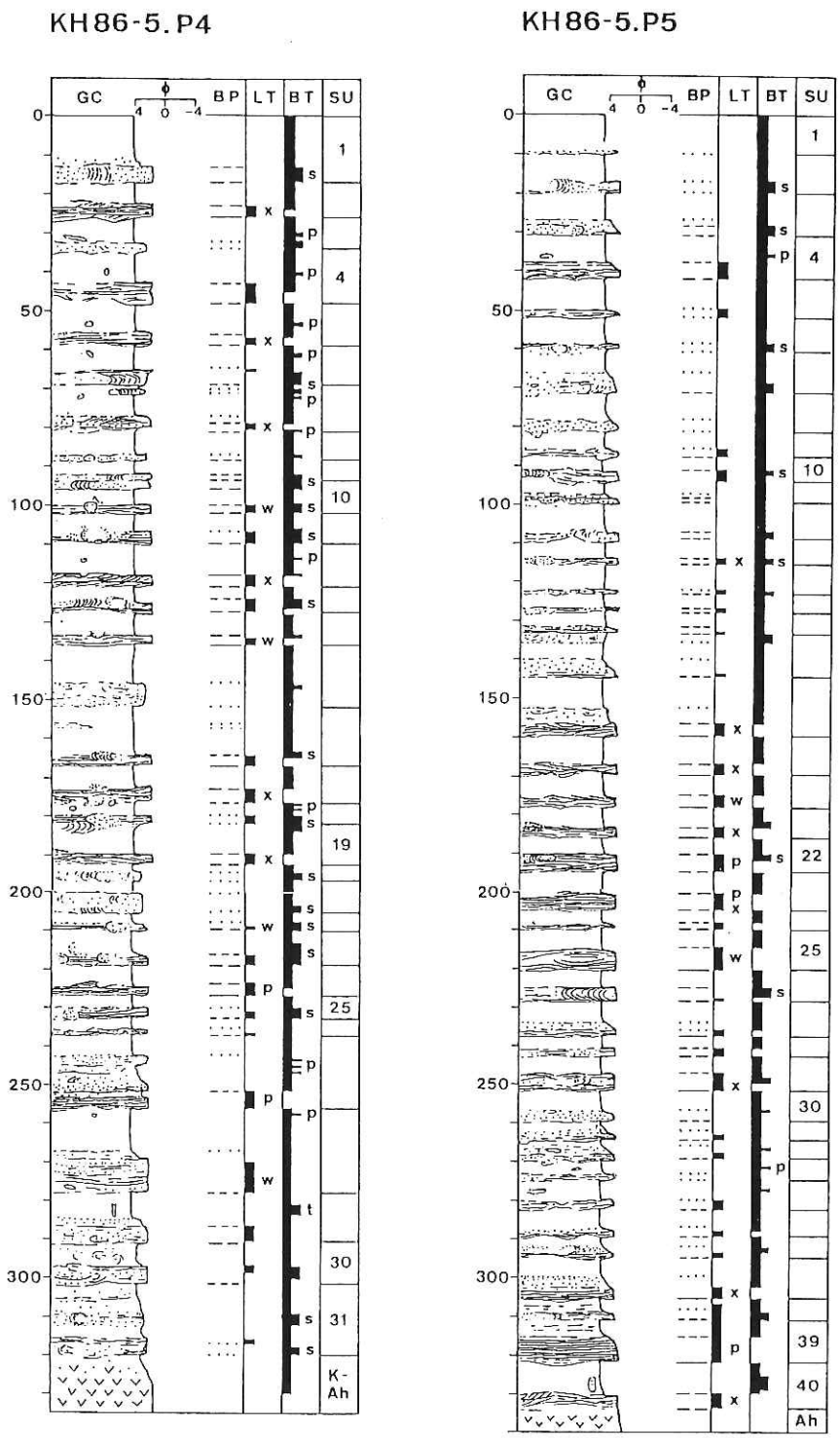

Fig. 2 Graphic representation of cores P4 and P5. Structures are interpreted from x-radiographs. K-Ah: Kikai-Akahoya ash.

LEGEND

GC **Graphic Coloumn**

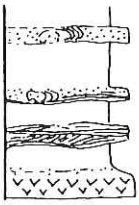

bioturbated sand layer with Scolicia trace

bioturbated mud layer

bioturbated sand layer with Scolicia trace, original lamination partly preserved

undisturbed laminated sand layer

volcanic ash layer

BP **Bedding Plane**

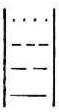

gradual transition

gradual, but rapid transition

distinct boundary

sharp boundary

LT **Lamination - Type**

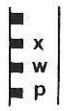

laminated, type not determinable

cross lamination

wavy lamination

parallel lamination

BT **Bioturbation - Traces**

bioturbated

Scolicia trace

Planolites trace

Teichnichus? trace

SU **Sedimentation Units**

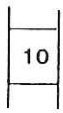

10th sedimentation unit from the top of the core

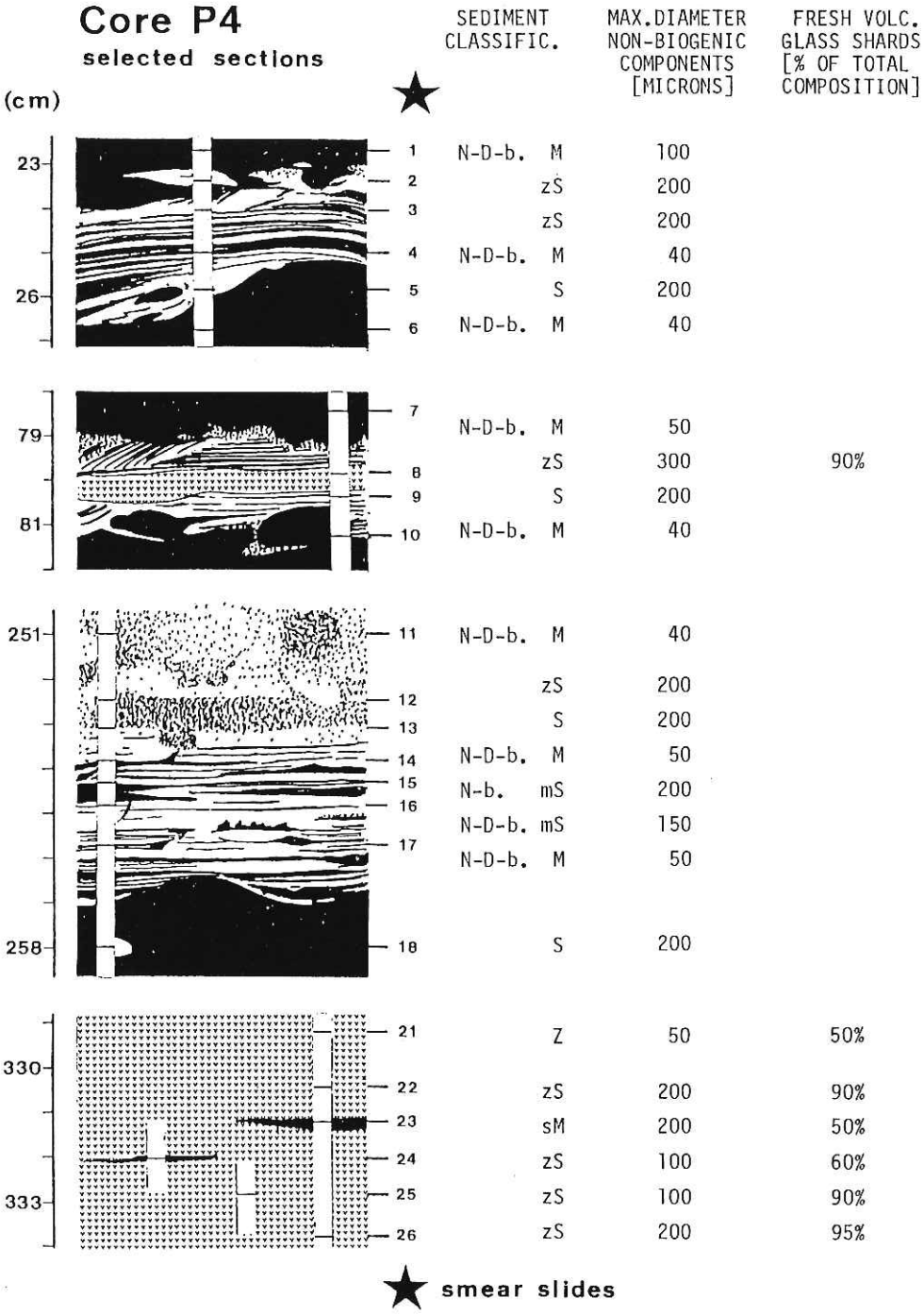

Fig. 3 Maximum grain size and fresh volcanic glass content in relation to sedimentary structures in some sections of core P4. Numbers to the right of the graphic sections indicate smear slide samples. N-D-b: nannofossil-diatom-bearing; M: mud; s: sand; m:muddy; z: silty; s:sandy.

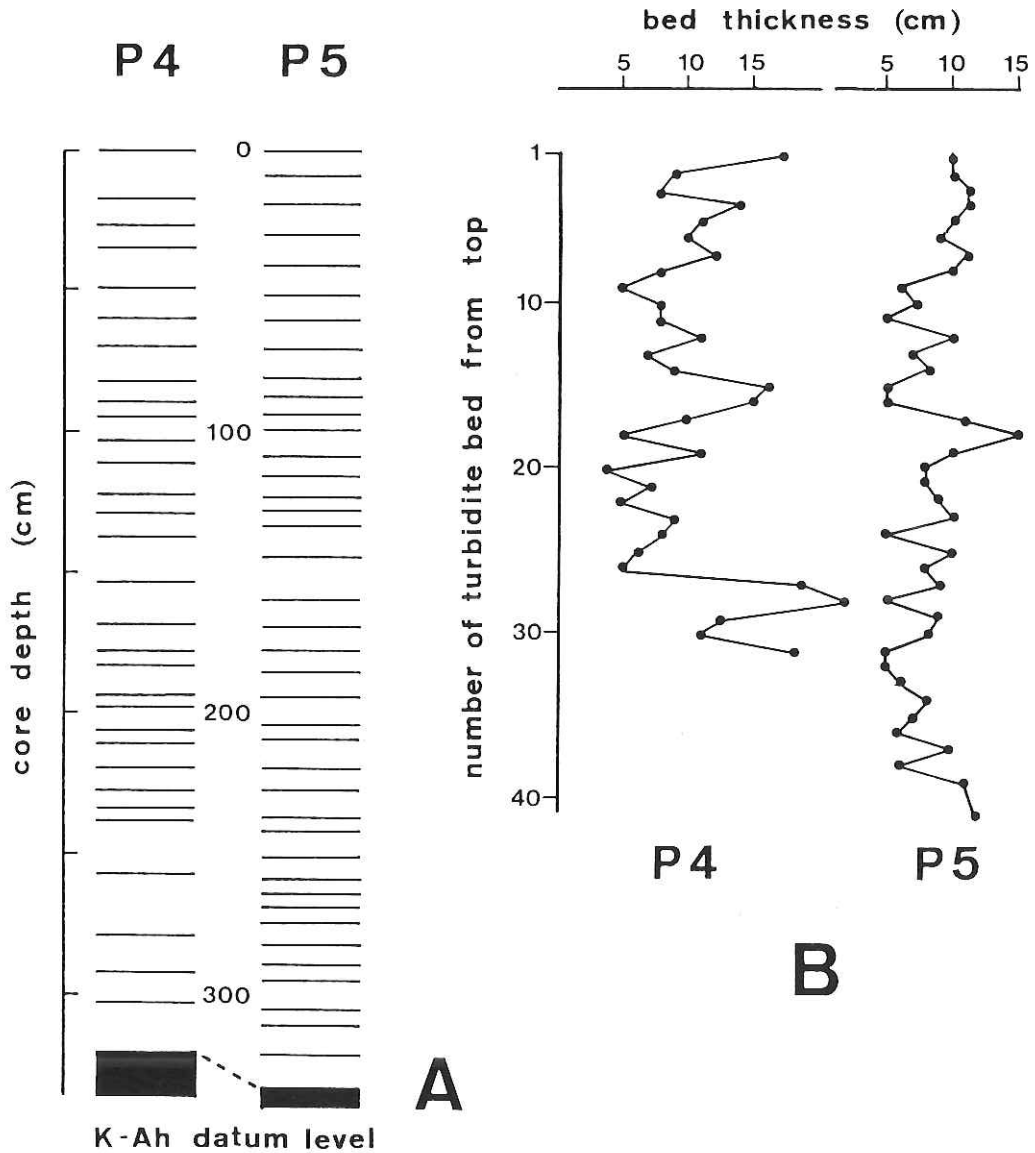

Fig. 4 Seqential patterns of the sedimentation units in cores P4 and P5. A: sedimentation unit coloumns from Fig.2; B: unit thickness vs. bed number, counted from the top of the cores.

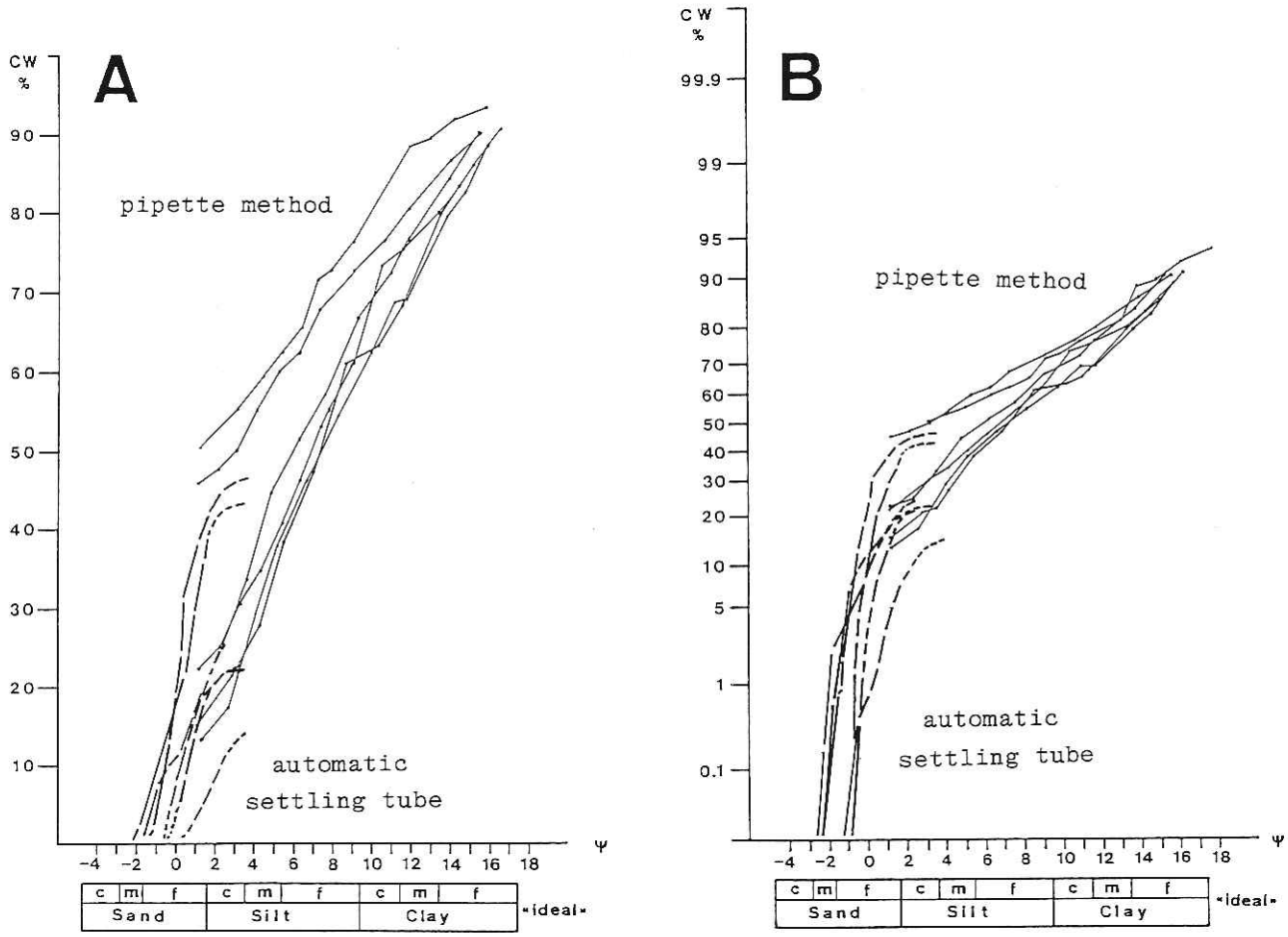

Fig. 5 Settling velocity (psi) versus cumulative weight percent (CW%) for all measured samples. A: logarithmic-arithmetic, B: logarithm-probability; psi=-log (v[cm*s]/1cm*s).

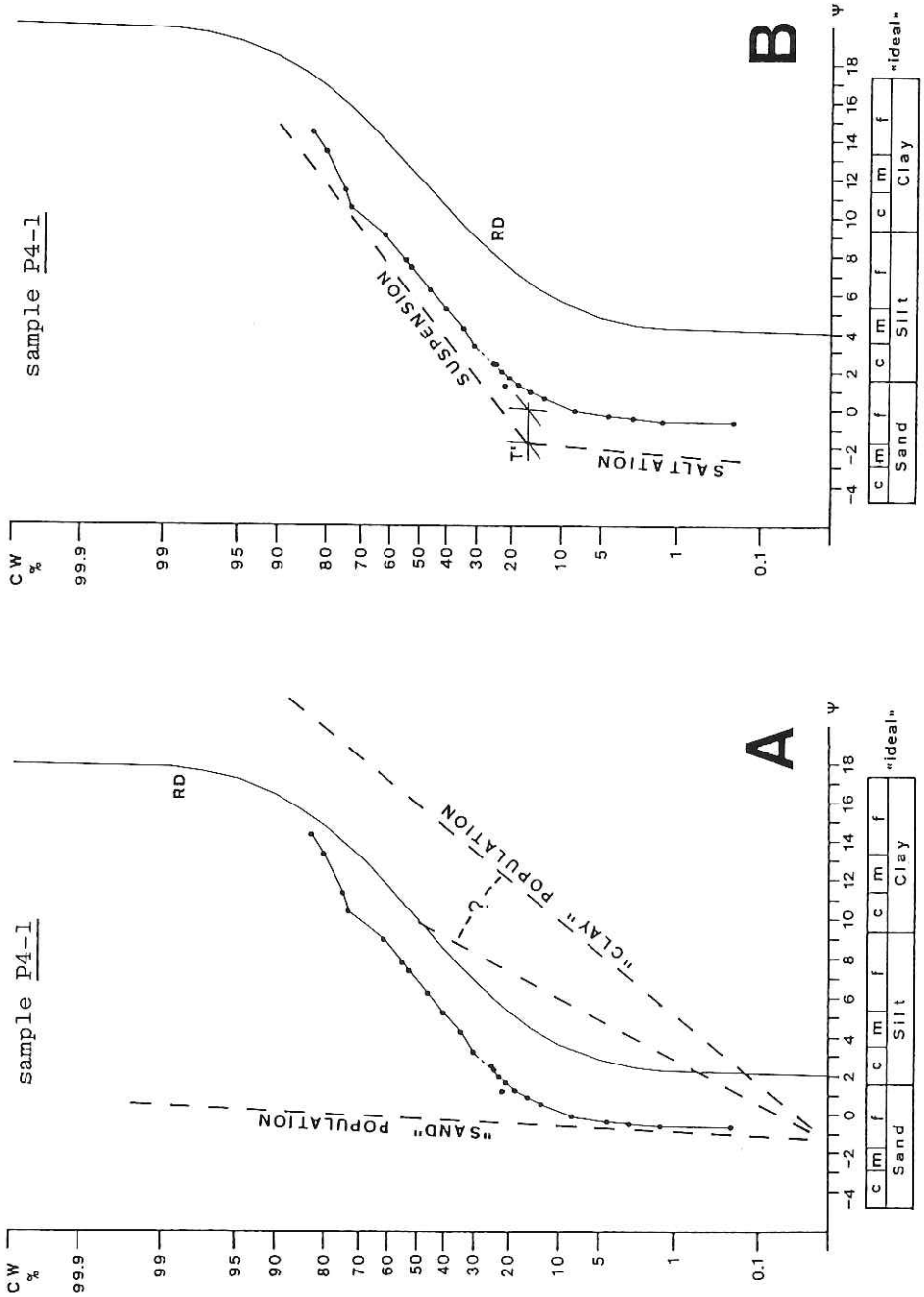

Fig. 6 Two graphical interpretation methods, exemplified for sample P4-1: A, after SPENCER (1963), B, after VISHER (1969). RD: "rectangular distribution", T: truncation point. Explanation see text.

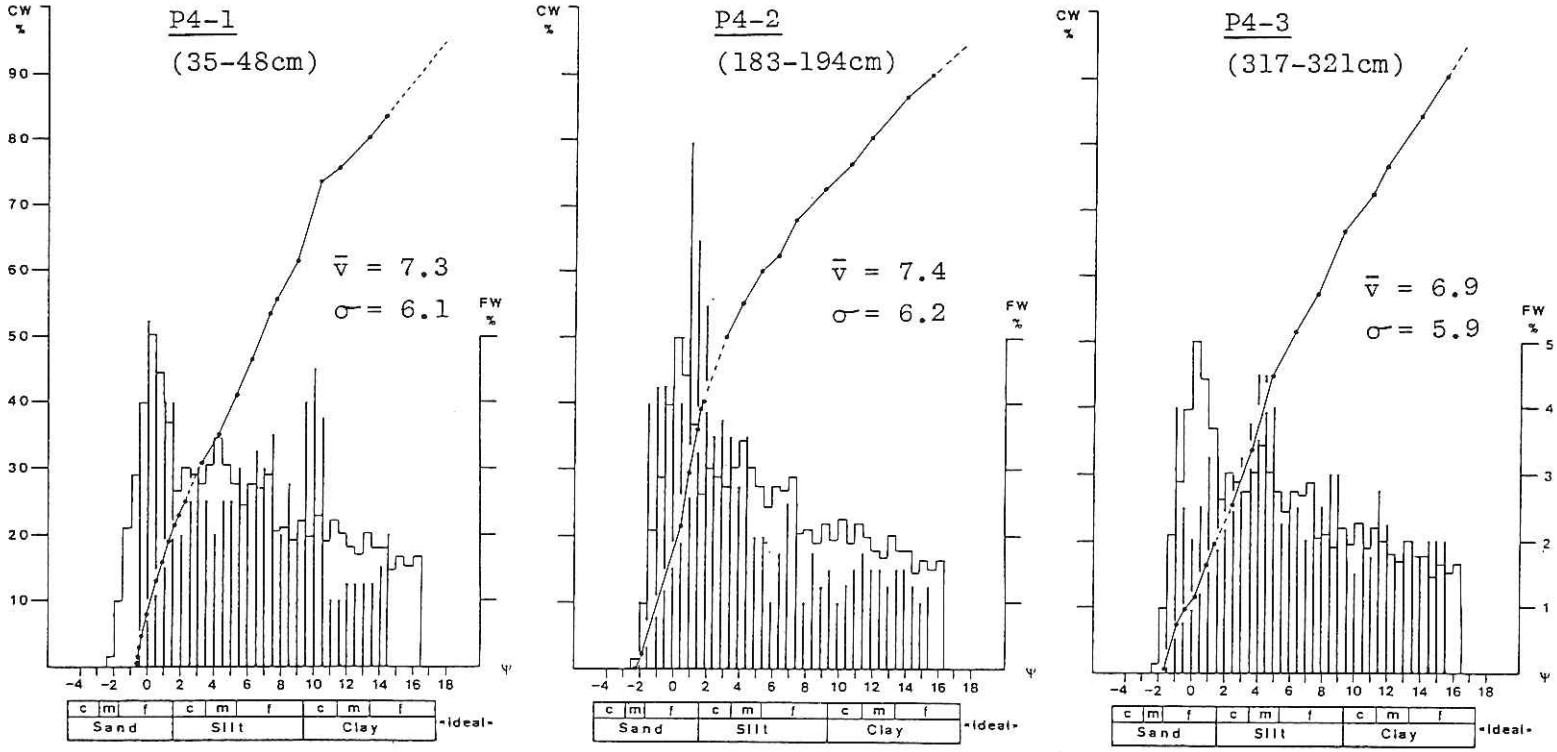

Fig. 7 Settling velocity (psi) versus cumulative weight (CW%) and frequency weight (FW%) percent. Individual frequency distributions are given in vertical lines (0.5 psi intervals), the computed average histogram is shown as contour line. Mean velocity (V) and standard deviation (sigma) after percentile method of FOLK & WARD (1957). Explanation see text.

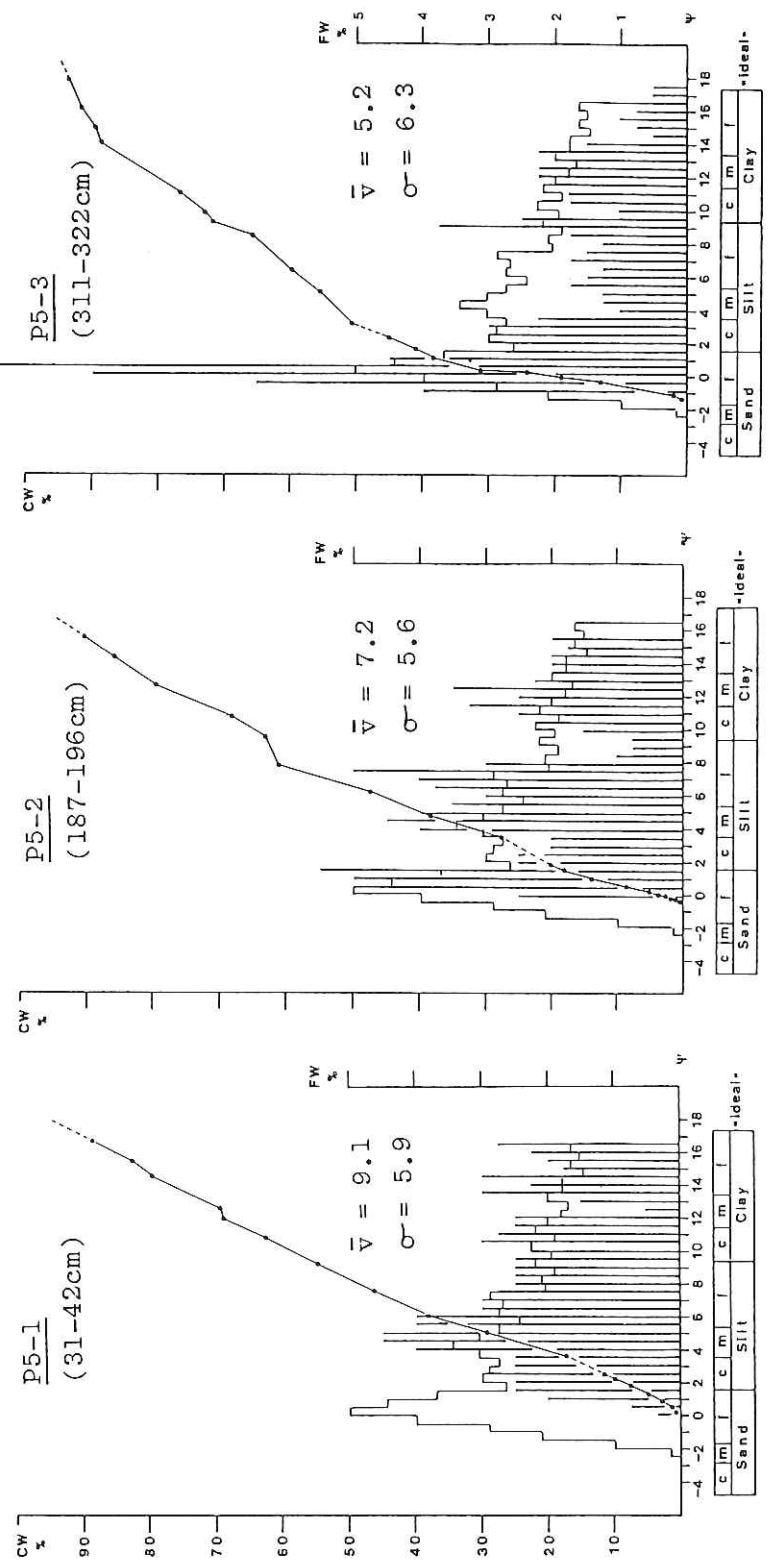
P5-1
(31-42cm)
$\bar{v}$ = 9.1
σ = 5.9
P5-2
(187-196cm)
$\bar{v}$ = 7.2
σ = 5.6
P5-3
(311-322cm)
$\bar{v}$ = 5.2
σ = 6.3
CW %
FW %
Ψ
Sand
Silt
Clay
-ideal-

REFRACTIVE INDICES AND CHEMICAL COMPOSITION OF VOLCANIC GLASS SHARDS OBTAINED FROM THE CORE SAMPLES, KH86-5 CRUISE

W. SOH and T. FURUTA

Ocean Research Institute, University of Tokyo, Nakono, Tokyo164

Widespread tephra is well known to be useful as a geologic time marker, that distributes form a terrestrial to deep-water environments (e.g. Furuta, 1976; Cadet and Fujioka, 1980; Fujioka and Cadet, 1985; Furuta et al., 1986).

Seven piston core samples are obtained during KH 86-5 cruise, R/V Hakuho-maru. Many tephra layers are intercalated in the piston core samples (Table 1). The measurements of refractive index and of chemical composition of volcanic glass shards were performed to investigate depositional age and sedimentary rates of the core samples. Seven samples were selected as shown in Table 2.

The refractive indices of volcanic glass shards could be obtained by RIMS-86 System of the Ocean Research Institute, University of Tokyo. This system allows direct measurement of the refractive indices flake-by-flake, using the temperature change of the immersion liquid, that is automatically controlled by the thermo-module on the microscope stage (see, Yokoyama et al., 1986). In each sample more than 45 flakes, chiefly buble-wall type glass shards, approximately 50 to 100 mm in diameter, were measured. The chemical composition of glass shard was analysed on a real-time basis by an automated JCXA-733 (JEOL) four-channel electron probe microanalyzer, interfaced with a computer to perform a standard correction. The analysed samples are 20 phi in diameter.

Results of the measurements are shown in Table 2 and Fig. 1. The analyses of the refractive indices and chemical composition suggest that P5-1 and P4-2 are the Kikai-Akahoya ash, 6,300 B.P. (Table 2 and Fig. 1). This interpretation would support 5,260 +90 yrs B.P.by ^{14}C age of plant debris contained in P4 (B. Suk et al., in this volume).

The refractive indices suggest that P2-1 and P7-2 tephra are similar to those of Aira-Tn ash, 21,000-23,000 B.P. However, the chemical composition of P2-1 strongly reject this interpretation. Oba and Ohta (in this report) pointed out that the depositional age of P2-1 horizon could be correlated with 5,000 to 8,000 BP.

REFERENCE

Cadet, J.P. and Fujioka, K., 1980, Ash layers from deep sea drilling project leg. 84: Middle America Trench transect. In Science party, Init. Repts. DSDP.84, 609-618.

Fujioka, K. and Cadet, J. P., 1985, Volcanic ash at site 584, Japan Trench. In Science party, Init. Repts. DSDP, 87, 681-694,

Furta, T., 1976, Petrographic and magnetic properties of tephra in a deep-sea core from the northwest Pacific. Mar.Geol.,20, 229-237.

Furata, T., Fujioka, K. and Arai, F., 1986, Widespread submarine tephras around Japan-Petrographic and chemical properties, Mar. Geol., 72, 125-142.

Yokoyama, T., Danhara, T. and Yamashita, T., 1986, A new refractometer for volcanic glass, Daiyonki-Kenkyu (the Quat. Res.), 25, 21-30.

Table 1 list of tephra layers of the piston core samples, KH 86-5 cruise.

Sample Number	lithology	Sedimentary Structure	Thickness (cm)	Depth below Surface (cm)
P2-1	glass	parallel lamination	4	68
P2-2	scoria	normal grading	3	138
P2-3	glass		1	177
P2-4	scoria	normal grading (?)	1	206
P3-1	glass	parallel lamination	2	592
P4-1	glass	parallel lamination	1	80
P4-2	glass	massive to parallel lamination	18	315
P5-1	glass	massive to parallel lamination	27	318
P7-1	glass	massive	22	8
P7-2	glass	crude parallel lamination	10	245
P7-3	glass	massive	10	260

Table 2 List of refractive indices of KH86-5 tephra samples

No. sample	Number	mean	max.	min.	range	st. dev.	skew.	
P2-1 (68 cm)	54	1.4993	1.4965	1.5000	0.0035	0.0007	-0.0829	AT
P3-1 (592 cm)	11	1.5074	1.5084	1.5084	0.0041	0.0011	-1.7448	?
P4-2 (315 cm)	51	1.5113	1.5131	1.5078	0.0053	0.0010	-0.9871	Ah
P5-1 (318 cm)	50	1.5104	1.5130	1.5078	0.0049	0.0013	0.1699	Ah
P7-1 (22 cm)	61	1.5030	1.5060	1.5006	0.0054	0.0014	0.3888	
P7-2 (245 cm)	45	1.4979	1.5010	1.4964	0.0046	0.0008	1.0291	
P7-3 (260 cm)	51	1.5009	1.5024	1.4993	0.0031	0.0006	-0.1093	

AT:Aira-Tn ash (6300 B.P.)
Ah:Kiaki-Akahoya ash (22000 B.P.)

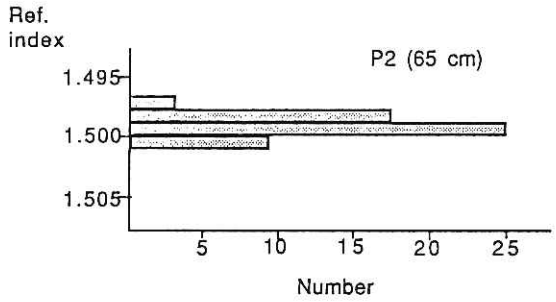

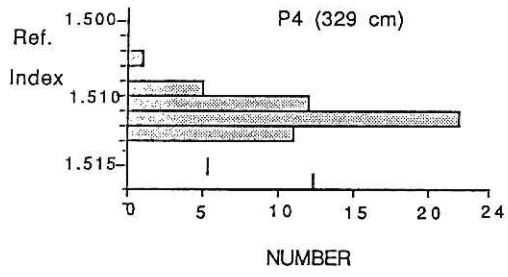

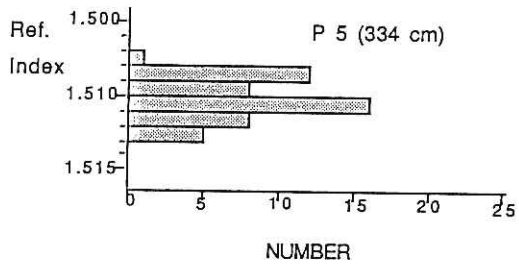

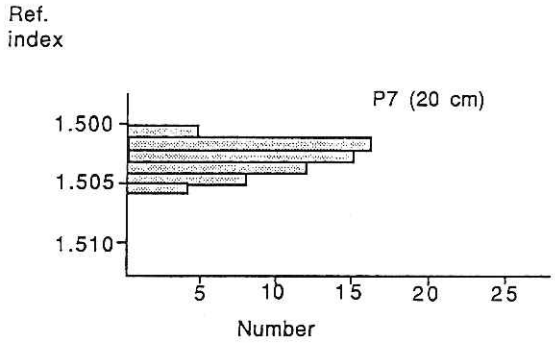

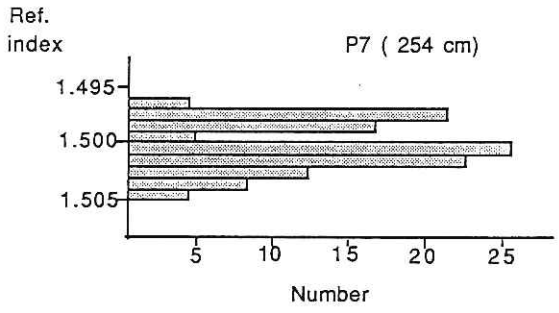

Fig. 1 Results of refractive index measurements by RIMS-86 system.

TRENCH FILL SEDIMENT THICKNESS DISTRIBUTION PATTERN, FRACTURE OF PACIFIC PLATE OCEANIC CRUST AND ACCRETION HISTORY AT THE TRIPLE JUNCTION

K. OTSUKA and X. GUO

Department of Earth Sciences, Shizuoka University, Shizuoka 422

INTRODUCTION

Thickness of trench fill sediments is an essentially important factor for the character of arc-trench systems and tectonic mechanisms in fore-arc regions. In order to realize sediment thickness distribution and also infer the basement deformation at the triple junction areas between Sagami Trough, Japan Trench and Izu-Bonin Trench, the thickness of turbiditic trench fill sediments is measured.

DATA USED IN THE STUDY

The seismic reflection profiles of KH-86-5 line 2 and the data from KAIKO phase I crossing the trench axis near triple junction are used in this study. The result is shown in Figs. 1 and 2.

RESULTS AND DISCUSSION

The results are described as follows;

1) Development of thick trench fill sediments is only recognozed in a very limited zone from 34°20' N to 33°50' N around the triple junction.

2) The thickness distribution pattern suggests influence of three major tectonic components, probably due to the fracture of oceanic crust of Pacific Plate. These tectonic components are ;

a)Component I, parallel with the trench axis direction. The trench fill sediment thickness increases toward the inner trench wall. However, increase-decrease repetition parallel with the trench axis is characteristic. This component represents Pacific Plate subduction itself and tensile rupture of oceanic crust by bending of Pacific Plate.

b)Component II, with NW-SE direction and recognizable thickenning of trench fill is distinct at its SW side.

c)Component III, with NE-SW direction. The trench fill thickenns at the NW side.

Component II and III are considered to be related to the deformation or fracture of Pacific Plate at the triple junction. Seno and Takano (1986) and Seno et al. (1986) show that NW-SE trending normal fracturings with the southwest block downthrown and NE-SW trending normal faulting with the northwest block downthrown are characteristically occurring in the triple juction area from the seismotectonic anaysis. They thought these normal faults as trench parallel and trench normal components. Trench fill thickness change patterns of component II and III represent direct influences of these normal faults. However, it seems more appropriate to interpret these faultings as oblique sets to the trench axis according to Fig. 1. One of these sets, in NW-SE direction, looks like paralleling with the Sagami Trough.

Fig. 1 indicates distinctly two sites of maximum trench fill sediment accumulation; the northern so-called Mogi Fan area (near lines 2 and 83) and the southern present Sagami Trough channel influx region (between line 81 and 79). At Mogi Fan area trench fill thickness increases abruptly at the toe of the inner trench wall even more than 2.0 sec, leaving most of the trench floor thinner sediment filling area almost same as more northern area. Contrary to Mogi Fan area, present Sagami Trough channle influx region is distinct by its wide distribution of sediment thickness augmentation in the trench floor as a form of buried trough extending from Sagami Trough channle in NW-SE direction. However, notable thickenning at the foot of inner trench wall is not recognized as yet.

These differences are probably attributed to the elapsed time and history of each site of sediment accumulation. The present Sagami Trough influx area is now becoming a main sediments accumulation site. However, Mogi Fan represent deformation morphology of accreted trench fill sediments.

Estimated from the rate of Pacific Plate movement against NE Japan and westward advance of accumulated trench fill of Mogi Fan to the inner wall, active sedimentation at Mogi Fan area ended about 0.2 Ma before present there. Then, Sagami Trough and its main channel shifted its position from already accreted impedimental area to southern newly forming tectonic depression. Terrigeneous sediments have buried the basement depression at this site. These interpretations suppose the possibility of migration of Sagami Trough axis in a rather short period, in relation to the sediment accretion and normal faulting of the oceanic basement of Pacific Plate in the direction parallel to the Sagami Trough.

REFERENCE

Seno, T. and Takano, T. (1986) Seismotectonics of the trench-trench-trench triple juction off central Honshu. Abst. Intern. KAIKO conf.,158-159.

Seno, T., Moriyama, T. and Takano, T. (1986) Seismotectonics of trench triple junction areas, The Earth Monthly (Gekkan-Chikyu), 8, 265-270.

KAIKO I Research Group (1986) Topography and structure of trenches around Japan. - Data atlas of Franco-Japanese KAIKO Project, Phase I-, 305 pp.

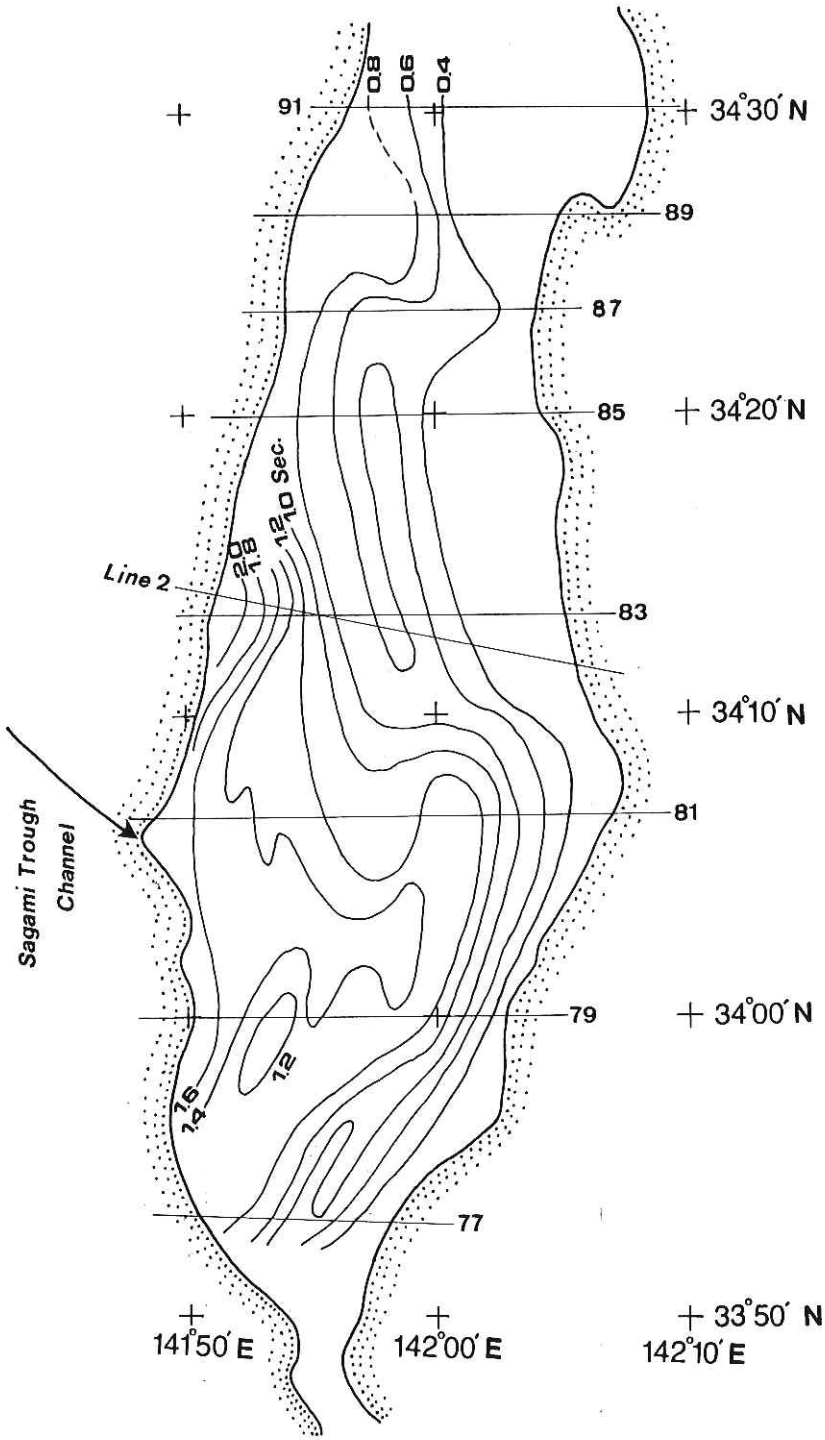

Fig. 1 Thickness distribution of trench fill turbidite at triple junction area between Sagami Trough, Japan and Izu-Bonin Trenches.

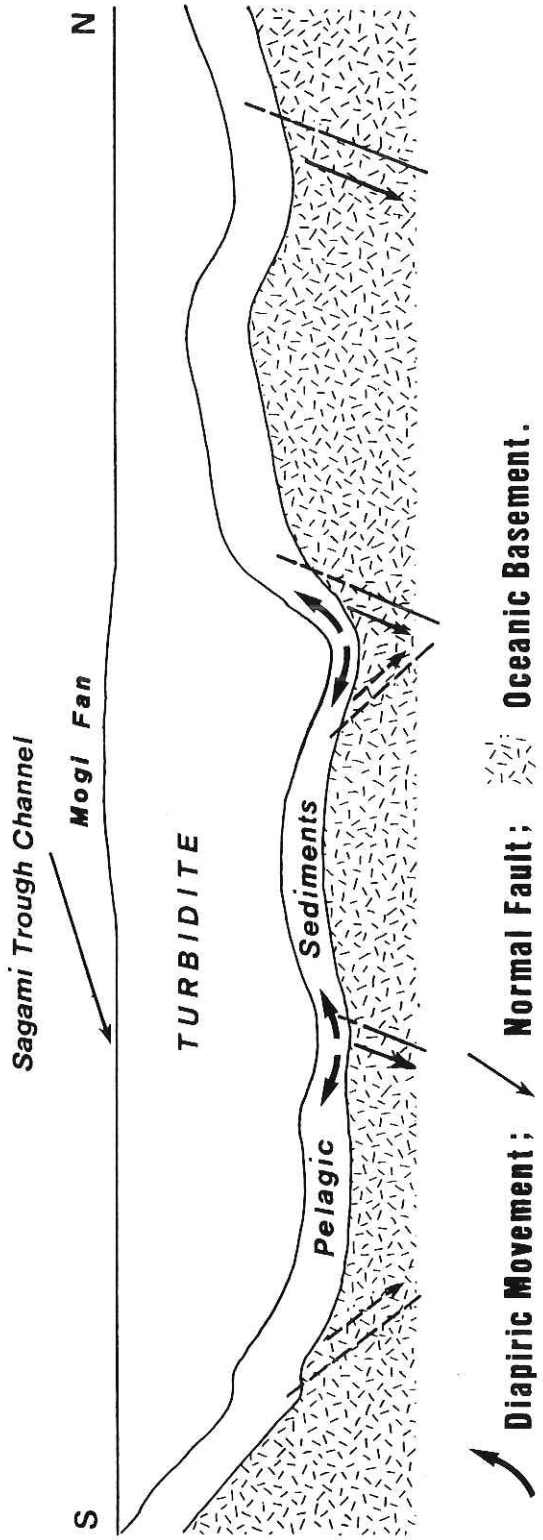

Fig. 2 Cross section of Japan and Izu-Bonin Trenches at the triple junction.

WHERE DO THE ORGANIC MATERIALS OF DEEP-SEA NANKAI TROUGH SEDIMENT COME FROM?

W. SOH and T. ISHIZUKA
Ocean Research Institute, University of Tokyo, Nakano, Tokyo 164
K. KOJIMA
Department of Earth Siences, Kanazawa University, Marunouchi, Kanazaw 920

KH86-5 P6 piston core was obtained from the Nankai Trough off Muroto Peninsula, Shikoku. Sample location is 32°17.9 N latitude, 135°00.9 E longitude, 4800 m in water depth. The core sample contained a large amount of organic materials as well as natural gasses. The organic gasses contained in P 6 core sample would be composed mainly of methane. Total organic carbon and nitrogen in the sediments, and amino acid in the pore water of the core were analyzed to investigate origin of the organic materials of the core sample. Results are shown in Fig. 1 and, Table 1 and 2.

As shown in Fig. 1, it can be well understood that the total amount of organic carbon depends chiefly on the sedimentational process of the deposits. The total amount of organic carbon in the hemipelagic sediment is fairly constant from 1 to 2 mg C/g, but the total amount in turbidites tends to vary widely by approximately two or three times higher than those of the hemipelagic sediment. In contrast, the total amount of organic nitrogen ranges from 1 to 2 mg N/g, and it shows relatively constant through the core sample.

It is known that the C/N ratio of plankton is 6 to 7, but the ratio of cellulose or lignite is ranging from 30 to 40, and that the C/N ratio of materials could reflect the difference of organic material source (Nakai et al., 1982). That the C/N ratio of turbiditic mud is much higher than those of plankton indicates strongly that the organic materials of turbiditic origin would include a large amount of terrestrial organic materials.

On the other hand, the free amino acids are almost less than 13 μm, and the proteins remain more than 100 μm (Table 1 & 2). It shows that the decomposition of organic materials of KH86-5, P6 has not been proceeded so much by bacteria. It suggests that the natural gasses mainly of the methane would not be the products of *in situ* bacteria activity in the subsurface of anoxidic condition. We believe that the natural gas would come up from the deeper level of the trough fill sediment from the bacterial fermentation zone or decarboxylation zone.

REFERENCE

Nakai, N., Ohata, T., Fujisawa, H. and Yoshida, M., 1982, Paleoclimate and Sea-level changes deduced from organic carbon isotope ratios, C/N ratios and pyrite contents of cored sediments from Nagoya Harbor, Japan. Daiyonki-Kenkyu (the Qauternary Research), 21, 169-177.

Table 1 List of the hydrolyzable amino acid of interstitial water in the Nankai Trough fill, KH86-5, P-6, off the Muroto Basin.

AMINOACIDS	(cm)	44	40-50	60-70	110-130	144-150	160-170	180-190	230-240	263-266
Taurine			0.91	0.80	0.84	0.96	1.02	0.89	1.06	0.76
Aspartic acid		0.09	12.60	11.05	12.20	11.95	12.57	11.40	12.68	8.50
Threoline		0.08	8.82	7.07	8.09	7.73	7.20	7.71	8.36	5.40
Serine		0.28	6.33	5.36	4.32	4.03	3.82	4.19	9.17	3.01
Asparagine			0.28						0.59	0.16
Glutamic acid		0.03	16.69	14.19	11.98	12.56	12.01	12.18	10.38	8.27
a-amino adpic acid			1.18	1.05	1.35	1.41	1.39	1.31	1.26	1.33
Glycine		0.51	33.89	29.99	26.23	31.63	32.25	30.79	31.56	23.93
Alanine		0.35	26.77	19.78	18.16	21.68	21.10	22.32	21.78	17.05
Citrulline			10.09	7.79	10.25	9.92	10.04	10.84	10.82	9.60
a-amino-n-butric acid						1.15	0.65	3.93	3.61	
Valine		0.34	5.18	4.60	4.68	4.44	3.94	4.27	4.23	2.87
Clystine										2.51
Methionine			0.48	0.54	0.96	0.57	0.55	0.66	0.81	0.64
Cystathionine			0.21	0.24	0.49			0.33	0.37	0.39
Isoleucine		0.09	3.31	2.88	3.49	2.87	2.58	7.97	2.75	1.84
Leucine		0.11	3.50	2.91	3.52	2.85	2.65	3.04	2.94	2.05
Tyrosine			0.49	0.42	0.25	0.26	0.24	0.36	0.91	0.55
Phenylalanine		0.05	1.53	1.10	0.96	1.53	1.05	1.31	1.33	0.94
b-Alanine			4.07	3.92	5.25	4.81	4.90	4.33	2.82	3.53
b-Amino iso butyric acid			0.16	0.09		0.13	0.15	0.15		
a-amino-n-butyric acid		0.12	2.06	1.87	2.38	2.24	2.18	2.06	1.52	1.43
Ethanolamine			1.64	1.33	1.42	1.59	1.72	1.44	1.52	1.43
Ornithine		0.18	2.47	1.92	0.71	0.85	0.76	0.89	3.16	0.65
Lysine		0.17	1.74	1.34	1.21	1.28	1.28	1.38	1.44	1.31
Histidine		0.03	0.48	0.46	0.24	0.21	0.15	0.22	0.88	0.17
Arginine			1.00	0.78	0.67	0.67	0.67	0.78	0.67	0.67
Total	2.43	145.88	121.40	119.65	125.57	125.37	131.47	136.96	102.59	

Table 2 List of the free amino acid of interstitial water in the Nankai Trough fill, KH86-5, P-6, off the Muroto Basin.

AMINOACIDS	29 cm	40-50	60-70	110-130	144-150	160-170	180-190	210-220	230-240	263-266	
Taurine											
Aspartic acid		0.21		0.08				0.28	0.44		
Threoline		0.17						0.28	0.44		
Serine		0.48	1.66	1.82	0.13			0.65	1.14		
Asparagine							0.22	0.23			
Glutamic acid				0.49				0.96	1.51	1.10	1.71
a-amino adpic acid								0.32			
Glycine		0.41	2.42	3.06	0.42	0.29	0.10	2.03	2.95		
Alanine		0.25	1.30	1.49	0.11			1.42	2.05	0.03	0.17
Citrulline							0.03	0.17			
Valine							0.71	0.99			
Clystine									2.51		
Methionine				0.04				0.51			
Cystathionine							0.67	0.57			
Isoleucine		0.36	0.79	0.79	0.45	0.36	1.53	0.86	0.96	0.08	0.06
Leucine		0.21	0.62	0.61	0.17	0.14	0.21	0.58	0.52		
Tyrosine		0.15	0.10	0.23					0.16		
Phenylalanine		0.03	0.18	0.21	0.08			0.37			
b-Alanine			0.82	1.06	0.89	0.95	1.70	1.19	1.09		0.05
b-Amino iso butyric acid											
a-amino-n-butyric acid				0.08			0.42		0.23		
Ethanolamine							0.23	0.14	0.14		
Ornithine		1.17	1.46	1.44	0.13	0.09		0.24			
Lysine		0.03	0.42	0.27			0.08	0.13	0.19		0.05
Histidine		0.18	0.33	0.38			0.06	0.09	0.20		
Arginine							0.03	0.03	0.05		
Total	3.65	10.10	12.05	2.38	1.83	4.36	11.71	14.11	1.56	1.99	

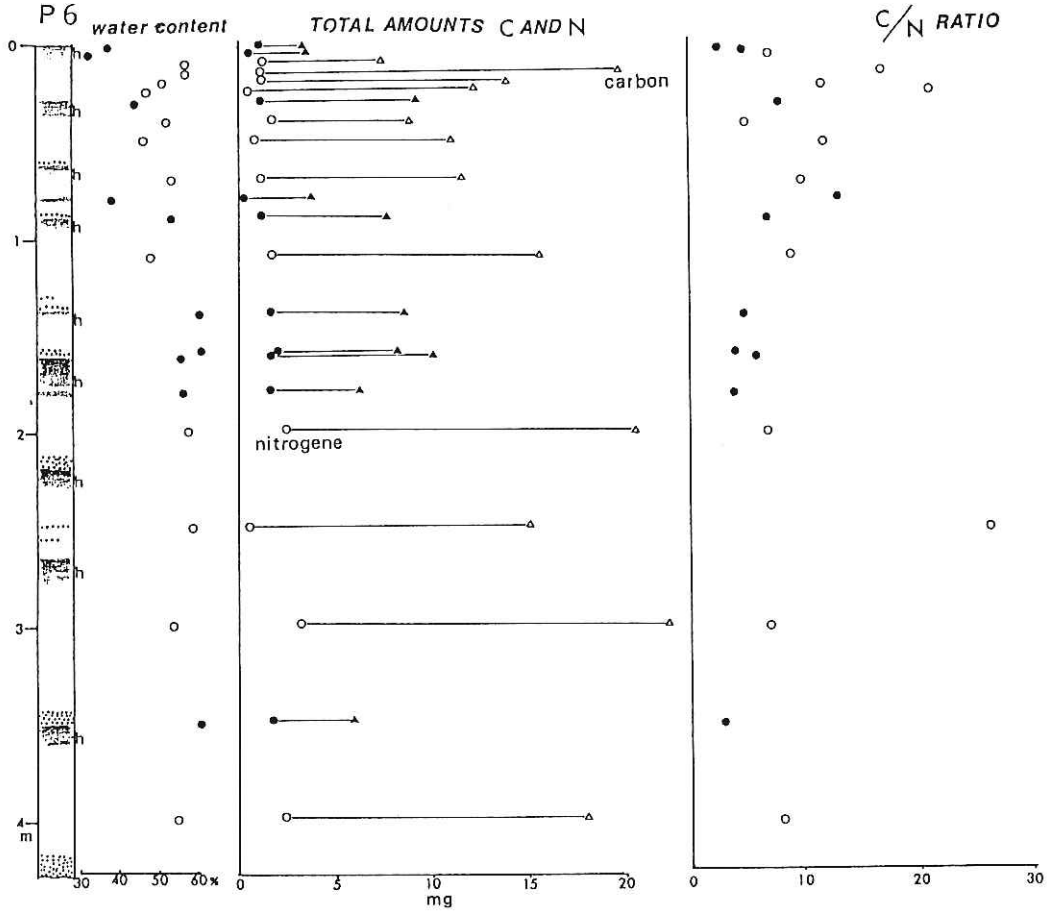

Fig. 1 KH86-5 P6 piston core log and characterisric properties showing water content, total amounts of carbon and itrogene, and C/N ratio. h is hemipelagite. Solid circle: hemipelagite;open circle: turbidite.

FACIES DIFFERENCE BETWEEN THE AXIS FLOOR AND THE SLOPE BASIN SEDIMENTS AROUND NANKAI TROUGH OFF SHIKOKU REGION AND POSSIBILITY OF DISPERSED GAS HYDRATE OCCURENCE

K. OTSUKA and X. GUO

Department of Earth Sciences, Shizuoka University, Otani, Shizuoka 422

INTRODUCTION

Piston core KH86-5 P-6, taken in the axis of the Nankai Trough off Shikoku was peculiarly notable as for blowing out a vast volume of gasses smelling of hydrogen sulfide. The soupy sediments were partly pushed out of the tightly taped core liner by the pressure of the generated gasses before the opening of the core. This means that the sediments of Nankai Trough axis contain a large amount of gaseous matter. In this paper, the authors describe the facies of the sediments around Nankai Trough, and also offer some ideas on the origin and occurrence of gaseous materials in the sediments.

FACIES DIFFERENCES AROUND NANKAI TROUGH OFF SHIKOKU

The texture of the sediments of P-6 core was partly distributed by blow out of gasses. Many voids and crevices due to generated gas bubbles were formed through the core. However, the facies of P-6 can be described as well to poorly-laminated black-coloured mud intercalated by intermittent distal turbidite layers as a whole (Fig. 1), excepting the uppermost 41 cm of bioturbated oxidation zone. On the contrary, the facies of slope basin sediments KH-86-5 P-7, taken near the toe of the accretionary prism of the inner trough wall, were very intensely-bioturbated olive to grayish-coloured mud with turbiditic layers (Fig. 2).

These differences are attributed to the difference of oxidation-reduction condition at the sediment-water interface. Very intense activity of benthic organisms inferred from the slope basin. In the axis floor of Nankai Trough oxygen deficient environment is likely to be maintained excepting the most recent years of the upper most section. Thus, benthic bioactivity was very low or frequently near absent.

This oxidation-reduction state depends at least on the amount of organic materials contained in the supplied sediments to these environments. Decomposition of a large

amount of organic matter exhausted oxygen in the trough axis floor and resulted in warning of benthic bioactivity, although relatively amount of organic materials in the supplied sediments were completely decomposed in the slope basin.

The difference of the supplied sediments to these two environments suggest that the main source of organic substances to the trough axis floor is terrigeneous sediments containing a large amount of on-land plant debris, transported through the major conduits as canyons and Suruga Trough from land areas.

POSSIBILITY OF DISPERSED GAS HYDRATE OCCURENCE

Aoki et al. (1982), Kagami et al (1982) and Yamano et al. (1982) reported the existence of a gas hydrate layer from the Nankai Trough region off Shikoku, inferred from BSR (Bottom Simulating Reflector). However, the results of DSDP leg 87, sites 582 and 583, could not obtain the direct evidence for gas hydrate layer (Kagami et al., 1986). The conclusion was indistinct, and the possibility of dispersed state of gas hydrate was pointed out from 10 m to 193 m below sea floor at the trough axis.

KH-86-5 P-6 has similarity not presented any direct evidence for the gas hydrate. However, the phase diagrams by Shipley et al. (1979) and others, indicate that the gas hydrate is stable even at the sea floor of the Nankai Trough. If enough gas is available beneath the sediment-water interface, generated gasses should be present as the gas hydrate.

The amount of organic matter is considered to be sufficient as described above. Thus, the presence of the gas hydrate depends on whether gas hydrate production rate from dissolved methaen is higher or not than the rate of seepage out of interstitial water that would be effectively obstructed. The generated gaseous material would quickly crystallize around the sites of organic material decomposition. Consequently minute gas hydrate inclusion would be formed.

At the depth of the sea-floor of this region, where gas hydrate is stable, 0.07 m mol of methane can be dissolved in the 1 kg of sea water. Estimation shows that about the same volume of gasses are released from a certain amount of sediments with porosity of 60-70 % at 1 atm. P-6 core at least partly includes almost this rate of voids and crevices. Furthermore, the blowing out gasses from sediments before and after the opening of P-6 core were fairly voluminous. Thus, the gasses in P-6 core would exceed the soluble amount in interstitial water. This might support the dispersed occurrence of gas hydrate directly beneath the sediment-water interface at P-6 site in the Nankai Trough axis. X-ray radiographs (Fig. 1) show various forms of crevices scattering in the sediments throughout

the core length. These might be investigate of gas bubbles released from minute gas hydrate inclusion dispersed in the organic material-rich sediments.

REFERENCE

Aoki, Y., Tamano, T. and Kato, S., 1982, Detailed structure of the Nankai Trough from migrated seismic sections. Am. Assc. Petrol.Geol. Mem., 34, 309-322.

Kagami, H., Tokuyama, E., Kong, Y. S., Igarashi, C. and Nasu, N., 1982, Multi channel seismic survey of Nankai Trough. Marine Sciences Monthly (Gekkan Kaiyo kagaku), 14, 351-357. (in Japanese)

Matsumoto, R., 1987, Nature and occurence of gas hydrates and their implications to geologic phenomena. Jour. Geol. Soc. Japan, 93, 597-615. (in Japanese)

Ocean Research Institute, University of Tokyo, 1982, Multi-channel seismic reflection data across Nankai Trough, IPOD Japan basic data series, 4, 34.

Shipley, T. H., Houston, M.H., Buffler, R. T., Shaub, F. J., McMillen, K. J., Ladd, J. W. and Worzel, J. L., 1979, Seismic evidence for wide spread possible gas hydrate horisons on continental slopes and rises. Am. Assoc. Petrol. Geol. Bull., 63, 2204-2213.

Yamano, M., Uyeda, S., Aoki, Y. and Shipley, T.H., 1982, Estimates of heat flow derived from gas hydrates, Geology, 10, 339-343.

Fig. 1 a X-ray radiograph of laminated sediment of Nankai Trough axis floor. KH-86-5 P6 132-152cm. The upper 6cm is turbiditic layers, but the other part is hemipelagic laminated mud. Many crevices by generated gasses are distinct.

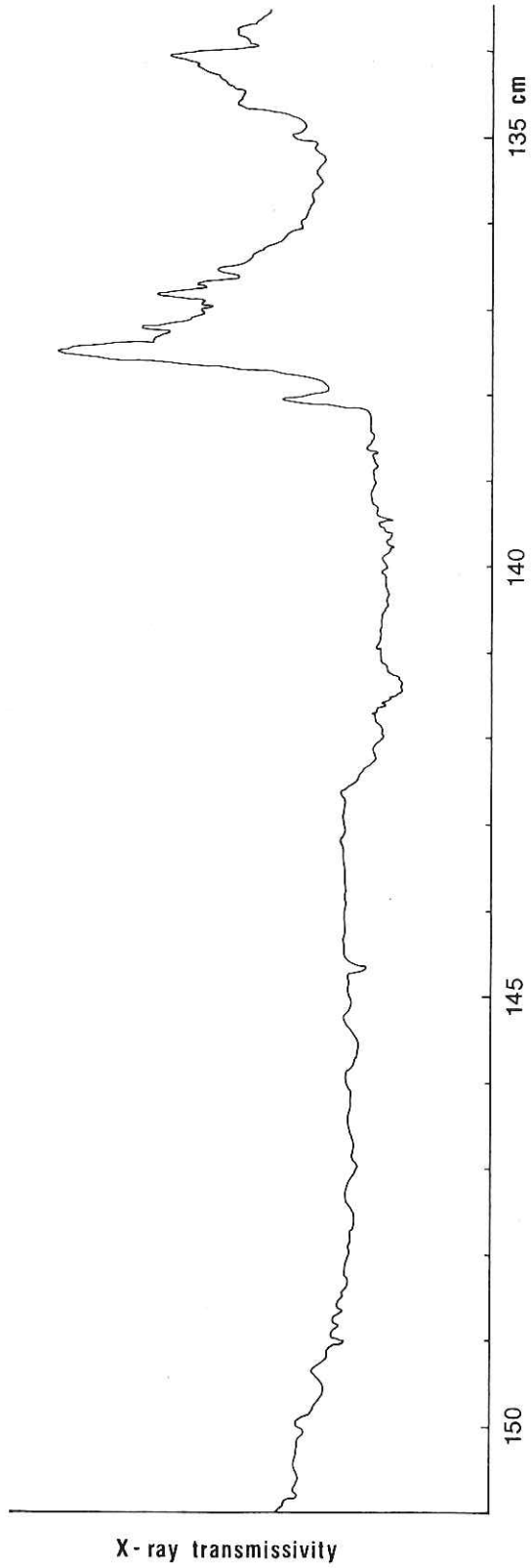

Fig. 1 b X-ray transmissivity of the same section as Fig. 1 a. Density grading of turbiditic layers of upper part is clearly indicated. The lower laminated hemipelagic part has distinctly lower density, and can be distinguished from turbiditic lyers.

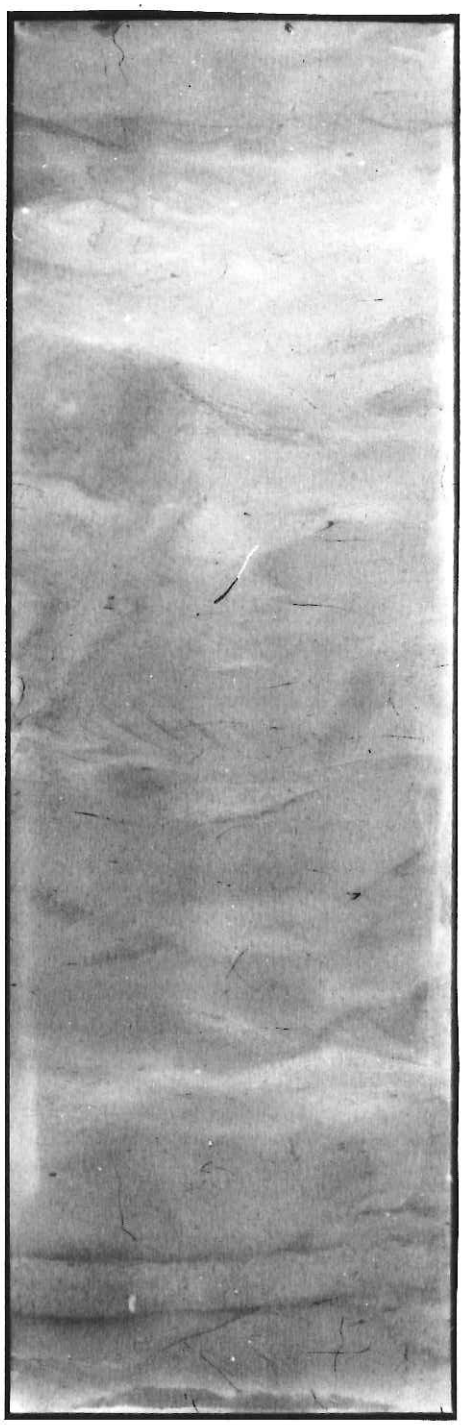

Fig. 2 X-ray radiograph of intensely bioturbated siope basin sediment around Nankai Trough region KH-86-5 P7 100-120cm.

RADIOCARBON AGE DETERMINATION WITH ACCELERATOR MASS SPECTROMETRY (AMS)

B. S. SUK
Ocean Research Institute, University of Tokyo, Nakano, Tokyo,164
T. NAKAMURA
Radio Isotope Center, Nagoya University, Chikusa, Nagoya 440
W. SOH and A. TAIRA
Ocean Research Institute, University of Tokyo, Nakano, Tokyo 164

A large fragment of plant debris was taken at 270-275 cm of piston core P-4, KH86-5 cruise during 22nd November and 15th December, 1986 which was recovered at 32°32'18"N, 134°59'03"E with water depth of 1,270 m from the southern slope of the Muroto Trough basin off Kii Peninsula (Fig. 1). Dimension of the plant debris is 510 by 120 by 60 mm in size with well- preserved plant tissues (Fig. 2). Radio-carbon age has been performed by Mass Spectrometry (AMS) techniques (Nakamura et al., 1987; Nakai & Nakamura, 1984). The plant debris was treated in a hot water bath with 4 % NaOH several times after sample cleaning in an ultrasonic bath, then with 1.2N HCl followed by washing with distilled water. After that the sample was pyrolyzed at 400°C in evecuated ampoules to produce element carbon. Finally sample target for AMS dating was prepared by mixing 2 to 5 mg of amophous carbon obtained with silver powder (1:1 mol) and then pressing the mixture into a pellet of 3 mm in diameter. One aspect of the acceleration mass spectrometry technique is that sample can be dated which are essentially smaller than required fro conventional 14C dating.

The lithofacies in the P-4 core where a plant debris was included shows crude parallel-laminated sand and silt, and was overlaid on the foraminifera-rich parallel-laminated silt layer (Fig. 3). Oba and Ohta (in this volume) described the chronology of the P-2 and C-6 core samples which were recovered from the slope bench off the Boso Peninsula. The age by conventional 14C technique and by tephrochronology assumed that sedimentation rate of core P-2 and C-6 recorded 0.01-0.02 cm/yr from 9,700 yrs BP to the present.

At the 270 to 275 cm of the core P-4, the age of a plant debris recorded 5,260+90 yrs BP by the AMS technique. At the 331 cm of the bottom of core composed of tephra

layer which was originated from the Akahoya Volcanic Eruption by the 6,350 yrs BP. On the basis of the age records, mean sedimentation rate shows 0.05 cm/yr, which the rate are two to four times higher than that of core P-2 and C-6. It is one of the reason why the water depths and depositional environments are different between these two areas.

There are two possibilities of transporting mechanism, one is terrigeneous in origin, and the alternative is come from the seismicitic disturbance on the adjacent sea-bottom occurred by the complex origin. On the basis of lithofacies and age determination, it is reasonable to interpret the sedimentary environments of the area as follows; parallel-laminated sand and silt deposit is terrigeneous in origin because of relative short distance of sediment input source of land, high gradient of continental slope, well-preserved plant debris in core and of turbiditic facies although boundary of bottom of the sequence is not clear comparative with the typical turbidites sequences. Parallel-laminated foraminiferal layers and parallel-laminated sand and silt deposits including well-preserved plant debris also accumulated in turbiditic regime.

REFERENCE

Nakai, N. and Nakamura, T., 1984, Dating and measurements of radioactive isotopes with the Accelerator Mass Spectrometry. Radioisotopes, 32, 645-655.

Nakamura, T., Nakai, N., Ohashi, S., Onoda, S. and Tsubota, S., 1987, 14C measurements with Accelerator Mass Spectrometry-Performance of the spectrometer and some applications to the earth sciences-, Application of Ion Beams in Materials Science, the 12th Intern. Symp. Hosei Univ., Tokyo, Sep. 2-4, pp.6.

Oba T. and Ohta, H., 1988, oxygen and carbon isotopic analysis (in this volume)

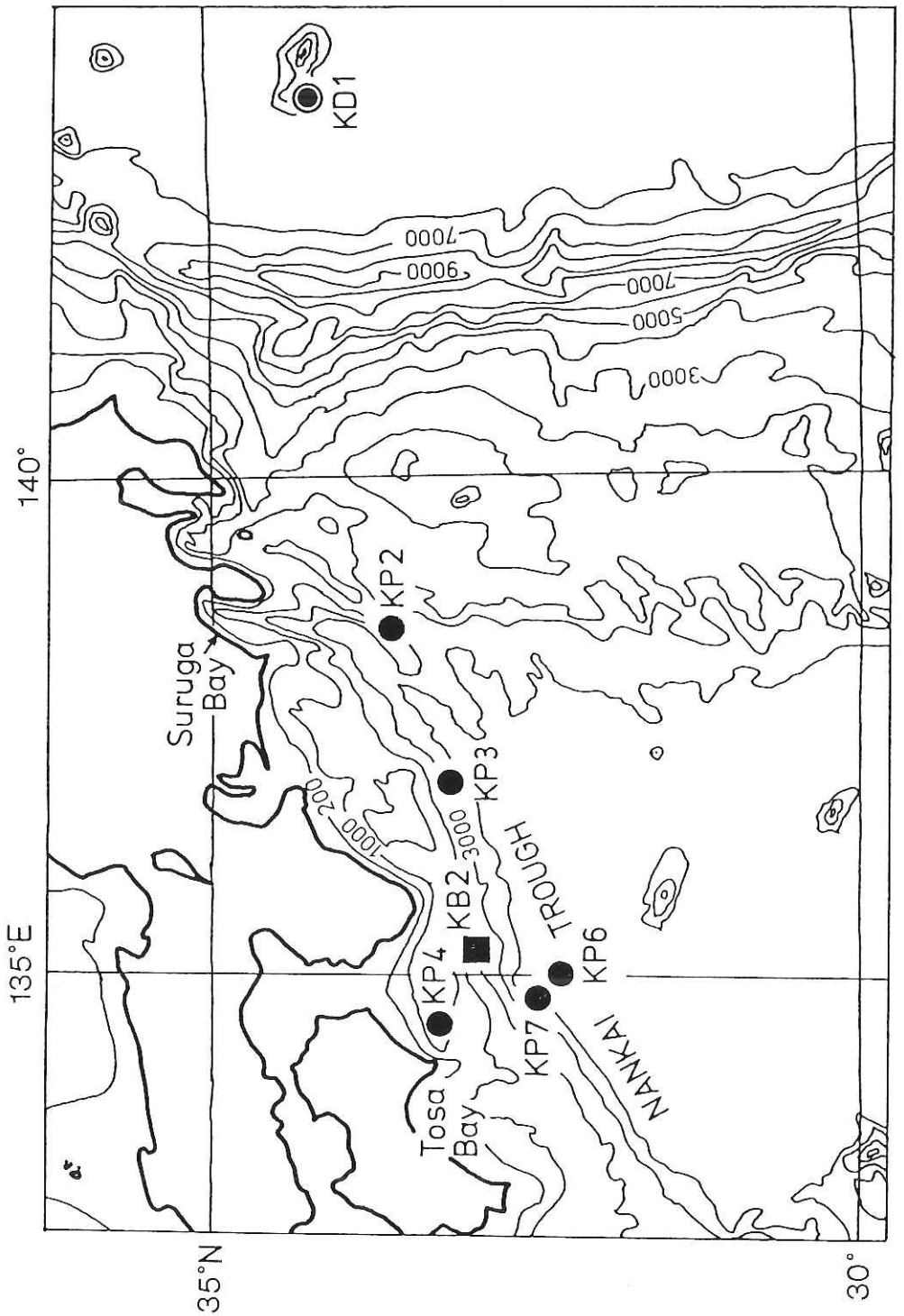

Fig.1 Locality of KH-86-5 cruise and the core station P-4.

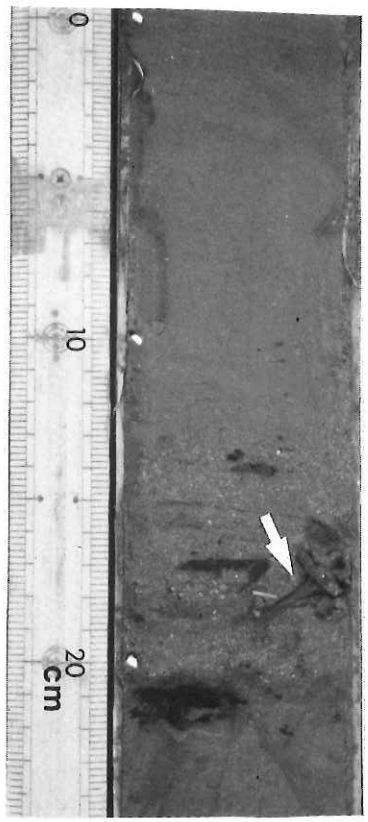

Fig.2 A part of real photographs of the sediment core P-4. Arrow points out the well-preserved plant debris in the core.

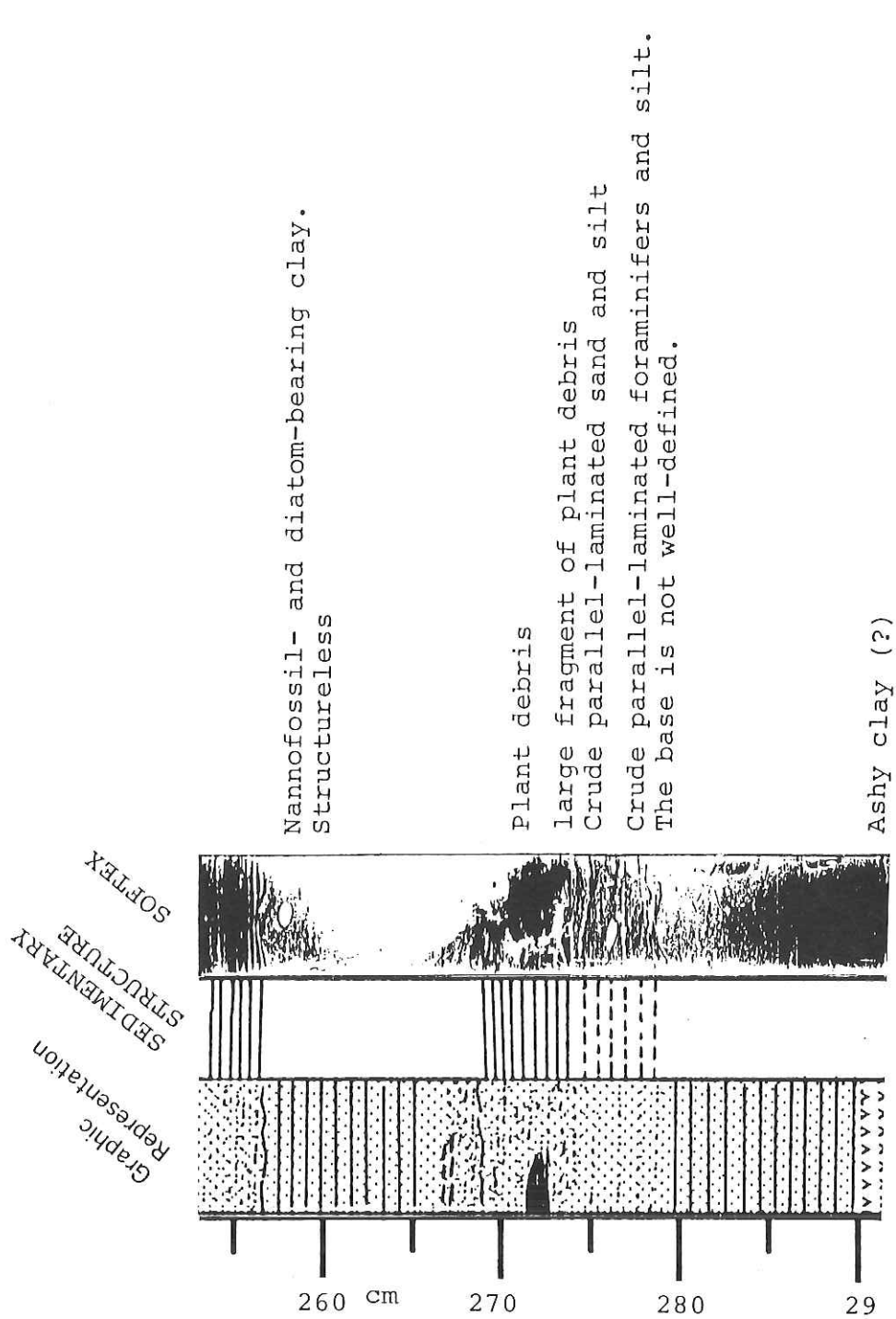

Fig. 3 Lithofacies and sedimentary structure at a part of core P-4, KH-86-5 cruise.

OXYGENE AND CARBON ISTOPIC ANALYSIS

T. OBA

Department of Geology, College Liberal Arts, Kanazawa University, Kanazawa 920

H. OHTA

Department of Earth Sciences, Kanazawa University, Marunouchi 920

Sediment samples for oxgene and carbon isotopic analysis were taken at 20-cm intervals of piston core KH-86-5 P-2 which was recovered from the Zenisu Ridge off Suruga Bay (Fig. 1). About 10 to 20 sepeciments of planktonic formainifera (*Globorotalia inflata*. 250-350 mm in diameter) in each sample were reacted under vaccum at 60.0°C with 100 % phosphoric acid without any pretreatment. The resultant CO_2 gas was analyzed with a Finnigan MAT 251 mass spectrometer at the Department of Geology, College of Liberal Arts, Kanazawa University.

The chronology of the core P-2 is based on the correlation of the oxygen isotopic curves between cores of P-2 and KH-79-3 C-6, which was recovered from the continental bench off the Boso Peninsula (Fig. 1). The top, 155 cm and bottom (315 cm) of the core P-2 are correlated to the top, 205 cm and 305 cm of the core C-6, respectively (Fig. 2). The most enriched $\delta\ ^{18}O$ value are observed at 155 cm in the core P-2 and 205 cm in the core C-6. The age of the enriched $\delta\ ^{18}O$ peak corresponds to the Younger Dryas cold stage of about 11,000 yrs BP, if linear interpolation is assumed between two radio-carbon ages of 10,700 yrs BP at 190 cm and 13,500 yrs BP at 300 cm of the core C-6.

After the Younger Dryas the oxygen isotopic values of the core P-2 are lighter by about 0.3 to 0.4 ‰ than those of the core C-6. The difference is mainly due to the temperature variation of the subsurface water in which *G. inflata* dwelled. On the other hand, the isotopic difference is relatively large (approx. 0.6 to 0.9 ‰) before the Youger Dryas. This is interpreted by the introdution of a mixed water mass of the Oyashio and Kuroshio Currents into the site of the core C-6 between 11,000 and 13,500 yrs BP. While the Kuroshio Current would have flowed through the site of the core P-2 during this period. The depletion of the carbon isotopes in the core C-6 during this period also supports this interpretation.

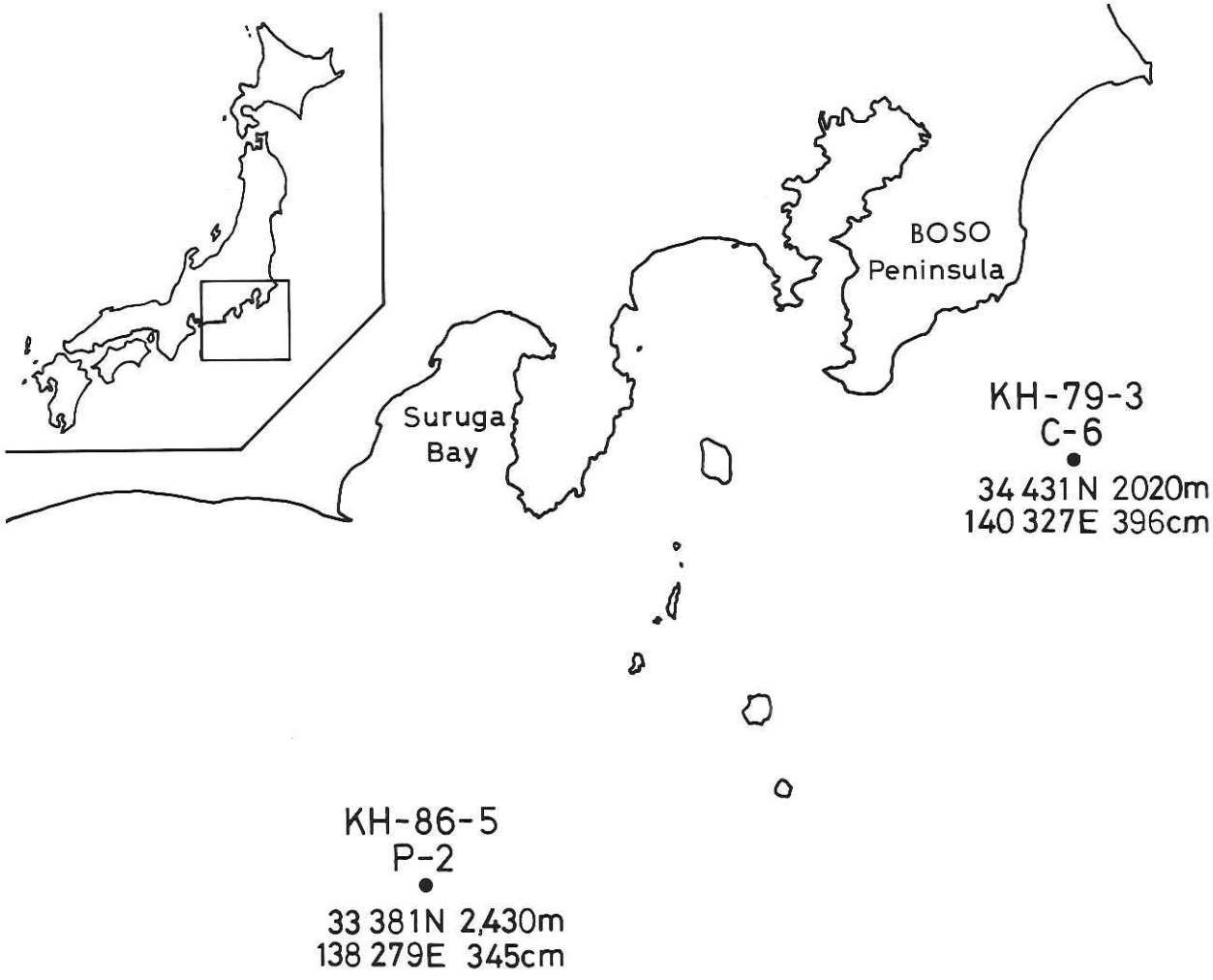

Figure 1. Location of two piston cores KH-79-3 C-6 and KH-86-5 P-2.

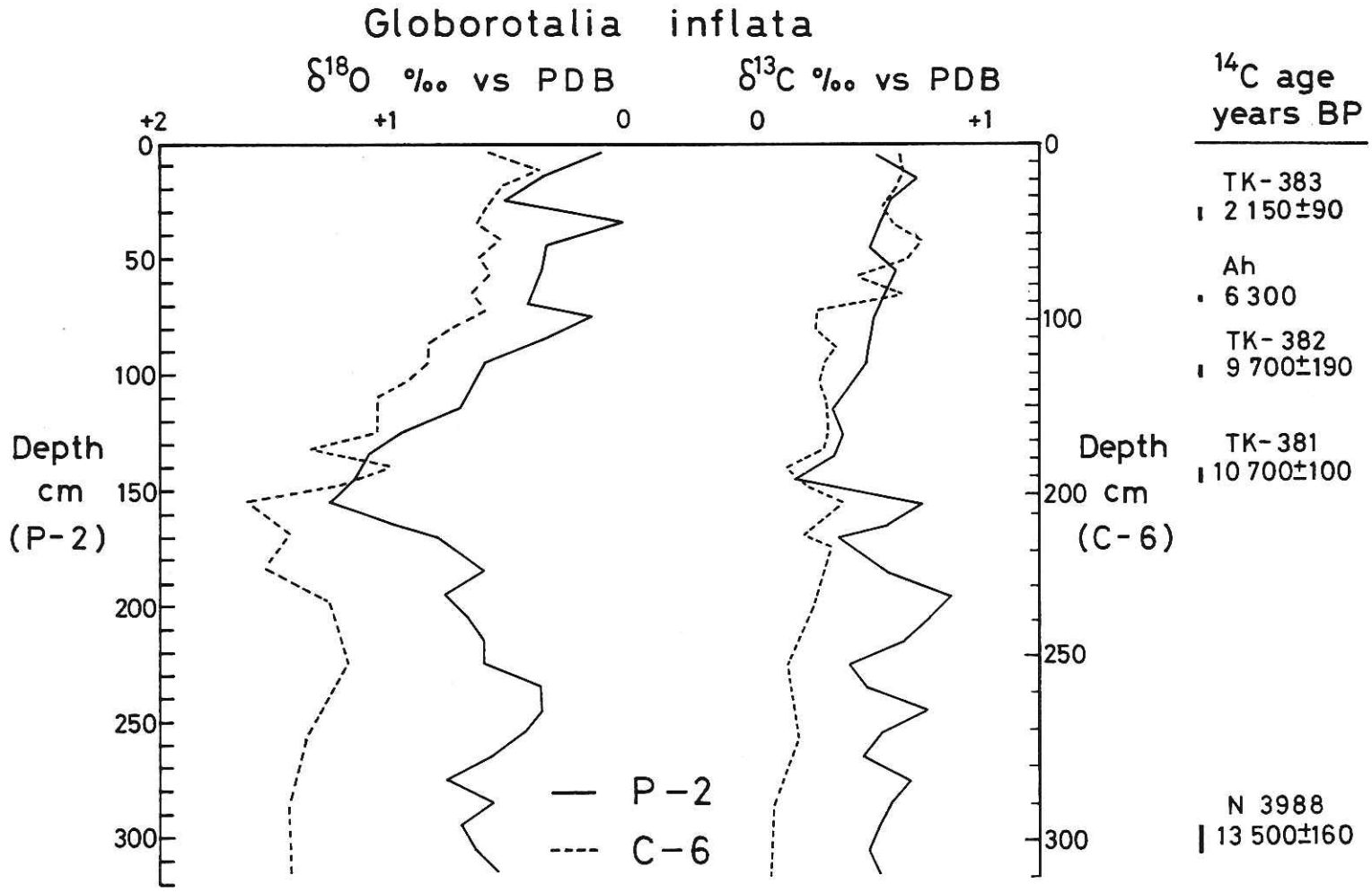

Figure 2. Oxygen and carbon isotopic curves of Globorotalia inflata in cores KH-79-3 C-6 and KH-86-5 P-2.

PRELIMINARY REPORT ON A DACITE LAVA DREDGED ON THE ZENISU RIDGE

J. HERNANDEZ
Universite P. et M. Curie, Laboratoere de Petrologie Mineralo-gique, 4, place jussieu, 75252 Paris Cedex 05
S. LALLEMANT
Ecolo Normale Superieure, Paris

Located at the eastern end of the Nankai trough, the Zenisu ridge is a zone of intraoceanic thrusting related to the vicinity of Izu collision zone (Le Pichon et al. , 1987). Three volcanoes are found on the back of the western part of the ridge (Fig. 1), far from the active volcanic arc related to the Pacific plate subduction. The present study concern six samples (D2 01 to D2 06) dredged on these volcanoes.

PETROGRAPHY

In hand specimen the lava present plagioclase and amphibole phenocrysts in a light grey glassy matrix. Manganese oxydes form a thin coating (3 to 5mm) around the samples. The six samples have the same texture and mineralogical composition.

The texture is hyaloporphyritic, composed of phenocrysts or microphenocrysts of plagioclase, amphibole, biotite and oxydes in a fine hyalopilitic groundmass, olivine is present in two samples and clinopyroxene in one sample. Some microdoleritic basic inclusions and cumulates are also present.

Three different types of plagioclase phenocrysts have been observed. The first one forms euhedral to subeuhedral microphenocrysts (200 to 300 µm), frequently with a fine dusty zone. The other one consist of larger rounded phenocrysts with a large dusty zone and glass inclusions. The last one is frequently associated with biotite in aggregates. This kind of phenocrysts is partly resorbed and contains also glass inclusions.

Amphibole microphenocrysts (green to olive green) are always associated with the first type of plagioclase phenocrysts and could indicate cotectic crystallization.

Biotite, brown to light brown, is frequently present as smalle sidual (?) inclusions in the core of amphibole phenocrysts and within plagioclase - biotite clusters.

Magnesian olivine has been found in two samples, in the first one as an rounded isolated crystal. In the other one as small rounded crystal, In the other one as small rounded crystals in an amphibole aggregate.

Finally, clinopyroxene of diopsidic to salitic composition occurs in one sample,

also in a small amphibole phenocrysts cluster.

"BASIC' INCLUSION

Small inclusions (3 cm diameter) composed of plagioclase, amphibole and oxydes, show evidence of quench textures (elongated or acicular morphology of amphiboles, hollow plagioclases). the presence of a rounded olivine crystal at the border of one inclusion, suggest, as known in other calc-alkaline lavas, mixing between a dacitic magma and a more basic liquid.

CUMULATES

Two types of cumulative association have been encountered. In the first case the paragenesis is similar to the phenocryst assemblage, and in the other one composed of biotite + plagioclase +/- magnetite. It seems that magnetite can be a reaction product between biotite and the host magma.

To summarize, this rock gives evidence of a complex paragenesis composed of an equilibrium assemblage (plagioclase, amphibole, magnetite), and inherited crystals (plagioclase, biotite, pyroxene, olivine). Associated with this assemblage, the presence of basic inclusions, is indicative of a stage of magma mixing.

MAJOR AND TRACE ELEMENTS COMPOSITION

In table 1, two analyses of the two D2-01 samples are presented. The analyses are very similar and the variation of major elements, essentially Mn, are probably due to the penetration of manganese oxydes through microfractures.

In the Peccerillo and Taylor (1976) classification, the rock plots in the upper part of the dacite field and shows a high K_2O content, clearly higher than the Izu -Bonin rocks (see for example Ewart, 1982 or Aramaki and Ui, 1982). It is interesting to note that rocks with K_2O content higher than 2.0% appear only in the western and south western parts of the Japanese arc (for Quaternary volcanic rocks). However, it seems that in the Kozu-shima island, lavas with high K_2O contents are also present (Aramaki an Ui, 1982; Matsuda et al, 1977), and the normalized K_2O content to SiO_2 = 60%, gives and average value for this island of 2.23% (Aramaki and Ui,1982), similar to the analyzed dacite, such contents remaining exceptional. Rb and Sr values are also high.

By their low contents in MgO, CaO and $TiO_2$and relatively high Al_2O_3, the rocks studied approach the "hypersthenic rock series" of Kuno (1968)

MINERALOGY

A preliminary set of mineralogical data has been obtained through 175 analyses of plagioclase, aphibole, biotite, pyroxene, olivine and magnetite (samples D2 - 01, D2-03 et D2-04) with a Camebax automatized electron microprobe (U.P.M.c. - Paris).

Plagioclase

It is possible to confirm three differect types of plagioclase crystals in the samples analyzed (Table 2 and Fig. 2).

Calcic plagioclase phenocrysts

They form phenocrysts and microphenocrysts, associated with amphibole. Their An content reaches 88 % at the core, the more frequent compositions being between An 60 - 70. They are normally zoned, the border composition is An 45 - 50. Frequently a fine zone of inclusions exists near the outerpart of the crystal. Potassium content of this plagioclase is low (.0025 to 0.187 cation per formula unit).

Resorbed agglomerate crystals

Frequently associated in small clusters of three to five crystals, with a well developed patchy zoning at the core and a zone of melting towards the border. Biotite is clearly linked with this type. The An content is low (An 51 - 54) decreases to An 38 - 40 before it increases again to a content of An 50 - 55. These changes are the nost frequent but are not systematic, and other compositions trends have been noted, always complex and inverse. The composition of the fusion zone is comprised generally btween An 52 - 53, but in two cases the An content of the zone was An 38 - 40. The iron content of these plagioclases is slightly higher than that in the preceding crystals.

Plagioclase of "basic" inclusions

In the inclusions, crystals are small microphenocrystals or quench crystals. The core of the microphenocrysts is An rich (An 68 - 71) and the microcrysts between An 51 to 57.

Other trace elements in plagioclase (Mg, Ba) have been measured. If variations exists, they does not appear significant at this stage of the study.

Olivine

They are magnesian olivine (Fo 81 to 86) (Fig. 3). In a same crystal the Fo content is constant (Fo 81.24 to 82.05 in the most ferrous crystal for example). The Ni content varie from .03. The Ca content is scattered between .53 and .69 cation.

Pyroxene

Clinopyroxene of salitic composition is present in a small aggregate of amphibole phenocrysts (Table 3, Fig. 3). TiO_2 contents are low (.29 to1.31 %) but Al_2O_3 contents are relatively high for pyroxene of calc-alkaline magmas (2.41 to 8.52 %). This high Al-content is not correlated with an increase of the sodium content.

Amphibole

Amphibole (Table 4, Figs. 3 and 4) has a composition varying from magnesio-hornblende to tschermakitic hornblende (Si: 6.21 to 6.78 for Mg/Mg+Fe = .54 to .70). The alumina content (1.50 to 2.62 cations) is relatively high and this type of composition is most frequently observed in andesitic magmas rather than in dacitic one.

Biotite

Biotites encountered in the lava (Table 5) are poor in TiO_2 (2.85 to 3.42 %) and relatively almina-rich (15.28 to 15.81 %). Their Mg/Mg+Fe ratio is comprised between .66 and .72, and therefore higher than the amphibole phenocrysts core. When they are associated the Mg* Amph/Mg* Biot varies from .85 to .90 and it seems that the two minerals are not in equilibrium. Their composition is, however, similar to that of other biotites known in andesitic magmas (Fig. 5).

Oxydes

Only Ti-poor magnetite has been found in microphenocrysts, with TiO_2 values of 5.03 to 6.21 % (Table 6).

CONCLUSION

The dacitic lava studied here give much evidence of disequilibrium assemblages. If we summarize:

-magnesian olivine and clinopyroxene could be associated with a stage of magma mixing between a dacitic magma and a basic liquid, now represented by quenched amphibole-rich inclusions;

-An-poor plagioclase and biotite have no clear relations with the host magma. The An content variations of the plagioclase are indicative of an increaseof the Ca content of the liquid and/or an increase of H_2O. In some cases (Wones & Dodge, 1977) in potassium-rich magmas, low H_2O activity favors earlier precipitation of biotite. This point remains unresolved for the moment.

-finally, the equilibrium assemblage of the dacitic magma, is formed as in many calc-alkaline SiO_2-rich rocks, by an amphibole + Ca-plagioclase + Ti-poor magnetite.

These paragenesis could indicate the existence of a plumbing system under the volcanic edifice.

The potassic character of the lava, in comparison with other lavas of the area, poses a problem. The Kozushima island, also of potassic character (Aramaki & Ui, 1982; Matsuda, 1977) is in the continuation of the volcanic alignment defined in the introduction. It would be essential to sample the other volcanoes of the ridge to precise their nature and a better understanding of this complex zone.

REFERENCE

Aramaki, S. and Ui, T., 1982, Japan, in Andesites, R. S. Thorpe (ed.) J Willey & sons, p.25-95

Ewart A., 1982, The mineralogy and petrology of Tertiary-Recent orogenic volcanic rocks with sepecial references to the andesitic basaltic compositional range. in Andesites, R. S. Thorpe (ed.) J. Willey & sons, p.25-95.

Kuno, I., 1968, Lateral variations of basalt magma types across continental margins and island arcs. Bull. Volcanol., 29, 195-222

Le Pichon X., Iiyama T., et al., 1987, The eastern and western ends of Nankai Trough: results of Box 5 and Box 7 Kaiko survey. Earth Planet. Sci. Lett., 83, 199-213.

Matsuda, J., Zashu, S. and Ozima, M., 1977, Sr isotopic studies of volcanic rocks from island arcs in the western Pacific, Thectonophysics, 37, 141-151.

Matsuda, J., 1985, Sr isotopic studies of rocks from the Philippine Sea and some implication for the mantle material. (ed.) T. Shiki, In. Geology of the Northern Philippine Sea, p.63-81., Tokai Univ. Press.

Pecerillo A. and Taylor S. R., 1976, Geochemistry of Eocene calc-alkaline volcanic rocks from Kastamanou area, Northern Turkey. Contrib. Mineral. Petrol., 58, 63-81.

Wones D. R. and Dodge F. C. W., 1977, The stability of phlogopite in the presence of quartz and diopside. (ed.) D. G. Fraser, In Thermodynamics and geology, p.229-247., Reidel, Dortrecht.

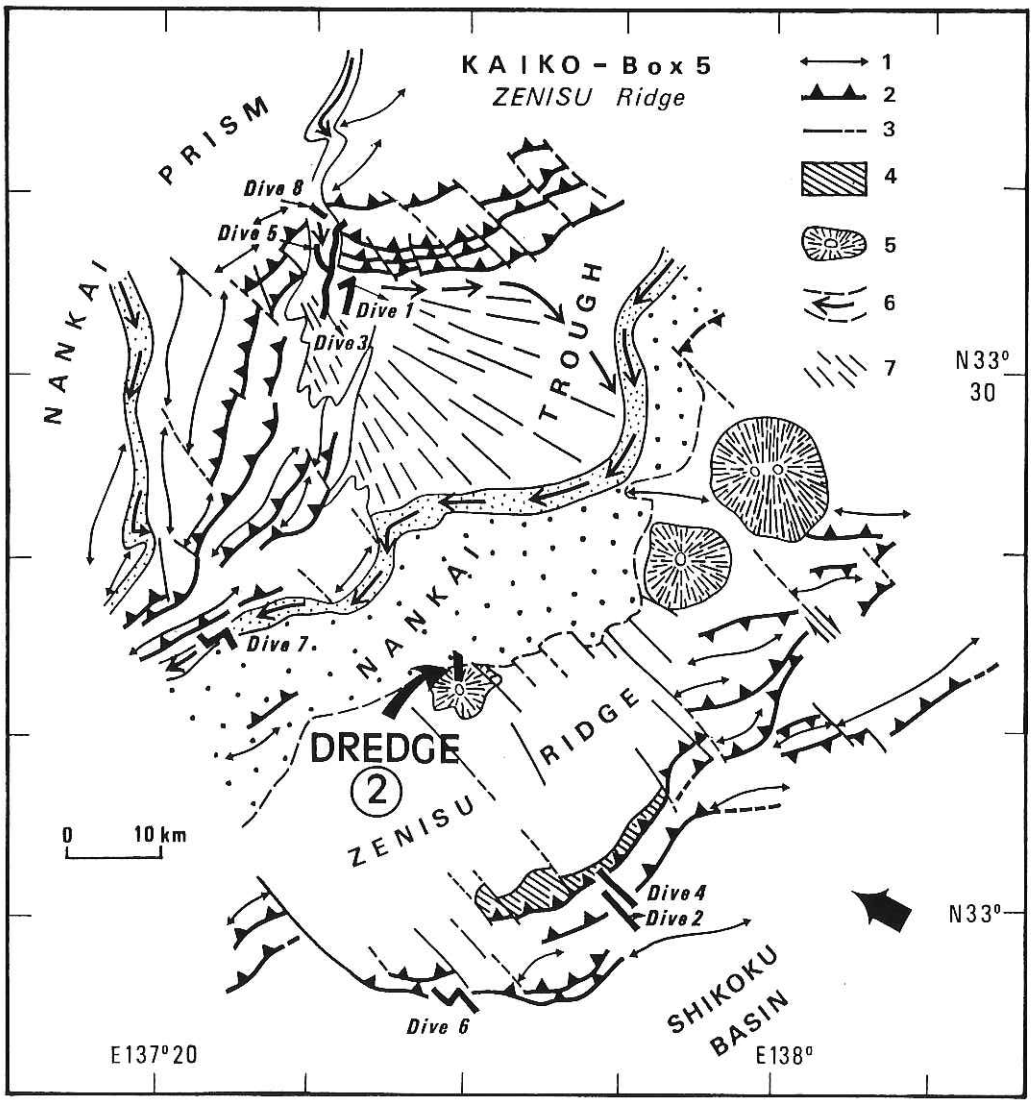

Fig. 1 Simplified structural sketchmap of the Zenisu ridge western end (Kaiko survey). Dredged samples sites are located
1 : anticlinal axis; 2: thrust; 3 : fault; 4 : outcrop of Zenisu acoustic basement; 5 : volcano; 6 : channel; 7: Tenryu deepsea fan.

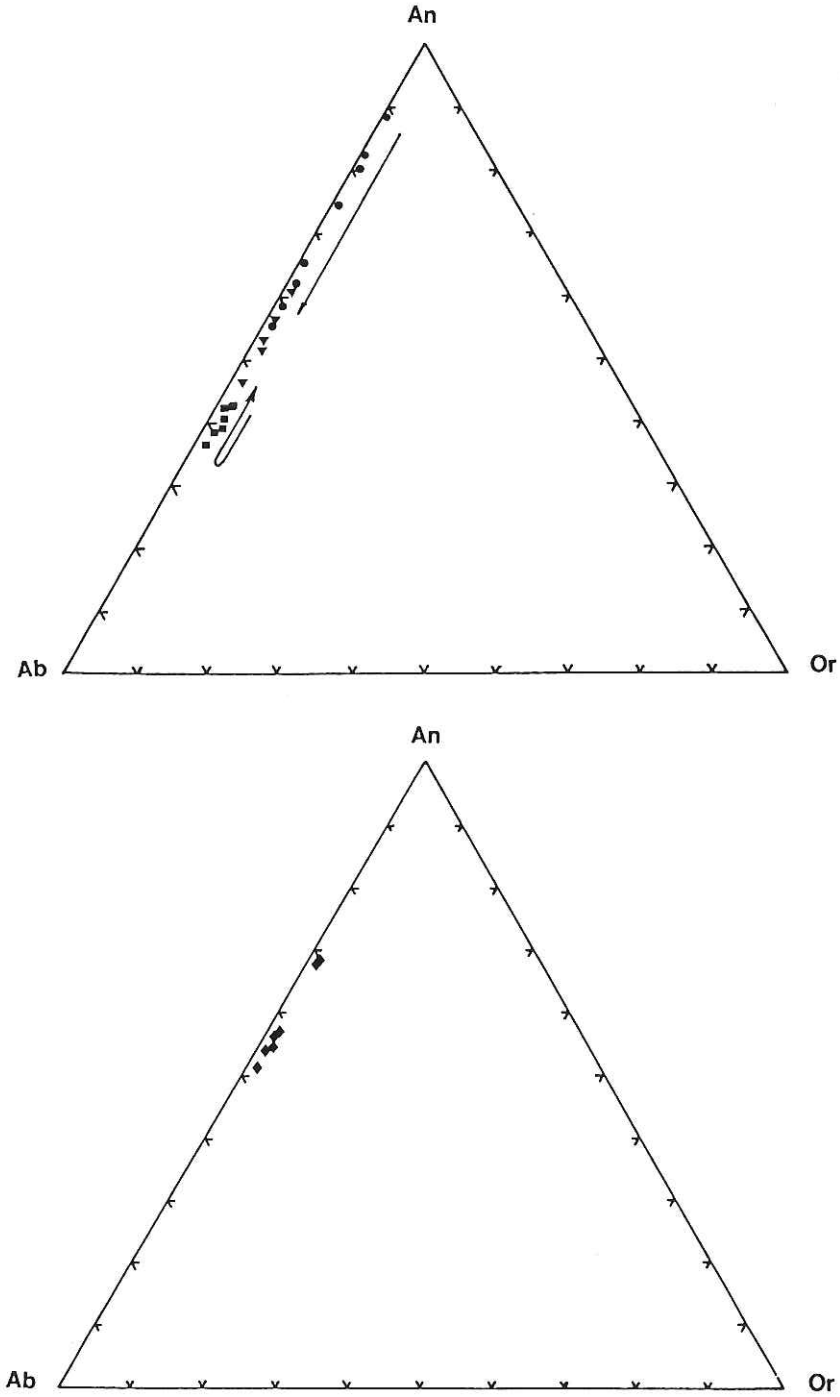

Fig 2b

Fig. 2 Composition of the plagioclases in the An-Ab-Or triangle Filled circles: core of phenocrysts; squares: core of resorbed phenocrysts; triangles: border of the two types of phenocrysts.

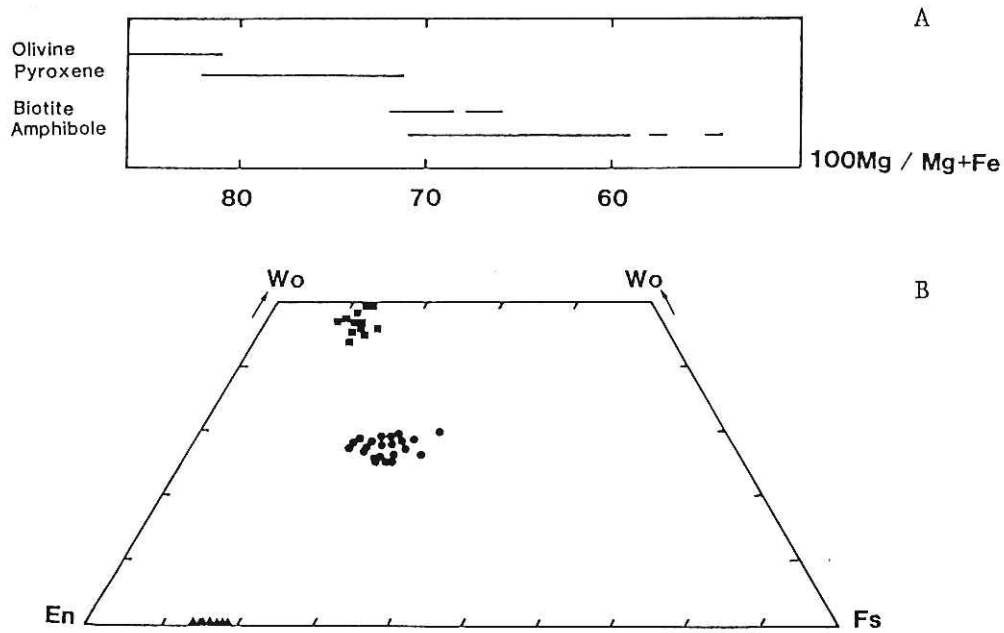

Fig. 3 a: 100 Mg/(Mg+Fe) of olivine, pyroxene, biotite and amphibole. b: Composition of clinopyroxenes (squares) amphibole (circles) and olivine (triangle) in the wollastonite-enstatite-ferrosilite triangle.

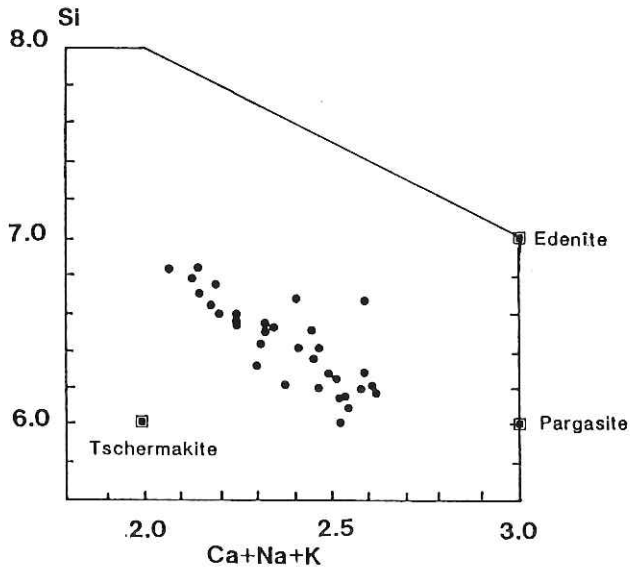

Fig.4 plot of Ca + Na + K versus Si for the amphibole compositions.

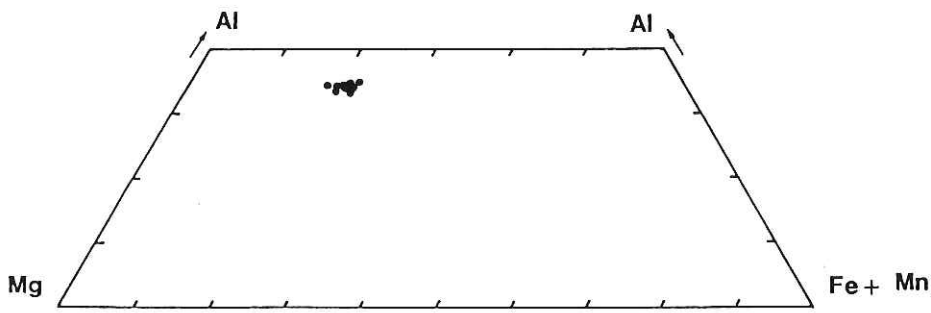

Fig. 5 Composition of the biotites in the Al-Mg-(Fe+Mn) triangle.

Table 1 - Major and trace elements, C.I.P.W. norm of sample D2 - 01.

	1	2		1	2
SiO2	65.33	65.21	Cu	29	<10
Al2O3	16.69	16.42	Rb	79	91
Fe2O3	1.85	1.58	Sr	507	414
FeO	1.46	1.69	Co	13	14
MnO	0.28	0.17	Cr	<10	<10
MgO	1.14	1.12	Ni	10	<10
CaO	4.17	4.16	V	56	55
Na2O	3.76	3.78	Zn	34	50
K2O	2.18	2.19			
TiO2	0.35	0.34			
P2O5	0.15	0.15			
CO2					
H2O+	1.98	1.98			
H2O-	0.47	0.50			
	99.81	99.89			
C.I.P.W. Norm					
Q	25.06	24.76			
Or	13.23	13.36			
Ab	32.67	33.33			
An	20.23	20.30			
Cor	0.95	0.65			
Hy	4.04	4.48			
Ma	2.75	2.37			
Ilm	0.68	0.67			
Ap	0.39	0.38			

Table 2 - Representative analyses of plagioclases.
49 - 52: plagioclases phenocrysts
7 - 9: resorbed phenocrysts
17 - 19: inclusions plagioclases.

	49	52	7	9	17	19
SiO2	47.66	52.36	53.39	56.99	50.77	55.81
AL2O3	33.62	30.13	29.62	27.18	31.06	28.03
Fe2O3	.30	.38	.30	.26	.79	.25
MgO	.01	.01			.04	.01
CaO	17.04	13.49	12.22	9.54	14.73	10.64
Na2O	1.96	3.91	4.61	6.15	3.32	5.43
K2O	.06	.13	.15	.25	.09	.26
BaO				.12		.02
	100.69	100.42	100.31	100.50	100.81	100.47
Si	2.171	2.369	2.411	2.551	2.302	2.504
Al	1.807	1.607	1.576	1.434	1.659	1.482
Fe3+	.010	.011	.013	.101	.088	.027
Mg	.001	.002	.001		.003	.001
Ca	.833	.654	.591	.456	.715	.512
Na	.173	.343	.404	.534	.292	.473
K	.003	.007	.009	.014	.005	.015
	5.004	4.995	5.000	5.001	5.003	4.995

Table 3 - Representative analyses and structural formulae of clinopyroxenes.

	2	15	17	18
SiO2	51.84	46.44	46.45	50.69
Al2O3	2.41	8.34	8.52	4.51
Fe2O3	0.00	0.00	0.00	0.00
FeO	7.95	7.29	7.36	5.91
MgO	14.07	12.44	12.46	14.66
CaO	22.13	22.74	22.50	22.99
Na2O	0.33	0.25	0.26	0.23
MnO	0.50	0.12	0.14	0.15
TiO2	0.29	1.31	1.37	0.61
Cr2O3	0.01	0.01	0.03	0.10
ZnO	0.00	0.00	0.00	0.00
SrO	0.00	0.00	0.00	0.00
V2O5	0.00	0.00	0.00	0.00
Total	99.53	98.94	99.09	99.85
Fe2O3	1.30	3.52	3.30	1.72
FeO	6.78	4.12	4.39	4.36
Si	1.933	1.738	1.736	1.868
Al	0.106	0.368	0.375	0.196
Fe3	0.036	0.099	0.093	0.048
Fe2	0.211	0.129	0.137	0.134
Mg	0.782	0.694	0.694	0.805
Ca	0.884	0.912	0.901	0.908
Na	0.024	0.018	0.019	0.016
Mn	0.016	0.004	0.004	0.005
Ti	0.008	0.037	0.039	0.017
Cr	0.000	0.000	0.001	0.003
Zn	0.000	0.000	0.000	0.000
Sr	0.000	0.000	0.000	0.000
V	0.000	0.000	0.000	0.000
Total	4.000	4.000	4.000	4.000

Table 4 - Representative analyses and structural formulae of amphibole.

SiO2	37.59	37.83
Al2O3	15.28	15.12
FeO	13.33	13.56
MgO	15.59	15.77
MnO	0.25	0.33
TiO2	0.03	2.85
CaO	0.06	0.08
Na2O	0.94	0.79
K2O	8.27	8.19
BaO	0.22	0.37
SrO	0.00	0.00
F	0.00	0.24
Cl	0.09	0.03
H2O	0.00	3.91
Total	91.65	99.07
Si	5.776	5.622
Al	2.768	2.649
Fe2	1.713	1.685
Mg	3.570	3.493
Mn	0.033	0.042
Ti	0.003	0.319
Ca	0.010	0.013
Na	0.280	0.228
K	1.621	1.553
Ba	0.013	0.022
Sr	0.000	0.000
F	0.000	0.113
Cl	0.000	0.008
OH*	0.000	3.880
Total	15.787	19.625
F/F+OH	0.000	0.028

Table 5 - Representative analyses and structural formulae of biotite.

SiO2	46.94	41.56	41.23	43.96
Al2O3	9.33	13.24	14.03	11.63
FeO	12.76	15.96	12.68	11.27
MgO	14.75	10.85	12.57	14.80
MnO	1.03	0.43	0.20	0.20
TiO2	1.05	1.71	1.57	1.81
CaO	10.34	11.85	11.79	11.37
Na2O	1.40	1.92	2.15	2.10
K2O	0.33	0.64	0.64	0.51
BaO	0.09	0.03	0.00	0.09
SrO	0.00	0.00	0.00	0.00
F	0.05	0.00	0.00	0.18
Cl	0.03	0.09	0.02	0.00
H2O	2.03	0.00	0.00	1.97
Total	100.13	98.28	96.88	99.89
Si	6.615	6.116	6.059	6.302
Al	1.550	2.297	2.430	1.965
Fe2	1.504	1.964	1.559	1.351
Mg	3.098	2.380	2.753	3.162
Mn	0.123	0.054	0.025	0.024
Ti	0.111	0.189	0.174	0.195
Ca	1.561	1.869	1.857	1.747
Na	0.383	0.548	0.613	0.584
K	0.059	0.120	0.120	0.093
Ba	0.005	0.002	0.000	0.005
Sr	0.000	0.000	0.000	0.000
F	0.023	0.000	0.000	0.083
Cl	0.007	0.000	0.000	0.000
OH*	1.970	0.000	0.000	1.917
Total	17.488	15.773	15.815	17.723
F/F+OH	0.012	0.000	0.000	0.042
Fe3	1.429	0.685	0.658	0.865
Fe2	0.075	1.279	0.901	0.486

Table 6 - Represnetative analyses and structural formulae of magnetite.

	65	64
SiO2	0.07	0.12
Al2O3	2.99	3.09
Fe2O3	0.00	0.00
FeO	82.76	85.22
MgO	2.13	0.02
CaO	0.10	0.14
Na2O	0.00	0.00
MnO	0.63	0.95
TiO2	5.97	5.15
Cr2O3	0.08	0.06
ZnO	0.00	0.00
SrO	0.00	0.00
V2O5	0.00	0.00
Total	97.99	97.98
Fe2O3	55.03	55.30
FeO	33.25	35.46
Si	0.003	0.005
Al	0.130	0.137
Fe3	1.530	1.562
Fe2	1.028	1.113
Mg	0.117	0.001
Ca	0.004	0.006
Na	0.000	0.000
Mn	0.020	0.030
Ti	0.166	0.145
Cr	0.002	0.002
Zn	0.000	0.000
Sr	0.000	0.000
V	0.000	0.000
Total	3.000	3.000
TiO2	6.30	5.57
FeO	35.32	34.64
Fe2O3	58.38	59.79